Technische Universität München

TUM School of Medicine and Health

TUM

Insulin signaling regulates localization and translation of *Pink1* mRNA via modulation of AMPK activity to support mitophagy in neurons

Jara Tabitha Hees

TABLE OF CONTENTS

_____

_____

_____

LIST OF FIGURES

LIST OF ABBREVIATIONS

AA	Antimycin A
Aβ	amyloid beta
AD	Alzheimer's disease
ADP	adenosine diphosphate
AICAR	AMP analogue 5-aminoimidazole-4-carboxamide ribonucleoside
AKAP1	A-kinase anchor protein 1
AMP	adenosine monophosphate
AMPK	AMP-activated protein kinase
ANXA11	Annexin A11
ApoE2	apolipoprotein E2
ApoE3	apolipoprotein E3
ApoE4	apolipoprotein E4
ATG	autophagy-related
ATP	adenosine triphosphate
Atp5f1b	ATP synthase F1 subunit beta
BBB	blood-brain barrier
BNIP3L	BCL2/adenovirus E1B 19-kDa interacting protein 3-like
Ca^{2+}	calcium
CAMKK2	Ca^{2+}/calmodulin-dependent protein kinase kinase 2
CBS	cystathionine-β-synthase
CC	Compound C
CIP	calf intestinal phosphatase
CLEM	correlative light electron microscopy
Cox4i	cytochrome c oxidase subunit 4 isoform I
Cox7c	cytochrome c oxidase subunit 7c
Djp1	DnaJ-like protein 1
DMEM	Dulbecco's modified Eagle medium
DNA	deoxyribonucleic acid
DNAJB6	DnaJ heat shock protein family (Hsp40) member B6
Drp1	Dynamin-related protein 1
EEA1	early endosomal antigen 1

eIF4E	eukaryotic translation initiation factor 4E
ER	endoplasmic reticulum
FAHD$_2$	flavin adenine dinucleotide
FBS	fetal bovine serum
FERRY	Five-subunit Endosomal Rab5 and RNA/ribosomes intermediary complex
FLIM	fluorescent lifetime imaging
FOXO1	Forkhead Box Protein O1
FRET	Förster Resonance Energy Transfer
FUNDC1	FUN14 domain containing protein 1
GAP	GTPase-activating protein
GATOR	GAP activity towards the Rags 1
G3BP1	GTPase-activating protein SH3 domain-binding protein 1
GEF	guanine nucleotide exchange factor
GFP	green fluorescent protein
HDL	high-density lipoprotein
HEK293T	Human embryonic kidney 293T
iBAQ	intensity-based absolute quantification
IGF-1	insulin-like growth factor 1
IMM	inner mitochondrial membrane
IMS	intermembrane space
iPSCs	induced pluripotent stem cells
IR	insulin receptor
IRS	insulin receptor substrates
LAMP1	lysosomal-associated membrane protein 1
LAMTOR	late endosomal/lysosomal adaptor, MAPK and mTOR activator
LFQ	label free quantification
LKB1	liver kinase B1
MCS	membrane contact site
meGFP	monomeric enhanced green fluorescent protein
Mff	mitochondrial fission factor
Mfn1/2	Mitofusin 1/2
MiD49	mitochondrial dynamics protein 49
MiD51	mitochondrial dynamics protein 51

MPP	matrix processing peptidase
mRNP	messenger ribonucleoprotein
MS	mass spectrometry
mtDNA	mitochondrial DNA
MTFR1L	mitochondrial fission regulator 1-like protein
mTOR	mammalian target of rapamycin
mTORC1	mammalian target of rapamycin complex 1
NADH	nicotinamide adenine dinucleotide
NBR1	neighbor of BRCA1 gene 1
NDP52	nuclear dot protein 52
NFTs	neurofibrillary tangles
NGN-2	neurogenin-2
NIX	NIP3-like protein X
NRF-1	nuclear respiration factor 1
NRF-2	nuclear respiration factor 2
OMM	outer mitochondrial membrane
Opa1	optic atrophy 1
OXPHOS	oxidative phosphorylation
PARL	Presenilin-associated rhomboid-like protein
PBR-A	phos binding reagent acrylamide
PD	Parkinson's disease
PDZ	postsynaptic density protein-95/discs large/zonula occludens-1
PDZD8	PDZ domain-containing protein 8
PFA	paraformaldehyde
PGC-1α	peroxisome-proliferator-activated γ co-activator 1α
Phospho-MS	phospho-peptide enrichment followed by mass spectrometry
PI3K	phosphatidylinositol 3-kinase
Pink1	PTEN-induced kinase 1
PIP_2	phosphatidylinositol-4,5-bisphosphate
PIP_3	phosphatidylinositol-3,4,5-trisphosphate
PLA	proximity ligation assay
PLL	poly-L-lysine
P/S	penicillin/streptomycin

PTEN	phosphatase and tensin homolog
p-ubiquitin	phosphorylated ubiquitin
Raptor	regulatory-associated protein of mTOR
RBP	RNA-binding protein
RFP	red fluorescent protein
Rheb	Ras homolog enriched in brain
RNA	ribonucleic acid
ROS	reactive oxygen species
Rpl22	ribosomal protein L22
Rps6	ribosomal protein S6
RRBP1	ribosome-binding protein 1
RT-qPCR	reverse transcription quantitative polymerase chain reaction
scFv-GFP	single-chain variable fragment antibody fused to GFP
SECFP	super enhanced cyan fluorescent protein
shRNA	short hairpin RNA
SMP	Synaptotagmin-like Mitochondrial lipid-binding proteins
SNPH	Syntaphilin
SYNJ2a	Synaptojanin 2a
SYNJ2BP	Synaptojanin 2 binding protein
TAX1BP1	Tax1-binding protein 1
TBC1D7	TBC1 domain family member 7
TFAM	mitochondrial transcription factor A
TIM	translocase of the inner mitochondrial membrane
TMEM192	transmembrane protein 192
TOM	translocase of the outer mitochondrial membrane
TSC	tuberous sclerosis protein complex
ULK1	Unc-51-like kinase 1
UTR	untranslated region
v-ATPase	vacuolar H^+-ATPase
Ypet	yellow fluorescent protein for energy transfer

SUMMARY

Neurons rely heavily on mitochondrial function including ATP synthesis and calcium buffering, due to the high energy demand of the brain. The extended and complex architecture of neurons presents a significant challenge in the maintenance and distribution of mitochondria throughout the cell. Given that neurons are postmitotic, they are highly susceptible to mitochondrial dysfunction. Timely degradation of damaged mitochondria through mitophagy is crucial to prevent the accumulation of defective mitochondria, which can lead to neurodegeneration. More than 99 % percent of mitochondrial proteins are encoded in the nucleus and imported into mitochondria after synthesis on cytosolic ribosomes. To ensure a constant supply of fresh mitochondrial proteins in every part of the neuron, short-lived proteins need to be locally translated in distal parts since transport from the soma would exceed their lifetime. The short-lived protein PTEN-induced kinase 1 (PINK1) is an important player in the removal of defective mitochondria via mitophagy by acting as a sensor for mitochondrial damage. *Pink1* mRNA is co-transported with mitochondria along neurites, which allows for on-demand local translation in distal parts of the neuron. The mitochondrial outer membrane protein Synaptojanin 2 binding protein (SYNJ2BP) and Synaptojanin 2a (SYNJ2a), which contains an RNA-binding domain, are involved in tethering *Pink1* mRNA to mitochondria. However, it still remains to be elucidated how mRNA transport as well as subsequent protein translation and function are regulated in response to local stimuli in neurons. Here, I report that activation of the insulin signaling cascade, which inhibits the AMPK-activated protein kinase (AMPK), reduces *Pink1* mRNA association with mitochondria. Mechanistically, AMPK phosphorylates the mitochondrial anchor protein SYNJ2BP at serine 21, which increases its interaction with SYNJ2a. Interestingly, loss of mitochondrial *Pink1* mRNA association upon AMPK inhibition increases PINK1 translation at endolysosomes, which supply amino acids required for protein synthesis. Furthermore, the ER-chaperone DNAJB6 localizes to the translation hotspots indicating that DNAJB6 could be involved in guiding PINK1 to its mitochondrial destination. As insulin drives *Pink1* mRNA translation via modulation of AMPK activity, the activation of the PINK1 protein as well as its role as a ubiquitin kinase in the mitophagy pathway rely on the presence of insulin. Insulin resistance, which is induced *in vitro* by addition of apolipoprotein E4, a key genetic risk factor for Alzheimer's disease, leads to the retention of *Pink1* mRNA at mitochondria and disrupts proper functioning of PINK1 in neurons. These findings collectively demonstrate a metabolic shift that governs the localization of *Pink1* mRNA as well as translation and function of PINK1 through signaling pathways involving insulin and AMPK. Furthermore, they propose a mechanistic link between mitochondrial dysfunction, insulin resistance, and the development of neurodegenerative disorders.

ZUSAMMENFASSUNG

Neuronen sind aufgrund des hohen Energiebedarfs des Gehirns stark von Mitochondrien abhängig, da diese ATP herstellen und die Calcium-Homöostase erhalten. Die komplexe Architektur von Neuronen stellt eine besondere Herausforderung bei der Aufrechterhaltung der Mitochondrien in der gesamten Zelle dar. Da Neuronen postmitotisch sind, sind sie außerdem sehr anfällig für mitochondriale Dysfunktion. Ein rechtzeitiger Abbau von geschädigten Mitochondrien durch Mitophagie ist notwendig, da eine Anhäufung defekter Mitochondrien zu Neurodegeneration führen kann. Über 99 % der mitochondrialen Proteine werden im Zellkern kodiert und nach der Synthese auf zytosolischen Ribosomen in die Mitochondrien importiert. Um eine konstante Versorgung mit frisch-synthetisierten mitochondrialen Proteinen in jedem Teil des Neurons zu gewährleisten, müssen kurzlebige Proteine in distalen Teilen lokal translatiert werden, da der Transport vom Soma ihre Lebensdauer überschreiten würde. Das kurzlebige Protein PTEN-induzierte Kinase 1 (PINK1) spielt eine wichtige Rolle bei der Beseitigung defekter Mitochondrien durch Mitophagie. *Pink1* mRNA wird zusammen mit Mitochondrien entlang den Neuriten transportiert, was eine bedarfsgerechte lokale Translation in distalen Teilen des Neurons ermöglicht. Das mitochondriale Protein Synaptojanin 2-bindendes Protein (SYNJ2BP) und Synaptojanin 2a (SYNJ2a), das eine RNA-bindende Domäne besitzt, ermöglichen die Lokalisierung von *Pink1* mRNA an die Mitochondrien. Es bleibt jedoch noch zu klären, wie der mRNA-Transport sowie die anschließende Translation und Funktion in Neuronen in Reaktion auf lokale Reize reguliert werden. Hier zeige ich, dass die Aktivierung der Insulinsignalkaskade, die die AMP-aktivierte Proteinkinase (AMPK) hemmt, die Assoziation von *Pink1* mRNA mit Mitochondrien reduziert. AMPK phosphoryliert das mitochondriale Ankerprotein SYNJ2BP an Serin 21, was seine Interaktion mit SYNJ2a erhöht. Interessanterweise führt der Verlust der mitochondrialen Bindung von *Pink1* mRNA induziert durch AMPK-Hemmung zu einer erhöhten Translation von PINK1 an Endolysosomen, die die benötigten Aminosäuren bereitstellen. Darüber hinaus lokalisiert das ER-Chaperon DNAJB6 an die Translation-Hotspots, was darauf hinweist, dass DNAJB6 an der Translokation von PINK1 zu seinem mitochondrialen Bestimmungsort beteiligt sein könnte. Da Insulin die Translation von *Pink1* mRNA mittels Modulation von AMPK steuert, sind die Aktivierung des PINK1-Proteins sowie seine Rolle als Ubiquitin-Kinase in der Mitophagie von Insulin abhängig. Insulinresistenz, die *in vitro* durch Zugabe von Apolipoprotein E4, einem genetischen Risikofaktor für die Alzheimer-Krankheit, induziert wird, führt zum Verbleiben von *Pink1* mRNA an Mitochondrien und stört die Funktion von PINK1 in Neuronen. Diese Ergebnisse zeigen einen metabolischen Schalter auf, der die Lokalisierung von *Pink1* mRNA sowie die Translation und Funktion von PINK1 über Signalwege, die Insulin und AMPK umfassen, steuert. Darüber hinaus schlagen sie eine mechanistische Verbindung zwischen mitochondrialer Dysfunktion, Insulinresistenz und der Entwicklung neurodegenerativer Erkrankungen vor.

1 INTRODUCTION

1.1 Mitochondria: origin, function and dynamics

Mitochondria are believed to have evolved from bacteria by endosymbiosis about 1.5 billion years ago (Archibald, 2015). As remnants of their bacterial origin, mitochondria still contain their own genome. In mammals, the mitochondrial DNA (mtDNA) encodes for 13 proteins, while the remaining 99 % of mitochondrial proteins are nuclear-encoded. Mitochondria are double membrane organelles with an outer mitochondrial membrane (OMM) facing the cytosol and an inner mitochondrial membrane (IMM) forming invaginations known as cristae that protrude into the mitochondrial matrix. The compartment inbetween the two membranes is referred to as intermembrane space (IMS).

Mitochondria play a critical role in many essential cellular processes placing them in a critical position for the regulation of cellular life and death. Mitochondria are best known for their function as powerhouses of the cell by producing energy in form of adenosine triphosphate (ATP) via oxidative phosphorylation (OXPHOS). The OXPHOS system consists of five main protein complexes that are embedded in the IMM. Electron transfer from nicotinamide adenine dinucleotide (NADH) and flavin adenine dinucleotide ($FADH_2$) to oxygen across the protein complexes as well as proton translocation across the IMM creates an electrochemical gradient that drives ATP synthesis via the final complex ATP synthase (Papa et al., 2012). Apart from ATP synthesis, however, mitochondria have several other functions including the regulation of apoptotic cell death, maintenance of calcium (Ca^{2+}) homeostasis, innate immunity and redox signalling (Kamer & Mootha, 2015; McBride et al., 2006; Nikoletopoulou et al., 2013; Rambold & Pearce, 2018).

For a long time, mitochondria have been considered to be static structures. This concept has dramatically changed over the past 30 years, as live cell imaging has revealed mitochondria to be highly dynamic organelles. They are not only very mobile due to transport along the cytoskeleton (Hollenbeck & Saxton, 2005) but they also constantly change their morphology by undergoing fission and fusion events (Bereiter-Hahn & Vöth, 1994). These processes are also referred to as mitochondrial dynamics.

Mitochondrial fusion is characterized by conjunction of two mitochondria resulting in one organelle, whereas fission divides one mitochondrion into two independent organelles. Fusion of the OMM and IMM is mediated by Mitofusin 1/2 (Mfn1/2) and optic atrophy 1 (OPA1), respectively (Cipolat et al., 2004; Eura et al., 2003; Griparic et al., 2004). The opposing fission reaction is primarily regulated by the cytosolic Dynamin-related protein 1 (Drp1) (Fröhlich et al., 2013; Ingerman et al., 2005; Smirnova et al., 2001) as well as its receptors mitochondrial fission factor (Mff) (Gandre-Babbe & van der Bliek, 2008) and mitochondrial dynamics proteins 49 and 51 (MiD49 and MiD51) (Losón et al., 2013; Palmer et al., 2011). The balance between fusion and fission contributes to a healthy mitochondrial network

_____

(Fig. 1a). While mitochondrial fission resulting in smaller organelles is critical for proper mitochondrial distribution (Ishihara et al., 2009; Z. Li et al., 2004), mitochondrial fusion facilitates exchange of organellar content to compensate for damaged DNA or proteins (H. Chen et al., 2005; Detmer & Chan, 2007).

In addition to morphological changes, mitochondria also show very complex mobility patterns as they are transported along microtubule and actin tracks in a dynamic and bidirectional fashion. They frequently change direction, pause or remain stationary. Tight regulation of mitochondrial transport is particular important in highly polarized and structurally complex cells such as neurons (as described in chapter 1.2). Whereas long-range mitochondrial trafficking is mainly mediated by microtubule-associated motors (kinesin and dynein), shorter movements are dependent on actin and its motor proteins (myosin) (Hirokawa & Takemura, 2005; Hollenbeck & Saxton, 2005; Morris & Hollenbeck, 1993; Quintero et al., 2009). Mitochondrial transport is mediated by the OMM Rho (Miro) GTPases and the motor adaptor proteins Milton/TRAK, which couple mitochondria to kinesin and dynein motors to allow for anterograde and retrograde trafficking, respectively (Fransson et al., 2006; Glater et al., 2006; López-Doménech et al., 2018; Oeding et al., 2018; Stowers et al., 2002; van Spronsen et al., 2013). Apart from the mobile mitochondrial pool, there is always a stationary fraction. Syntaphilin (SNPH) has been identified as a docking protein that anchors mitochondria on microtubules (Kang et al., 2008) (Fig. 1b).

Due to their essential role in cells, mitochondrial health maintenance is critical for cell survival (Nunnari & Suomalainen, 2012). As neurons are very dependent on mitochondrial function, maintaining a healthy mitochondrial network is particularly important in neurons.

_____
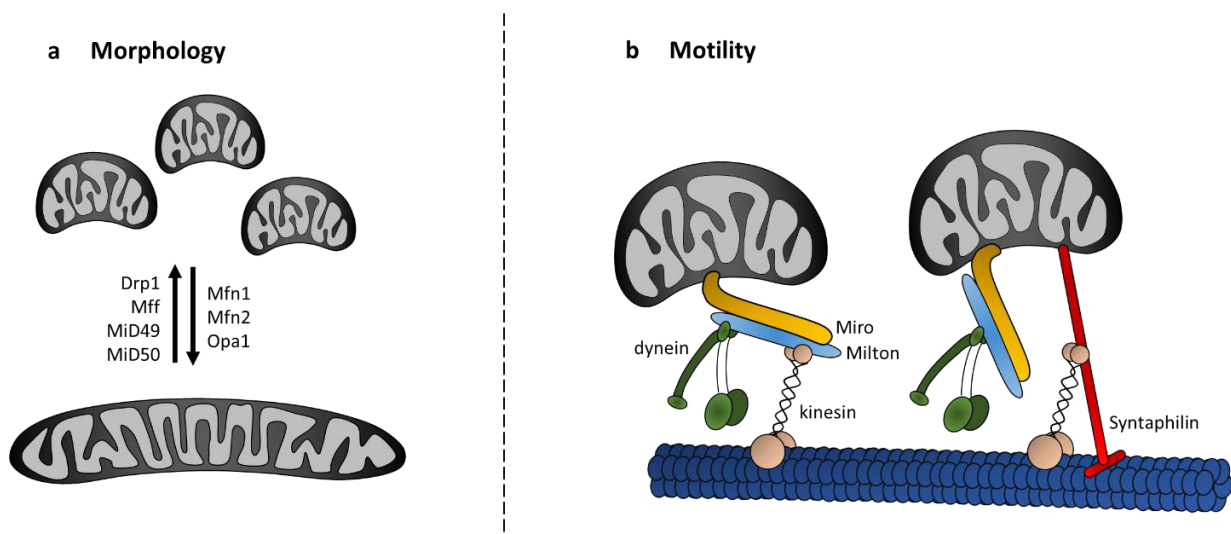
Figure 1: Mitochondrial morphology and motility.
(a) Mitochondrial fusion is mediated by Mfn1, Mfn2 and Opa1, while mitochondrial fission is regulated by Drp1 and its receptors Mff, MiD49, and MiD50. **(b)** Mitochondria are coupled to kinesin and dynein motors via the OMM GTPase Miro and the motor adaptor protein Milton, which allows for anterograde and retrograde transport along microtubules. Syntaphilin is a docking protein that anchors stationary mitochondria on microtubules.

1.2 Mitochondrial maintenance in neurons

Compared to other cell types, neurons are especially challenged in maintaining and distributing mitochondria throughout the entire cell due to their extended architecture (W. Matsuda et al., 2009; Misgeld & Schwarz, 2017). Neurons are highly polarized cells that contain different cellular subcompartments including a cell body (soma), dendrites, an axon, and synapses. This complex structure consisting of long and highly branched processes has evolved due to the neuron's function, which is to transmit information in form of electric signals over long distances. While axons can be up to one meter long in humans, individual highly branched neurons of certain brain regions even have a cumulative total axon length of 4.5 m (Bolam & Pissadaki, 2012; W. Matsuda et al., 2009). Apart from their extraordinary architecture, neurons are postmitotic cells and hence need to survive a human's lifetime. Most proteins, on the other hand, last only for minutes, hours, days or weeks due to constant turnover by proteolytic degradation and synthesis (Goldberg, 2003). While neurons are particularly challenged in maintaining a healthy mitochondrial network, they are at the same time, however, very dependent on mitochondrial function. Although the brain only makes up 2 % of the body weight, ATP generation via OXPHOS in brain mitochondria consumes about 20 % of the body's oxygen (Attwell & Laughlin, 2001). Synaptic transmission including the firing of action potentials as well as the maintenance of resting membrane potential requires a large amount of energy. OXPHOS, in contrast to glycolysis, is believed to be the primary ATP source in neurons (Erecińska & Silver, 1994; Hall et al., 2012; Harris et al., 2012).

The process that maintains a healthy mitochondrial pool in each compartment throughout the neuron's life has been termed mitostasis (Misgeld & Schwarz, 2017). Several issues need to be taken into account when considering neuronal mitostasis. As the majority of mitochondrial proteins are nuclear-encoded and the translational machinery is mainly present in the soma, it has been assumed that mitochondrial biogenesis is mainly restricted to the somatodendritic compartment. This raises, however, the question how distal mitochondria are maintained. Considering the long distances between the soma and the synapses in neurons and the speed of mitochondrial transport (around 0.5 µm/s, Bros et al., 2015; Ligon & Steward, 2000), several mitochondrial proteins would not survive the transport as the travel duration exceeds their lifetime. Furthermore, neurons and in particular synapses are very plastic and therefore constantly changing while adapting to their environment.

Consequently, mitochondria are also required to respond to these local demands by changing their distribution accordingly (Misgeld & Schwarz, 2017).

The answer to how the complex process of mitostasis is achieved in neurons lies in the highly dynamic nature of mitochondria and the control of mitochondrial dynamics. Furthermore, local stimuli triggering specific signaling pathways likely allows mitochondria to precisely adapt to the shifting needs of neurons and their different subcompartments. It is possible that neurons have developed their own, neuron-specific signaling pathways to deal with all the challenges that come along with the complex neuronal shape. Furthermore, tight regulation of mitochondrial biogenesis and mitochondrial degradation critically contribute to mitochondrial homeostasis as described in the chapters 1.4 and 1.5.

1.3 Important signaling pathways relevant for mitochondrial homeostasis in neurons

1.3.1   Role of AMPK in mitochondrial homeostasis

AMP-activated protein kinase (AMPK) is known as the master regulator of energy metabolism. Structurally, AMPK is a heterotrimeric complex composed of three subunits: one catalytic α-subunit and two regulatory β- and γ-subunits (Hardie, 2007). In mammals, there are multiple isoforms of each subunit (α1, α2, β1, β2, γ1, γ2, γ3), which are encoded by separate genes (Cheung et al., 2000; Stapleton et al., 1996; Thornton et al., 1998). Hence, 12 different combinations of distinct AMPK complexes are possible as each complex contains one isoform of each subunit (Ross, MacKintosh, et al., 2016). The catalytic α-subunit contains the kinase domain including a regulatory threonine 172 (T172) residue that is phosphorylated by upstream kinases resulting in AMPK activation (Hawley et al., 1996). The β-subunit allows AMPK to associate with glycogen as it contains a conserved carbohydrate-binding domain (Hudson et al., 2003). The γ-subunit contains the adenine nucleotide binding region composed of a tandem of four cystathionine-β-synthase (CBS) domains (Xiao et al., 2007). AMP binding to the γ-subunit results in AMPK activation (Gowans et al., 2013). Apart from AMP, ADP and ATP are also able to bind to the CBS domains (Fig. 2). While ADP also leads to increased AMPK activity, however to a lesser extent than AMP, ATP does not. Consequently, AMPK is a real sensor for energy levels as it senses changes in the ATP-to-ADP/AMP ratio rather than total changes in only one nucleotide (Gowans et al., 2013; Hardie et al., 2011; Ross, Jensen, et al., 2016). Mechanistically, AMP activates AMPK by two main actions. First, binding of AMP protects the critical T172 site from phosphatases thereby preventing its dephosphorylation and keeping AMPK in an active state (Davies et al., 1995). Second, AMP allosterically activates AMPK that is already phosphorylated at T172 (Gowans et al., 2013; Suter et al., 2006). There are two main upstream kinases that phosphorylate T172 in the activation loop of the catalytic AMPK subunit α: liver kinase B1 (LKB1) (in complex with STRAD and MO25) (Hawley et al.,

2003; Shaw et al., 2004; Woods et al., 2003) and Ca^{2+}/calmodulin-dependent protein kinase kinase 2 (CAMKK2) (Hawley et al., 2005; Hurley et al., 2005; Woods et al., 2005). LKB1 is mainly responsible for AMPK activation during energy stress as well as upon induction of mitochondrial damage (Shackelford & Shaw, 2009). In contrast, CAMKK2 stimulates AMPK activity in response to increased intracellular Ca^{2+} levels (Hawley et al., 2005; Hurley et al., 2005; Woods et al., 2005) (Fig. 2). This form of AMPK activation does not depend on LKB1 and nucleotide levels.

Once activated, AMPK's main function is to restore energy homeostasis in the cell by stimulating ATP-producing catabolic processes and inhibiting energy-consuming anabolic processes. AMPK is known to have more than 100 substrates that are phosphorylated by AMPK on at least 130 sites (Steinberg & Hardie, 2022). Since AMPK is the central regulator of energy sensing, it is not surprising that AMPK has been reported to be involved in various aspects of mitochondrial homeostasis such as mitochondrial morphology, transport, autophagy and mitophagy as well as mitochondrial biogenesis (Herzig & Shaw, 2018) (Fig. 2).

AMPK plays a critical role in the regulation of mitochondrial dynamics. It has been shown to phosphorylate MFF at S155 and S172 thereby promoting mitochondrial fission (Ducommun et al., 2015; Toyama et al., 2016). Mechanistically, MFF phosphorylation by AMPK increases mitochondrial localization of DRP1 (Toyama et al., 2016). Furthermore, the OMM localized mitochondrial fission regulator 1-like protein (MTFR1L) has recently been identified as a novel AMPK substrate (Tilokani et al., 2022). AMPK-mediated phosphorylation of MTFR1L at S103 and S238 negatively regulates mitochondrial fusion leading to a more fragmented mitochondrial network (Tilokani et al., 2022).

Mitochondrial transport has also been reported to be influenced by AMPK in neurons. During local energetic stress, retrograde transport of axonal mitochondria was repressed in an AMPK-dependent manner (Watters et al., 2020). In line with that, synaptic activity-induced energy deficits in the presynapse have been shown to activate the AMPK/p21-activated kinase pathway, which recruits and captures mitochondria via myosin VI and SNPH (Li et al., 2020). Together, these AMPK-dependent mechanisms increase mitochondrial number in axons to restore energy levels upon energetic stress caused by synaptic activity.

Additionally, both mitochondrial biogenesis (see chapter 1.4) and mitochondrial degradation via mitophagy as well as bulk autophagy (see chapter 1.5) are regulated by AMPK signaling. Thus, AMPK plays a critical role in regulating various aspects of mitochondrial homeostasis. However, it is very likely that the complex relationship between mitochondria and AMPK is still underestimated. Future studies might discover many more mitochondrial AMPK substrates.

_____
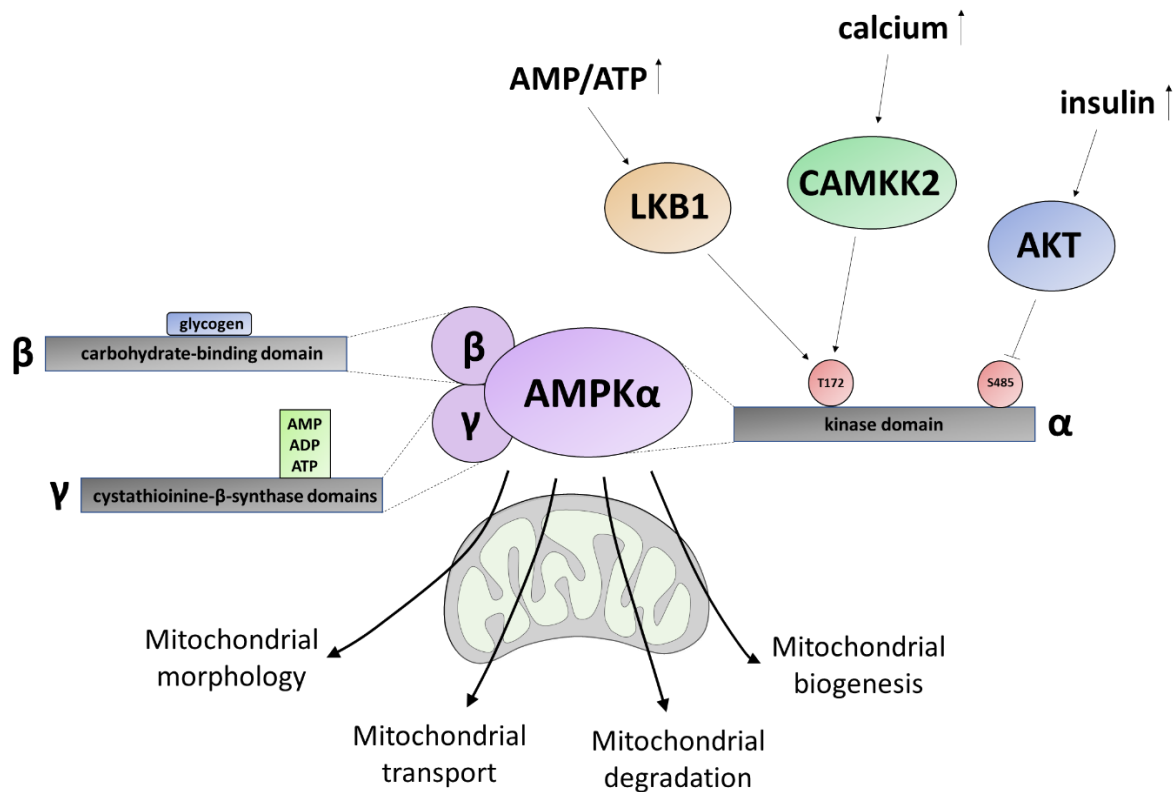
Figure 2: Structure and regulation of AMPK.
AMPK is a heterotrimeric complex composed of three subunits. The catalytic α-subunit contains the kinase domain including regulatory threonine 172 (T172) and serine 485 (S485) residues. Phosphorylation of T172 by LKB1 (upon energy stress) or CAMKK2 (upon calcium) results in activation of AMPK, while phosphorylation of S485 by AKT (upon insulin) leads to inhibition of AMPK. The β-subunit contains a conserved carbohydrate-binding domain, which allows AMPK to associate with glycogen. The γ-subunit comprises the adenine nucleotide binding region consisting of a tandem of four cystathionine-β-synthase (CBS) domains, which enables binding to AMP, ADP and ATP. AMPK signaling regulates several aspects of mitochondrial homeostasis including mitochondrial morphology, mitochondrial transport, mitochondrial degradation, and mitochondrial biogenesis.

1.3.2   Role of insulin in mitochondrial homeostasis

Historically, the polypeptide hormone insulin is best known for its action on peripheral glucose homeostasis, whereas the brain was considered an insulin-insensitive organ for the longest time. However, this view changed when high insulin levels as well as expression of the insulin receptor (IR) were found in brain tissues (Havrankova et al., 1978). The highest density of the IR has been detected in the olfactory bulb, hypothalamus, hippocampus, cerebellum, choroid plexus and cerebral cortex (Havrankova et al., 1981; Hill et al., 1986; Hopkins & Williams, 1997; Mielke & Wang, 2011; Schulingkamp et al., 2000). The presence of insulin in the brain raised the question about its origin, which is still controversially discussed. While some are convinced that insulin is of peripheral origin and enters the brain through the blood-brain barrier (BBB), others have reported that insulin is directly synthesized by neurons (Ghasemi et al., 2013). It is likely that the majority of the insulin found in the

brain comes from the periphery, whereas a small amount might be produced *de novo* in the brain (Agrawal et al., 2021).

Upon insulin binding, the IR triggers several downstream signaling cascades. Subsequently, the active insulin-IR complex is internalized by endocytosis. After reaching the early endosome, the majority is recycled back to the plasma membrane, whereas a small portion is sorted into late endosomes for degradation via lysosomes (Baldwin et al., 1980; Trischitta et al., 1989). This internalization pathway contributes to the intensity and duration of the insulin action (Iraburu et al., 2021). One of the best characterized signaling cascades induced by insulin is mediated via phosphatidylinositol 3-kinase (PI3K) and AKT (also known as protein kinase B). Insulin binding to the IR stimulates its kinase activity leading to autophosphorylation as well as phosphorylation of the insulin receptor substrates (IRS). Phosphorylated IRSs interact with and activate PI3K, which converts phosphatidylinositol-4,5-bisphosphate (PIP_2) to phosphatidylinositol-3,4,5-trisphosphate (PIP_3). The second messenger PIP_3 in turn stimulates activity of the serine/threonine protein kinase AKT (Taniguchi et al., 2006). A key downstream substrate of AKT is mammalian target of rapamycin complex 1 (mTORC1). mTORC1 is composed of the mTOR serine/threonine kinase, the scaffold protein regulatory-associated protein of mTOR (RAPTOR) as well as associated subunits (G. Y. Liu & Sabatini, 2020). The small GTPase Ras homolog enriched in brain (Rheb) is an essential activator of mTORC1 (Sancak et al., 2008; Saucedo et al., 2003), whereas the tuberous sclerosis protein complex (TSC) consisting of TSC1, TSC2 and TBC1 domain family member 7 (TBC1D7) (Dibble et al., 2012) inhibits mTORC1. TSC acts as a GTPase-activating protein (GAP) towards Rheb and thus inhibits Rheb-induced mTORC1 activation (Inoki, Li, et al., 2003; Tee et al., 2003; Yang et al., 2021). Insulin-induced activation of AKT phosphorylates TSC2, which leads to disinhibition of Rheb and thus activation of mTORC1 (Inoki et al., 2002; Manning et al., 2002). mTORC1 is known as the master regulator of protein synthesis as well as cell growth and activated when nutrients such as amino acids are sufficient, in contrast to AMPK. Both kinases are inversely regulated and have been shown to control one another. AMPK inhibits mTORC1 signaling via two signaling pathways. Firstly, AMPK directly phosphorylates and thereby activates TSC2 leading to inhibition of Rheb-mediated mTORC1 activity (Inoki, Zhu, et al., 2003). In the second pathway, AMPK directly phosphorylates the scaffold protein RAPTOR leading to its inhibition (Gwinn et al., 2008). mTORC1, on the other hand, can also downregulate AMPK signaling by direct phosphorylation (Ling et al., 2020). Interestingly, insulin has also been shown to inhibit AMPK activity via AKT-mediated phosphorylation at serine 485 in its catalytic α-subunit (Berggreen et al., 2009; Dagon et al., 2012; Horman et al., 2006; Kovacic et al., 2003; J. Ning et al., 2011; Soltys et al., 2006; Valentine et al., 2014) (Fig. 2). This pathway has mainly been described in non-neuronal cells. There are, however, a few studies confirming its relevance in neurons (Minokoshi et al., 2004; Zakharova et al., 2019).

Importantly, insulin signaling is tightly associated with neuronal mitochondrial function including ATP production, respiration, Ca^{2+} buffering as well as protein biogenesis and homeostasis (Schell et al., 2021). In cortical neurons, insulin has been shown to increase mitochondrial ATP production (Ruegsegger et al., 2019; N. Zhao et al., 2017). Additionally, insulin treatment enhances mitochondrial polarisation and reduces intracellular Ca^{2+} levels under resting conditions in sensory neurons (Huang et al., 2003). In Huntingtin striatal cells, insulin and insulin-like growth factor 1 (IGF-1) treatment decreases mitochondrial reactive oxygen species (ROS) production as well as mitochondrial fission thereby overall improving mitochondrial function in a PI3K/AKT-dependent manner (Ribeiro et al., 2014). Also in mice, intranasal insulin application has been observed to increase brain mitochondrial respiration (Ruegsegger et al., 2018). Insulin signaling elicits its effect on neuronal mitochondria at several levels, from transcriptional regulation to direct regulation of mitochondrial processes via AKT/mTORC1/AMPK signaling. The role of insulin in mitochondrial biogenesis is described in chapter 1.4. However, its role in neuronal mitostasis is less clear.

1.4 Mitochondrial biogenesis

Mitochondria cannot be made *de novo* but must derive from already existing organelles as mitochondrial biogenesis requires mtDNA replication. Furthermore, since the majority of mitochondrial proteins is encoded in the nucleus, mitochondrial import of over 1000 proteins is required for proper mitochondrial biogenesis. The co-transcriptional regulation factor PGC-1α (peroxisome-proliferator-activated γ co-activator-1α) is generally known as the master regulator of mitochondrial biogenesis. It regulates the activity of different transcription factors including the nuclear respiration factors 1 and 2 (NRF-1 and NRF-2). NRF-1 and NRF-2 in turn drive the expression of several nuclear-encoded mitochondrial genes such as the mitochondrial transcription factor A (TFAM), which promotes transcription and replication of mtDNA (Diaz & Moraes, 2008; Jornayvaz & Shulman, 2010). Several signaling pathways have been shown to regulate mitochondrial biogenesis via the PGC-1α-NRF-1/2-TFAM pathway including the AMP/ATP ratio (via AMPK), Ca^{2+} levels (via CAMK and p38 MAPK) and the NAD^+/NADH ratio (via SIRT1). All three pathways result in activation of PGC-1α by either phosphorylation via AMPK as well as CAMK-stimulated p38 MAPK or by deacetylation via SIRT1 (Cardanho-Ramos & Morais, 2021; Hees & Harbauer, 2022). The described signals are not only all part of mitochondrial feedback mechanisms within the cell but are also primarily involved in transcriptional upregulation of mitochondrial genes. In contrast, the hormone insulin plays a role in translational regulation of mitochondrial biogenesis. The insulin/PI3K/AKT-mediated activation of mTORC1 (as described in chapter 1.3.2) upregulates the translation of nuclear-encoded mitochondrial proteins via stimulation of the eukaryotic translation initiation factor 4E (eIF4E) (Morita et al., 2013). Insulin, however, also increases the activity of PGC-1α via AKT-induced inhibition of the transcription factor

_____

Forkhead Box Protein O1 (FOXO1) (Brunet et al., 1999; Cheng et al., 2009; Kops et al., 1999; Mootha et al., 2003; Nakae et al., 1999; Patti et al., 2003; Yan et al., 2020). Furthermore, insulin can inhibit AMPK activity via AKT-mediated phosphorylation (as described in chapter 1.3.2) (Berggreen et al., 2009; Dagon et al., 2012; Horman et al., 2006; Kovacic et al., 2003; J. Ning et al., 2011; Soltys et al., 2006; Valentine et al., 2014), thereby decreasing AMPK-mediated transcriptional upregulation of mitochondrial biogenesis via PGC-1α while at the same time promoting translation of mitochondrial proteins via mTORC1. This differential regulation of mitochondrial biogenesis at the transcriptional versus the translational level is supported by the reciprocal inhibition of AMPK and mTORC1 (as described in chapter 1.3.2). Consequently, inhibition of AMPK signaling by insulin and mTORC1 would increase mitochondrial protein biogenesis in spite of transcriptional downregulation and vice versa (Hees & Harbauer, 2022) (Fig. 3).
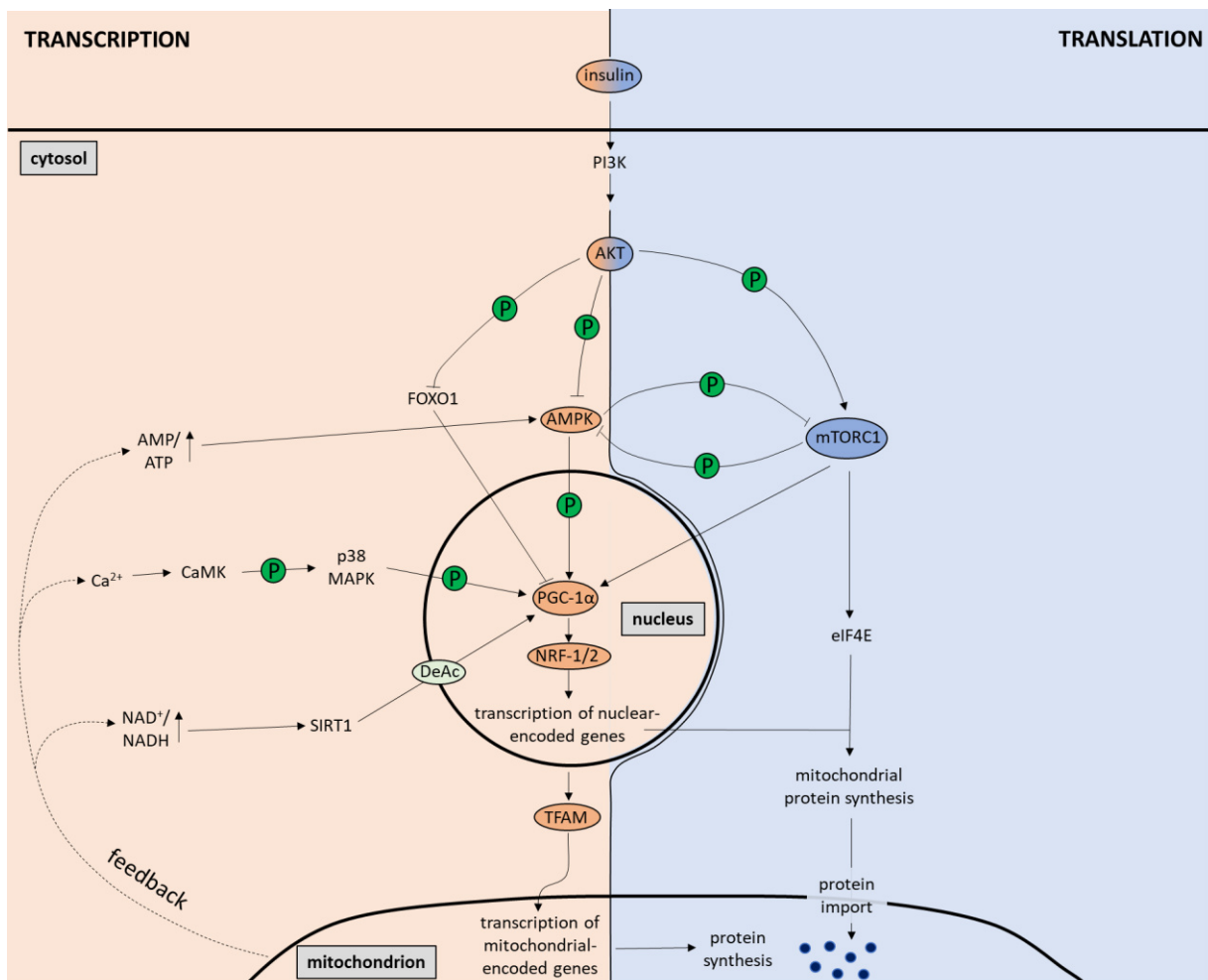
Figure 3: Regulation of mitochondrial biogenesis.
Transcriptionally, the PGC-1α-NRF-1/2-TFAM pathway serves as the master regulator of mitochondrial biogenesis. Cellular signals such as increased AMP/ATP ratio, NAD$^+$/NADH ratio, and Ca^{2+} levels activate AMPK, SIRT1, and CaMK, respectively, which results in PGC-1α stimulation. PGC-1α facilitates the transcription of nuclear-encoded mitochondrial genes through NRF-1/2 and the transcription of mitochondrial-encoded genes by promoting TFAM expression. Translationally, the insulin-induced PI3K/AKT/mTORC1 pathway significantly influences mitochondrial biogenesis. Through the activation of eIF4E, mTORC1 enhances the translation of

_____

nuclear-encoded mitochondrial proteins. AKT, in addition to its translational impact, also affects transcription by inhibiting FOXO1, thereby activating PGC-1α. Additionally, AKT phosphorylation inhibits AMPK. Notably, AMPK and mTORC1 can directly phosphorylate and inhibit each other, creating a regulatory interplay (adapted from Hees & Harbauer, 2022).

Very little is known about regulation of mitochondrial biogenesis in neurons, as the majority of the studies have been performed in non-neuronal cells. However, as in other cells, PGC-1α is critically involved in transcriptional control of mitochondrial biogenesis (Cardanho-Ramos & Morais, 2021). Furthermore, also insulin has been shown to play an important role in the regulation of mitochondrial protein synthesis in neurons (Ruegsegger et al., 2019). It is, however, very likely that neurons have developed their own mechanisms and signaling pathways to regulate mitochondrial biogenesis that specifically meet the needs of cells that are as complex as neurons. One potential mechanism is controlled localization and transport as well as local translation of mRNAs encoding mitochondrial proteins in different subcompartments of the neuron as described in chapter 1.6.

1.5 Mitophagy: a selective form of autophagy

Macroautophagy (hereafter autophagy; Greek: 'self-eating') is the biological process that involves bulk degradation and recycling of cytosolic components such as damaged or unwanted proteins or organelles including mitochondria through lysosomal delivery. Autophagy is highly conserved and serves both as quality control and recycling mechanism (Mizushima & Komatsu, 2011). It is generally induced by starvation to facilitate bulk recycling of cellular components and provide the cell with nutrients. Autophagy, however, can also be activated during stress to prevent accumulation or aggregation of harmful cellular constituents. The autophagic process is either a non-selective bulk removal of cytosolic components or a selective, targeted degradation of damaged or unwanted proteins and organelles.

Briefly, during autophagy an isolation membrane develops to encircle and sequester degradation cargo thereby forming the autophagosome. After maturation, the autophagosome fuses with a lysosome to generate an autolysosome, which eventually results in degradation of the engulfed cargo (Mizushima & Komatsu, 2011). Autophagy is a highly complex process and by now, many autophagy-related (ATG) proteins have been identified including the serine/threonine protein kinase Unc-51-like kinase 1 (ULK1) (K. H. Kim & Lee, 2014). As ULK1 has a critical role in the initiation of autophagy during formation of the autophagosome, its activity is tightly regulated. Under nutrient-rich conditions, mTORC1 inhibits autophagy initiation by phosphorylation of ULK1 at S637 and S757, which suppresses its catalytic activity (Ganley et al., 2009; J. Kim et al., 2011). In contrast, during starvation, AMPK directly

phosphorylates ULK1 on four residues: S467, S555, T574 and S637 (Egan et al., 2011; J. Kim et al., 2011). The AMPK-dependent phosphorylation of ULK1 is critically required for autophagy initiation.

Since damaged mitochondria produce an excess amount of ROS, which is harmful for the cell, they need to be rapidly degraded via mitophagy, a selective form of the autophagy pathway. In mammals, mitophagy is commonly regulated in a ubiquitin-dependent or a receptor-dependent manner. The receptor-dependent pathway is mediated by FUN14 domain containing protein 1 (FUNDC1) (M. Chen et al., 2016), BCL2/adenovirus E1B 19-kDa interacting protein 3-like (BNIP3L/NIX) (Y. Li et al., 2021; Sandoval et al., 2008), and BCL2-L-13 (Guan et al., 2018; Yamaguchi et al., 2016). The ubiquitin-dependent pathway, on the other hand, is the best characterized mitophagy pathway, which is mediated by two main players: the nuclear-encoded mitochondrial serine/threonine protein kinase PTEN-induced kinase 1 (PINK1) and the E3-ubiquitin ligase Parkin (N. Matsuda et al., 2010; Narendra et al., 2008, 2010; Vives-Bauza et al., 2010). Both proteins are commonly mutated in certain autosomal-recessive forms of Parkinson's disease (PD) (Kitada et al., 1998; Valente et al., 2004). PINK1 functions as a sensor for mitochondrial damage since it constantly surveys mitochondrial health making it a critical player in mitochondrial quality control. In healthy mitochondria, driven by the mitochondrial membrane potential, PINK1 is imported into mitochondria via the translocase of the outer and inner mitochondrial membrane (TOM and TIM, respectively). In the IMM, PINK1 is first processed by the matrix processing peptidase (MPP) leading to removal of the N-terminal mitochondrial targeting signal of PINK1 (Greene et al., 2012). Afterwards, PINK1 is cleaved by the rhomboid protease presenilin-associated rhomboid-like (PARL) between the amino acids A103 and F104 within its transmembrane domain (Deas et al., 2011; Jin et al., 2010; Meissner et al., 2011). After retrotranslocation back into the cytosol, cleaved PINK1 is rapidly degraded by the ubiquitin proteasome system via the N-end rule pathway (Yamano & Youle, 2013). The import and rapid degradation of PINK1 prevents the removal of functional mitochondria (Fig. 4a). In damaged mitochondria, on the other hand, mitochondrial PINK1 import is inhibited due to a loss of mitochondrial membrane potential or accumulation of misfolded proteins (Jin et al., 2010; Jin & Youle, 2013). As a result, PINK1 stabilizes on the OMM bound to the TOM complex (Maruszczak et al., 2022; Narendra et al., 2010). In this position, PINK1 is protected from PARL cleavage and proteasomal degradation. After undergoing autophosphorylation required for its full kinase activity (Okatsu et al., 2012), PINK1 phosphorylates several substrates on the mitochondrial surface including ubiquitin bound to mitochondrial surface proteins, which initiates the mitophagy pathway. Phosphorylated ubiquitin at S65 serves as receptor for the E3-ubiquitin ligase Parkin (Okatsu et al., 2015). Recruitment of Parkin to the mitochondria (Narendra et al., 2008) leads to its partial activation. Full activation is achieved after phosphorylation by PINK1 at S65. Parkin then conjugates ubiquitin onto proteins on the OMM, which can be further phosphorylated by PINK1. This in turn leads to additional rounds of Parkin

recruitment and activation resulting in a positive feedback mechanism. The coordinated action of PINK1 and Parkin leads to the decoration of damaged mitochondria with phosphorylated ubiquitin chains. Autophagy receptors are recruited due to binding to the ubiquitin chains, while at the same time bound to LC3-associated autophagosomal membranes (Stolz et al., 2014). The autophagy receptors involved in PINK1/Parkin-dependent mitophagy include Optineurin, nuclear dot protein 52 (NDP52), p62, neighbor of BRCA1 gene 1 (NBR1), and Tax1-binding protein 1 (TAX1BP1), with Optineurin and NDP52 being the most important ones (Heo et al., 2015; Lazarou et al., 2015; Sarraf et al., 2013; Wong & Holzbaur, 2014). After formation of an autophagosomal membrane around the damaged mitochondrion, the autophagosome fuses with a lysosome, eventually resulting in mitochondrial degradation (Lazarou et al., 2015) (Fig. 4b).
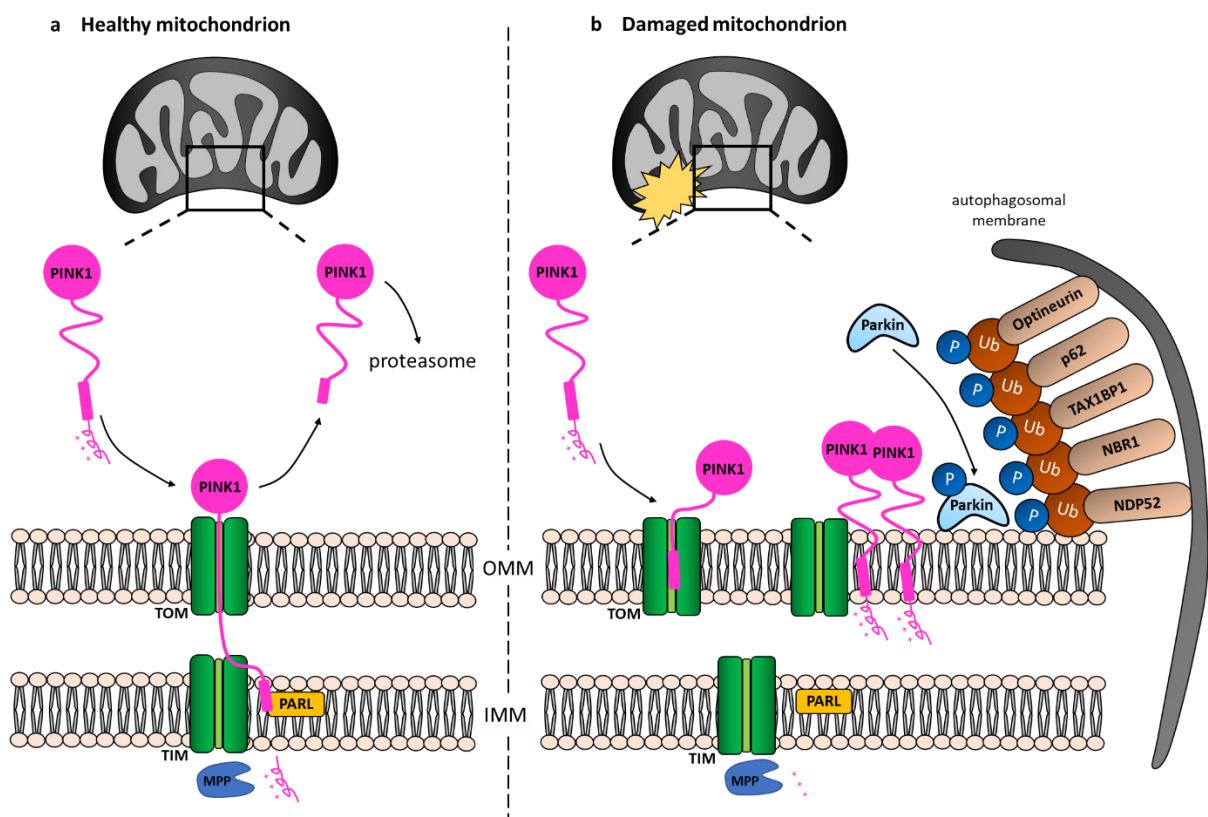
Figure 4: PINK1/Parkin-dependent mitophagy pathway.
(a) In healthy mitochondria, PINK1 is imported via TOM and TIM driven by the mitochondrial membrane potential. In the IMM, PINK1 is processed by MPP, which removes the N-terminal mitochondrial targeting signal, before being cleaved by PARL within its transmembrane domain. Following retrotranslocation back into the cytosol, cleaved PINK1 is degraded via the N-end rule pathway. **(b)** In damaged mitochondria, a loss of the mitochondrial membrane potential results in import inhibition of PINK1 and thus stabilization and activation of PINK1 on the outer mitochondrial membrane. PINK1 phosphorylates multiple substrates including ubiquitin attached to mitochondrial surface proteins. Phosphorylated ubiquitin acts as a receptor for Parkin. Mitochondrial recruitment of Parkin and PINK1-mediated phosphorylation result in full activation of Parkin. Once activated, Parkin conjugates ubiquitin molecules to proteins on the OMM, which are further phosphorylated by PINK1 leading to a positive feedback mechanism. The emerging phosphorylated ubiquitin chains recruit autophagy receptors such as Optineurin, NDP52, p62, NBR1 and TAX1BP1 resulting in formation of an autophagosomal membrane around the damaged mitochondrion, which is eventually degraded in lysosomes.

1.6 mRNA localization, transport and translation in neurons

The complex architecture of neurons combined with the short half-life of some mitochondrial proteins makes it very challenging for the neuron to maintain mitochondrial functionality within distal parts of the cell. Given that the majority of mitochondrial proteins is nuclear-encoded and components required for protein synthesis are mainly present in the cell body, it has long been assumed that mitochondrial biogenesis is restricted to the somato-dendritic region. However, as mentioned in chapter 1.2, short-lived mitochondrial proteins would not survive the transport required to reach distal parts of the axons. A possible solution for this problem is local translation of mitochondrial proteins in every part of the neurons. Fittingly, nuclear-encoded mitochondrial transcripts have not only been detected in axons (Aschrafi et al., 2016; Gumy et al., 2011; Shigeoka et al., 2016; Zivraj et al., 2010) but some of them are even enriched in axons compared to the somatodendritic compartment (Andreassi et al., 2010; Briese et al., 2016).

There are several ways of how transcripts can be transported within the cell. RNA-binding proteins (RBPs) play an important role as they can interact with cis-acting factors or 'zipcodes' within the mRNA. 'Zipcodes' are most frequently found in the 3´ untranslated region (UTR) of transcripts (Dalla Costa et al., 2021; Das et al., 2019; Gomes et al., 2014). Together, mRNAs and RBPs form so-called messenger ribonucleoprotein (mRNP) granules, which are important for stability of mRNAs as well as regulation of subcellular transport and localization. mRNPs can interact with cytoskeletal motor proteins or other adaptor proteins allowing for transport along the neuron (Kanai et al., 2004; McClintock et al., 2018; Tauber et al., 2020). An emerging concept is organellar tethering of mRNPs allowing for hitchhiking of mRNAs on different organelles including mitochondria, early and late endosomes as well as lysosomes (Cioni et al., 2019; Cohen et al., 2022; Harbauer et al., 2022; Liao et al., 2019; Schuhmacher et al., 2023).

1.6.1 mRNA hitchhiking on mitochondria and other organelles

Our lab has recently shown that the transcript encoding for the mitophagy protein PINK1 and potentially other nuclear-encoded mitochondrial mRNAs are associated with mitochondria allowing for long-distance transport into axons as well as on-demand local translation (Harbauer et al., 2022). As PINK1 has a very short half-life of about 30 minutes (W. Lin & Kang, 2008; Vincow et al., 2013) due to its function in the removal of damaged mitochondria (as described in chapter 1.5), a constant supply of fresh PINK1 protein is critical for mitochondrial health maintenance. By tethering the *Pink1* transcript to mitochondria, the organelle carries the mRNA required for its own maintenance and repair. Interestingly, sequences within the coding region rather than the 3´ UTR are required for association with mitochondria (Harbauer et al., 2022). The tethering complex is composed of the

_____

mitochondrial outer membrane protein Synaptojanin 2 binding protein (SYNJ2BP, also called OMP25) and the RNA-binding motif-containing (Hsu & Mao, 2015) phosphatidylinositol phosphatase Synaptojanin 2 (SYNJ2) (Harbauer et al., 2022) (Fig. 5a). SYNJ2BP is a ubiquitously expressed protein that localizes to the outer mitochondrial membrane due to its C-terminal transmembrane domain, while the N-terminal part faces towards the cytosol. SYNJ2a, a splice variant of SYNJ2 that is primarily expressed in neurons (Harbauer et al., 2022), is recruited to the mitochondria via the specific interaction between the so-called postsynaptic density protein-95/discs large/zonula occludens-1 (PDZ) motif at its C-terminus and the corresponding PDZ domain at the N-terminus of SYNJ2BP (Nemoto & De Camilli, 1999). Whereas SYNJ2a binds to the *Pink1* transcript, SYNJ2BP acts as mitochondrial anchor by tethering both SYNJ2a and *Pink1* mRNA to the mitochondria. Apart from a few interacting proteins including SYNJ2a as well as the ribosome-binding protein 1 (RRBP1) (V. Hung et al., 2017), very little is known about the function of SYNJ2BP. Recently, SYNJ2BP itself has been described as an RBP (Mullari et al., 2017; Qin et al., 2021). Most likely, this mechanism is not exclusive to *Pink1*, as multiple other transcripts were found to be associated with SYNJ2a (Harbauer et al., 2022). Another recent study has found the *cytochrome c oxidase subunit 7c* (*Cox7c*) transcript similarly associated with mitochondria (Cohen et al., 2022). *Cox7c* mRNA encodes for a subunit of complex IV of the electron transport chain (Fig. 5a). In both cases, the coding region rather than the 3´UTR contained the critical sequences necessary for mitochondrial localization and co-transport along axons. Furthermore, active translation was necessary to target the mRNAs to the organelle (Cohen et al., 2022; Harbauer et al., 2022).

Apart from mitochondria, several transcripts have recently been found to associate with early endosomes in a translation-dependent or -independent manner (Popovic et al., 2020) (Fig. 5b). One example is the mRNA of the early endosomal antigen 1 (EEA1), which encodes an endosomal tethering factor and fusogen. Again, the 3´ UTR is not required for endosomal association, whereas the coding region is sufficient (Popovic et al., 2020). Lastly, endolysosomal hitchhiking of mRNPs has also been shown. Rab7-positive endolysosomes associate with RNA granules that contain nuclear-encoded mitochondrial transcripts allowing for co-transport along axons (Cioni et al., 2019). Furthermore, RNA granules containing the RBP GTPase-activating protein SH3 domain-binding protein 1 (G3BP1) have been reported to hitchhike on moving lysosomal-associated membrane protein 1 (LAMP1)-positive endolysosomes in axons (Liao et al., 2019). Annexin A11 (ANXA11) was identified as the tether between lysosomes and RNA granules (Liao et al., 2019) (Fig. 5c). It remains to be elucidated what kind of transcripts are associated with G3BP1-containing RNA granules and specifically whether nuclear-encoded mitochondrial transcripts are part of them.

1.6.2   mRNA translation in neurons

Hitchhiking of transcripts on various organelles does not only represent an energy efficient way to transport mRNAs along the neuron but also allows for on-demand local translation. In this way, a constant supply of fresh proteins required for maintenance and repair of mitochondria and other organelles is ensured. The importance of this mechanism becomes particularly evident when looking at very short-lived proteins such as PINK1. Both prevention of *Pink1* mRNA transport by knock down of the tethering protein SYNJ2BP as well as inhibition of axonal protein translation abolishes PINK1/Parkin-dependent mitophagy in axons (Harbauer et al., 2022). Hence, local axonal translation of PINK1 is required for the degradation of damaged mitochondria via local mitophagy in axons (Ashrafi et al., 2014; Harbauer et al., 2022).

Apart from PINK1, translation of other nuclear-encoded (Cioni et al., 2019; Yoon et al., 2012) as well as mitochondrial-encoded (Yousefi et al., 2021) mitochondrial transcripts has been observed in axons. Both mitochondria (Spillane et al., 2013) as well as early endosomes (Schuhmacher et al., 2023) and endolysosomes (Cioni et al., 2019) have been shown to serve as mRNA translation platforms in axons.

However, the localization of ribosomes to those axonal translation hotspots as well as the general presence of ribosomes in axons is still controversial. Ribosomes contain two major components, the small (40S) and the large (60S) ribosomal subunit. Furthermore, ribosomes exist in two different forms: polysomes and monosomes (80S). A polysome is defined as a group of two or more ribosomes bound to a single mRNA molecule. A monosome, on the other hand, consists of a single ribosome bound to an mRNA molecule. Whereas polysomes are considered to be the translationally active ribosome population, monosomes are thought to be involved in initiation and termination but not in the active process of elongation (Warner et al., 1963; Warner & Knopf, 2002; Warner & Rich, 1964). Considering the diversity of nuclear-encoded transcripts present in axons, polysomes, usually easily recognized in electron microscopy, are surprisingly scarce in axons. Interestingly, a recent study has shown that 80S monosomes rather than polysomes contribute to local translation in axons thereby bridging the gap between scarce ribosomal distribution in axons and observed local protein synthesis (Biever et al., 2020).

Rab7-positive endolysosomes have been found to associate with ribosomes in axons. At these sites, transcripts encoding mitochondrial proteins are actively translated (Cioni et al., 2019). Furthermore, an early endosomal Rab5 effector complex called Five-subunit Endosomal Rab5 and RNA/ribosome intermediary (FERRY) has recently been identified (Schuhmacher et al., 2023). This complex interacts both with the translation machinery and transcripts enriched for mRNAs encoding for mitochondrial proteins (Schuhmacher et al., 2023) (Fig. 5b). Therefore, this suggests that both moving early

endosomes as well as endolysosomes transport ribosomes that actively translate nuclear-encoded mitochondrial transcripts thereby contributing to local mitochondrial biogenesis.
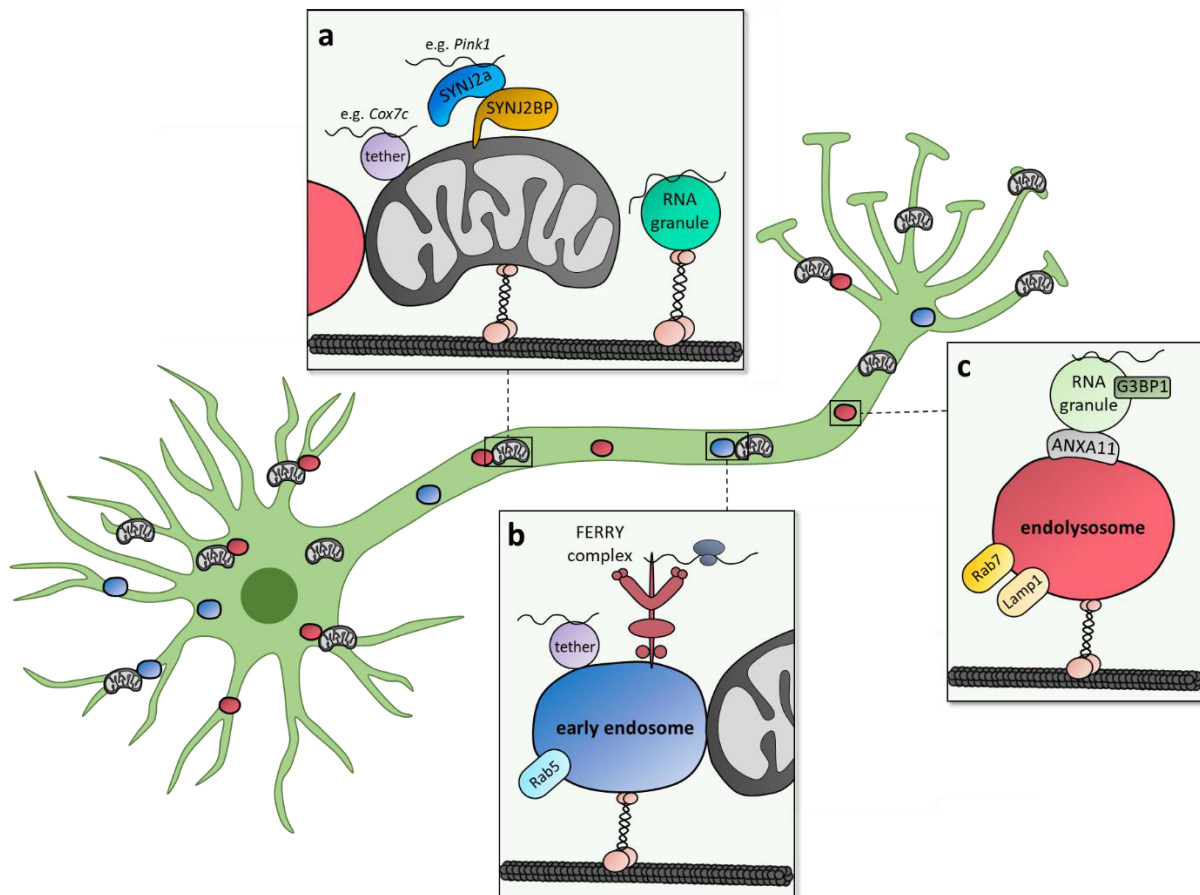
Figure 5: Transport of nuclear-encoded mitochondrial mRNAs in neurons.
RNA granules as well as mitochondria, Rab5-positive early endosomes and Rab7- and Lamp1-positive endolysosomes are actively transported along axons. Hitchhiking nuclear-encoded mitochondrial transcripts, whether they are part of RNA granules or attached to organelles, can reach distal regions of the neurons allowing for on-demand local translation. **(a)** *Cox7c* and *Pink1* mRNA are associated with mitochondria. While the tether for the *Cox7c* transcript is not known, *Pink1* mRNA is tethered via SYNJ2BP and SYNJ2a. **(b)** The early-endosomal localized FERRY complex interacts with the translation machinery and many transcripts that are enriched for nuclear-encoded mitochondrial genes. **(c)** Endolysosomes carry G3BP1-positive RNA granules that are tethered via ANXA11 (adapted from Hees & Harbauer, 2022).

1.7 Lysosomes: a signaling hub for protein translation

Lysosomes are classically associated with the process of degradation and recycling and play an important role in autophagy as described in chapter 1.5. The lysosomal membrane consists of more than 100 proteins including the vacuolar H^+-ATPase (v-ATPase), which is a proton pump that is required to pump H^+ ions from the cytosol into the lysosomal lumen to maintain the acidic environment (Forgac, 2007; Mindell, 2012). The low pH provides an optimal environment for the lysosomal hydrolases

required for the degradation of macromolecules and organelles. Following degradation, amino acids and other building blocks are transported back into the cytosol to be recycled in anabolic processes.

It has become more and more clear that the lysosome does not exclusively function as a degradation and recycling hotspot but that it is also an important hub for metabolic signaling (Lamming & Bar-Peled, 2019). These two functions are not in conflict but rather act in concert thereby providing an ideal environment for protein translation.

Interestingly, lysosomes are a crucial hub for the signaling of the two inversely regulated kinases: AMPK and mTORC1 (Carroll & Dunlop, 2017). It has been found that localization of mTORC1 to Rab7-positive vesicles is needed for its activation (Sancak et al., 2008). Due to the lack of specific markers for late endosomes and lysosomes, the distinction between those two organelles and their importance as signaling hubs is currently not clear. For simplicity, they will be referred to as endolysosomes. Endolysosomal recruitment of mTORC1 requires the so-called Rag GTPases and a pentameric complex called Ragulator, which consists of the late endosomal/lysosomal adaptor, MAPK and mTOR activator (LAMTOR) 1-5 (E. Kim et al., 2008; Sancak et al., 2008, 2010). The Rag GTPases are tethered to the endolysosomal membrane via Ragulator, which also functions as guanine nucleotide exchange factor (GEF) for the Rag GTPases (Bar-Peled et al., 2012; Sancak et al., 2010). The v-ATPase senses high nutrient levels, which results in stimulation of Ragulator's GEF activity (Bar-Peled et al., 2012; Efeyan et al., 2013; Zoncu et al., 2011). Upon activation, Rag GTPases bind RAPTOR thereby recruiting mTORC1 to the endolysosomal surface (E. Kim et al., 2008; Sancak et al., 2008, 2010), where it can interact with its activator protein Rheb1 (Bai et al., 2007) (Fig. 6a). Rag GTPase activation and endolysosomal mTORC1 recruitment is primarily controlled by amino acid (E. Kim et al., 2008; Sancak et al., 2008) and glucose availability (Efeyan et al., 2013). GAP activity towards the Rags (GATOR) 1 complex acts as the GAP of the Rag GTPases and thus terminates mTORC1 signaling (Bar-Peled et al., 2013; Panchaud et al., 2013).

Intriguingly, the v-ATPase-Ragulator complex is not only required for mTORC1 activation but also for activation of AMPK signaling. The scaffold protein AXIN, which mediates AMP-induced AMPK activation by LKB1 (Y.-L. Zhang et al., 2013), has been identified as an interaction partner of LAMTOR1 (C.-S. Zhang et al., 2014). Furthermore, starvation increases the interaction between LKB1-AMPK/AXIN and LAMTOR1 as well as the other Ragulator members (C.-S. Zhang et al., 2014). In this way, AMPK is actively recruited to the endolysosomes and activated by phosphorylation via LKB1. Interestingly, AXIN has been shown to be the key component in regulating endolysosomal recruitment of AMPK and mTORC1. While AXIN translocates to the endolysosome to activate AMPK, it at the same time mediates inhibition and endolysosomal dissociation of mTORC1 by impairing the GEF activity of Ragulator (C.-S. Zhang et al., 2014) (Fig. 6b).
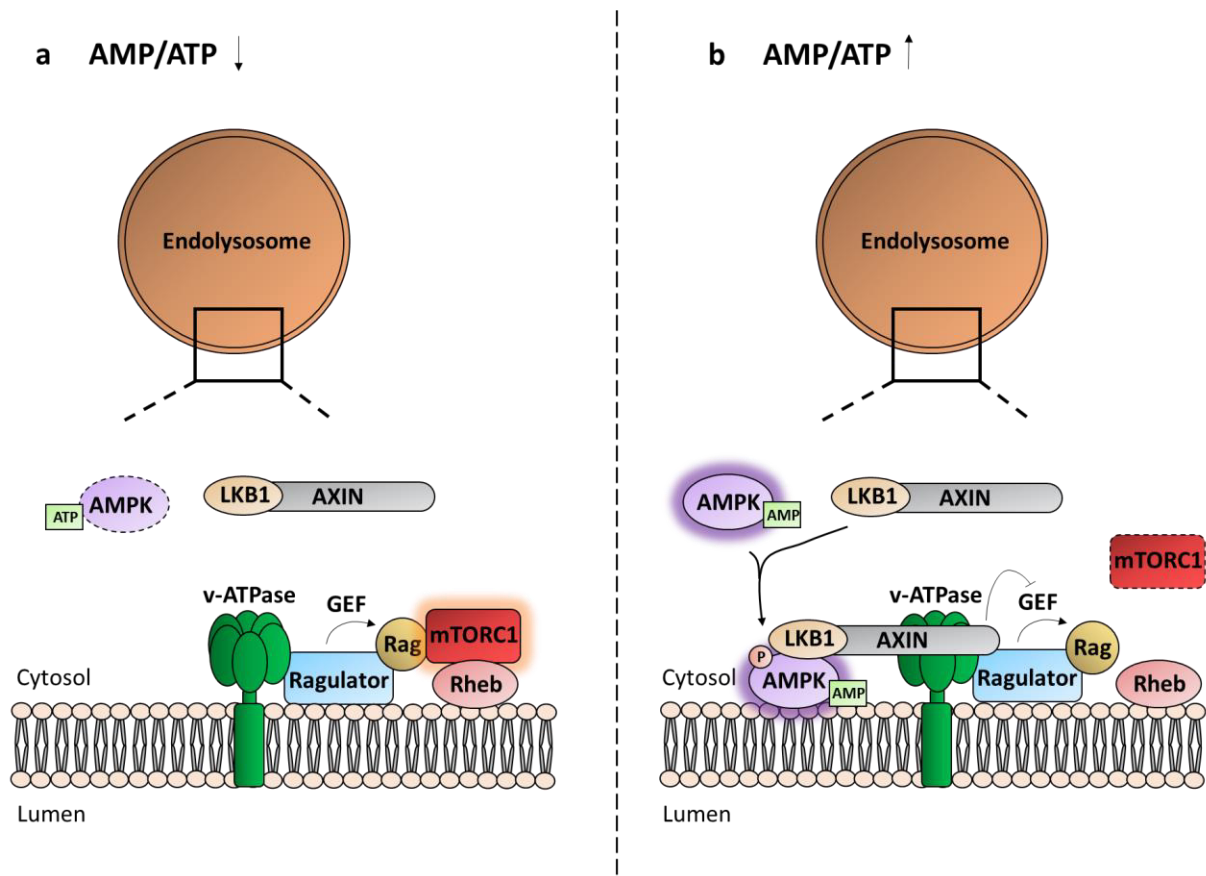
Figure 6: AMPK and mTORC1 activation at endolysosomes.
(a) Under conditions of sufficient energy and nutrient availability, the v-ATPase stimulates the GEF activity of the endolysosomal-localized Ragulator complex, which leads to activation of the Rag GTPases and recruitment of mTORC1. At the endolysosomal membrane, mTORC1 gets stimulated by interacting with its activator protein Rheb1. **(b)** Under conditions of limited energy and nutrient availability, the scaffold protein AXIN mediates AMPK activation by LKB1 phosphorylation in response to increased AMP levels. AXIN interacts with the Ragulator complex thereby recruiting AMPK to the endolysosomal membrane. Furthermore, AXIN suppresses the GEF activity of Ragulator, which results in inhibition and endolysosomal dissociation of mTORC1.

1.8 The importance of membrane contact sites between different organelles in neurons

Membrane contact sites (MCSs) between different organelles including mitochondria, endoplasmic reticulum (ER) and endolysosomes play very distinct roles in maintaining cellular functions (Elbaz & Schuldiner, 2011; Murley & Nunnari, 2016; Phillips & Voeltz, 2016; H. Wu et al., 2018). MCSs are defined as regions where the membranes of two organelles are brought in close proximity (10-30 nm) via a protein tether (Eisenberg-Bord et al., 2016).

Mitochondria-ER contact sites are to date one of the most well-studied membrane contact sites and are present in all neuronal compartments. They fulfil many important functions including lipid transfer, Ca^{2+} homeostasis, mitochondrial dynamics, and autophagy (Markovinovic et al., 2022). To date, several

mitochondria-ER tethers have been identified that physically connect the two organelles (Wilson & Metzakopian, 2021).

Mitochondria-endolysosome MCSs have also recently been shown to play a critical role in maintaining neuronal homeostasis (Cisneros et al., 2022). They are not only involved in regulating both mitochondrial and endolysosomal dynamics (Cisneros et al., 2022), but they also serve as translation platforms for mitochondrial proteins in neurons. As described in chapter 1.6, Rab7-positive endolysosomes transport nuclear-encoded mitochondrial transcripts along axons (Cioni et al., 2019). These mRNA-carrying endolysosomes have been shown to often pause at axonal mitochondria thereby forming mitochondria-endolysosome MCSs, which remain for prolonged periods (Cioni et al., 2019). In line with this, hotspots of Rab5-positive early endosome-associated translation are also observed in close proximity to mitochondria in neurons (Schuhmacher et al., 2023). This suggests an important role for contact sites between mitochondria and the endolysosomal compartment in local translation of nuclear-encoded mitochondrial proteins.

Interestingly, the ER has also been associated with translation of nuclear-encoded mitochondrial proteins by targeting them to the mitochondrial surface after their translation in the cytosol. In a recent study, a mechanism called ER-SURF has been identified in yeast (Hansen et al., 2018). ER-associated chaperones such as DnaJ-like protein 1 (Djp1) can bind to certain mitochondrial membrane protein precursors and facilitate their transfer to the mitochondria (Hansen et al., 2018). Although there are indications that the ER-SURF pathway is also present in mammalian cells (Lalier et al., 2021), its relevance as well as the involved proteins need to be elucidated.

So far, only one contact site involving all three organelles (mitochondria, ER and endolysosomes) has been characterized in mammalian cells. Relevant tethering proteins for this contact site are the ER transmembrane proteins PDZ domain-containing protein 8 (PDZD8) and Protrudin as well as the late endosomal protein Rab7 (Elbaz-Alon et al., 2020). PDZD8 contains a Synaptotagmin-like Mitochondrial lipid-binding Proteins (SMP) domain and has also been shown to be part of an ER-mitochondria MCS (Hirabayashi et al., 2017). In line with that, PDZD8 can recruit mitochondria to the ER-endolysosome MCS thereby forming a three-way contact (Elbaz-Alon et al., 2020). The function of this three-way MCS as well as its presence in neurons remains to be determined.

Taken together, this suggests that the tight interplay of mitochondria, ER and endolysosomes forming various MCSs is required for proper cellular homeostasis and function. Dysregulation of inter-organellar communication through MCSs has been observed in several neurodegenerative diseases including PD and Alzheimer's disease (AD) (Vrijsen et al., 2022).

1.9 Alzheimer's disease, insulin resistance and Apolipoprotein E4

AD is a devastating neurodegenerative disease and the most common form of dementia (Thies, W. & Bleiler, L., 2011). Typically, AD predominantly affects individuals over the age of 65, known as late-onset AD. However, when it manifests in individuals younger than 65, it is termed early-onset AD. Memory loss and cognitive decline are common features of AD. The two main neuropathological hallmarks include the presence of amyloid plaques consisting of amyloid beta (Aβ) protein and neurofibrillary tangles (NFTs) containing hyperphosphorylated tau protein.

Interestingly, it has been shown that brain insulin resistance, which is defined as the failure of neurons to respond to insulin, as well as insulin deficiency are pathological hallmarks of both metabolic and cognitive dysfunctions including type 2 diabetes and AD (Kullmann et al., 2016; Laws et al., 2017; Talbot et al., 2012). Mechanistically, compromised insulin signaling in the brain results in increased accumulation of Aβ (Chua et al., 2012) as well as hyperphosphorylated tau protein (Schubert et al., 2004). In line with that, type 2 diabetes represents a risk factor for AD and general cognitive impairment (Chatterjee & Mudher, 2018; Han & Li, 2010). As the connection between AD and type 2 diabetes is so evident, AD is sometimes considered as 'diabetes of the brain' or 'type 3 diabetes' (de la Monte & Wands, 2008; Nguyen et al., 2020).

Apart from type 2 diabetes, there are several genetic and environmental risk factors for AD (Armstrong, 2019). A major genetic risk factor for developing late onset AD is a polymorphism in the apolipoprotein E (APOE) gene (Belloy et al., 2020; Corder et al., 1993; Serrano-Pozo et al., 2021; Strittmatter, Saunders, et al., 1993; Strittmatter, Weisgraber, et al., 1993). Functionally, ApoE is involved in regulating lipid homeostasis by facilitating the transport of lipids such as cholesterol and phospholipids between cells. Due to their water insolubility, lipids have to be transported by so-called lipoproteins, which are hydrophile-lipophile particles. In the brain, lipoproteins are referred to as high-density lipoproteins (HDL)-like as they are similar to plasma HDL in size and density (Koch et al., 2001; Vitali et al., 2014). ApoE is their major apolipoprotein component, which is primarily produced by astrocytes and to a lesser extent by microglia in the brain (Vance & Hayashi, 2010). Furthermore, neurons have been shown to express ApoE upon excitotoxic injury (Boschert et al., 1999; Xu et al., 2006). In humans, ApoE is expressed in three isoforms (ApoE2, ApoE3 and ApoE4), which differ only in one or two residues. While ApoE3 has a cysteine at position 112 and an arginine at position 158, ApoE2 and ApoE4 contain cysteines and arginines, respectively, at both positions. Despite only minor amino acid changes the structure and function of ApoE is dramatically affected. The differences at position 112 affects lipid binding properties, while position 158 has an effect on the receptor-binding affinity to ApoE receptors (Weisgraber, 1990). The differences in the structure also affect their ability to bind and clear Aβ (Strittmatter, Weisgraber, et al., 1993). The most common allele is ε3, which is considered to be risk-

_____

neutral regarding AD, while ε2 is neuroprotective. The presence of the ε4 allele, on the other hand, is the strongest risk factor for late-onset AD (Bu, 2009; C.-C. Liu et al., 2013). Interestingly, a recent study found a link between ApoE4 and insulin resistance. ApoE4 has been shown to interact with the IR leading to compromised trafficking and signaling by trapping the receptor in early endosomes (N. Zhao et al., 2017). As described in chapter 1.3.2 the insulin-IR complex is internalized by endocytosis as part of the normal action of insulin. Following internalization, the majority of the IR is recycled and translocated back to the plasma membrane where insulin can trigger another round of signalling (Baldwin et al., 1980; Trischitta et al., 1989). Hence, ApoE4-mediated endosomal trapping of the IR impairs neuronal insulin signaling and causes insulin resistance (N. Zhao et al., 2017).

Given the growing evidence that central insulin resistance is a primary feature of AD pathology, intranasal administration of insulin has been used to increase brain insulin levels. This leads to improved cognitive performance in healthy humans as well as in patients with type 2 diabetes and AD (Benedict et al., 2007; Brünner et al., 2015; Claxton et al., 2015; Craft, 2012; Novak et al., 2014; Reger et al., 2008; H. Zhang et al., 2015). Apart from improving cognitive performance, intranasal insulin has also been shown to improve mitochondrial function (Galizzi & Di Carlo, 2022). Mitochondrial dysfunction is also a common characteristic of AD (Perez Ortiz & Swerdlow, 2019). However, to date, the contribution of both insulin resistance and mitochondrial dysfunction to the pathogenesis of the disease as well as the interplay between each other is not clear (Fig. 7).
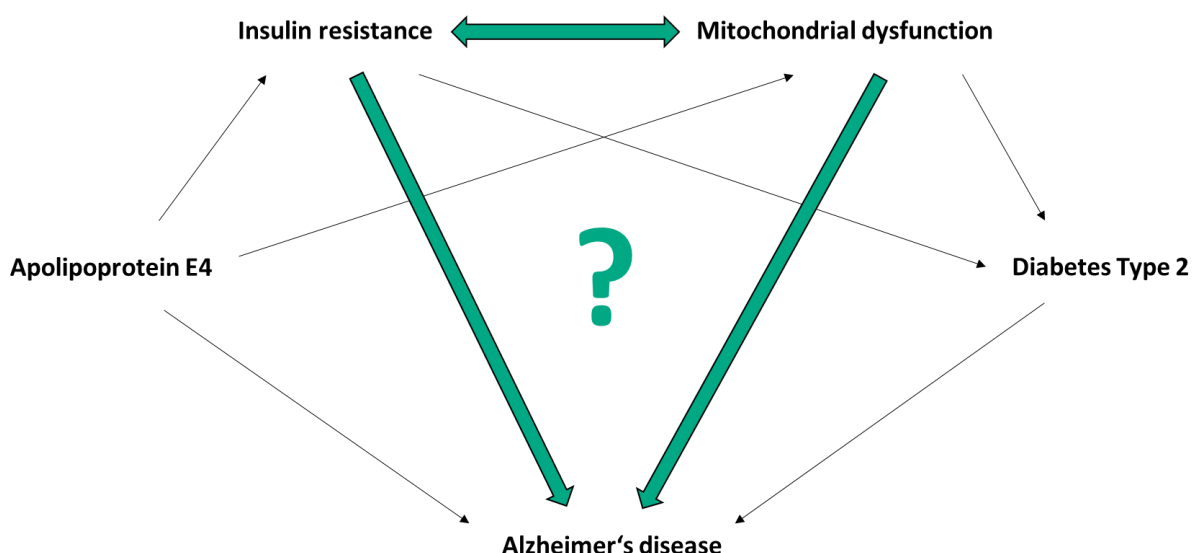
Figure 7: Link between insulin resistance, mitochondrial dysfunction and Alzheimer's disease.
Insulin resistance and mitochondrial dysfunction are common characteristics of both type 2 diabetes and Alzheimer's disease (AD). Furthermore, type 2 diabetes is considered a risk factor for AD and apolipoprotein E4, another key genetic risk factor for AD, causes insulin resistance *in vitro*. Despite the intricate interconnection among these factors, the precise contribution of insulin resistance and mitochondrial dysfunction to the pathogenesis of AD as well as the complex interplay between them remain incompletely understood.

1.10 Aims and objectives

The protein PINK1 is critical for mitochondrial health maintenance as it plays an important role in mitochondrial quality control via the PINK1/Parkin-dependent mitophagy pathway (N. Matsuda et al., 2010; Narendra et al., 2008, 2010; Vives-Bauza et al., 2010). Due to its short lifetime PINK1 needs to be synthesized locally in order to ensure a constant supply of fresh protein in every part of the neuron. To achieve this, *Pink1* mRNA is co-transported with mitochondria in neurons, which allows for on-demand local translation also in distal parts of the cell. *Pink1* mRNA is tethered to mitochondria via the RNA-binding protein SYNJ2a and its OMM binding partner SYNJ2BP (Harbauer et al., 2022). However, it is still unknown what signaling pathways regulate *Pink1* mRNA transport as well as translation and function of PINK1 in neurons. AMPK is known as the master regulator of energy metabolism and therefore tightly associated with mitochondrial homeostasis (Herzig & Shaw, 2018) making it a potential candidate for regulating the biology of *Pink1* mRNA and PINK1 protein in neurons. In the context of my thesis, I aimed at elucidating the mechanisms governing the regulation of *Pink1* mRNA and PINK1 protein in neurons, with a specific focus on AMPK signaling. More specifically, I aimed to address the following questions:

1. Does AMPK signaling regulate mitochondrial *Pink1* mRNA localization in neurons?

2. How does this regulation occur at the molecular level?

3. What is the effect on PINK1 translation?

4. What is the effect on PINK1 function in mitochondrial quality control via mitophagy?

5. Are the identified pathway and mechanism relevant in the context of neurodegenerative diseases?

2 MATERIALS AND METHODS

2.1 Mice

All mouse procedures were approved by the Government of Upper Bavaria and performed in accordance with the relevant regulations and guidelines. C57BL/6 WT as well as B6N.129-Rpl22$^{tm1.1Psam}$/J (Rpl22-HA) mice (Sanz et al., 2009, JAX stock #011029) were housed in the animal facility of the Max Planck Institute for Biological Intelligence, Martinsried, Germany under a controlled environment with *ad libitum* access to food and water. Animals of either sex were used for the experiments.

2.2 Cell culture

2.2.1 Primary hippocampal and cortical mouse neurons

Primary mouse neurons were obtained from E16.5 embryos of timed-pregnant mice as described previously (Harbauer et al., 2022; Hees & Harbauer, 2023). The pregnant mouse was euthanized with CO_2 and the embryos were rapidly extracted from the abdomen and put into ice-cold dissociation medium (Ca^{2+}-free Hank's Balanced Salt Solution with 10 mM kynurenic acid, 100 mM $MgCl_2$, and 100 mM HEPES). The embryos were removed from the amniotic sac and immediately decapitated with forceps. Under a dissecting microscope, the brains were taken out of the skull and the cerebellum, the midbrain as well as the meninges were removed leaving the two cortices. The hippocampus was carefully dissected from each hemisphere and hippocampi and cortices were collected in two separate tubes containing ice-cold dissociation medium. The tissue was enzymatically dissociated using papain/L-cysteine (Sigma-Aldrich) for 5 min at 37 °C, which was stopped by addition of trypsin inhibitor (Abnova). Afterwards, the tissue was washed three times with Neurobasal medium supplemented with B27 (Thermo Fisher Scientific), L-glutamine, and penicillin/streptomycin (NB+B27+PSG) and finally dissociated into single cells by trituration (10-15 times) using a p1000 pipette. Hippocampal and cortical neurons were plated in 3.5 µg/ml laminin (Thermo Fisher Scientific) and 20 µg/ml poly-L-lysine (PLL; Sigma-Aldrich) coated glass bottom 24 well plates (CellVis), 6 well plates (Greiner) or on acid-washed glass coverslips (1.5 mm, Marienfeld) in NB+B27+PSG. Primary neurons were kept in a humidified incubator at 37 °C with 5 % CO_2. Every 5 days, 50 % of the medium was replaced with fresh NB+B27+PSG.

2.2.2 Human induced pluripotent stem cell (iPSC)-derived cortical neurons

Human iPSCs (cell line: HPSI0314-hoik_1) were purchased from the Wellcome Trust Sanger Institute HipSci Repository and maintained in StemFlex medium (Thermo Fisher Scientific) on Matrigel

(Corning)-coated 10 cm dishes (Falcon). The medium was exchanged every day with fresh StemFlex and iPSCs were passaged at 80 % confluency using ReLeSR (Stem Cell Technologies) enzyme free passaging reagent.

The differentiation of iPSCs into cortical neurons was achieved by overexpression of the transcription factor neurogenin-2 (NGN-2) as described previously (Hees & Harbauer, 2023; Y. Zhang et al., 2013). On day -2, iPSCs were dissociated into single cells using Accutase (Thermo Fisher Scientific) and plated in Matrigel-coated 10 cm dishes ($2.5*10^6$ per dish) in StemFlex supplemented with 10 µM Y-27632 (Tocris). After 24 h, on day -1, cells were lentivirally transduced with pLV-TetO-hNGN2-eGFP-puro and FudeltaGW-rtTA in StemFlex medium required for differentiation into cortical neurons. After 5 h, the medium was replaced with fresh StemFlex containing 2 µg/ml doxycycline (Takara) to induce TetO gene expression. On day 0, N2/DMEM/F12/NEAA (N2 medium; Thermo Fisher Scientific) containing 2 µg/ml doxycycline, 0.2 µg/ml laminin (Thermo Fisher Scientific), 10 ng/ml NT-3 (PeproTech) and 10 ng/ml BDNF (PeproTech) was added to the cells. On day 1, a 24 h puromycin selection period was started by adding fresh N2 medium supplemented with 1 µg/ml puromycin (Enzo Life Sciences), 2 µg/ml doxycycline, 10 ng/ml NT-3, 10 ng/ml BDNF and 0.2 µg/ml laminin to the cells. On day 2, the N2 medium was replaced by B27/Neurobasal-A/Glutamax (B27 medium; Thermo Fisher Scientific) supplemented with 2 µg/ml doxycycline, 0.2 µg/ml laminin, 10 ng/ml NT-3, 10 ng/ml BDNF, and 2 µM Ara-C (Sigma-Aldrich). From day 3 to 6, medium was exchanged every other day (day 3 and 5) with fresh B27 medium supplemented with 2 µg/ml doxycycline, 0.2 µg/ml laminin, 10 ng/ml NT-3, 10 ng/ml BDNF, and 2 µM Ara-C. On day 7, medium was changed to conditioned Südhof neuronal growth medium (NGN2 glial conditioned medium/B27/Neurobasal-A/ $NaHCO_3$/Glucose/ Transferrin/ L-Glutamine) containing 0.2 µg/ml laminin, 10 ng/ml NT-3, and 10 ng/ml BDNF. Furthermore, the medium was supplemented with 10 µM Y-27632 to prepare the cells for re-plating. The iPSC-derived cortical neurons were re-plated on day 8. To this end, cells were dissociated using TrypLE Express (Thermo Fisher Scientific) at 37 °C for 5 min. After inactivation of the enzyme using fetal bovine serum (FBS), centrifugation at 1000 rpm for 5 min, resuspension in fresh conditioned Südhof neuronal growth medium containing 0.2 µg/ml laminin, 10 ng/ml NT-3 and 10 ng/ml BDNF and filtering through a 70 µm cell strainer, cells were seeded in laminin- and PLL-coated 6 well plates (Greiner) ($2*10^6$ cells per well). Human iPSC-derived neurons were kept in a humidified incubator at 37 °C with 5 % CO_2. Every other day, 50 % of the medium was replaced with fresh conditioned Südhof neuronal growth medium supplemented with 0.2 µg/ml laminin, 10 ng/ml NT-3 and 10 ng/ml BDNF.

2.2.3 Human embryonic kidney (HEK) 293T cells

HEK293T cells were acquired from ATCC®. They were maintained in Dulbecco's modified Eagle medium (DMEM; Thermo Fisher Scientific) supplemented with 10 % FBS and 1 % penicillin/streptomycin (P/S)

in T75 flasks (Falcon). HEK293T cells were kept in a humidified incubator at 37 °C with 5 % CO_2. The cells were passaged twice a week at approximately 80 % confluency using Trypsin (Thermo Fisher Scientific). After 15 passages, a new vial of HEK293T cells was thawed.

2.2.4 HeLa cells

HeLa cells were a kind gift from Danny Nedialkova, Max Planck Institute of Biochemistry, Martinsried, Germany. They were maintained in DMEM (Thermo Fisher Scientific) supplemented with 10 % FBS and 1% P/S in T75 flasks (Falcon). HeLa cells were kept in a humidified incubator at 37 °C with 5 % CO_2. The cells were passaged twice a week at approximately 80 % confluency using Trypsin (Thermo Fisher Scientific). After 15 passages, a new vial of HeLa cells was thawed.

2.3 DNA constructs

Mito-mRaspberry-7, mito-meGFP, mito-BFP, EBFP2-C1 (cell fill), YFP-Parkin, pPBbsr2-4031NES (AMPK FRET biosensor), Mito-ABKAR, Cyto-ABKAR, LAMP1-ABKAR, mCherry-Rab7A, TMEM192-mRFP-3xHA, pLAMP1-mCherry, Snap-Omp25, pLV-EGFP-Cre, pLJM1-EGFP and scFv-GCN4-sfGFP were purchased from Addgene (55931, 172481, 49151, 54665, 23955, 105241, 61509, 61510, 65068, 61804, 134641, 45147, 69599, 86805, 19319 and 60907, respectively). Plasmids encoding shRNA targeting AMPKα1, AMPKα2 and SYNJ2BP (TRCN0000024000, TRCN0000024046 and TRCN0000139049, respectively) along with a non-targeting control shRNA plasmid (TR30021) in a pLKO vector backbone were acquired from Sigma-Aldrich. Pink1-kinase dead-MS2-PP7, Cox4i-MS2-PP7, Atp5f1β-MS2-PP7, split-Venus, SYNJ2mito WT and VQL/AAA as well as shRNA-resistant myc-tagged SYNJ2BP WT plasmids have previously been described (Harbauer et al., 2022). The phospho-ablative (S21A) and phospho-mimetic (S21E) mutations of SYNJ2BP were generated by site-directed mutagenesis (Hees & Harbauer, 2023). For SYNJ2BP purification from *E. Coli*, the amino acids 1-110 of rat SYNJ2BP WT (cytosolic domain) were C-terminally tagged with 6xHis-tag and cloned into the bacterial expression vector pET19b vector. The phospho-ablative (S21A) mutation of SYNJ2BP was generated by site-directed mutagenesis (Hees & Harbauer, 2023). The Pink1-kinase dead-10xGCN4-12xMS2-PP7 and PINK1-GFP plasmids were a kind gift from Inmaculada Segura and Angelika Harbauer, Max Planck Institute for Biological Intelligence, Martinsried, Germany, respectively. The lentiviral packaging plasmids used for virus production pMD2.G, pRSV-Rev and pMDLg/pRRE as well as the plasmids used for iPSC differentiation into cortical neurons pLV-TetO-hNGN2-eGFP-puro and FudeltaGW-rtTA were obtained from Addgene (12259, 12253, 12251, 79823 and 19780, respectively).

2.4 Protein purification of recombinant SYNJ2BP

The purification of SYNJ2BP WT and SYNJ2BP S21A was performed in collaboration with Leopold Urich and Sabine Suppmann from the Max Planck Institute of Biochemistry, Martinsried, Germany as described previously (Hees & Harbauer, 2023). The plasmids pET19b-SYNJ2BP-6xHis WT and S21A, respectively, were transformed into Rosetta *E. coli* bacteria. The bacteria were initially cultured in 15 ml of ZY auto-induction medium overnight followed by fermenter inoculation when the optical density reached 0.04. After a 24 h growth period, the bacteria were collected by centrifugation at 8000 rpm for 10 min at 4 °C, resulting in a pellet weighing 50 g. 50 % of the pellet was then reconstituted in 100 ml of lysis buffer, which consisted of HisBinding Buffer (50 mM Na_3PO_4/Na_2HPO_4 pH 8, 500 mM NaCl, 10 mM imidazole, and 10% glycerol) supplemented with 2 mM $MgCl_2$ 1 mM AEBSF-HCl, 1 µg/ml Leupeptin, 2 µg/ml Aprotinin, 1 µg/ml Pepstatin, and 2.4 U/ml Benzonase Corefa,. An Avestin system was used to lyse the bacteria through homogenization, and the resulting lysate was clarified by centrifugation at 20500 rpm for 30 min at 4 °C. To purify the his-tagged proteins, NiNTA-affinity chromatography was employed. This involved subjecting the cleared lysate to a linear gradient ranging from 4 to 100% elution buffer (50 mM Na_3PO_4/Na_2HPO_4 pH 8, 500 mM NaCl, 250 mM imidazole, and 10% glycerol) over 10 column volumes. The eluate was collected in 1 ml fractions that contained the recombinant SYNJ2BP. After pooling the fractions, they were subjected to size-exclusion chromatography using a HiLoad 16/60 Superdex 75 column with SE/storage Buffer (20 mM Tris pH 7.2, 30 mM NaCl, and 10% glycerol). Lastly, the purified protein was concentrated by employing Amicon Ultra 15 columns in two separate batches, ultimately reaching a final concentration of 1 mg/ml. The protein was subsequently snap-frozen at -80 °C for storage.

2.5 *In vitro* phosphorylation assay with recombinant AMPK

The *in vitro* phosphorylation assay using recombinant AMPK was performed as described previously (Hees & Harbauer, 2023). From *E. Coli* purified SYNJ2BP WT and S21A protein were first dephosphorylated using calf intestinal phosphatase (CIP). In a total volume of 10 µl, 0.5 µg of the purified SYNJ2BP protein was mixed with 1 µl of CIP (NEB) in 1x rCutSmart Buffer and incubated at 37 °C for 1 h. The dephosphorylation reaction was terminated by addition of 1x PhosStop (Roche). For the *in vitro* phosphorylation assay, 16 ng active recombinant AMPK (Sigma-Aldrich) was added to the dephosphorylated SYNJ2BP WT and S21A protein, respectively. The reaction was performed in kinase reaction buffer (8 mM MOPS/NaOH pH 7, 200 µM EDTA) containing 500 µM ATP (Serva) and 200 µM AMP (Serva) in a final volume of 30 µl. After incubation at 30 °C for 2 h (shaking at 300 rpm), the reaction was terminated by addition of 1x Laemmli sample buffer and boiling at 95 °C for 5 min.

2.6 *In vitro* phosphorylation assay with neuronal cytosolic extracts

The *in vitro* phosphorylation assay using neuronal cytosolic extracts was performed as described previously (Hees & Harbauer, 2023). Mouse primary cortical neurons were plated in PLL- and laminin-coated 6 well plates (Greiner) ($2*10^6$ cells per well) and cultivated in NB+B27+PSG as described above. On DIV6, neurons were treated with 1 mM AICAR (Abcam) for 2 h or cultured in medium lacking B27 (NB+PSG), and therefore insulin, for 2 h. Afterwards, the cortical neurons were washed twice in ice-cold PBS, collected in a buffer containing 20 mM Tris/HCl pH 7.2, 10 mM $MgCl_2$, 30 mM NaCl, 1 mM EDTA, 10 % glycerol, protease inhibitor cocktail (Roche) and 200 µM PMSF (80 µl per well) and mechanically lysed by performing 50 strokes using the tight pestle of a dounce homogenizer. The lysates were cleared by centrifugation at 5000 rpm for 1 min at 4 °C, snap-frozen and stored at -80 °C. For the *in vitro* phosphorylation assay, 25 µl of the neuronal cytosolic extracts as well as 500 µM ATP (Serva) were added to 0.5 µg of the dephosphorylated SYNJ2BP WT and S21A protein, respectively (preparation as described above), in a total volume of 40 µl. Following incubation at 30 °C for 2 h (shaking at 300 rpm), the reaction was terminated by addition of 1x Laemmli sample buffer and boiling for 5 min at 95 °C.

2.7 Zn^{2+}-Phos-Tag SDS-PAGE

Zn^{2+}-Phos-Tag sodium dodecyl sulfate polyacrylamide gel electrophoreses (Zn^{2+}-Phos-Tag SDS-PAGE; Kinoshita et al., 2006) was used to analyze the samples of the SYNJ2BP *in vitro* phosphorylation assay as described previously (Hees & Harbauer, 2023). To this end, 20 % polyacrylamide gels were prepared using 1.4 M Bis-Tris/HCl (pH 6.8) for both separating and stacking gel. Furthermore, 50 µM Phos binding reagent acrylamide (PBR-A, APExBIO) and 100 µM $Zn(NO_3)_2$ were added to the separating gel. Electrophoresis was performed for 120 min at 40 mA using a buffer containing 100 mM Tris, 100 mM MOPS, 5 mM $NaHSO_3$, and 0.1 % SDS. Afterwards, the gel was washed three times for 10 min in standard transfer buffer containing 1 mM EDTA followed by one 10 min wash in transfer buffer without EDTA. For immunoblotting, a standard transfer buffer containing 10 % methanol and a PVDF membrane was used. The transfer was performed for 90 min at 400 mA. Following blocking in 1x Fluorescent Blocking Buffer (Thermo Scientific) for 60 min at RT, the membrane was decorated with anti-SYNJ2BP rabbit antibody (1:500; Proteintech, #15666-1-AP) diluted in 5 % milk/TBS-T at 4 °C overnight. After three washes in TBS for 5 min at RT, the membrane was incubated in secondary antibody Alexa Fluor Plus goat anti-rabbit 647 (Invitrogen, 1:5000) diluted in 5 % milk/TBS for 120 min at room temperature followed by another wash in TBS.

2.8 Immunoblotting

2.8.1 Validation of AMPK knockdown

Mouse primary cortical neurons were plated in PLL- and laminin-coated 6 well plates (Greiner) ($2*10^6$ cells per well) and cultivated in NB+B27+PSG as described above. On DIV1, cortical neurons were lentivirally transduced with a non-targeting control shRNA or shRNAs against AMPKα1 and α2, respectively, for about 8 h. On DIV5, neurons were lysed in a buffer containing 25 mM Tris/HCl pH 7.4, 150 mM NaCl, 1 mM EDTA and 1 % NP-40 supplemented with protease inhibitor cocktail (Roche) and 200 μM PMSF (40 μl per well). The lysates were cleared by centrifugation at 10000 rpm for 1 min at 4 °C. The pellet was discarded, while the supernatant was mixed with Laemmli sample buffer and boiled for 5 min at 95 °C. The samples were analyzed by SDS-PAGE and immunoblotting on a 12 % polyacrylamide gel following standard protocols. Anti-βIII tubulin mouse (2G10) antibody (1:2000; Invitrogen, #MA1-118), anti-AMPKα1 rabbit (Y365) antibody (1:500; Abcam, #ab32047), and anti-AMPKα2 mouse (A6A10) antibody (1:500; Invitrogen, #MA5-42560) were used.

2.8.2 Detection of SYNJ2BP and SYNJ2 protein levels

Mouse primary cortical neurons were plated in PLL- and laminin-coated 6 well plates (Greiner) ($2*10^6$ cells per well) and cultivated in NB+B27+PSG as described above. To assess the expression levels of myc-tagged SYNJ2BP WT, S21A and S21E constructs, cortical neurons were lentivirally transduced with the corresponding constructs for about 8 h on DIV1. For detection of endogenous expression levels of SYNJ2BP and SYNJ2 under different conditions, cortical neurons were treated with 1 mM AICAR (Abcam), 20 μM CC (Abcam), 500 nM insulin (Sigma-Aldrich) or cultured in NB+B27+PSG lacking insulin for 2 h on DIV6. Afterwards, the cells were lysed in a buffer containing 25 mM Tris/HCl pH 7.4, 150 mM NaCl, 1 mM EDTA and 1 % NP-40 supplemented with protease inhibitor cocktail (Roche) and 200 μM PMSF (40 μl per well). The lysates were cleared by centrifugation at 10000 rpm for 1 min at 4 °C. The pellet was discarded, while the supernatant was mixed with Laemmli sample buffer and boiled for 5 min at 95 °C. The samples were analyzed by SDS-PAGE and immunoblotting on 15 % and 7.5 % polyacrylamide gels for SYNJ2BP and SYNJ2 detection, respectively, following standard protocols. Anti-SYNJ2 rabbit antibody (1:500; Proteintech, #13893-1-AP), anti-SYNJ2BP rabbit antibody (1:500; Proteintech, #15666-1-AP), and anti-βIII tubulin mouse (2G10) antibody (1:2000; Invitrogen, #MA1-118) were used.

2.8.3 Detection of PINK1 expression levels

PINK1 levels were determined as described previously (Hees & Harbauer, 2023). Human iPSC-derived cortical neurons were plated in PLL- and laminin-coated 6 well plates (Greiner) ($2*10^6$ cells per well)

and maintained in conditioned Südhof neuronal growth medium as described above. HEK293T cells were seeded in 6 well plates (Greiner) ($0.5*10^6$ cells per well) and cultivated in DMEM supplemented with 10 % FBS and 1 % P/S as described above. On DIV14, human iPSC-derived cortical neurons were cultured in conditioned Südhof neuronal growth medium lacking insulin or treated with 10 µM AKT inhibitor VIII (TCI), 1 mM AICAR (Abcam) or 20 µM CC (Abcam) for 2 h. Two days after seeding, HEK293T cells were treated with 1 µM GSK1904529A (Abcam) or 10 µM AKT inhibitor (TCI) for 2 h. HEK293T cells and human iPSC-derived cortical neurons were lysed in buffer containing 25 mM Tris/HCl pH 7.4, 150 mM NaCl, 1 mM EDTA and 1 % NP-40 supplemented with protease inhibitor cocktail (Roche) and 200 µM PMSF. The lysates were cleared by centrifugation at 10000 for 1 min at 4 °C. After addition of 1x Laemmli sample buffer the supernatants were boiled for 5 min at 95 °C. The samples were analyzed by SDS-PAGE and immunoblotting on a 12 % polyacrylamide gel following standard protocols. Anti-PINK1 rabbit antibody (1:500; Novus Biologicals, #BC100-494), anti-βIII tubulin mouse (2G10) antibody (1:2000; Invitrogen, #MA1-118), and anti-β-actin mouse (AC-74) antibody (1:500; Sigma-Aldrich, A5316) and were used.

2.9 Lentivirus production

HEK293T cells were used for the production of lentiviral particles as described previously (Hees & Harbauer, 2023). The cells were plated in collagen (Sigma-Aldrich)-coated 10 cm dishes (Falcon) ($6*10^6$ cells per dish) and maintained in DMEM supplemented with 10 % FBS and 1 % P/S as described above. 24 h after seeding, each 10 cm dish of HEK293T cells was transfected with 5 µg of the respective transfer plasmid (mycSYNJ2BP WT, S21A, S21E, pLV-TetO-hNGN2-eGFP-puro, FudeltaGW-rtTA, GFP-Cre, control GFP, non-targeting control shRNA, AMPKα1 shRNA or AMPKα2 shRNA) and 5 µg of the packaging plasmid mix (pMDLg/pRRE, pRSV-Rev, pMD2.G; ratio 4:1:1) using TransIT-Lenti reagent (Mirus Bio). After 48 h, the medium of the cells, which contained the lentiviral particles, was collected and cleared by centrifugation at 300xg for 10 min at room temperature. The supernatant was mixed with lentivirus precipitation solution (Alstem) in a 4:1 ratio (10 ml supernatant and 2.5 ml precipitation solution per dish) and incubated at 4 °C overnight. On the next day, the mix was centrifuged at 1500xg for 30 min at 4 °C to sediment the lentiviral particles. The supernatant was discarded and the pellet was resuspended in 1 ml ice-cold PBS per 10 cm dish, aliquoted and stored at -80 °C.

2.10 Co-immunoprecipitation

Co-immunoprecipitation experiments for assessing the interaction between SYNJ2BP and SYNJ2 were performed as described previously (Hees & Harbauer, 2023). Mouse primary cortical neurons were plated in PLL- and laminin-coated 6 well plates (Greiner) ($2*10^6$ cells per well) and cultivated in

NB+B27+PSG as described above. On DIV1, cortical neurons were lentivirally transduced with mycSYNJ2BP WT for about 8 h. On DIV6, neurons were lysed in a buffer containing 25 mM Tris/HCl pH 7.4, 150 mM NaCl, 1 mM EDTA and 1 % NP-40 supplemented with protease inhibitor cocktail (Roche), 200 µM PMSF and PhosStop (Roche) (40 µl per well). The lysates were cleared by centrifugation at 10000 rpm for 1 min at 4 °C. The pellet was discarded, while the supernatant was treated either with or without CIP (NEB) for 1 h at 37 °C in 1x rCutSmart buffer. 10 % of the total lysate volume was kept as input. The remaining lysate was mixed with buffer containing 20 mM Tris/HCl pH 8, 5 mM MgCl$_2$, 140 mM NaCl, 0.1 % Triton-X, 0.5 mM DTT and 200 µM PMSF in a 1:1 ratio and incubated with either 2 µg anti-SYNJ2BP rabbit antibody (Proteintech, #15666-1-AP) or anti-flag rabbit antibody (Sigma-Aldrich; #F7425) as IgG control per ml lysate for 30 min, rotating, at 4 °C. Afterwards, 10 mg of 1 % BSA-blocked protein A sepharose beads were added to each sample and incubated for another 60 min, rotating, at 4 °C. For the following washing steps, the beads were transferred to columns (MoBiTec) and washed five times with buffer containing 20 mM Tris/HCl pH 8, 5 mM MgCl$_2$, 140 mM NaCl, 0.1 % Triton-X, 0.5 mM DTT and 200 µM PMSF. Finally, proteins were eluted in 1x Laemmli sample buffer for 2 min at 95 °C. The samples were analyzed by SDS-PAGE and immunoblotting on a 7.5 – 15 % gradient polyacrylamide gel following standard protocols. Anti-SYNJ2BP rabbit antibody (1:500; Proteintech, 15666-1-AP), anti-SYNJ2 rabbit antibody (1:500; Proteintech, #13893-1-AP), and anti-βIII tubulin mouse (2G10) antibody (1:2000; Invitrogen, #MA1-118) were used.

2.11 Phospho-mass spectrometry

2.11.1 Sample Preparation

Phospho-mass spectrometry experiments were performed in collaboration with Barbara Steigenberger from the Max Planck Institute of Biochemistry, Martinsried, Germany as described previously (Hees & Harbauer, 2023). Mouse primary cortical neurons were plated in PLL- and laminin-coated 6 well plates (Greiner) ($2*10^6$ cells per well) and cultivated in NB+B27+PSG as described above. On DIV1, cortical neurons were lentivirally transduced with mycSYNJ2BP WT for about 8 h. On DIV6, the cells were cultured for 2 h in NB+B27+PSG lacking insulin and simultaneously treated with or without 20 µM CC (Abcam) and 500 nM insulin (Sigma-Aldrich), respectively. Afterwards, cells were collected in ice-cold PBS and pelleted at 10000 rpm for 1 min. The following steps were performed at the mass spectrometry facility of the Max Planck Institute of Biochemistry, Martinsried. The harvested cell pellets of approximately $10*10^6$ mouse cortical neurons were mixed with 200 µl of preheated SDC buffer (1% SDC, 40 mM CAA, 10 mM TCEP in 100 mM Tris, pH 8.0) and incubated at 95 °C for 2 min. Subsequently, ultrasonication was performed using a Bioruptor Plus sonication system (Diogenode) for a total of 10 min, with 10 cycles of 30 s at high intensity followed by a 30 s pause. The incubation

and ultrasonication process was performed twice. Afterwards, MS grade water was used to dilute the sample in a 1:1 ratio. Protein digestion was carried out by adding 2 µg of Lys-C for a 4 h incubation, followed by an overnight incubation at 37 °C with 4 µg of trypsin. The resulting peptide solution was acidified with trifluoroacetic acid (TFA) to a final concentration of 1 %. Desalting of the peptides was performed using Sep-Pak C18 5cc vacuum cartridges. The desalted peptides were then dried and resuspended in 220 µl of equilibration buffer (80 % acetonitrile and 0.1 % TFA) right before the phospho-peptide enrichment process. Alternatively, the peptides were resuspended in buffer A (0.1 % formic acid (FA)) for the measurement of the total proteome.

2.11.2   Phospho-peptide enrichment

Phospho-peptide enrichment was conducted using an automated AssayMAP Bravo Platform (Agilent Technologies), employing AssayMAP FE(III)-NTA cartridges (Agilent Technology). Initially, the cartridges were primed with 200 µl of priming buffer (100 % acetonitrile and 0.1 % TFA). And equilibrated with 250 µl of equilibration buffer (80 % acetonitrile and 0.1% TFA). After loading the sample onto the cartridges, the cartridges were washed with 250 µl of equilibration buffer to remove any unbound or non-specifically bound peptides. The enriched phospho-peptides were then eluted using 35 µl of elution buffer (10 % NH_3 in H_2O). To acidify the eluted peptides, 35 µl of 10 % FA was added. Afterwards, the samples were concentrated using a SpeedVac apparatus for 45 min at 37 °C. The SpeedVac process involves evaporation of solvents under vacuum to concentrate the peptides.

2.11.3   LC MS/MS data acquisition

The peptides were introduced into a 30 cm column with a 75 µm inner diameter (packed in-house with ReproSil-Pur C18-AQ 1.9 µm beads, Dr. Maisch GmbH). This loading process was performed via the autosampler of the Thermo Easy-nLC 1200 system (Thermo Fisher Scientific), with the column temperature maintained at 60 °C. The eluted peptides were directly transferred to the benchtop Orbitrap mass spectrometer Exploris 480 (Thermo Fisher Scientific) using a nanoelectrospray interface. During peptide separation, buffer A (0.1 % FA) was used for peptide loading. The separation was achieved at a flow rate of 300 nL/min, utilizing a gradient of buffer B (80 % acetonitrile and 0.1 % FA). The gradient started at 5 % buffer B and gradually increased to 30 % over a duration of 105 min. Subsequently, there was a rapid increase to 65 % buffer B in 5 min, followed by a further increase to 95 % buffer B over the next 5 min. The percentage of buffer B was then maintained at 95 % for an additional 5 min. Operating in a data-dependent mode, the mass spectrometer performed survey scans in the range of 300 to 1650 m/z, with a resolution of 60000 at m/z = 200. Up to 15 of the most intense precursor ions were selected for fragmentation using higher energy collisional dissociation

(HCD) with a normalized collision energy set at 28. The resulting MS2 spectra were captured at a resolution of 30000 (at m/z = 200). The Automatic Gain Control (AGC) target was set to 3E6 for MS scans and 1E5 for MS2 scans with a maximum injection time of 25 ms for MS1. The injection time for MS2 scans was automatically determined. Dynamic exclusion was set to 30 ms, preventing the reselection of previously fragmented ions within that time window.

2.12   RNA isolation and RT-qPCR

RNA isolation and RT-qPCR experiments were performed as described previously (Hees & Harbauer, 2023). Mouse primary cortical neurons were plated in PLL- and laminin-coated 6 well plates (Greiner) ($2*10^6$ cells per well) and cultivated in NB+B27+PSG as described above. On DIV6, RNA was isolated from neurons treated with or without 20 µM CC (Abcam) for 2 h and with 50 nM ApoE3 (PeproTech) or 50 nM ApoE4 (PeproTech) overnight, respectively, using the QIAGEN RNeasy Mini Kit following the manufacturer's instructions. The RNA concentration was determined using a NanoDrop® spectrophotometer and 500 ng were used for complementary DNA (cDNA) synthesis with qScriptTM cDNA SuperMix (Quantabio). The RT-qPCR assay was performed in a Mic (magnetic induction cycler) PCR machine (Bio Molecular Systems) using the PerfeCTa SYBR® Green FastMix (Quantabio) and the following primers (5' → 3'): Pink1 forward: GCGAAGCCATCTTAAGCAAA; Pink1 reverse: AGTAGTGTGGGGGCAGCATA; β-actin forward: ACACTGTGCCCATCTACG and β-actin reverse: GCTGTGGTGGTGAAGCTGTAG.

2.13   Live cell mRNA imaging

Live cell imaging of *Pink1, Cox4i or Atp5f1*β mRNA in mouse primary hippocampal neurons was conducted as described previously (Harbauer et al., 2022; Hees & Harbauer, 2023). Neurons were plated in PLL- and laminin-coated 24-well glass bottom plates (CellVis) ($100*10^3$ cells per well) and cultivated as described above. On DIV5-7, neurons were transfected with the Pink1 kinase dead (Pink1-kinase dead-MS2-PP7), Cox4i or Atp5f1β construct containing the MS2 and PP7 binding sites and the split-Venus construct along with organellar markers (mito-mRaspberry-7, TMEM192-mRFP-3xHA or mCherry-Rab7a) as well as shRNAs against SYNJ2BP, AMPKα1 or AMPKα2 and constructs encoding mycSYNJ2BP WT, S21A, S21E, SYNJ2mito WT, VQL/AAA and Snap-Omp25 using Lipofectamine® 2000 transfection reagent (Thermo Fisher Scientific). While 2 µl Lipofectamine® was used per well, 4 µg of the Pink1-kinase dead-MS2-PP7 construct was transfected to prevent retention of RNA inside the nucleus. Furthermore, the optimal ratio between the two plasmids, Pink1-kinase dead-MS2-PP7 and split-Venus, was empirically determined to be 4:1. 0.3 µg of the DNA encoding for the organellar markers, the shRNAs and the SYNJ2BP and SYNJ2 constructs was used per well. Briefly, Lipofectamine®

and DNAs were mixed in NB+PSG and incubated for at least 20 min at room temperature. After changing the medium of the neurons from NB+B27+PSG to NB+PSG, prepared DNA-lipofectamine complexes were added. Following a 20 min incubation, conditioned and fresh NB+B27+PSG was added to the cells in a 1:1 ratio. The cells were imaged 2 days after transfection, except in the case of co-transfection with shRNAs against SYNJ2BP, AMPKα1 or AMPKα2, where expression was allowed for 4 days to achieve an effective knock down of the respective proteins. On DIV9, the neurons were imaged with an Eclipse Ti2 spinning disk microscope (Nikon) using a 60×/NA 1.2 oil immersion objective, a DS-Qi2 high-sensitivity monochrome camera and NIS-Elements software (version 5.21.03) at the Imaging Facility of the Max Planck Institute for Biological Intelligence, Martinsried. Prior to imaging, the neuronal medium was replaced by Hibernate E medium without phenol red (BrainBits). Furthermore, the following treatments were performed depending on the respective experiment: 500 nM insulin (Sigma-Aldrich) for 1 h, 10 µM AKT inhibitor VIII (TCI) for 2 h, 1 µM Wortmannin (EMD Millipore) for 2 h, 1 µM GSK1904529A (Abcam) for 2 h, 20 µM CC (Abcam) for 2 h, 1 mM AICAR (Abcam) for 2 h, 50 nM ApoE3 or ApoE4 (PeproTech) overnight.

2.14 Protein translation assays

2.14.1 SunTag system

Mouse primary hippocampal neurons and HeLa cells were plated in PLL- and laminin-coated 24-well glass bottom plates (CellVis) ($100*10^3$ and $50*10^3$ cells per well, respectively) and cultivated as described above. HeLa cells were transfected with the Pink1 kinase dead construct containing the SunTag repeats (Pink1-kinase dead-10xGCN4-12xMS2-PP7) and the scFv-GFP construct. In neurons, depending on the respective experiment, transfection of Pink1-kinase dead-10xGCN4-12xMS2-PP7 and scFv-GFP was combined with organellar markers (mito-mRaspberry-7, mCherry-Rab7A, TMEM192-mRFP-3xHA or pLAMP1-mCherry) or plasmids encoding mycSYNJ2BP WT or S21E. While 1 µg of the Pink1-kinase dead-10xGCN4-12xMS2-PP7 construct was transfected, 0.3 µg of the DNA encoding for the organellar markers and the mycSYNJ2BP constructs was used per well. Furthermore, the optimal ratio between the two plasmids, Pink1-kinase dead-10xGCN4-12xMS2-PP7 and scFv-GFP, was empirically determined to be 4:1. HeLa cells were transfected one day after plating using calcium phosphate, while neurons were transfected on DIV7 in NB+PSG using Lipofectamine® 2000 transfection reagent (Thermo Fisher Scientific) as described above. On DIV9 or 2 days after transfection, neurons and HeLa cells were imaged with an Eclipse Ti2 spinning disk microscope (Nikon) using a 60×/NA 1.2 oil immersion objective, a DS-Qi2 high-sensitivity monochrome camera and NIS-Elements software (version 5.21.03) at the Imaging Facility of the Max Planck Institute for Biological Intelligence, Martinsried. Prior to imaging, the medium was replaced by Hibernate E medium without phenol red (BrainBits). Furthermore, the following treatments were performed depending on the

_____

respective experiment: 500 nM insulin (Sigma-Aldrich) for 1 h, 10 µM AKT inhibitor VIII (TCI) for 2 h, 1 µM Wortmannin (EMD Millipore) for 2 h, 1 µM GSK1904529A (Abcam) for 2 h, 20 µM CC (Abcam) for 2 h, 1 mM AICAR (Abcam) for 2 h, 10 nM Torin-2 (Sigma-Aldrich) for 30 min, 100 nM Bafilomycin A1 (Abcam) for 2 h, 200 µg/ml Puromycin (Enzo Life Sciences) for 2 h.

2.14.2   RiboTag assay

Mouse primary cortical neurons from heterozygous B6N.129-Rpl22$^{tm1.1Psam}$/J (Rpl22-HA) (Sanz et al., 2009) E16.5 mouse embryos were plated in PLL- and laminin-coated 6-well plates (Greiner) ($2*10^6$ cells per well) and cultivated as described above. On DIV1, cortical neurons were transduced either with lentivirus packaged Cre-GFP or control-GFP plasmid for 5-8 h. In the presence of Cre recombinase, expression of the modified allele of the ribosomal gene *Rpl22 (Rpl22-HA)* is induced. The immunoprecipitation of the HA-tagged ribosomes was performed as described above. Briefly, on DIV6, cells were treated with 1 mM AICAR or 20 µM CC for 2 h followed by lysis (25 mM Tris/HCl pH 7.4, 1 % NP-40, 150 mM NaCl, supplemented with protease inhibitor cocktail (Roche) and 200 µM PMSF) and centrifugation at 10000 rpm for 1 min. After discarding the pellets, 10 % of the supernatant was kept as input and the rest was incubated with 0.5 µg anti-HA rabbit antibody (Cell Signaling, #3724) per ml lysate for 30 min at 4 °C. Following blocking using 1 mg/ml BSA, protein A sepharose beads were added to the lysate-antibody mix and incubated for additional 60 min at 4 °C. Finally, the beads underwent five washing steps in columns (MoBiTec) using a buffer containing 20 mM Tris/HCl pH 8, 5 mM MgCl$_2$, 140 mM NaCl, 0.1 % Triton X-100, 0.5 mM DTT and 200 µM PMSF and were eluted by addition of Laemmli sample buffer followed by boiling at 95 °C for 2 min. Half of each sample was analyzed by immunoblotting to confirm the successful isolation of HA-tagged ribosomes using anti-HA rabbit antibody (1:500; Cell Signaling, #3724) and anti-βIII tubulin mouse (2G10) antibody (1:2000; Invitrogen, #MA1-118). The other half was used for RNA isolation followed by RT-qPCR as described above. Briefly, RNA was isolated using the QIAGEN RNeasy Mini Kit following the manufacturer's instructions. cDNA synthesis was performed with qScriptTM cDNA SuperMix (Quantabio), while the RT-qPCR assay was conducted in a Mic PCR machine (Bio Molecular Systems) using the PerfeCTa SYBR® Green FastMix (Quantabio) and the following primers (5' $\rightarrow$ 3'): Pink1 forward: GCGAAGCCATCTTAAGCAAA; Pink1 reverse: AGTAGTGTGGGGGCAGCATA.

2.15   PINK1-GFP imaging

Mouse primary hippocampal neurons were plated in PLL- and laminin-coated 24-well glass bottom plates (CellVis) ($100*10^3$ cells per well) and cultivated as described above. On DIV7, neurons were transfected with 0.3 µg PINK1-GFP and 0.3 µg mito-BFP per well. The transfection was performed in

NB+PSG using Lipofectamine® 2000 transfection reagent (Thermo Fisher Scientific) as described above. On DIV9, neuronal medium was replaced by NB+B27+PSG supplemented either with or without insulin for 2 h. Subsequently, neurons were imaged with an Eclipse Ti2 spinning disk microscope (Nikon) using a 60×/NA 1.2 oil immersion objective, a DS-Qi2 high-sensitivity monochrome camera and NIS-Elements software (version 5.21.03) at the Imaging Facility of the Max Planck Institute for Biological Intelligence, Martinsried. Prior to imaging, the neuronal medium was replaced by Hibernate E medium without phenol red (BrainBits) supplemented with or without 500 nM insulin.

2.16   Proximity Ligation Assay

Mouse primary hippocampal neurons were plated on acid-washed, PLL- and laminin-coated glass coverslips (1.5 mm, Marienfeld) (50*10^3 cells per well) and cultivated as described above. For detection of PLA signal between endogenous SYNJ2 and SYNJ2BP WT, S21A and S21E, respectively, neurons were transfected with 0.3 µg mito-meGFP as well as 0.3 µg of the respective SYNJ2BP construct per coverslip on DIV5. For detection of PLA signal between the PINK1 SunTag signal and ribosomes, neurons were transfected with 1 µg Pink1-kinase dead-10xGCN4-12xMS2-PP7 and 0.25 µg scFv-GFP on DIV5. The transfection was performed in NB+PSG using Lipofectamine® 2000 transfection reagent (Thermo Fisher Scientific) as described above. For detection of PLA signal between endogenous SYNJ2BP and SYNJ2, no transfection was conducted. Before fixation on DIV7, the following treatments were performed depending on the respective experiment: 1 mM AICAR (Abcam) or 20 µM CC (Abcam) were added to either NB+B27+PSG or Hibernate E medium (BrainBits) and incubated with the neurons for 2 h. For the starvation condition, neurons were kept for 2 h in NB+B27+PSG lacking insulin. Furthermore, 500 nM insulin (Sigma-Aldrich) and 1 µM GSK1904529A (Abcam) were added to the neurons cultured in NB+B27+PSG for 1 h and 2 h, respectively. Additionally, the untransfected cells were stained with 100 nM MitoTracker Deep Red (Invitrogen) at 37 °C for 20 min followed by three quick washes in the appropriate medium. Subsequently, neurons were fixed with 4 % paraformaldehyde (PFA; pre-heated to 37 °C) for 15 min at room temperature and permeabilized with 0.3 % Triton/PBS for 10 min at room temperature. The following steps were performed according to the manufacturer's instructions (Sigma-Aldrich) and as described (Harbauer et al., 2022; Hees & Harbauer, 2023). Neurons were blocked using the Duolink blocking solution for 60 min at 37 °C in a humidity chamber and afterwards incubated with the primary antibodies (anti-SYNJ2 rabbit antibody, Proteintech, #13893-1-AP, 1:50; anti-SYNJ2BP mouse antibody, Sigma-Aldrich, #SAB1400613, 1:50; anti-RPS6 rabbit (5G10) antibody, Cell Signaling Technology, #2217, 1:200) diluted in Duolink antibody diluent at 4 °C overnight. On the next day, cells were washed with buffer A (0.01 M Tris, 0.15 M NaCl, 0.05 % Tween 20) two times for 5 min at room temperature and afterwards incubated with the Duolink anti-rabbit plus and anti-mouse minus PLA probes, which were diluted in a 1:5 ratio in the Duolink

_____

antibody diluent, at 37 °C for 60 min. After two washes with buffer A for 5 min at RT, cells were treated with a ligase, diluted in the Duolink ligation buffer (1:40), at 37 °C for 30 min, which was again followed by two washes with buffer A for 5 min at room temperature. Afterwards, a polymerase diluted in the Duolink amplification buffer (1:80) that contains fluorescently-labeled oligonucleotides (green or far-red) was added and the cells were incubated at 37 °C for 100 min. Following two washing steps in buffer B (0.2 M Tris, 0.1 M NaCL) for 10 min at room temperature and a final washing step in 0.01x buffer B for 1 min at RT, coverslips were mounted using Fluoromount G (Invitrogen) and imaged with an Eclipse Ti2 spinning disk microscope (Nikon) using a 60×/NA 1.2 oil immersion objective, a DS-Qi2 high-sensitivity monochrome camera and NIS-Elements software (version 5.21.03) at the Imaging Facility of the Max Planck Institute for Biological Intelligence, Martinsried.

2.17   Fluorescence Lifetime Imaging (FLIM)

Mouse primary hippocampal neurons were plated in PLL- and laminin-coated 24-well glass bottom plates (CellVis) ($100*10^3$ cells per well) and cultivated as described above. On DIV6, neurons were transfected with 0.3 µg of the AMPK FRET biosensor pPBbsr2-4031NES (Konagaya et al., 2017), Mito-ABKAR, Cyto-ABKAR or LAMP1-ABKAR (Miyamoto et al., 2015) per well. The transfection was performed in NB+PSG using Lipofectamine® 2000 transfection reagent (Thermo Fisher Scientific) as described above. On DIV7, one day before imaging, neuronal medium was replaced by NB+B27+PSG supplemented either with or without insulin as well as with or without 50 nM ApoE3 (PeproTech) or 50 nM ApoE4 (PeproTech). On DIV8, the neurons were imaged with a LEICA (Wetzlar, Germany) SP8 FALCON confocal laser scanning microscope using an HCX PL APO 63x/1.2 motCORR CS water immersion objective and the LAS-X software (version 3.5.5) at the Imaging Facility of the Max Planck Institute of Biochemistry, Martinsried. Prior to imaging, the neuronal medium was replaced by Hibernate E medium without phenol red (BrainBits) supplemented with or without 500 nM insulin as well as with or without 50 nM ApoE3 or ApoE4. Furthermore, the following additional treatments were performed 2 h before imaging to inhibit the insulin pathway: 1 µM GSK1904529A (Abcam), 1 µM Wortmannin (EMD Millipore) and 10 µM AKT inhibitor VIII (TCI). To analyze AMPK activity, fluorescence lifetime imaging (FLIM) was performed at 37 °C as described previously (Hees & Harbauer, 2023). To this end, a pulsed diode laser (PicoQuant) was used to excite the donor of either AMPK FRET biosensor at 440 nm. The donor lifetime was determined by detection of photon arrival times of a maximum of 1000 photons per brightest pixel between 470 and 512 nm using the phasor analysis approach (Digman et al., 2008; Hinde et al., 2012).

2.18   Mitophagy assays

2.18.1   Phospho-ubiquitin and optineurin immunostaining

Immunostaining of phospho-ubiquitin and optineurin was performed as described previously (Hees & Harbauer, 2023). Mouse primary hippocampal neurons were plated on acid-washed, PLL- and laminin-coated glass coverslips (1.5 mm, Marienfeld) ($50*10^3$ cells per well) and cultivated as described above. On DIV6, neurons were transfected with 0.3 µg mito-meGFP as well as 0.3 µg SYNJ2BP WT, S21A or S21E depending on the experiment. The transfection was performed in NB+PSG using Lipofectamine® 2000 transfection reagent (Thermo Fisher Scientific) as described above. On DIV7, one day before fixation, neuronal medium was replaced by NB+B27+PSG supplemented either with or without insulin as well as with or without 50 nM ApoE3 or ApoE4 (PeproTech). On the next day, neurons were treated with or without 1 mM AICAR (Abcam) for 2 h as well as with or without 10 nM Torin-2 (Sigma-Aldrich) for 30 min. Following induction of mitochondrial damage using 20 µM AA (Alfa Aesar) for 45 min, neurons were fixed with 4 % PFA (pre-warmed to 37 °C) for 15 min at room temperature. After permeabilization in 0.3 % Triton X-100/PBS for 10 min and blocking in 1 % BSA/PBS for 1 h at room temperature, neurons were incubated with primary antibodies (anti-optineurin rabbit antibody (1:500; Abcam, #ab23666), anti-phospho-ubiquitin S65 rabbit antibody (1:200; Millipore, #ABS1513-I), and anti-βIII tubulin mouse (2G10) antibody (1:1000; Invitrogen, #MA1-118)) diluted in 1 % BSA/PBS at 4 °C overnight. On the next day, the fixed neurons were washed three times in PBS for 5 min each at room temperature and incubated with secondary fluorescent antibodies (Alexa Fluor 568 goat anti-mouse and Alexa Fluor 647 goat anti-rabbit (Invitrogen, 1:500)) diluted in 1 % BSA/PBS at room temperature for 2 h followed by additional three washes in PBS. Finally, the coverslips were mounted using Fluoromount G (Invitrogen) and imaged with an Eclipse Ti2 spinning disk microscope (Nikon) using a 60×/NA 1.2 oil immersion objective, a DS-Qi2 high-sensitivity monochrome camera and NIS-Elements software (version 5.21.03) at the Imaging Facility of the Max Planck Institute for Biological Intelligence, Martinsried.

2.18.2   Parkin translocation

Mouse primary hippocampal neurons were plated in PLL- and laminin-coated 24-well glass bottom plates (CellVis) ($100*10^3$ cells per well) and cultivated as described above. On DIV7, neurons were transfected with 0.3 µg YFP-Parkin, 0.3 µg mito-mRaspberry-7 and 0.3 µg EBFP2-C1 (cytosolic BFP) per well. The transfection was performed in NB+PSG using Lipofectamine® 2000 transfection reagent (Thermo Fisher Scientific) as described above. On DIV8, one day before imaging, neuronal medium was replaced by NB+B27+PSG supplemented either with or without insulin. On DIV9, the neurons were imaged with an Eclipse Ti2 spinning disk microscope (Nikon) using a 60×/NA 1.2 oil immersion objective, a DS-Qi2 high-sensitivity monochrome camera and NIS-Elements software (version 5.21.03)

at the Imaging Facility of the Max Planck Institute for Biological Intelligence, Martinsried. Prior to imaging, the neuronal medium was replaced by Hibernate E medium without phenol red (BrainBits) supplemented with or without 500 nM insulin. To visualize Parkin translocation to damaged mitochondria, the same dendrites were imaged before and 30 min after 20 µM AA (Alfar Aesar) treatment as described previously (Harbauer et al., 2022; Hees & Harbauer, 2023).

2.18.3   Mitochondrial and lysosomal colocalization assay

Mouse primary hippocampal neurons were plated in PLL- and laminin-coated 24-well glass bottom plates (CellVis) (100*10^3 cells per well) and cultivated as described above. On DIV7, neurons were transfected with 0.3 µg mito-meGFP and 0.3 µg LAMP1-mCherry per well. The transfection was performed in NB+PSG using Lipofectamine® 2000 transfection reagent (Thermo Fisher Scientific) as described above. On DIV8, one day before imaging, neuronal medium was replaced by NB+B27+PSG supplemented either with or without insulin. On DIV9, the neurons were imaged with an Eclipse Ti2 spinning disk microscope (Nikon) using a 60×/NA 1.2 oil immersion objective, a DS-Qi2 high-sensitivity monochrome camera and NIS-Elements software (version 5.21.03) at the Imaging Facility of the Max Planck Institute for Biological Intelligence, Martinsried. Prior to imaging, the neuronal medium was replaced by Hibernate E medium without phenol red (BrainBits) supplemented with or without 500 nM insulin. Furthermore, AA (Alfar Aesar, 20 µM) was added to the neurons 45 min before imaging.

2.19   DNAJB6 immunostaining

Mouse primary hippocampal neurons were plated on acid-washed, PLL- and laminin-coated glass coverslips (1.5 mm, Marienfeld) (50*10^3 cells per well) and cultivated as described above. On DIV6, neurons were transfected with 1 µg Pink1-kinase dead-10xGCN4-12xMS2-PP7 and 0.25 µg scFv-GFP. The transfection was performed in NB+PSG using Lipofectamine® 2000 transfection reagent (Thermo Fisher Scientific) as described above. On DIV8, neurons were treated with or without 20 µM CC (Abcam) for 2 h. Afterwards, neurons were fixed with 4 % PFA (pre-warmed to 37 °C) for 15 min at room temperature. After permeabilization in 0.3 % Triton X-100/PBS for 10 min and blocking in 1 % BSA/PBS for 1 h at room temperature, neurons were incubated with the primary antibody anti-DNAJB6 rabbit antibody (1:500; Proteintech, #11707-1-AP) diluted in 1 % BSA/PBS at 4 °C overnight. On the next day, the fixed neurons were washed three times in PBS for 5 min each at room temperature and incubated with the secondary fluorescent antibody Alexa Fluor 647 goat anti-rabbit (Invitrogen, 1:500) diluted in 1 % BSA/PBS at room temperature for 2 h followed by additional three washes in PBS. Finally, the coverslips were mounted using Fluoromount G (Invitrogen) and imaged with an Eclipse Ti2 spinning disk microscope (Nikon) using a 60×/NA 1.2 oil immersion objective, a DS-Qi2 high-sensitivity

monochrome camera and NIS-Elements software (version 5.21.03) at the Imaging Facility of the Max Planck Institute for Biological Intelligence, Martinsried.

2.20   Correlative light and scanning electron microscopy

For correlative imaging, mouse primary hippocampal neurons were plated in PLL- and laminin-coated 35 mm glass bottom dishes (1.5 gridded coverslip, 14 mm glass diameter, MatTek) ($150*10^3$ cells per dish) and cultivated as described above. On DIV7, neurons were transfected with 1 µg Pink1-kinase dead-10xGCN4-12xMS2-PP7, 0.25 µg scFv-GFP, 0.3 µg mito-BFP and 0.3 µg TMEM192-mRFP-3xHA. The transfection was performed in NB+PSG using Lipofectamine® 2000 transfection reagent (Thermo Fisher Scientific) as described above. On DIV9, the neurons were imaged with an Eclipse Ti2 spinning disk microscope (Nikon) using a 60×/NA 1.2 oil immersion objective, a DS-Qi2 high-sensitivity monochrome camera and NIS-Elements software (version 5.21.03) at the Imaging Facility of the Max Planck Institute for Biological Intelligence, Martinsried. Prior to imaging, the neuronal medium was replaced by Hibernate E medium without phenol red (BrainBits) and the neurons were treated with or without 20 µM CC (Abcam) for 2 h. Immediately after imaging, the neurons were fixed using freshly prepared 2.5 % glutaraldehyde in 0.1 M cacodylate buffer (Science Services). The fixative was prepared as a 2x solution, pre-warmed to 37 °C and added directly into the Hibernate E medium of the neurons in a ratio of 1:1. After 5 min at 37 °C, it was replaced by 1x fixative and incubated for additional 25 min on ice. The fixative was removed by three 5 min washes with 0.1 M cacodylate buffer on ice. Afterwards, the samples were further processed by Martina Fetting at the electron microscopy hub at the German Center for Neurodegenerative Diseases (DZNE), Munich, Germany. A reduced osmium thiocarbohydrazide osmium (rOTO) en bloc staining protocol was applied including postfixation in 2 % osmium tetroxide (EMS), 1.5 % potassium ferricyanide (Sigma-Aldrich) in 0.1 M sodium cacodylate buffer (pH 7.4) (Kislinger et al., 2020). Staining was enhanced through a 45-min reaction with 1 % thiocarbohydrazide (Sigma-Aldrich) at 40 °C. Neurons were subsequently rinsed in water and immersed in a 2 % aqueous solution of osmium tetroxide. Following another wash, they were further contrasted by an overnight incubation in a 1 % aqueous solution of uranyl acetate at 4 °C and for an additional 2 h incubation at 50 °C. To prepare the samples for further processing, they were dehydrated using a series of increasing ethanol concentrations and infiltrated with LX112 (LADD). After curing the block was removed from the glass cover slip by freeze-thaw cycles. The region of interest was trimmed (TRIM2, Leica) according to the grid pattern that has previously been acquired by confocal imaging. Serial sections were obtained using a 35° ultra-diamond knife (Diatome) on an ATUMtome (Powertome, RMC). The sections had a nominal thickness of 80 nm and were collected onto Kapton tape that had been freshly treated with plasma (custom-built, based on Pelco easiGlow, adopted from M. Terasaki, U. Connecticut, CT) and was carbon-coated (kindly provided by Jeff

_____

Lichtman and Richard Schalek). Subsequently, the tape stripes were assembled onto adhesive carbon tape (Science Services), which in turn was attached to 4-inch silicon wafers (Siegert Wafer) and grounded using adhesive carbon tape strips (Science Services). EM micrographs were captured using an Apreo S2 SEM (Thermo Fisher Scientific) as described previously (Kislinger et al., 2023). Hierarchical imaging of serial sections was performed by mapping the plastic tape strips at low lateral resolution and acquisition of entire tissue sections at medium resolution (100-200 nm). The region of interest was correlated by the grid pattern and cellular morphologies and serial sections thereof acquired at 5 nm lateral resolution. Serial section data were aligned using a combination of automated and manual processing procedures within Fiji TrakEM2 (Kislinger et al., 2023). Single sections bearing the organellar structures of interest were selected.

2.21   Quantification and statistical analysis

All data are shown as mean ± SEM. GraphPad Prism (version 9.1.0) for Windows, GraphPad Software, San Diego, California, USA, www.graphpad.com, was used for graphical representation and statistical analysis. For comparison of two conditions, a student's or Welch's t-test was performed, whereas a one-way ANOVA with Tukey's or Dunnett's multiple comparisons was done for comparison of multiple groups. A p-value of $p<0.05$ (*) was considered statistically significant and further significance levels were defined as $p<0.01$ (**), $p<0.001$ (***) and $p<0.0001$ (****). The p-values are mentioned in the figure in case of statistically non-significant comparisons.

2.21.1   Analysis of immunoblots

The Invitrogen iBright FL1000 Imaging System (Thermo Fisher Scientific) was used to acquire immunoblot images as described previously (Hees & Harbauer, 2023). Densitometry analysis of images was performed in Fiji/ImageJ (National Institutes of Health) (Schindelin et al., 2012). The values were exported to Excel where the protein of interest was normalized to its respective loading control.

2.21.2   Analysis of mRNA imaging

The microscopy images from the *Pink1* mRNA imaging were analyzed in Fiji/ImageJ. The 'Just Another Colocalization Plugin' (JaCoP) (Bolte & Cordelières, 2006) was used to quantify the Manders' colocalization coefficient of the Venus (mRNA signal) and the respective organelle channel (mitochondria, late endosomes, lysosomes) as previously described (Graber et al., 2013; Harbauer et al., 2022; Hees & Harbauer, 2023). The quantification was performed on z-stack images. For the cell body, a squared region containing the entire cell body was chosen and no maximum z-projection was done. The dendrites were straightened with a 20 pixel margin following maximum z-projection. For

the rotated Venus quantification, a 10 x 10 µm square in the cell body was chosen based on the organelle channel and excluding the nucleus. The Manders' coefficient was determined before and after rotation of the Venus channel. The values of the Manders' coefficient were exported to Excel and plotted in GraphPad Prism. Additionally, the length of the mitochondria as well as the number of *Pink1* mRNA dots per mitochondrion were determined in the analyzed dendrites. The values were exported to Excel and the number of *Pink1* mRNA dots per µm mitochondrion were determined. The data were plotted in GraphPad Prism.

2.21.3   Analysis of SunTag imaging

The microscopy images from the PINK1 SunTag imaging were analyzed in Fiji/ImageJ. All quantifications were performed on z-stack images. A squared region containing the entire cell body was chosen and maximum z-projection was performed. A thresholded image of the GFP (SunTag signal) channel was created and the SunTag clusters were identified using the particle analyzer. The area as well as the intensities of the non-thresholded images were determined. The JaCoP plugin was used to quantify the Manders' colocalization coefficient of the GFP (SunTag signal) and the respective organelle channel (mitochondria, late endosomes, lysosomes). The quantification was performed on z-stack images. A squared region containing the entire cell body was chosen and no maximum z-projection was performed. The values of the Manders' coefficient as well as the mean gray values (intensity) and area values were exported to Excel and plotted in GraphPad Prism.

2.21.4   Analysis of proximity ligation assay

The microscopy images from the proximity ligation assay (PLA) were analyzed in Fiji/ImageJ. The cell body of the neuron was identified based on the mitochondrial channel and labeled by a self-drawn ROI. The number of PLA puncta per cell body was manually counted after maximum z-projection of the stacked images as previously described (Harbauer et al., 2022; Hees & Harbauer, 2023). The values were exported to Excel and plotted in GraphPad Prism.

2.21.5   Analysis of p-ubiquitin and optineurin immunostaining

The microscopy images from the p-ubiquitin and optineurin staining were analyzed in Fiji/ImageJ. The JaCoP plugin was used to quantify the Manders' colocalization coefficient of the p-ubiquitin/optineurin and the mitochondrial channel as described in Harbauer et al., 2022 and Hees & Harbauer, 2023. The quantification was performed on z-stack images. The βIII tubulin signal was used to identify intact

dendrites, which were straightened with a 20 pixel margin following maximum z-projection. The values of the Manders' coefficient were exported to Excel and plotted in GraphPad Prism.

2.21.6 Analysis of Parkin translocation

The microscopy images from the Parkin translocation imaging were analyzed in Fiji/ImageJ. The quantification was performed on z-stack images. Images of dendrites before and 30 min after AA treatment were straightened with a 20 pixel margin following maximum z-projection. The plot profile function of Fiji/ImageJ was used to generate plots of fluorescence intensity against the position along dendrites for the mitochondrial and the YFP-Parkin channel as previously described (Hees & Harbauer, 2023). Comparison of the intensities of the two channels allowed the identification of Parkin-positive mitochondria. When the intensity of a YFP-Parkin peak overlapping with a mitochondrial peak was at least twice as high as the baseline intensity level, the mitochondrion was counted as Parkin positive. The data were plotted in GraphPad Prism.

2.21.7 Analysis of the mitochondrial and lysosomal colocalization assay

The microscopy images from the mitochondrial and lysosomal colocalization assay were analyzed in Fiji/ImageJ. The 'Just Another Colocalization Plugin' (JaCoP) (Bolte & Cordelières, 2006) was used to quantify the Manders' colocalization coefficient of the mitochondrial and the lysosomal channel. The quantification was performed on z-stack images. For the cell body, a squared region containing the entire cell body was chosen and no maximum z-projection was done. The values of the Manders' coefficient were exported to Excel and plotted in GraphPad Prism.

2.21.8 Analysis of Ct values from RT-qPCR

The Ct values were obtained from the micPCR software version 2.8.10 (Bio Molecular Systems) and exported to Excel. The Ct values were analyzed using the $2^{-\Delta\Delta Ct}$ method as described previously (Hees & Harbauer, 2023). The *Pink1* transcript levels were first normalized to β-*actin* levels before normalization to the respective control treatment. For the RiboTag assay, the ribosome-associated *Pink1* transcript levels following the different treatments were normalized to their respective inputs as well as to the control condition where the control-GFP instead of the Cre-GFP virus was used. The final values were plotted in GraphPad Prism.

2.21.9 Analysis of mass spectrometry

The MaxQuant computational platform (version 2.0.1.0; standard settings) (Cox & Mann, 2008) was used to analyze the raw data as described previously (Hees & Harbauer, 2023). Briefly, the peak list was compared to the sequence of rat SYNJ2BP and the reviewed mouse proteome database. A precursor mass deviation and fragment mass deviation of 4.5 ppm and 20 ppm, respectively, was allowed. The default individual peptide mass tolerances by MaxQuant were used in the search and the match-between runs option was turned on. While phosphorylation on serine, threonine and tyrosine, methionine oxidation, N-terminal acetylation and deamidation on asparagine and glutamine were set as variable modifications, cysteine carbamidomethylation was defined as static modification. Furthermore, the label free quantification (LFQ) algorithm and the intensity-based absolute quantification (iBAQ) algorithm was used for quantification of proteins and for calculating the approximate abundances of the identified proteins, respectively.

3 RESULTS

The data and figures in the chapters 3.1 – 3.10, 3.12 and 3.17 – 3.19 are adapted from Hees & Harbauer, 2023 as well as from the unpublished data in the revised manuscript Hees et al., 2023 (under review).

3.1 AMPK signaling regulates *Pink1* mRNA localization to mitochondria

As mitochondria have a central role in neuronal energy metabolism and PINK1 is important for mitochondrial quality control, I aimed to investigate whether changes in energy metabolism affect the mitochondrial association of *Pink1* mRNA that was recently shown by our lab (Harbauer et al., 2022). I therefore treated primary mouse hippocampal neurons cultured *in vitro* with the AMP analog 5-aminoimidazole-4-carboxamide ribonucleoside (AICAR) and Compound C (CC), which have been shown to activate and inhibit AMPK, the master regulator of energy metabolism, respectively (Corton et al., 1995; Zhou et al., 2001). To examine the effect of AICAR and CC on mitochondrial *Pink1* mRNA localization, I visualized mitochondria by expression of mitochondrially-targeted mRaspberry and *Pink1* mRNA using the MS2/PP7-split Venus approach that has previously been established in our lab (Harbauer et al., 2022). Briefly, the gene of interest Pink1 is tagged with 12 alternating copies of MS2 and PP7 stem loops that are inserted downstream of the 3´ untranslated region (UTR). Additionally, a kinase-dead mutation (K219M) (Petit et al., 2005) was introduced to avoid effects caused by PINK1 overexpression. This construct is co-expressed together with the phage-derived MS2- and PP7-coat proteins that are fused each to one half of the yellow fluorescent protein Venus. As a result, only in the presence of *Pink1* mRNA the two halves of Venus are close enough to form a functional fluorescent protein, thereby visualizing *Pink1* mRNA in a background-free manner (B. Wu et al., 2014) (Fig. 8a). In the presence of the AMPK activator AICAR, mitochondrial *Pink1* mRNA localization was not affected, while inhibition of AMPK using CC resulted in a significant decrease of *Pink1* mRNA association with mitochondria. This effect was observed in the soma as well as in dendrites and was quantified using the Manders' colocalization coefficient (Fig. 8b-d). Through time-lapse imaging, I could show that *Pink1* mRNA dissociates from mitochondria as early as 20 min following CC treatment (Fig. 8e). Importantly, the decrease in colocalization was not caused by a general reduction in *Pink1* mRNA levels upon CC treatment (Fig. 8f). I also quantified the Manders' coefficient in a square within the soma before and after rotating the Venus channel (*Pink1* mRNA) 90 degrees. Under control conditions, the mitochondrial *Pink1* mRNA association was significantly increased compared to its rotated quantification, which represents the chance level. Upon CC treatment, however, the mitochondrial *Pink1* mRNA localization was comparable between the normal and the rotated quantification and therefore not different from chance level indicating a CC specific effect on *Pink1* mRNA localization (Fig. 8g).

_____
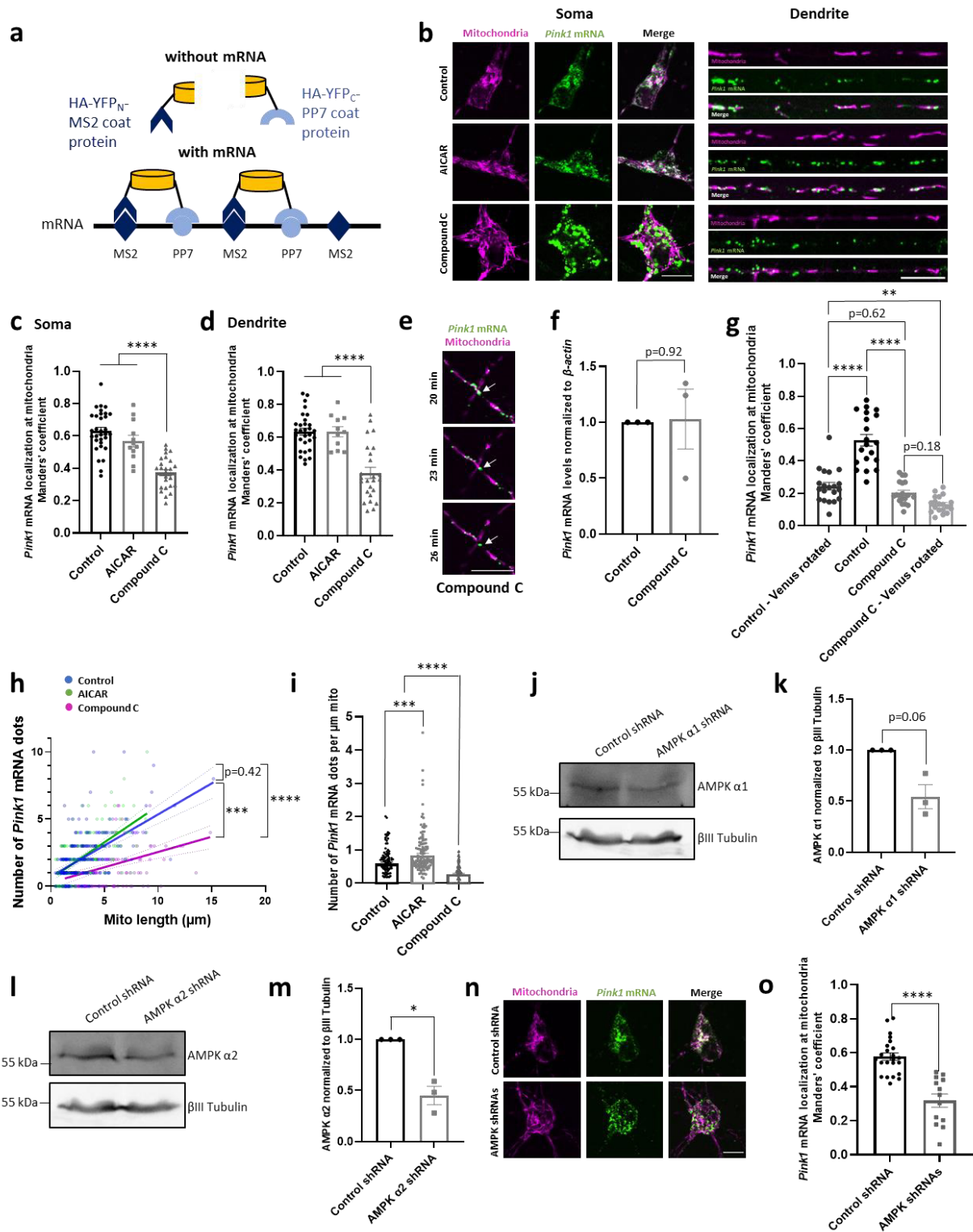
Figure 8: AMPK signaling regulates *Pink1* mRNA localization to mitochondria.
(a) Schematic illustrating the MS2/PP7-split Venus approach for mRNA imaging. **(b)** Representative images of *Pink1* mRNA as visualized using the MS2/PP7-split Venus approach and mRaspberry-labeled mitochondria following control, AICAR (1 mM, 2 h) or CC (20 µM, 2 h) treatment in the soma and in dendrites of primary hippocampal neurons. **(c)** Manders' coefficient based-quantification of the colocalization between the *Pink1* mRNA and the mitochondrial channel in the soma as in **b**. One-way ANOVA with Tukey's post hoc test; n = 21 - 38; p < 0.0001 (****). **(d)** Manders' coefficient-based quantification of the colocalization between the *Pink1* mRNA and the mitochondrial channel in dendrites as in **b**. One-way ANOVA with Tukey's post hoc test; n = 20 - 36; p < 0.0001 (****). **(e)** Representative images of *Pink1* mRNA as visualized using the MS2/PP7-split Venus

_____

approach and mRaspberry-labeled mitochondria 20 min, 23 min and 26 min after CC (20 µM) treatment. The white arrow indicates a *Pink1* mRNA cluster dissociating from mitochondria. **(f)** *Pink1* transcript levels normalized to β-*actin* transcript levels as assessed by RT-qPCR from primary cortical neurons treated with or without CC (20 µM, 2 h). Two-tailed Welch's t-test; n = 3. **(g)** Manders' coefficient-based quantification of the colocalization between the *Pink1* mRNA and the mitochondrial channel in primary hippocampal neurons treated without and with CC (20 µM, 2 h) as in **b**. The term 'Venus rotated' indicates that the *Pink1* mRNA channel underwent a 90-degree rotation, and this analysis was conducted within a square area of 10 by 10 µm in the soma. One-way ANOVA with Tukey's post hoc test; n = 19 - 20; $p < 0.01$ (**). **(h)** *Pink1* mRNA dot count plotted against the corresponding dendritic mitochondria length (µm) in primary hippocampal neurons following control, AICAR (1 mM, 2 h) or CC (20 µM, 2 h) treatment. Slope comparison among the three groups by simple linear regression and one-way ANOVA with Tukey's post hoc test; n = 140 - 218; $p < 0.001$ (***), $p < 0.0001$ (****). **(i)** Average number of *Pink1* mRNA dots per µm mitochondrion in dendrites of primary hippocampal neurons as in **h**. One-way ANOVA with Tukey's post hoc test; n = 167 - 310; $p < 0.0001$ (****). **(j)** Representative Western blot image of primary cortical neurons that were lentivirally transduced with control shRNA or shRNA targeting AMPKα1. **(k)** Densitometry analysis of the protein bands of AMPKα1 normalized to the corresponding βIII tubulin bands as in **j**. Two-tailed Welch's t-test; n = 3. **(l)** Representative Western blot image of primary cortical neurons that were lentivirally transduced with control shRNA or shRNA targeting AMPKα2. **(m)** Densitometry analysis of the protein bands of AMPKα2 normalized to the corresponding βIII tubulin bands as in **l**. Two-tailed Welch's t-test; n = 3; $p < 0.05$ (*). **(n)** Representative images of *Pink1* mRNA as visualized using the MS2/PP7-split Venus approach and mRaspberry-labeled mitochondria in the soma of primary hippocampal neurons overexpressing either control shRNA or shRNAs targeting AMPKα1 and α2. **(o)** Manders' coefficient-based quantification of the colocalization between the *Pink1* mRNA and the mitochondrial channel in the soma as in **n**. Two-tailed student's t-test; n = 13 - 23; $p < 0.0001$ (****).

All data are presented as mean ± SEM. Data points correspond to biological replicates (**f,k,m**), single cells (**c,d,g,o**) or single mitochondria (**h,i**) obtained from ≥3 biological replicates. Scale bars, 10 µm (adapted from Hees & Harbauer, 2023 and from the unpublished data in the revised manuscript Hees et al., 2023 (under review)).

Since AMPK is known to affect mitochondrial morphology by promoting mitochondrial fission (Ducommun et al., 2015; Toyama et al., 2016), I also correlated the number of *Pink1* mRNA dots to the mitochondrial length. In line with the results in Fig. 8b-d, CC treatment led to a significant reduction in the number of *Pink1* mRNA dots per µm mitochondrion (Fig. 8h,i) suggesting that the observed effect is independent of changes in mitochondrial morphology. As CC also inhibits other kinases apart from AMPK (Dasgupta & Seibel, 2018), I confirmed its effect by knockdown of both catalytic subunits of AMPK using short hairpin RNAs (shRNAs) (Didier et al., 2018). The AMPK α1 and α2 shRNAs led to a 60 % and 50 % reduction in expression, respectively (Fig. 8j-m). In line with the CC effect, I observed a reduced mitochondrial *Pink1* mRNA localization in the soma upon AMPK knockdown using both shRNAs (Fig. 8n,o).

Recently, *Cox4i* and *Atp5f1*β mRNA have been shown to localize to mitochondria, albeit to a lesser extent than *Pink1* mRNA (Harbauer et al., 2022). Interestingly, CC-mediated AMPK inhibition reduced mitochondrial association of *Atp5f1*β but not *Cox4i* mRNA (Fig. 9a-d) suggesting that, in contrast to *Cox4i*, mitochondrial *Atp5f1*β transcript tethering is regulated by a similar mechanism as *Pink1* mRNA binding. This is in line with the finding that only *Atp5f1*β and *Pink1* but not *Cox4i* mRNA were co-isolated with the RNA-binding protein SYNJ2a (Harbauer et al., 2022). *Pink1* mRNA is known to localize to mitochondria via binding to SYNJ2a, which is tethered to mitochondria via the mitochondrial anchor

protein SYNJ2BP (Harbauer et al., 2022). Therefore, I tested whether the AMPK-mediated regulation of mitochondrial *Pink1* mRNA localization is also dependent on SYNJ2a. CC treatment of neurons overexpressing a control protein (snap-tag) fused to the transmembrane domain of SYNJ2BP led to reduced mitochondrial *Pink1* mRNA localization, while overexpression of a SYNJ2a WT construct that is mitochondrially targeted by the SYNJ2BP transmembrane domain even in the absence of SYNJ2BP (SYNJ2mito) retained *Pink1* mRNA at mitochondria (Fig. 9e,f). In contrast, overexpressing an RNA-binding deficient mutant of SYNJ2mito VQL/AAA (Harbauer et al., 2022) did not prevent the CC-mediated dissociation of *Pink1* mRNA from mitochondria suggesting that the AMPK-dependent regulation of mitochondrial *Pink1* mRNA localization is also dependent on SYNJ2a. Taken together, AMPK signaling positively regulates *Pink1* mRNA association with mitochondria potentially by influencing the SYNJ2BP-SYNJ2a tethering complex.
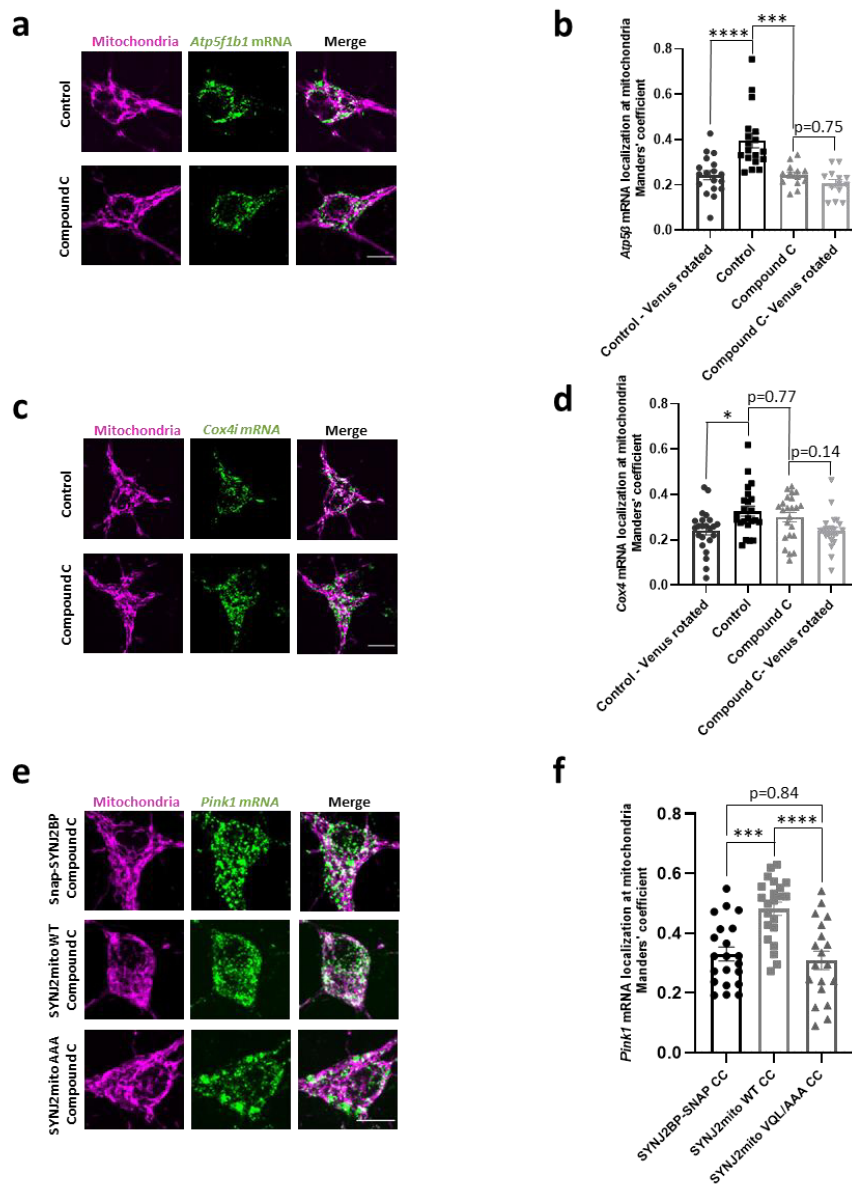
Figure 9: Regulation of *Atp5b* and *Cox4i* mRNA localization as well as dependence on SYNJ2a.
(a) Representative images of *Atp5b* mRNA as visualized using the MS2/PP7-split Venus approach and mRaspberry-labeled mitochondria with or without CC (20 μM, 2 h) treatment in the soma of primary hippocampal neurons. **(b)** Manders' coefficient-based quantification of the colocalization between the *Atp5b* mRNA and the mitochondrial channel as in **a**. The term 'Venus rotated' indicates that the *Atp5b* mRNA channel underwent a 90-degree rotation, and this analysis was conducted within a square area of 10 by 10 μm in the soma. One-way ANOVA with Tukey's post hoc test; n = 13 - 18; $p < 0.001$ (***), $p < 0.0001$ (****). **(c)** Representative images of *Cox4i* mRNA as visualized using the MS2/PP7-split Venus approach and mRaspberry-labeled mitochondria with or without CC (20 μM, 2 h) treatment in the soma of primary hippocampal neurons. **(d)** Manders' coefficient-based quantification of the colocalization between the *Cox4i* mRNA and the mitochondrial channel as in **c**. The term 'Venus rotated' indicates that the *Cox4i* mRNA channel underwent a 90-degree rotation, and this analysis was conducted within a square area of 10 by 10 μm in the soma. One-way ANOVA with Tukey's post hoc test; n = 23; $p < 0.05$ (*). **(e)** Representative images of *Pink1* mRNA as visualized using the MS2/PP7-split Venus approach and mRaspberry-labeled mitochondria in the soma of primary hippocampal neurons overexpressing either SYNJ2BP-Snap, SYNJ2mito WT or SYNJ2mito VQL/AAA following CC (20 μM, 2 h) treatment. **(f)** Manders' coefficient-based quantification of the colocalization between the *Pink1* mRNA and the mitochondrial channel in the soma as in **e**. One-way ANOVA with Tukey's post hoc test; n = 19 - 22; $p < 0.001$ (***), $p < 0.0001$ (****).

All data are presented as mean ± SEM. Data points correspond to single cells obtained from ≥3 biological replicates (**b,d,f**). Scale bars, 10 μm (adapted from the unpublished data in the revised manuscript Hees et al., 2023 (under review)).

3.2 AMPK signaling regulates the interaction between SYNJ2BP and SYNJ2

In order to better understand the mechanism underlying the AMPK-mediated mitochondrial *Pink1* mRNA association, I investigated the effect of AMPK signaling on the interaction between the mitochondrial tethering protein SYNJ2BP and the RNA binding domain-containing protein SYNJ2 by performing a proximity ligation assay (PLA) using antibodies against the endogenous proteins SYNJ2BP and SYNJ2 (Harbauer et al., 2022). Briefly, the so-called PLA probes, which are oligonucleotide-coupled secondary antibodies, bind to the primary antibodies. If the PLA probes are in close proximity, hybridizing connector oligos attach to them, which are then ligated resulting in a closed, circular DNA template. This is amplified by a DNA polymerase using the PLA probe as a primer. Finally, complementary, fluorescently-labeled oligos bind to the amplified sequences thereby visualizing protein interaction as discrete spots (PLA puncta) (Fig. 10a). In line with the decrease of mitochondrial *Pink1* mRNA association upon AMPK inhibition (Fig. 8b-d), CC reduced the interaction between SYNJ2BP and SYNJ2 as quantified by the number of PLA puncta per cell body (Fig. 10b-f). When I performed the treatments for the PLA experiment in the imaging medium Hibernate E, AICAR treatment had no effect on the interaction of the two proteins (Fig. 10b-d) consistent with the results from the *Pink1* mRNA localization (Fig. 8b-d), where I also used Hibernate E medium. However, when performing the treatments for the PLA experiment in the neuronal culture medium, B27-supplemented Neurobasal, instead of changing it to Hibernate E imaging medium, addition of AICAR resulted in an increased number of PLA puncta compared to the control condition (Fig. 10e,f). This was

caused by a drop in the number of baseline puncta (compare Fig. 10d and f). Importantly, the observed changes in the interaction were not due to altered expression of SYNJ2BP and SYNJ2. Neither AICAR nor CC significantly affected the protein levels (Fig. 10g-j). Taken together, AMPK signaling positively regulates the interaction between SYNJ2BP and SYNJ2 and therefore mitochondrial *Pink1* mRNA association. Furthermore, the AMPK-dependent mechanism seems to be responsive to components that differ between the two media Hibernate E and B27-supplemented Neurobasal.

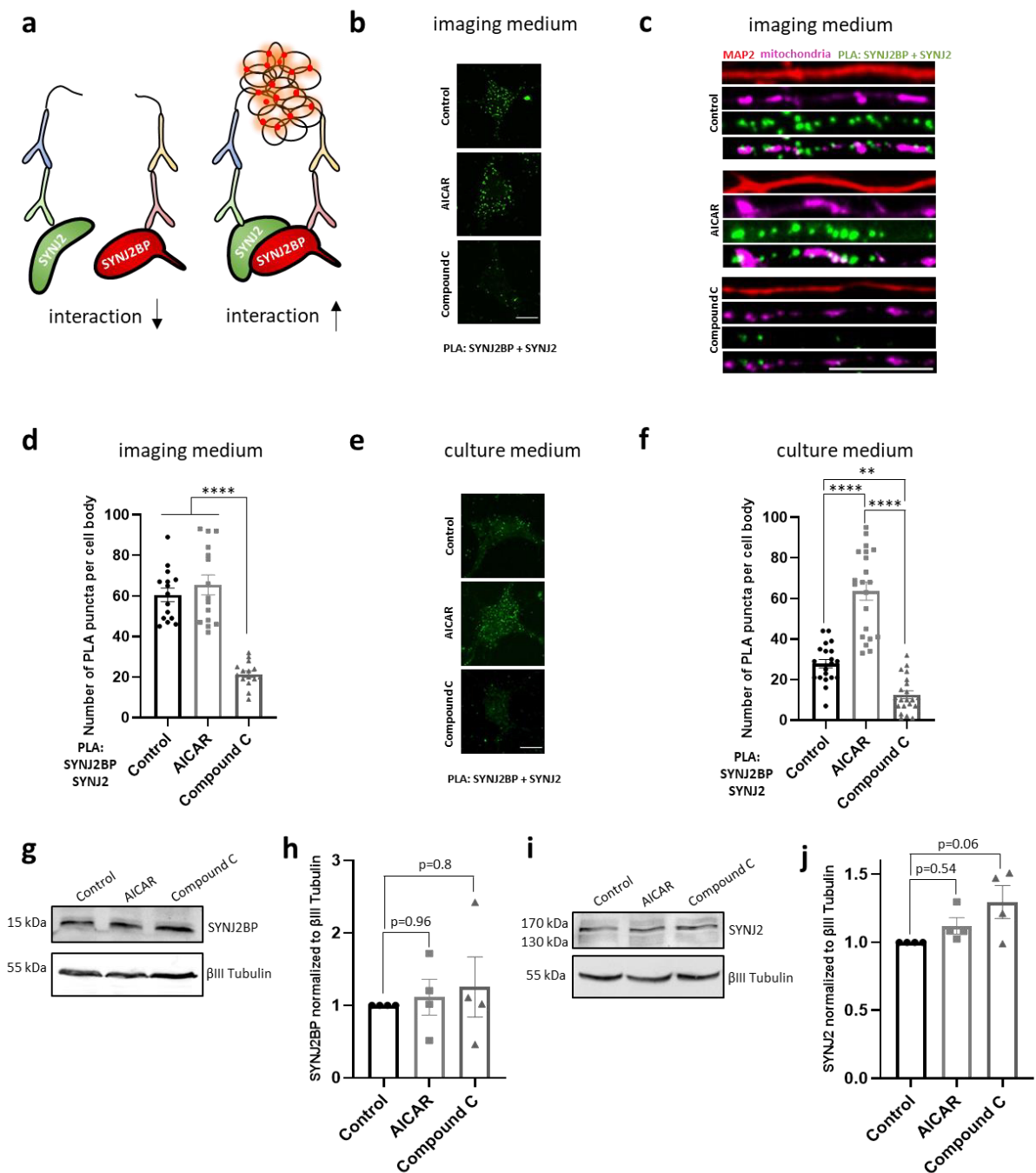**Figure 10: AMPK signaling regulates the interaction between SYNJ2BP and SYNJ2.**
(a) Schematic illustrating the proximity ligation assay (PLA) to visualize the interaction between SYNJ2BP and SYNJ2. **(b)** Representative soma images of primary hippocampal neurons exhibiting the PLA signal for interaction of SYNJ2BP and SYNJ2 following control, AICAR (1 mM, 2 h) or CC (20 µM, 2 h) treatment in imaging medium

_____

(Hibernate E medium). **(c)** Representative images of MAP2-positive dendrites of primary hippocampal neurons exhibiting the PLA signal for interaction of SYNJ2BP and SYNJ2 following control, AICAR (1 mM, 2 h) or CC (20 µM, 2 h) treatment in imaging medium (Hibernate E medium). **(d)** Number of PLA puncta per cell body as in **b**. One-way ANOVA with Tukey's post hoc test; n = 15; p < 0.0001 (****). **(e)** Representative soma images of primary hippocampal neurons exhibiting the PLA signal for interaction of SYNJ2BP and SYNJ2 following control, AICAR (1 mM, 2 h) or CC (20 µM, 2 h) treatment in culture medium (B27-supplemented Neurobasal). **(f)** Number of PLA puncta per cell body as in **e**. One-way ANOVA with Tukey's post hoc test; n = 21; p < 0.01 (**); p < 0.0001 (****). **(g)** Representative Western blot image of primary cortical neurons following control, AICAR (1 mM, 2 h) or CC (20 µM, 2 h) treatment. **(h)** Densitometry analysis of the protein bands of SYNJ2BP normalized to the corresponding βIII tubulin bands as in **g**. One-way ANOVA with Tukey's post hoc test; n = 4. **(i)** Representative Western blot image of primary cortical neurons following control, AICAR (1 mM, 2 h) or CC (20 µM, 2 h) treatment. **(j)** Densitometry analysis of the protein bands of SYNJ2 normalized to the corresponding βIII tubulin bands as in **i**. One-way ANOVA with Tukey's post hoc test; n = 4.

All data are presented as mean ± SEM. Data points correspond to biological replicates (**h,j**) or single cells obtained from ≥3 biological replicates (**d,f**). Scale bars, 10 µm (adapted from Hees & Harbauer, 2023 and from the unpublished data in the revised manuscript Hees et al., 2023 (under review)).

3.3 Insulin signaling inhibits AMPK in primary neurons

The growth factor and peptide hormone insulin is an important signaling molecule, which is absent in the imaging medium Hibernate E but present in the neuronal supplement B27. In line with my observation that AMPK activity seems to be reduced in neurons cultured in B27-supplemented Neurobasal containing insulin, it has already been shown that insulin inhibits AMPK activity. Mechanistically, insulin-mediated AKT activation results in an inhibitory phosphorylation in the catalytic subunit of AMPK (Berggreen et al., 2009; Dagon et al., 2012; Horman et al., 2006; Kovacic et al., 2003; J. Ning et al., 2011; Soltys et al., 2006; Valentine et al., 2014). To confirm the inhibitory effect of insulin on AMPK activity in neurons, I used a Förster Resonance Energy Transfer (FRET)-based AMPK activity sensor (Konagaya et al., 2017) (Fig. 11a). Briefly, the FRET sensor contains a super enhanced cyan fluorescent protein (SECFP) and a yellow fluorescent protein for energy transfer (Ypet) as donor and acceptor, respectively. Inbetween the two fluorescent proteins, there is an AMPK substrate sequence that can be phosphorylated by activated AMPK thereby leading to a conformational change within the sensor and as a result FRET occurs. To measure the changes in AMPK activity, I performed fluorescence lifetime imaging (FLIM). Compared to traditional intensity-based FRET techniques, FLIM measurements are insensitive to different expression levels of the sensor, bleaching of the sensor as well as bleed-through artifacts as only the fluorescence lifetime of the donor molecule is determined (Periasamy et al., 2015). In the context of FRET, energy is transferred from the donor to the acceptor molecule leading to quenching of the donor fluorescence. As a result, the fluorescence lifetime of the donor decreases indicating an increased AMPK activity. The addition of increasing insulin concentrations to Hibernate E medium ranging from 50 nm to 1 µM led to a dose-dependent inhibition of AMPK activity as quantified by an increased lifetime of the donor (Fig. 11b). This insulin-mediated

_____

inhibition of AMPK was prevented by addition of inhibitors against the IR (GSK1904529A), PI3K (Wortmannin) and AKT (AKT inhibitor VIII) (Fig. 11c,d). Taken together, insulin signaling inhibits AMPK in primary neurons via activation of PI3K and AKT.
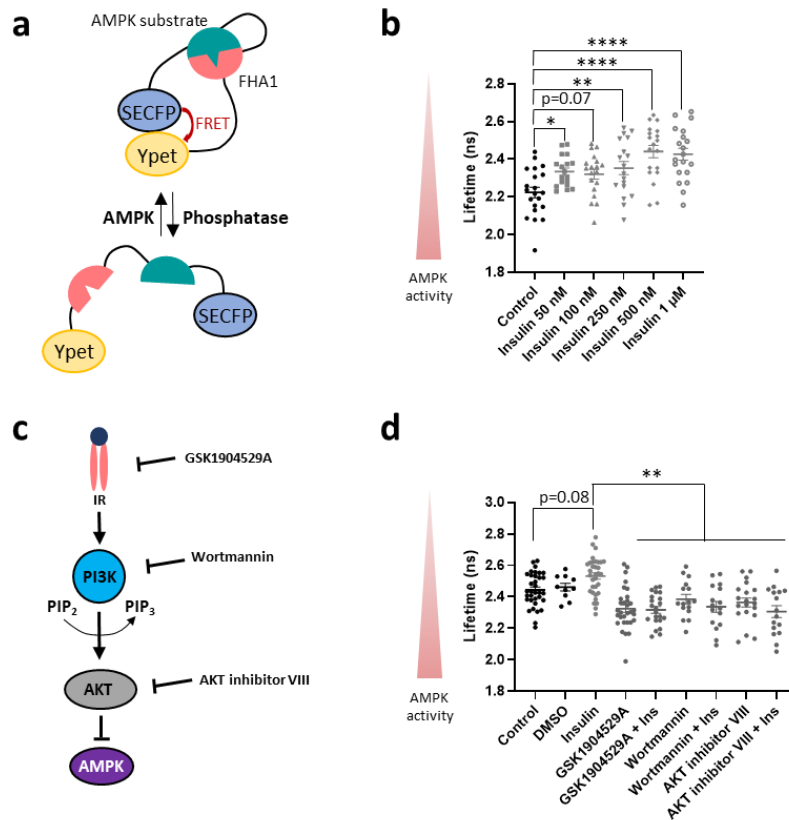
Figure 11: Insulin signaling inhibits AMPK in primary neurons.
(a) Schematic illustrating the FRET-based AMPK sensor to measure AMPK activity. **(b)** Analysis of AMPK activity by performing fluorescence lifetime imaging of the FRET-based AMPK activity sensor donor in primary hippocampal neurons exposed to increasing insulin concentrations for 1 h. One-way ANOVA with Dunnett's post hoc test; n = 18 - 21; $p < 0.05$ (*), $p < 0.01$ (**), $p < 0.0001$ (****). **(c)** Schematic illustrating the insulin signaling pathway. Insulin binding to IR results in activation of PI3K, which converts PIP_2 to PIP_3. PIP_3 in turn stimulates AKT, which phosphorylates and thereby inhibits AMPK. GSK1904529A, Wortmannin and the AKT inhibitor VIII inhibit the IR, PI3K and AKT, respectively. **(d)** Analysis of AMPK activity by performing fluorescence lifetime imaging of the FRET-based AMPK activity sensor donor in primary hippocampal neurons treated with insulin in the presence or absence of inhibitors targeting the insulin signaling pathway: IR inhibitor GSK1904529A (1 μM, 2 h); PI3K inhibitor Wortmannin (1 μM, 2 h) and AKT inhibitor VIII (10 μM, 2 h). One-way ANOVA with Tukey's post hoc test; n = 10 - 34; $p < 0.01$ (**).

All data are presented as mean ± SEM. Data points correspond to single cells obtained from ≥3 biological replicates (**b,d**) (adapted from Hees & Harbauer, 2023).

3.4 Insulin signaling regulates *Pink1* mRNA localization to mitochondria

To investigate whether insulin also reduces mitochondrial *Pink1* mRNA association similar to CC treatment, I again performed *Pink1* mRNA imaging using the MS2/PP7-split Venus approach. Addition of insulin to the Hibernate E imaging medium significantly reduced mitochondrial *Pink1* mRNA

_____

localization (Fig. 12a-c) both in the soma and in dendrites reflecting the CC effect (Fig. 8b-d). The insulin-mediated impact was prevented when the IR (Fig. 12a-c), PI3K or AKT were inhibited (Fig. 12d,e). This confirms the relevance of the insulin signaling pathway in regulating mitochondrial *Pink1* mRNA tethering.

Figure 12: Insulin signaling regulates *Pink1* mRNA localization to mitochondria.
(a) Representative images of *Pink1* mRNA as visualized using the MS2/PP7-split Venus approach and mRaspberry-labeled mitochondria following control or insulin (500 nM, 1 h) treatment in the presence or absence of the IR inhibitor GSK1904529A in the soma and in dendrites of primary hippocampal neurons. **(b)** Manders' coefficient-based quantification of the colocalization between the *Pink1* mRNA and the mitochondrial channel in the soma as in **a**. One-way ANOVA with Tukey's post hoc test; n = 22 - 29; $p < 0.0001$ (****). **(c)** Manders' coefficient-based quantification of the colocalization between the *Pink1* mRNA and the mitochondrial c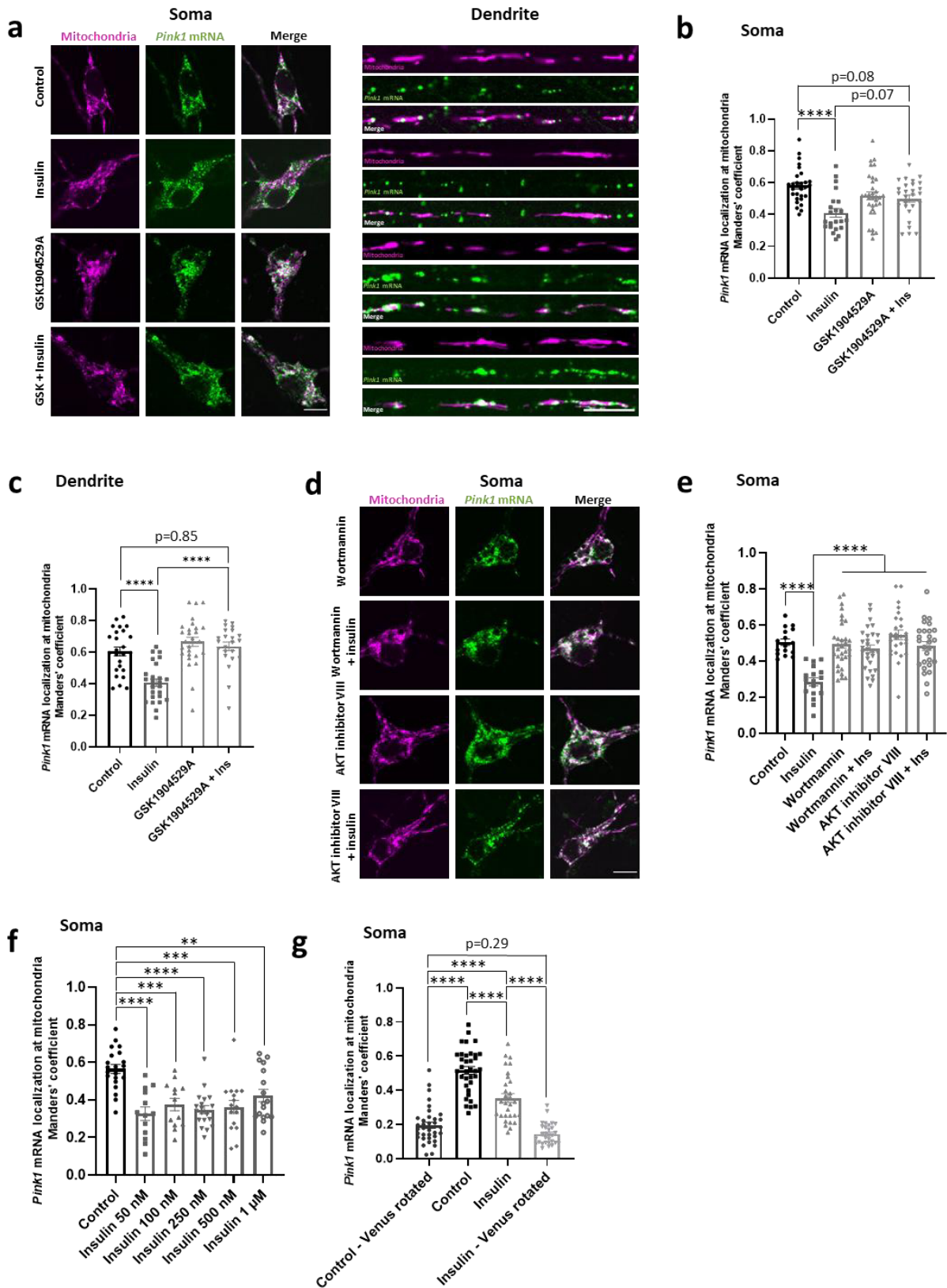hannel in dendrites as in **a**. One-way ANOVA with Tukey's post hoc test; n = 23 - 28; $p < 0.0001$ (****). **(d)** Representative images of *Pink1* mRNA as visualized using the MS2/PP7-split Venus approach and mRaspberry-labeled mitochondria following control or insulin (500 nM, 1 h) treatment in the presence of the PI3K inhibitor Wortmannin (1 µM, 2 h) or the AKT inhibitor VIII (10 µM, 2 h) in the soma of primary hippocampal neurons. **(e)** Manders' coefficient-based quantification of the colocalization between the *Pink1* mRNA and the mitochondrial channel in the soma as in **d**. One-way ANOVA with Tukey's post hoc test; n = 16 - 32; $p < 0.0001$ (****). **(f)** Manders' coefficient-based quantification of the colocalization between the *Pink1* mRNA and the mitochondrial channel in the soma of primary hippocampal neurons exposed to increasing insulin concentrations for 1 h. One-way ANOVA with Dunnett's post hoc test; n = 13 - 21; $p < 0.01$ (**); $p < 0.001$ (***), $p < 0.0001$ (****). **(g)** Manders' coefficient-based quantification of the colocalization between the *Pink1* mRNA and the mitochondrial channel in primary hippocampal neurons treated without and with insulin (500 nM, 1 h) as in **a**. The term 'Venus rotated' indicates that the *Pink1* mRNA channel underwent a 90-degree rotation, and this analysis was conducted within a square area of 10 by 10 µm in the soma. One-way ANOVA with Tukey's post hoc test; n = 30 - 35; $p < 0.0001$ (****).

All data are presented as mean ± SEM. Data points correspond to single cells obtained from ≥3 biological replicates (**b,c,e,f,g**). Scale bars, 10 µm (adapted from Hees & Harbauer, 2023).

As physiological insulin levels in the brain are in the low nanomolar range (Gray & Barrett, 2018), I also tested lower insulin concentrations. Importantly, the insulin-mediated effect on *Pink1* mRNA association was still present using a concentration of 50 nM (Fig. 12f) indicating that this could also happen physiologically in the brain. Furthermore, addition of insulin resulted in a partial reduction of mitochondrial *Pink1* mRNA localization when compared to the rotated quantification of the Manders' coefficient (Fig. 12g), consistent with a more physiological inhibition of AMPK.

3.5 Insulin signaling regulates the interaction between SYNJ2BP and SYNJ2

To test whether insulin signaling also affects the interaction between SYNJ2BP and SYNJ2, I performed the PLA in the B27-supplemented neuronal culture medium with and without insulin. Indeed, whereas insulin withdrawal for 2 h led to an enhanced interaction as quantified by an increased number of PLA puncta per soma, addition of 500 nM insulin for 1 h significantly reduced the interaction (Fig. 13a-c). The insulin-mediated effect was dependent on the IR since co-treatment with an inhibitor prevented this effect (Fig. 13a,c). Importantly, the observed changes in the interaction were not due to altered expression of SYNJ2BP and SYNJ2. Neither insulin withdrawal nor addition of insulin significantly affected the protein levels (Fig. 13d-g). Taken together, these findings indicate that insulin-mediated activation of IR signaling, PI3K and AKT negatively regulates mitochondrial *Pink1* mRNA association due to a decreased interaction between SYNJ2BP and SYNJ2, most likely via inhibition of AMPK.
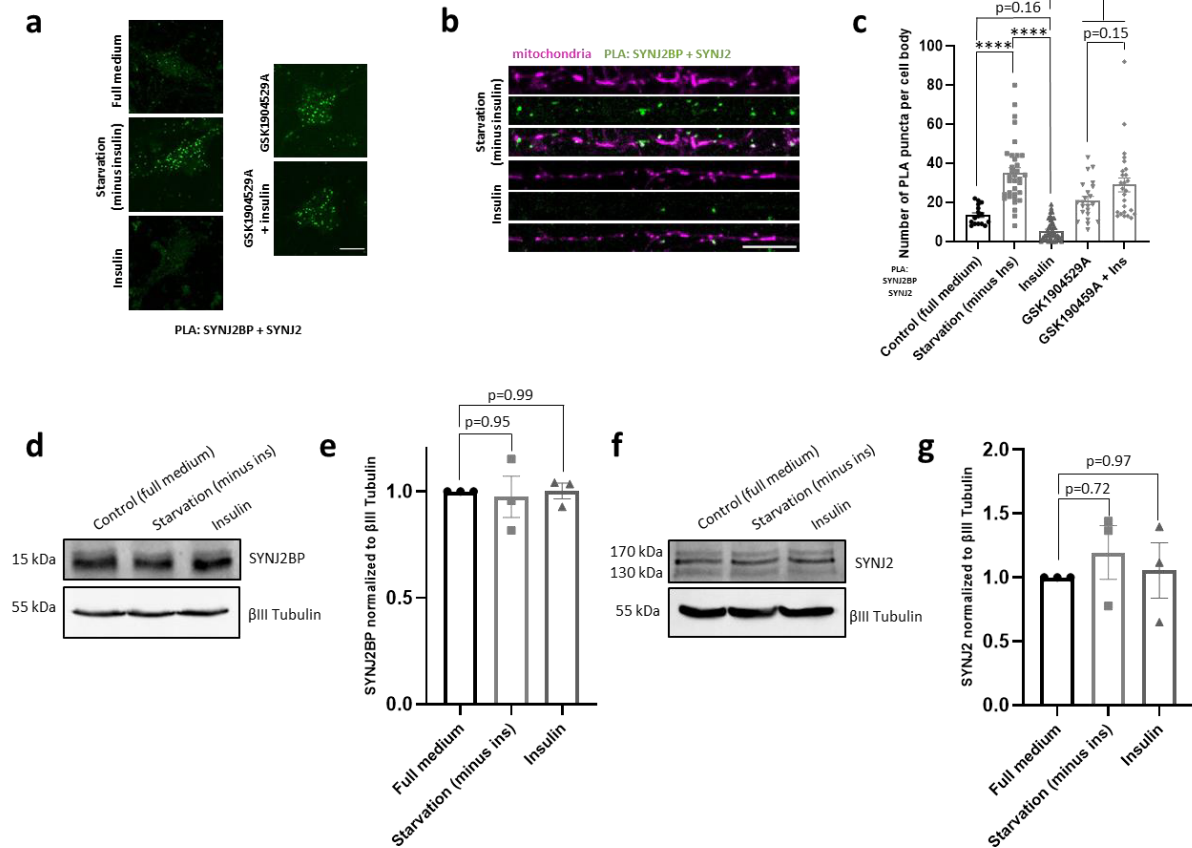
Figure 13: Insulin signaling regulates the interaction between SYNJ2BP and SYNJ2 upstream of AMPK.
(a) Representative soma images of primary hippocampal neurons exhibiting the PLA signal for interaction of SYNJ2BP and SYNJ2 in full culture medium (B27-supplemented Neurobasal), after insulin withdrawal (2 h) or after addition of insulin (500 nM, 1 h) in the presence or absence of the IR inhibitor GSK1904529A (1 µM, 2 h). **(b)** Representative dendrite images of primary hippocampal neurons exhibiting the PLA signal for interaction of SYNJ2BP and SYNJ2 after insulin withdrawal (2 h) or after addition of insulin (500 nM, 1 h). **(c)** Number of PLA puncta per cell body as in **a**. One-way ANOVA with Tukey's post hoc test; n = 16 - 45; p < 0.0001 (****). **(d)** Representative Western blot image of primary cortical neurons following control, insulin withdrawal (2 h) or addition of insulin (500 nM, 1 h). **(e)** Densitometry analysis of the protein bands of SYNJ2BP normalized to the corresponding βIII tubulin bands as in **d**. One-way ANOVA with Tukey's post hoc test; n = 3. **(f)** Representative Western blot image of primary cortical neurons following control, insulin withdrawal (2 h) or addition of insulin (500 nM, 1 h). **(g)** Densitometry analysis of the protein bands of SYNJ2 normalized to the corresponding βIII tubulin bands as in **f**. One-way ANOVA with Tukey's post hoc test; n = 3.

All data are presented as mean ± SEM. Data points correspond to biological replicates (**e,g**) or single cells obtained from ≥3 biological replicates (**c**). Scale bars, 10 µm (adapted from Hees & Harbauer, 2023 and from the unpublished data in the revised manuscript Hees et al., 2023 (under review)).

3.6 AMPK phosphorylates SYNJ2BP in its PDZ domain *in vitro*

As I observed that the interaction between SYNJ2BP and SYNJ2 is positively regulated by AMPK, I wondered whether one of the two proteins might be a direct phosphorylation target of AMPK. In line with that idea, a peptide of SYNJ2BP phosphorylated at serine 21 (S21) has been detected in a high-throughput phospho-proteomics screen (Mertins et al., 2014) and its sequence matches the consensus

motif of AMPK (Steinberg & Hardie, 2022) (Fig. 14a). To investigate whether SYNJ2BP indeed is a substrate of AMPK, I purified the cytosolic domain of *rat* SYNJ2BP from *E.Coli* in collaboration with the protein core facility at the Max Planck Institute of Biochemistry, Martinsried, Germany and performed an *in vitro* kinase assay using recombinant active AMPK. Due to the lack of a phospho-specific SYNJ2BP antibody, I analyzed the kinase assay using the Zn^{2+}-Phos-Tag approach (Kinoshita et al., 2006), which changes the electrophoretic mobility of phosphorylated proteins compared to their non-phosphorylated form. As the SYNJ2BP protein purified from *E.Coli* was already phosphorylated, I did a pre-treatment using calf intestinal phosphatase (CIP) before performing the kinase assay using AMPK (Fig. 14b). Following addition of active AMPK to the reaction, I could indeed observe a slower migrating species of SYNJ2BP. Importantly, this band was not present when the phospho-ablative form of SYNJ2BP containing an alanine instead of serine at position 21 (S21A) was used (Fig. 14c). To examine whether endogenous AMPK activity was also sufficient to induce SYNJ2BP phosphorylation I replaced the recombinant AMPK with lysates from cortical neurons cultured either in the absence of the B27 supplement (and therefore insulin) or treated with the AMPK activator AICAR. In line with the previous observation, I detected a slower migrating, phosphorylated SYNJ2BP species upon treatment of SYNJ2BP WT with B27-starved or AICAR-treated lysates but not when the phospho-ablative SYNJ2BP S21A mutant was used (Fig. 14d). Taken together, this suggests that SYNJ2BP is a novel substrate of AMPK.
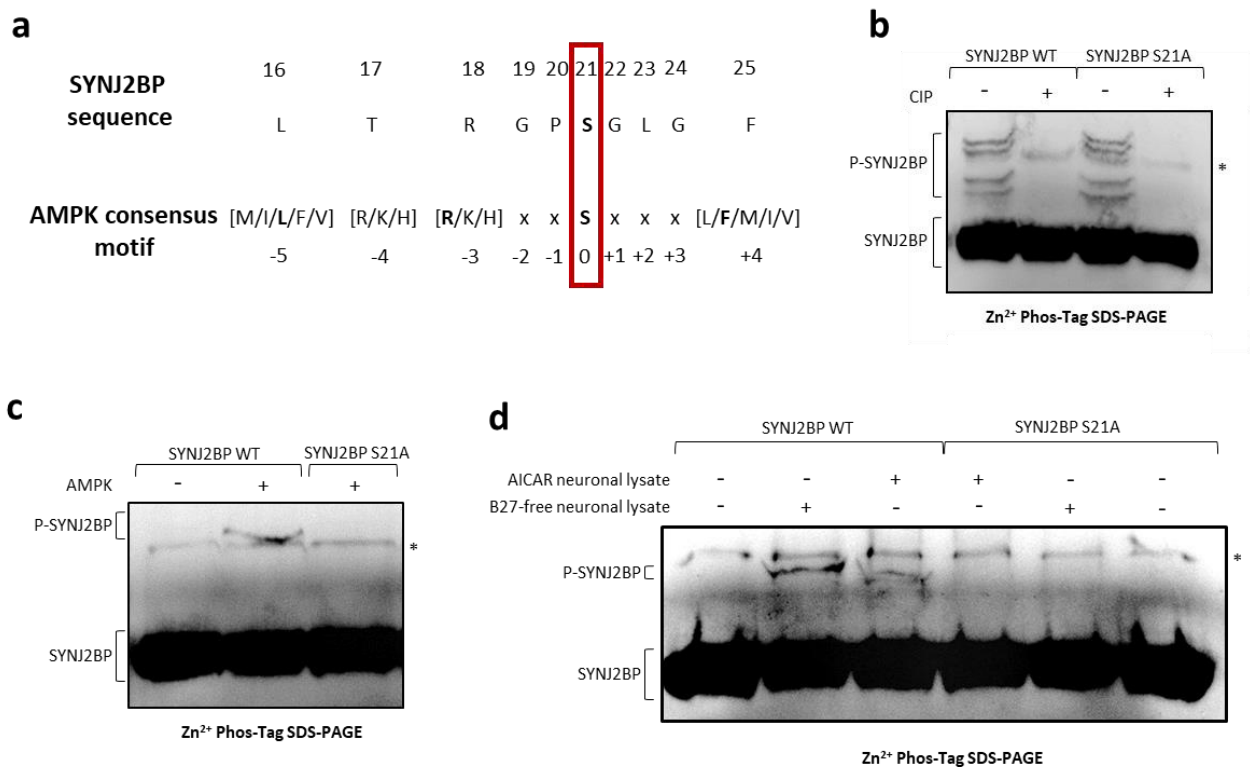
Figure 14: AMPK phosphorylates SYNJ2BP in its PDZ domain *in vitro*.
(a) Illustration depicting the AMPK recognition motif and the sequence of SYNJ2BP encompassing the suggested phosphorylation site S21. **(b)** Recombinant SYNJ2BP WT and S21A, respectively, were subjected to dephosphorylation using CIP and analyzed using Zn^{2+}-PhosTag SDS-PAGE. Note the presence of slower moving entities that vanish following CIP treatment indicating phosphorylated variants of SYNJ2BP. The asterisk (*) marks an unspecific band that does not respond to CIP treatment. **(c)** *In vitro* kinase assay using recombinant SYNJ2BP WT and S21A, respectively, as well as AMPK was analyzed on a Zn^{2+}-PhosTag SDS-PAGE. Note the presence of slower moving entities only in the presence of AMPK and SYNJ2BP WT but not S21A. The asterisk (*) marks an unspecific band observed in all samples. **(d)** *In vitro* phosphorylation assay using recombinant SYNJ2BP WT and S21A, respectively, as well as lysates from cortical neurons cultured in the absence of the B27 supplement (2 h) or in the presence of AICAR (1 mM, 2 h). The samples were analyzed on a Zn^{2+}-PhosTag SDS-PAGE. Note the presence of slower moving entities only in the presence of B27-starved or AICAR-treated lysates and SYNJ2BP WT but not S21A. The asterisk (*) marks an unspecific band observed in all samples (adapted from Hees & Harbauer, 2023).

3.7 AMPK phosphorylates SYNJ2BP in its PDZ domain in primary neurons

To investigate whether AMPK-dependent phosphorylation of SYNJ2BP is also detectable in living neurons, I performed phospho-peptide enrichment followed by mass spectrometry (phospho-MS) in collaboration with the mass spectrometry facility at the Max Planck Institute of Biochemistry, Martinsried, Germany. As endogenous SYNJ2BP is a very low abundant protein in cultured cortical neurons (Fig. 15a), I lentivirally overexpressed myc-tagged *rat* SYNJ2BP (Fig. 15b). Upon overexpression, I was able to detect a phosphorylated SYNJ2BP peptide, which indeed confirmed phosphorylation of SYNJ2BP at S21 (Fig. 15c).
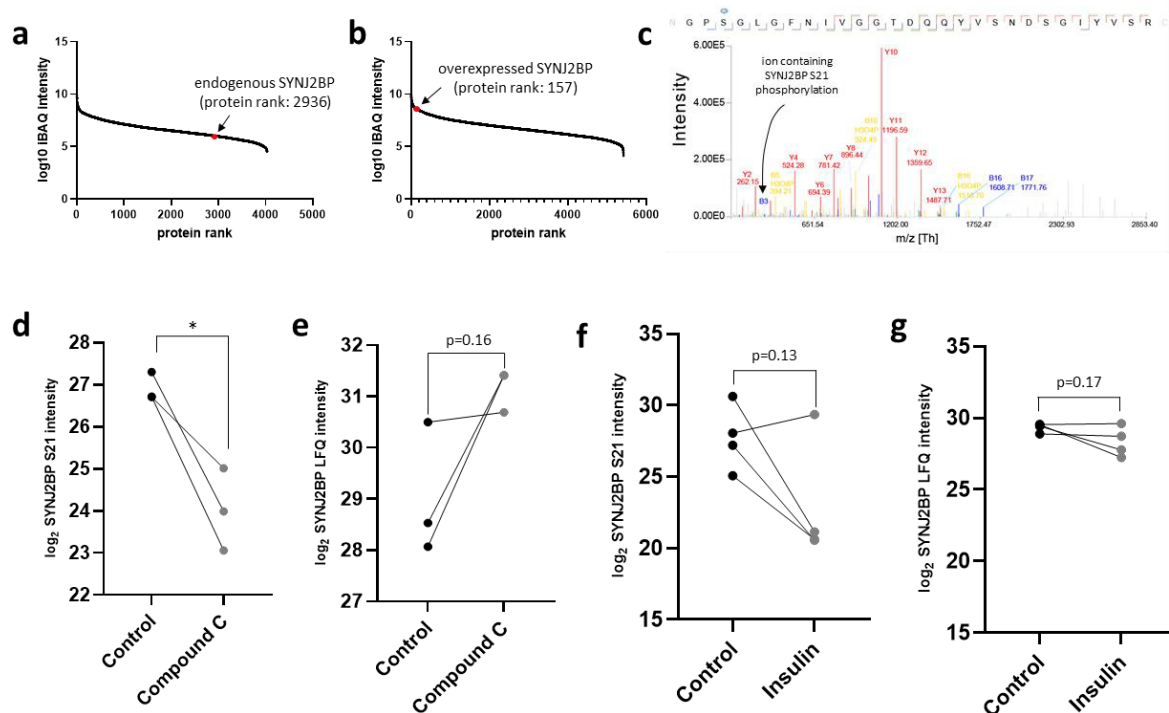
Figure 15: AMPK phosphorylates SYNJ2BP in its PDZ domain in primary neurons.
(a-b) The plots depict the relationship between the quantified proteins, obtained through LC MS/MS analysis, and the log10-transformed intensity-based absolute quantification (iBAQ) values. The iBAQ values serve as an estimate of the molar abundance of proteins in the sample. Note that the endogenous SYNJ2BP in cortical neurons **(a)** exhibits a relatively low protein rank, which can be enhanced by lentiviral overexpression of myc-tagged SYNJ2BP WT **(b)**. **(c)** Annotated MS/MS spectrum of the indicated SYNJ2BP peptide from primary cortical neurons lentivirally overexpressing myc-tagged SYNJ2BP WT. Note that the ion B3 is indicative of the phosphorylation of SYNJ2BP at the S21 site. **(d)** Log2-transformed intensity of SYNJ2BP S21 obtained through phospho-peptide enrichment followed by LC MS/MS analysis in primary cortical neurons overexpressing myc-tagged SYNJ2BP WT. The neurons were grown in insulin-free medium (2 h) and treated with or without CC (20 µM, 2 h). Two-tailed student's t-test; n = 3; p < 0.05 (*). **(e)** Log2-transformed LFQ intensity of SYNJ2BP analyzed through LC MS/MS in primary cortical neurons lentivirally overexpressing myc-tagged SYNJ2BP WT. The neurons were grown in insulin-free medium (2 h) and treated with or without CC (20 µM, 2 h) as in **d**. Two-tailed student's t-test; n = 3. **(f)** Log2-transformed intensity of SYNJ2BP S21 obtained through phospho-peptide enrichment followed by LC MS/MS analysis in primary cortical neurons overexpressing myc-tagged SYNJ2BP WT. The neurons were grown in insulin-free medium (2 h) and treated with or without insulin (500 nM, 1 h). Two-tailed student's t-test; n = 4. **(g)** Log2-transformed LFQ intensity of SYNJ2BP analyzed through LC MS/MS in primary cortical neurons lentivirally overexpressing myc-tagged SYNJ2BP WT. The neurons were grown in insulin-free medium (2 h) and treated with or without insulin (500 nM, 1 h) as in **f**. Two-tailed student's t-test; n = 4.

All data are presented as mean ± SEM. Data points correspond to biological replicates (**d,e,f,g**) (adapted from Hees & Harbauer, 2023 and from the unpublished data in the revised manuscript Hees et al., 2023 (under review)).

Consistent with my *in vitro* finding, primary cortical neurons cultured in the absence of insulin for 2 h and simultaneously treated with the AMPK inhibitor CC showed a decreased intensity for the phosphorylated SYNJ2BP peptide (Fig. 15d). Importantly, the total levels of SYNJ2BP did not decrease following CC treatment (Fig. 15e). Insulin treatment resulted in a similar trend. Within most biological replicates, addition of insulin led to a decreased intensity of the phosphorylated SYNJ2BP peptide (Fig. 15f), while the total levels of SYNJ2BP did not change (Fig. 15g). This indicates that SYNJ2BP is also phosphorylated by AMPK in cultured neurons.

3.8 SYNJ2BP S21 phosphorylation regulates *Pink1* mRNA localization to mitochondria

As I observed that AMPK positively regulates *Pink1* mRNA localization to mitochondria and phosphorylates SYNJ2BP, I aimed to investigate whether mitochondrial *Pink1* mRNA association is dependent on SYNJ2BP phosphorylation. As expected, knockdown of SYNJ2BP using shRNA significantly reduced *Pink1* mRNA tethering to mitochondria as visualized using the MS2/PP7-split Venus approach and quantified by the Manders' coefficient. Interestingly, only overexpression of SYNJ2BP WT and a phospho-mimetic mutant of SYNJ2BP containing glutamic acid instead of serine at position 21 (S21E) was able to rescue the SYNJ2BP knockdown-induced phenotype (Fig. 16a,b). Overexpression of the phospho-ablative SYNJ2BP S21A mutant, however, could not prevent *Pink1* mRNA dissociation from mitochondria (Fig. 16a,b). Importantly, the observed effect was not caused by different expression levels of the constructs (Fig. 16c,d).
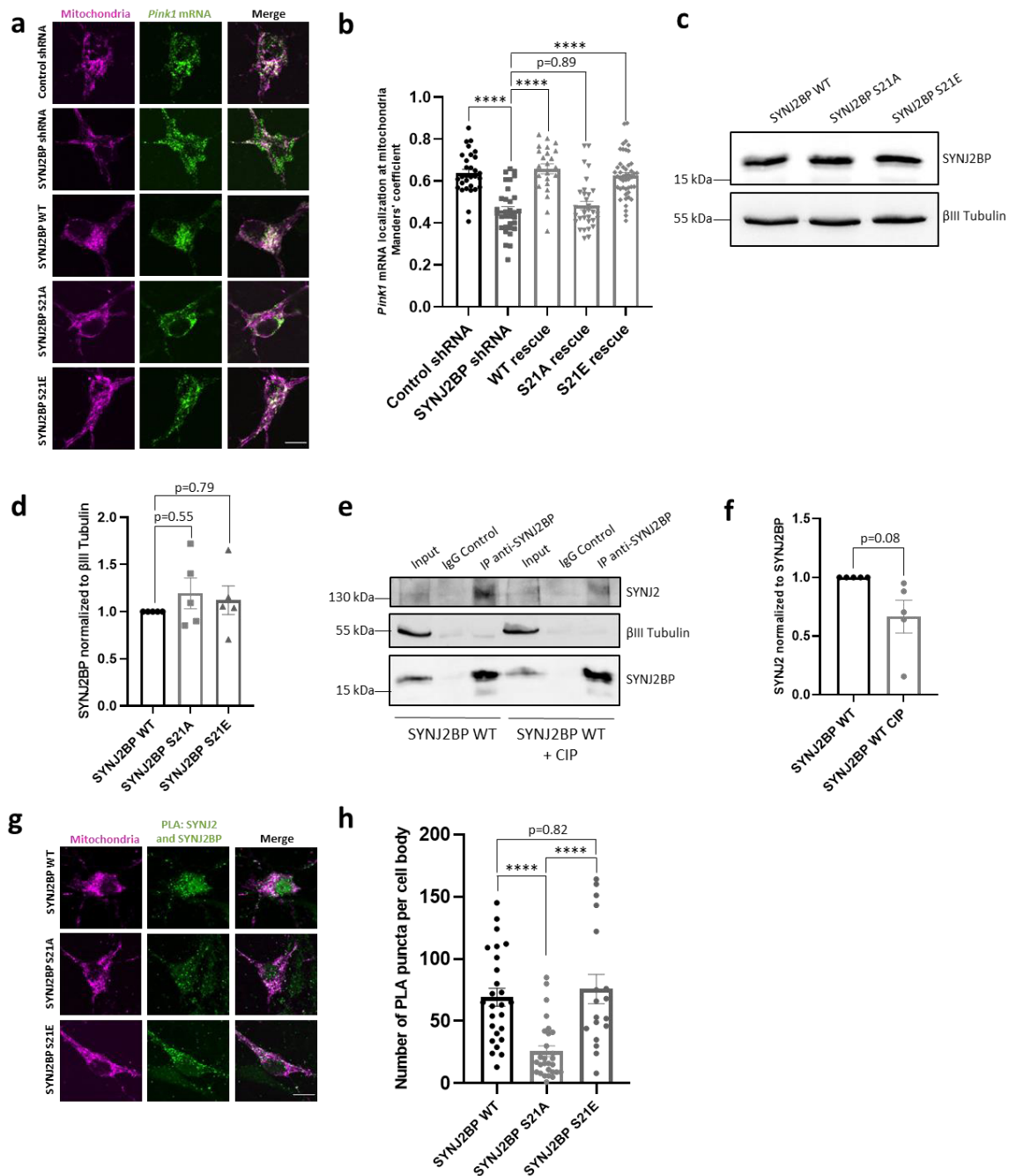
Figure 16: SYNJ2BP phosphorylation regulates *Pink1* mRNA localization to mitochondria.
(a) Representative images of *Pink1* mRNA as visualized using the MS2/PP7-split Venus approach and mRaspberry-labeled mitochondria in the soma of primary hippocampal neurons overexpressing either control shRNA or shRNA targeting SYNJ2BP as well as SYNJ2BP WT, S21A or S21E. **(b)** Manders' coefficient-based quantification of the colocalization between the *Pink1* mRNA and the mitochondrial channel in the soma as in **a**. One-way ANOVA with Tukey's post hoc test; n = 23 - 46; p < 0.0001 (****). **(c)** Representative Western blot image of primary cortical neurons lentivirally transduced with myc-tagged SYNJ2BP, S21A or S21E. **(d)** Densitometry analysis of the protein bands of SYNJ2BP normalized to the corresponding βIII tubulin bands as in **c**. One-way ANOVA with Tukey's post hoc test; n = 5. **(e)** Representative Western blot image of SYNJ2BP immunoprecipitation from cortical neuron lysates lentivirally transduced with myc-tagged SYNJ2BP WT treated with and without CIP. Note, reduced SYNJ2 co-precipitation observed with CIP-treated lysates. **(f)** Densitometry analysis of the protein bands of SYNJ2 normalized to the corresponding SYNJ2BP bands as in **e**. Two-tailed Welch's t-test; n = 5.

_____

(g) Representative images of somata of primary hippocampal neurons exhibiting the PLA signal indicating the interaction between SYNJ2BP and SYNJ2 upon SYNJ2BP WT, S21A or S21E overexpression. **(h)** Number of PLA puncta per cell body as in **g**. One-way ANOVA with Tukey's post hoc test; n = 18 - 28; p < 0.0001 (****).

All data are presented as mean ± SEM. Data points correspond to biological replicates (**d,f**) or single cells obtained from ≥3 biological replicates (**b,h**). Scale bars, 10 μm (adapted from Hees & Harbauer, 2023 and from the unpublished data in the revised manuscript Hees et al., 2023 (under review)).

Since AMPK activity positively regulates the interaction between SYNJ2BP and SYNJ2 (Fig. 10b-f), I tested whether the interaction between SYNJ2BP and SYNJ2a is also dependent on phosphorylation. To this end, I used two different strategies. First, I immunoprecipitated lentivirally overexpressed myc-tagged *rat* SYNJ2BP WT from primary cortical neurons grown in the absence of insulin for 2 h and quantified the amount of co-precipitated SYNJ2. I observed a specific interaction between SYNJ2BP and SYNJ2 since the neuronal protein βIII tubulin did not co-precipitate with SYNJ2BP and I did not detect SYNJ2 in a sample using IgG control antibodies (Fig. 16e). To investigate the dependence on the phosphorylation status, I treated the lysates with calf-intestinal phosphatase (CIP) prior to immunoprecipitation. In this condition, the amount of co-isolated SYNJ2 was diminished (Fig. 16e,f). Second, I performed a PLA for SYNJ2BP and SYNJ2a in hippocampal neurons overexpressing SYNJ2BP WT, S21A and S21E, respectively. While the PLA signal as quantified by number of PLA puncta per cell body was comparable between SYNJ2BP WT and S21E overexpression, there was a significant reduction in number of PLA puncta when the phospho-ablative SYNJ2BP S21A mutant was overexpressed (Fig. 16g,h). This suggests that SYNJ2BP phosphorylation at S21 promotes the interaction with SYNJ2. Taken together, this fully supports the model that AMPK-mediated phosphorylation of SYNJ2BP at S21 is required for *Pink1* mRNA tethering to mitochondria as phosphorylation strengthens the interaction between SYNJ2BP and SYNJ2.

3.9 Phospho-mimetic SYNJ2BP restores mitochondrial *Pink1* mRNA localization upon AMPK inhibition

The observation that overexpression of the phospho-mimetic SYNJ2BP S21E mutant rescues mitochondrial *Pink1* mRNA localization upon SYNJ2BP knockdown prompted me to investigate whether SYNJ2BP S21E expression could also prevent the effects mediated by AMPK inhibition. Indeed, CC-induced reduction of *Pink1* mRNA association with mitochondria as visualized by the MS2/PP7-split Venus approach was prevented both in the soma and in dendrites when the phospho-mimetic SYNJ2BP mutant was overexpressed (Fig. 17a-c). In line with that, the insulin-mediated effect on *Pink1* mRNA localization was also rescued if instead of SYNJ2BP WT the SYNJ2BP S21E mutant was overexpressed (Fig. 17d-f). Together, this indicates that phosphorylation of SYNJ2BP at S21 is regulated by insulin as well as AMPK signaling and influences *Pink1* mRNA association with mitochondria.
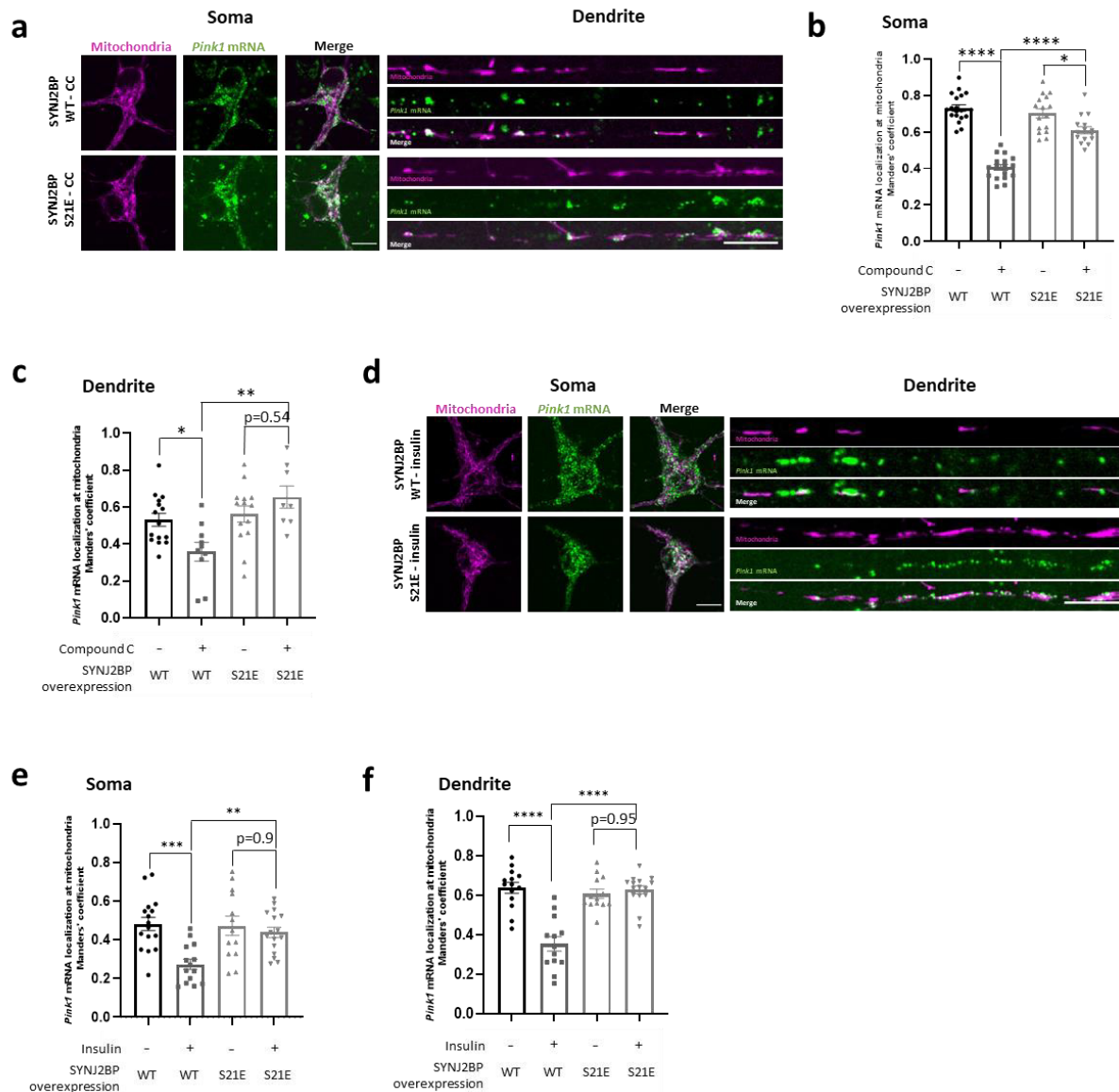
Figure 17: Phospho-mimetic SYNJ2BP restores mitochondrial *Pink1* mRNA localization upon AMPK inhibition. **(a)** Representative images of *Pink1* mRNA as visualized using the MS2/PP7-split Venus approach and mRaspberry-labeled mitochondria in the soma and dendrites of primary hippocampal neurons overexpressing SYNJ2BP WT or S21E and treated with or without CC (20 μM, 2 h). **(b)** Manders' coefficient-based quantification of the colocalization between the *Pink1* mRNA and the mitochondrial channel in the soma as in **a**. One-way ANOVA with Tukey's post hoc test; n = 16 - 19; $p < 0.05$ (*), $p < 0.0001$ (****). **(c)** Manders' coefficient-based quantification of the colocalization between the *Pink1* mRNA and the mitochondrial channel in dendrites as in **a**. One-way ANOVA with Tukey's post hoc test; n = 8 - 15; $p < 0.05$ (*), $p < 0.01$ (**). **(d)** Representative images of *Pink1* mRNA as visualized using the MS2/PP7-split Venus approach and mRaspberry-labeled mitochondria in the soma and dendrites of primary hippocampal neurons overexpressing SYNJ2BP WT or S21E and treated with or without insulin (500 nM, 1 h). **(e)** Manders' coefficient-based quantification of the colocalization between the *Pink1* mRNA and the mitochondrial channel in the soma as in **d**. One-way ANOVA with Tukey's post hoc test; n = 13 - 16; $p < 0.01$ (**), $p < 0.001$ (***). **(f)** Manders' coefficient-based quantification of the colocalization between the *Pink1* mRNA and the mitochondrial channel in dendrites as in **d**. One-way ANOVA with Tukey's post hoc test; n = 13 - 15; $p < 0.0001$ (****).

All data are presented as mean ± SEM. Data points correspond to single cells obtained from ≥3 biological replicates (**b,c,e,f**). Scale bars, 10 μm (adapted from Hees & Harbauer, 2023).

_____

3.10 PINK1 translation is upregulated upon AMPK inhibition

My findings that SYNJ2BP phosphorylation at S21 is important for *Pink1* mRNA tethering to mitochondria raised the question whether the phosphorylation status is also involved in regulating translation of the PINK1 protein. To address this question, I used three different approaches. First, I took advantage of the SunTag system. This method allows visualization of single mRNA translation in living cells in real time by fluorescently labeling nascent polypeptides (Ruijtenberg et al., 2018; Tanenbaum et al., 2014). Briefly, the SunTag consists of several short peptides that are inserted in frame within the gene of interest. This construct is co-expressed together with a single-chain variable fragment antibody fused to GFP (scFv-GFP), which specifically recognizes the SunTag peptides. Therefore, synthesis of the SunTag peptides by ribosomes leads to binding of several scFv-GFP and a GFP signal at the site of a translating mRNA (Fig. 18a). Between the transmembrane and the kinase domain of a *rat* Pink1 construct, 10 copies of the SunTag peptides were added. Furthermore, a kinase dead mutation (K219M) (Petit et al., 2005) was introduced to avoid effects caused by PINK1 overexpression. As upon mitochondrial PINK1 import, scFv-GFP can no longer bind to the construct, only cytosolic PINK1 will be highlighted, which represents the precursor form of PINK1 that will be targeted to mitochondria and immediately degraded unless mitochondrial damage is induced. Therefore, the SunTag clusters closely represent the amount of freshly translated PINK1. Unexpectedly, upon AMPK inhibition via CC I observed a striking increase in the mean intensity and mean area of the PINK1 SunTag clusters, whereas the AMPK activator AICAR did not significantly affect their appearance (Fig. 18b-d). As *Pink1* mRNA dissociates from mitochondria upon CC treatment (Fig. 8b-d), this suggests that mitochondrial *Pink1* mRNA tethering and its translation might be inversely regulated. The CC-mediated effect on the PINK1 SunTag clusters could be prevented by simultaneous addition of puromycin indicating that the signal indeed corresponds to ongoing protein translation (Fig. 18e-g), as puromycin disassembles the ribosome. Importantly, overexpression of the scFv-GFP alone did not result in an increased SunTag signal upon CC addition confirming that the clusters are not unspecific aggregates of the nanobody (Fig. 18h). Interestingly, an increase in the PINK1 SunTag signal was not observed in HeLa cells upon CC treatment indicating that this might be a neuron-specific effect (Fig. 18i-k). This is in line with the finding that *Pink1* mRNA only localizes to mitochondria in neurons due to the neuron-enriched splice variant SYNJ2a (Harbauer et al., 2022). As expected, also insulin treatment resulted in increased translation of PINK1 visualized by the SunTag system. This effect could be partly prevented by inhibition of the insulin signaling pathway using the IR inhibitor GSK1904529A, the PI3K inhibitor Wortmannin or the AKT inhibitor VIII (Fig. 18l-n).
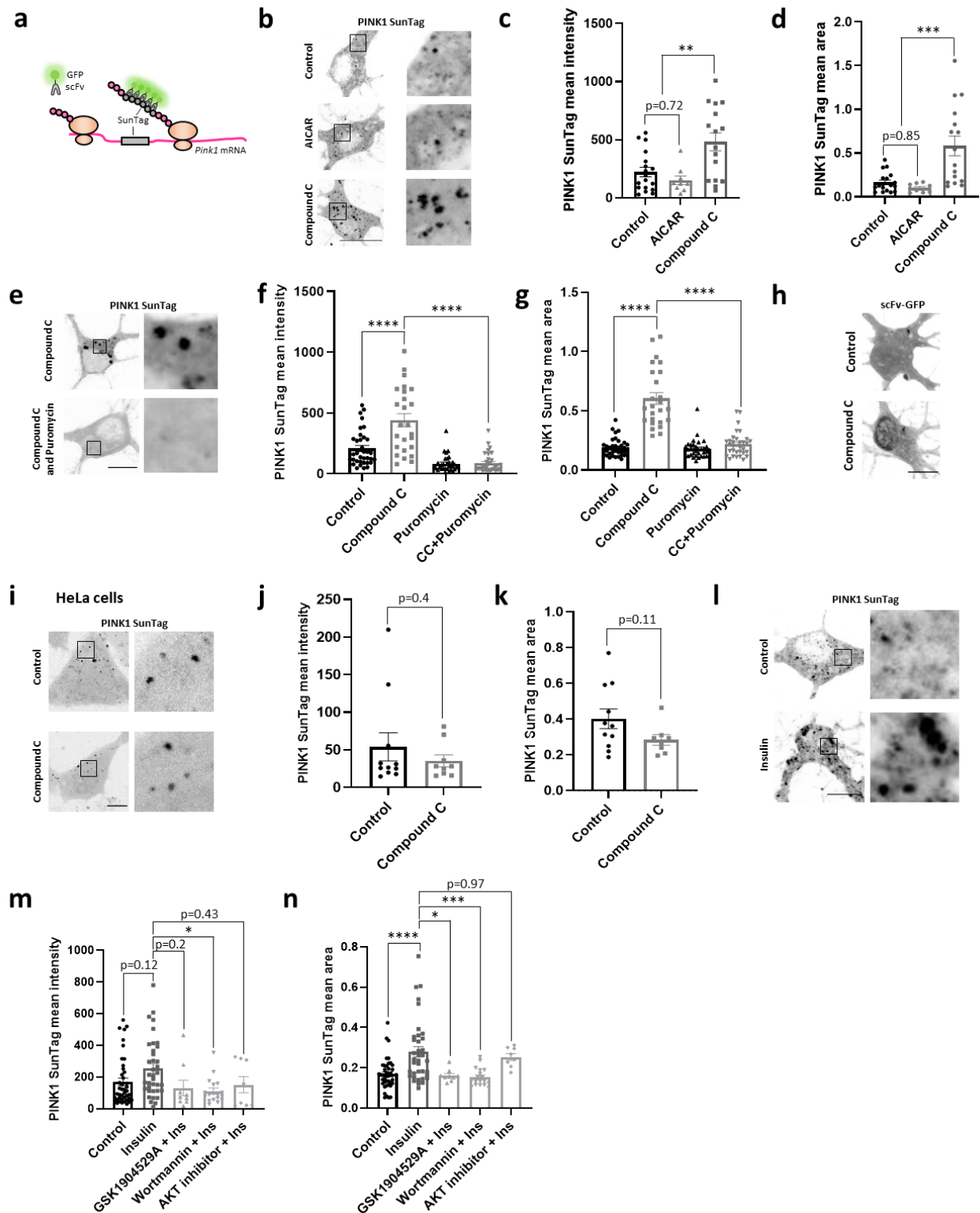
Figure 18: PINK1 translation is upregulated upon AMPK inhibition as reported by the SunTag system.
(a) Schematic illustrating the SunTag system to visualize active protein translation. **(b)** Representative images of PINK1 SunTag clusters following control, AICAR (1 mM, 2 h) or CC (20 µM, 2 h) treatment in the soma of primary hippocampal neurons. **(c)** Quantification of the mean intensity of the PINK1 SunTag clusters as in **b**. One-way ANOVA with Tukey's post hoc test; n = 9 - 18; p < 0.01 (**). **(d)** Quantification of the mean area of the PINK1 SunTag clusters as in **b**. One-way ANOVA with Tukey's post hoc test; n = 9 - 18; p < 0.001 (***). **(e)** Representative images of PINK1 SunTag clusters following CC (20 µM, 2 h) treatment in the presence or absence of puromycin (200 µg/ml, 2 h) in the soma of primary hippocampal neurons. **(f)** Quantification of the mean intensity of the

_____

PINK1 SunTag clusters as in **e**. One-way ANOVA with Tukey's post hoc test; n = 25 - 35; p < 0.0001 (****). **(g)** Quantification of the mean area of the PINK1 SunTag clusters as in **e**. One-way ANOVA with Tukey's post hoc test; n = 25 - 35; p < 0.0001 (****). **(h)** Representative images of the soma of primary hippocampal neurons overexpressing the scFv-GFP alone without the Pink1 construct with and without CC (20 μM, 2 h) treatment. Note that overexpression of only the scFv-GFP does not result in formation of clusters following CC treatment. **(i)** Representative images of PINK1 SunTag clusters following control or CC (20 μM, 2 h) treatment in the soma of HeLa cells. **(j)** Quantification of the mean intensity of the PINK1 SunTag clusters as in **i**. Two-tailed student's t-test; n = 9 - 11. **(k)** Quantification of the mean area of the PINK1 SunTag clusters as in **i**. Two-tailed student's t-test; n = 8 - 11. **(l)** Representative images of PINK1 SunTag clusters following control or insulin (500 nM, 1 h) treatment in the soma of primary hippocampal neurons. **(m)** Quantification of the mean intensity of the PINK1 SunTag clusters in the soma of primary hippocampal neurons following control or insulin treatment in the presence or absence of inhibitors targeting the insulin signaling pathway: IR inhibitor GSK1904529A (1 μM, 2 h); PI3K inhibitor Wortmannin (1 μM, 2 h) and AKT inhibitor VIII (10 μM, 2 h). One-way ANOVA with Tukey's post hoc test; n = 8 - 42; p < 0.05 (*). **(n)** Quantification of the mean area of the PINK1 SunTag clusters in the soma of primary hippocampal neurons following control or insulin treatment in the presence or absence of inhibitors targeting the insulin signaling pathway: IR inhibitor GSK1904529A (1 μM, 2 h); PI3K inhibitor Wortmannin (1 μM, 2 h) and AKT inhibitor VIII (10 μM, 2 h). One-way ANOVA with Tukey's post hoc test; n = 8 - 42; p < 0.05 (*), p < 0.001 (***), p < 0.0001 (****).

All data are presented as mean ± SEM. Data points correspond to single cells obtained from ≥2 biological replicates (**c,d,f,g,j,k,m,n**). Scale bars, 10 μm.

As a second approach, I utilized the RiboTag mouse line to analyze ongoing translation of *Pink1* mRNA (Sanz et al., 2009). Briefly, this mouse line has a modified allele of the 60S ribosomal gene *Rpl22 (Rpl22-HA)* that is induced in the presence of Cre recombinase. In this way, ribosomes can be tagged and subsequently isolated by immunoprecipitation. Ribosome-bound mRNAs can be further analyzed by RT-qPCR (Sanz et al., 2009) (Fig. 19a). I treated cortical neurons obtained from RiboTag mouse embryos with a control or Cre virus as well as with AICAR or CC to activate and inhibit AMPK, respectively, and isolated ribosomes from the lysates by immunoprecipitation using the HA-tag (Fig. 19b). Upon CC treatment I observed a trend towards increased *Pink1* mRNA association with the isolated HA-tagged ribosomes as measured by RT-qPCR (Fig. 19c). Together with the CC-mediated increase in mean intensity and mean area of the PINK1 SunTag clusters observed in the previous experiment (Fig. 18b-d), this could indicate increased PINK1 translation upon AMPK inhibition. It remains to be determined whether insulin addition also results in increased ribosomal association of *Pink1* mRNA. Finally, I investigated PINK1 expression in human iPSC-derived cortical neurons as commercially available PINK1 antibodies only reliably detect the human PINK1 protein. I analyzed PINK1 protein levels in neurons treated with AICAR or CC. In line with the SunTag and RiboTag data, I observed increased PINK1 protein levels upon CC treatment, while AICAR treatment had no effect (Fig. 19d,e). Furthermore, I compared PINK1 protein levels in neurons cultured in the presence or absence of insulin. Interestingly, already two hours of insulin withdrawal as well as inhibition of insulin signaling using the AKT inhibitor VIII reduced PINK1 protein levels (Fig. 19f,g), which is in line with the very short half-life of the protein (W. Lin & Kang, 2008; Vincow et al., 2013). To confirm this finding in mouse hippocampal neurons, I overexpressed GFP-tagged PINK1 and compared its protein levels in the presence or absence of insulin

specifically on mitochondria. In the presence of insulin, the intensity of mitochondrial GFP-tagged PINK1 was significantly increased (Fig. 19h,i). It remains to be determined whether the effect is due to decreased synthesis of PINK1 or changes in degradation rates in the absence of insulin. Interestingly, inhibition of the insulin signaling pathway in HEK293T cells using the IR inhibitor GSK1904529A or the AKT inhibitor VIII did not lead to reduced PINK1 expression indicating that this mechanism is neuron-specific (Fig. 19j,k). This is consistent with the observation that CC-mediated inhibition did not result in increased PINK1 SunTag clusters in HeLa cells (Fig. 18i-k). Altogether, these three lines of evidence suggest that dissociation of *Pink1* mRNA from mitochondria, as seen under conditions where AMPK is inactive, favors its translation.
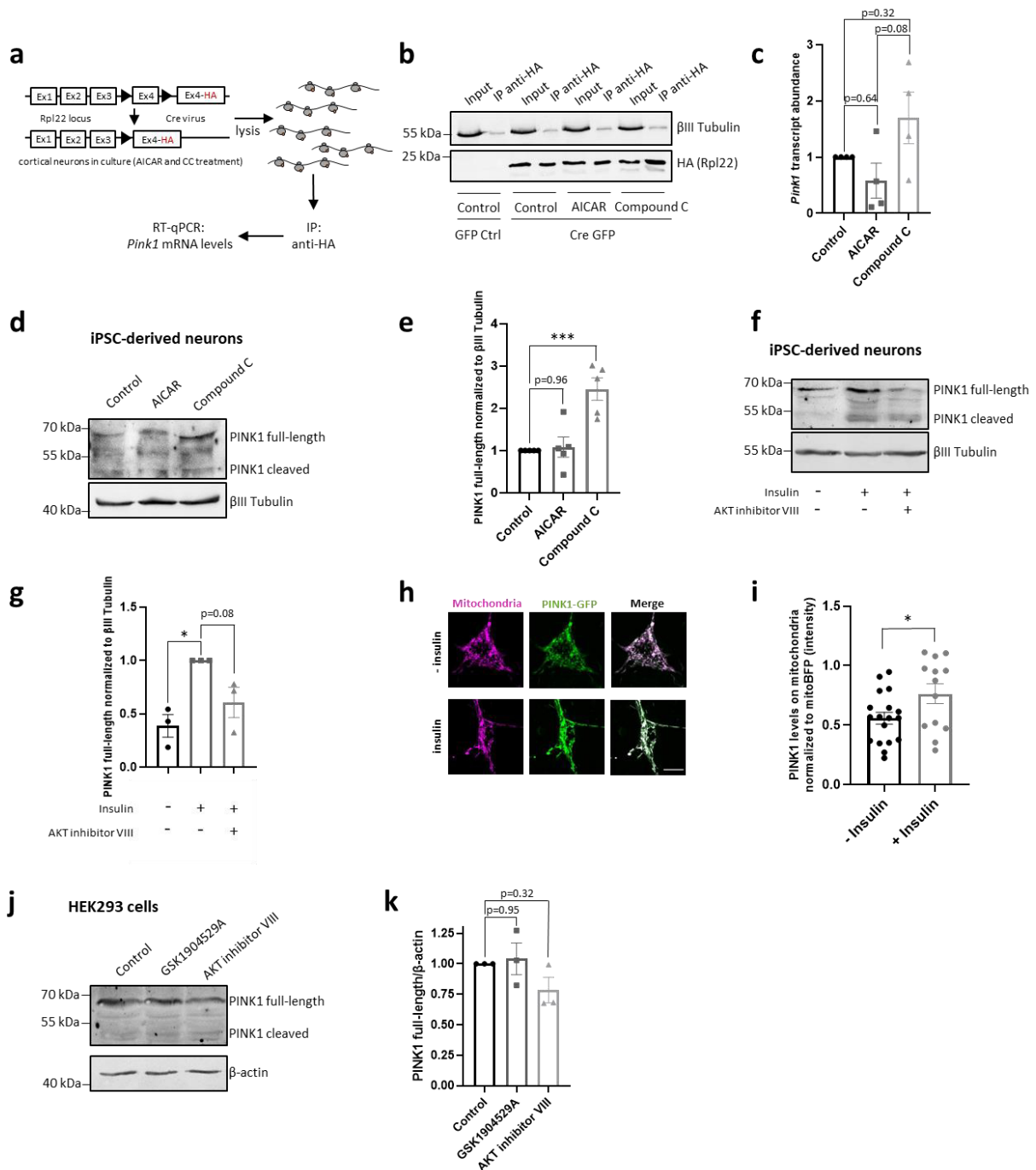
_____

Figure 19: PINK1 translation is upregulated upon AMPK inhibition as reported by the RiboTag assay and immunoblotting.
(a) Schematic illustrating the RiboTag assay to determine ribosomal association of *Pink1* mRNA. **(b)** Representative Western blot image of primary cortical neurons from the RiboTag mouse line. Cortical neurons were lentivirally transduced with GFP control or GFP-Cre to induce expression of HA-tagged Rpl22 and treated with AICAR (1 mM, 2 h) or CC (20 μM, 2 h). Ribosomes were isolated by immunoprecipitation against the HA-tag. **(c)** Ribosome-associated *Pink1* transcript levels as assessed by RT-qPCR following control, AICAR or CC treatment as in **b**. One-way ANOVA with Tukey's post hoc test; n = 4. **(d)** Representative Western blot image of human iPSC-derived cortical neurons following control, AICAR (1 mM, 2 h) or CC (20 μM, 2 h) treatment. **(e)** Densitometry analysis of the protein bands of PINK1 (full-length) normalized to the corresponding βIII tubulin bands as in **d**. One-way ANOVA with Tukey's post hoc test; n = 5; p < 0.001 (***). **(f)** Representative Western blot image of human iPSC-derived cortical neurons cultured in the presence or absence of insulin for 2 h and treated with or without the AKT inhibitor VIII (10 μM, 2 h). **(g)** Densitometry analysis of the protein bands of PINK1 (full-length) normalized to the corresponding βIII tubulin bands as in **f**. One-way ANOVA with Tukey's post hoc test; n = 3; p < 0.05 (*). **(h)** Representative images of somata of primary hippocampal neurons overexpressing PINK1-GFP and mitochondrially targeted BFP grown with or without insulin for 2 h. **(i)** Quantification of the intensity of the mitochondrially localized PINK1-GFP signal normalized to the mito-BFP signal as in **h**. Two-tailed student's t-test; n = 11 - 18; p < 0.05 (*). **(j)** Representative Western blot image of HEK293 cells treated with or without the IR inhibitor GSK1904529A (1 μM, 2 h) and the AKT inhibitor VIII (10 μM, 2 h). **(k)** Densitometry analysis of the protein bands of PINK1 (full-length) normalized to the corresponding β-actin bands as in **j**. One-way ANOVA with Tukey's post hoc test; n = 3.

All data are presented as mean ± SEM. Data points correspond to biological replicates (**c,e,g,k**) or single cells obtained from ≥3 biological replicates (**i**). Scale bars, 10 μm (adapted from Hees & Harbauer, 2023 and from the unpublished data in the revised manuscript Hees et al., 2023 (under review)).

3.11   Ribosomes as well as *Pink1* mRNA are present at the PINK1 translation hotspot

As one of the key components for translation are ribosomes, I next examined whether ribosomes are present at the PINK1 translation hotspots. The RiboTag experiment already indicates an increased ribosomal *Pink1* mRNA association upon AMPK inhibition using CC. However, I also tested whether I can detect ribosomes in close proximity to the PINK1 SunTag clusters to really confirm that these are true translation events. Therefore, I again took advantage of the PLA approach. As the scFv-GFP, which specifically binds to the SunTag peptides, contains a mouse Fc domain (H. Zhao et al., 2016), it can be recognized by the secondary anti-mouse PLA probe. In addition, a primary antibody against a protein in the 40S ribosomal subunit Rps6 was used, which can be recognized by the secondary anti-rabbit PLA probe (Fig. 20a). Both under control conditions and upon CC treatment, I observed a colocalization between the PLA signal and the PINK1 SunTag signal indicating that ribosomes are indeed in the same spot as the SunTag clusters (Fig. 20b). Importantly, the PLA signal was abolished when the Pink1 construct containing the SunTag peptides was not expressed (Fig. 20c). In this condition, the scFv-GFP was evenly distributed in the cytosol instead of being recruited to translation hotspots, which is in line with the reduced PLA signal. Furthermore, I performed a control experiment without addition of the Rps6 antibody and did not detect any PLA signal as expected (Fig. 20d). Apart from ribosomes, the *Pink1* mRNA is required for PINK1 translation. Hence, I co-transfected the constructs required for visualization of *Pink1* mRNA (MS2-PP7 split-Venus system) as well as PINK1 translation (SunTag system

_____

using scFv-mRaspberry instead of scFv-GFP). Both under control conditions and upon CC treatment, I observed a colocalization between the two signals (Fig. 20e). Together, this indicates that the PINK1 SunTag clusters indeed represent real translation hotspots.
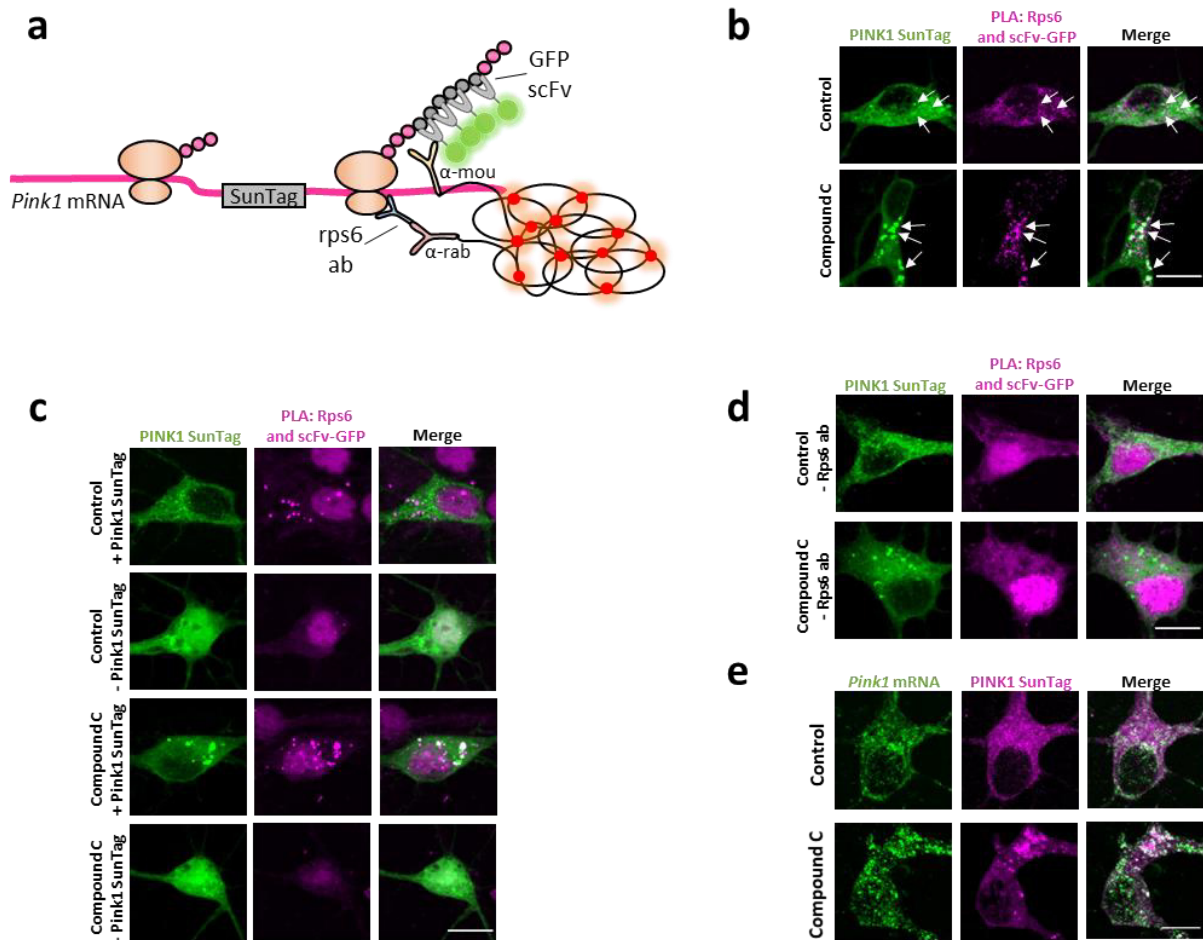
Figure 20: Ribosomes as well as *Pink1* mRNA are present at the PINK1 translation hotspot.
(a) Schematic illustrating the proximity ligation assay (PLA) to visualize the interaction between the SunTag signal and ribosomes. **(b)** Representative images of somata of primary hippocampal neurons overexpressing the Pink1 SunTag construct and exhibiting the PLA signal for the interaction between the SunTag signal and Rps6 following control or CC (20 µM, 2 h) treatment. **(c)** Representative images of somata of primary hippocampal neurons overexpressing the scFv-GFP with or without the Pink1 SunTag construct following control or CC (20 µM, 2 h) treatment. The PLA was performed as in **b** and serves as control. Note that there is no PLA signal when the Pink1 construct is not expressed. **(d)** Representative images of somata of primary hippocampal neurons overexpressing the Pink1 SunTag construct following control or CC (20 µM, 2 h) treatment. As a control for **b**, the PLA was performed without addition of the Rps6 antibody. Note that there is no PLA signal. **(e)** Representative images of somata of primary hippocampal neurons overexpressing the Pink1 MS2-PP7 split-Venus constructs and the Pink1 SunTag construct (using scFv-mRaspberry instead of scFv-GFP) following control or CC (20 µM, 2 h) treatment. Note the colocalization between the *Pink1* mRNA and the SunTag clusters.

Scale bars, 10 µm.

_____

3.12 *Pink1* mRNA localizes to endolysosomes upon AMPK inhibition

My observation that *Pink1* mRNA dissociates from mitochondria upon AMPK inhibition raised the question where the mRNA is localized when no longer associated with mitochondria. In a recent study, translation of nuclear-encoded mitochondrial proteins has been shown to occur at endolysosomes in close proximity to mitochondria in neurons (Cioni et al., 2019). I therefore tested whether AMPK inhibition would induce *Pink1* mRNA localization to endolysosomes visualized by expression of either the RFP-tagged lysosomal transmembrane protein 192 (TMEM192) or the mCherry-tagged late endosomal protein Rab7. Indeed, endolysosomal *Pink1* mRNA association using either TMEM192 or Rab7 as a marker significantly increased upon AMPK inhibition using CC (Fig. 21a-d). Consistent with the CC effect, insulin-induced inhibition of AMPK also resulted in an increased endolysosomal localization of the *Pink1* mRNA (Fig. 21e,f). Taken together, inhibition of AMPK signaling induces *Pink1* mRNA translocation from mitochondria to endolysosomes potentially promoting its translation at this organelle.
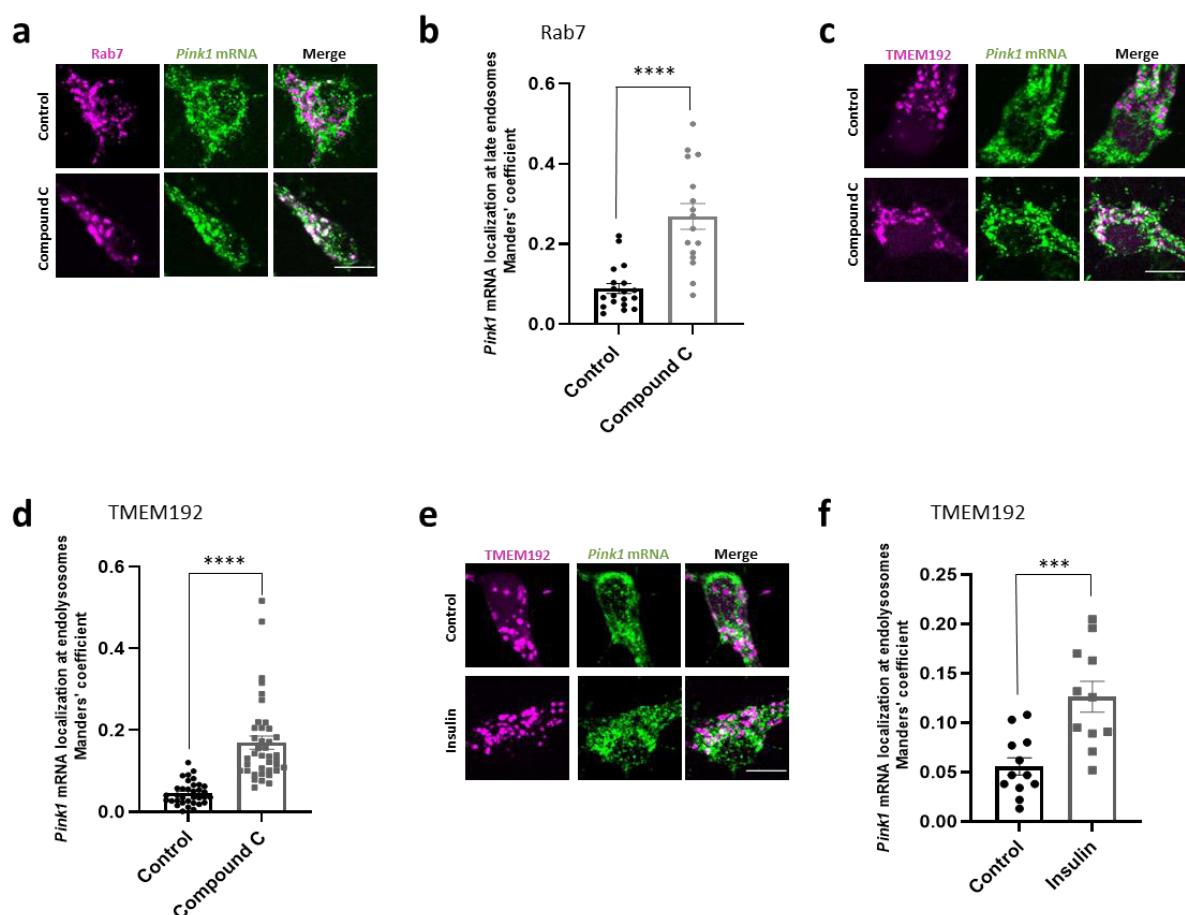
Figure 21: *Pink1* mRNA localizes to endolysosomes upon AMPK inhibition.
(a) Representative images of *Pink1* mRNA as visualized using the MS2/PP7-split Venus approach and endolysosomes visualized by overexpression of mCherry-tagged Rab7 in the soma of primary hippocampal neurons following control or CC (20 µM, 2 h) treatment. **(b)** Manders' coefficient-based quantification of the colocalization between the *Pink1* mRNA and the endolysosomal channel (Rab7) as in **a**. Two-tailed student's t-

_____

test; n = 34 - 39; p < 0.0001 (****). **(c)** Representative images of *Pink1* mRNA as visualized using the MS2/PP7-split Venus approach and endolysosomes visualized by overexpression of RFP-tagged TMEM192 in the soma of primary hippocampal neurons following control or CC (20 µM, 2 h) treatment. **(d)** Manders' coefficient-based quantification of the colocalization between the *Pink1* mRNA and the endolysosomal channel (TMEM192) as in **c**. Two-tailed student's t-test; n = 16 - 19; p < 0.0001 (****). **(e)** Representative images of *Pink1* mRNA as visualized using the MS2/PP7-split Venus approach and endolysosomes visualized by overexpression of RFP-tagged TMEM192 in the soma of primary hippocampal neurons following control or insulin (500 nM, 1 h) treatment. **(f)** Manders' coefficient-based quantification of the colocalization between the *Pink1* mRNA and the endolysosomal channel (TMEM192) as in **e**. Two-tailed student's t-test; n = 11 - 12; p < 0.001 (***).

All data are presented as mean ± SEM. Data points correspond to single cells obtained from ≥3 biological replicates (**b,d,f**). Scale bars, 10 µm (adapted from the unpublished data in the revised manuscript Hees et al., 2023 (under review)).

3.13 PINK1 translation occurs at endolysosomes upon AMPK inhibition

As I observed increased endolysosomal *Pink1* mRNA association upon AMPK inhibition, I next investigated whether its translation occurs at endolysosomes. Upon AMPK inhibition via CC or insulin, the PINK1 SunTag signal colocalized with endolysosomal markers such as Rab7, LAMP1 and TMEM192 indicating that PINK1 translation indeed occurs at the endolysosomal compartment (Fig. 22a,b). With an increase in endolysosomal localization, the mitochondrial localization of the SunTag signal decreased upon CC treatment (Fig. 22b).
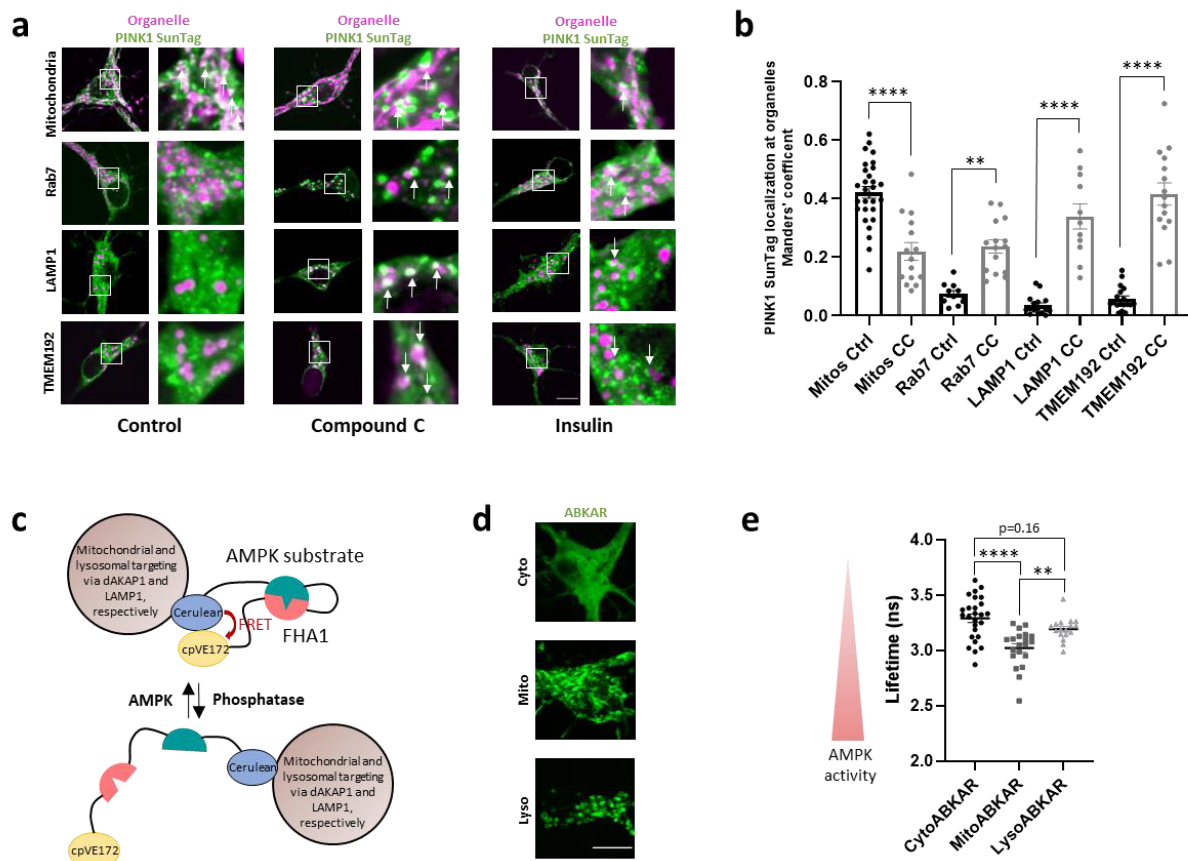
_____

Figure 22: PINK1 translation occurs at endolysosomes upon AMPK inhibition.
(a) Representative images of PINK1 SunTag clusters as well as mitochondria or endolysosomes visualized by overexpression of mitochondrially-targeted mRaspberry, mCherry-tagged Rab7, mCherry-tagged LAMP1 or RFP-tagged TMEM192 in the soma of primary hippocampal neurons following control, CC (20 μM, 2 h) or insulin (500 nM, 1 h) treatment. **(b)** Manders' coefficient-based quantification of the colocalization between the PINK1 SunTag and the organelle channel following CC treatment as in **a**. One-way ANOVA with Tukey's post hoc test; n = 11 - 29; $p < 0.01$ (**), $p < 0.0001$ (****). **(c)** Schematic illustrating the FRET-based AMPK activity sensor ABKAR targeted to mitochondria and to endolysosomes via dAKAP1 and LAMP1, respectively. **(d)** Representative images of primary hippocampal neurons overexpressing the FRET-based AMPK activity sensor ABKAR sensor targeted to the cytosol, to mitochondria or to endolysosomes. **(e)** Analysis of AMPK activity by performing fluorescence lifetime imaging of the FRET-based AMPK activity sensor donor ABKAR in primary hippocampal neurons as in **d**. One-way ANOVA with Tukey's post hoc test; n = 17 - 26; $p < 0.01$ (**), $p < 0.0001$ (****).

All data are presented as mean ± SEM. Data points correspond to single cells obtained from ≥3 biological replicates (**b,e**). Scale bars, 10 μm.

As mitochondrial *Pink1* mRNA association as well as translation at endolysosomes seems to be inversely regulated by AMPK activity, I next addressed the question whether AMPK activity differs between mitochondria and endolysosomes. To test this, I took advantage of the AMPK FRET (ABKAR) constructs tethered to the two organelles via A-kinase anchor protein 1 (AKAP1) and LAMP1 to measure AMPK activity specifically at mitochondria and endolysosomes, respectively (Miyamoto et al., 2015) (Fig. 22c,d). Interestingly, mitochondrial AMPK activity was significantly higher than lysosomal AMPK activity (Fig. 22e). Taken together, these results indicate that when a mitochondrion carrying *Pink1* mRNA reaches an endolysosome, the *Pink1* mRNA might be released due to a signaling environment that favors the dephosphorylated state of SYNJ2BP, allowing for ribosomal translation.

3.14   Phospho-mimetic SYNJ2BP decreases endolysosomal-localized PINK1 translation upon AMPK inhibition

Given the observation that AMPK-mediated SYNJ2BP phosphorylation is critical for *Pink1* mRNA tethering to mitochondria (Fig. 16a,b), I tested whether it is also involved in regulating its translation. Indeed, overexpression of the phosphomimetic SYNJ2BP S21E mutant compared to SYNJ2BP WT significantly reduced the mean intensity of the SunTag clusters upon AMPK inhibition using CC or insulin (Fig. 23a,b). A similar trend was observed for the mean area of the SunTag clusters (Fig. 23c). Furthermore, both CC- and insulin-induced endolysosomal localization of the PINK1 translation as visualized by the SunTag system was prevented if instead of SYNJ2BP WT the phospho-mimetic SYNJ2BP S21E mutant was overexpressed (Fig. 23d-f). Together, this indicates that phosphorylation of SYNJ2BP at S21 regulates the switch between *Pink1* mRNA tethering to mitochondria and its translation at endolysosomes.
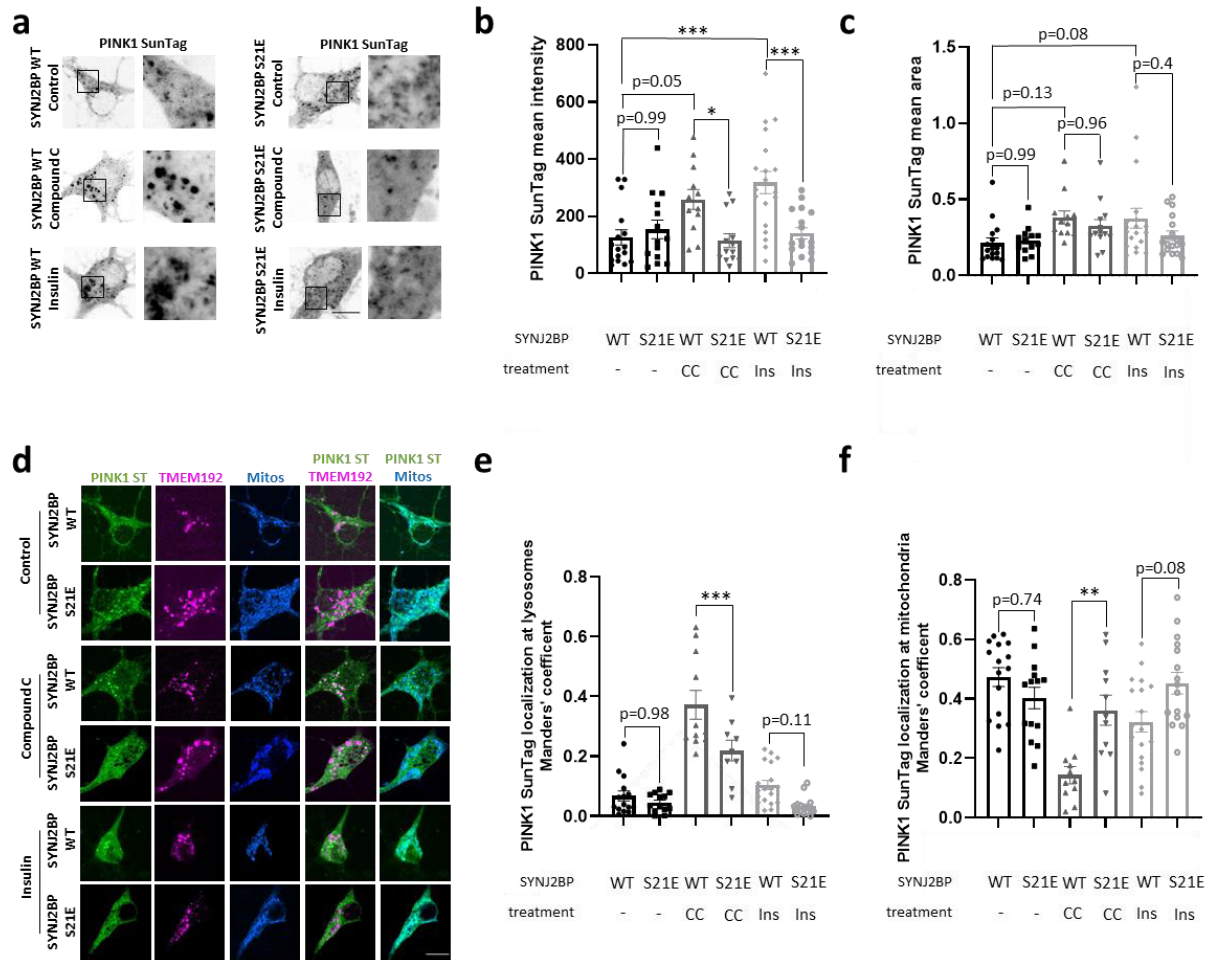
Figure 23: Phospho-mimetic SYNJ2BP decreases endolysosomal-localized PINK1 translation upon AMPK inhibition.

(a) Representative images of PINK1 SunTag clusters following control, CC (20 µM, 2 h) or insulin (500 nM, 1 h) treatment in the soma of primary hippocampal neurons overexpressing SYNJ2BP WT or S21E. **(b)** Quantification of the mean intensity of the PINK1 SunTag clusters as in **a**. One-way ANOVA with Tukey's post hoc test; n = 12 - 19; p < 0.05 (*), p < 0.001 (***). **(c)** Quantification of the mean area of the PINK1 SunTag clusters as in **a**. One-way ANOVA with Tukey's post hoc test; n = 12 - 19. **(d)** Representative images of PINK1 SunTag clusters as well as mitochondria and endolysosomes visualized by overexpression of mitochondrially-targeted BFP and RFP-tagged TMEM192, respectively, in the soma of primary hippocampal neurons overexpressing SYNJ2BP WT or S21E following control, CC (20 µM, 2 h) or insulin (500 nM, 1 h) treatment. **(e)** Manders' coefficient-based quantification of the colocalization between the PINK1 SunTag and the endolysosomal channel as in **d**. One-way ANOVA with Tukey's post hoc test; n = 9 - 19; p < 0.001 (***). **(f)** Manders' coefficient-based quantification of the colocalization between the PINK1 SunTag and the mitochondrial channel as in **d**. One-way ANOVA with Tukey's post hoc test; n = 11 - 18; p < 0.01 (**).

All data are presented as mean ± SEM. Data points correspond to single cells obtained from ≥3 biological replicates (**b,c,e,f**). Scale bars, 10 µm.

3.15 Increased PINK1 translation is not dependent on mTORC1 signaling but on endolysosomal activity

Endolysosomes are known to be important hubs for metabolic signaling (Lamming & Bar-Peled, 2019). Interestingly, both AMPK and mTORC1 are actively recruited to endolysosomes for activation (Carroll & Dunlop, 2017). Furthermore, mTORC1 is known as the master regulator of protein synthesis and has been shown to upregulate translation of nuclear-encoded mitochondrial proteins (Morita et al., 2013). AMPK and mTORC1 signaling are inversely regulated and AMPK can inhibit mTORC1 through different signaling pathways (Gwinn et al., 2008; Inoki, Zhu, et al., 2003). Therefore, I next tested whether the CC-induced increase of endolysosomal PINK1 translation is mTORC1-dependent. To test this, I used Torin-2, a known mTOR inhibitor (Q. Liu et al., 2011, 2013). As observed before, CC addition resulted in an increased mean intensity as well as mean area of the PINK1 SunTag clusters. Interestingly, simultaneous treatment with Torin-2 did not prevent this effect (Fig. 24a-c). In line with that, Torin-2 did not prevent the CC-mediated endolysosomal localization of the PINK1 SunTag signal either (Fig. 24d-f) indicating that the upregulation and localization of translation does not depend on mTOR signaling.

Another reason why endolysosomes are ideal platforms for protein translation is their role as degradation and recycling centers. During the degradation process amino acids are transported back into the cytosol, which can be recycled in the synthesis of new proteins. To test whether the degradative capacity of the endolysosomes plays a role, I combined Bafilomycin A1 with CC treatment and analyzed the mean intensity, mean area as well as localization of the PINK1 SunTag signal. Bafilomycin A1 inhibits the endolysosomal v-ATPase, a proton pump required for the acidification of the organelle (Forgac, 2007; Mindell, 2012). Interestingly, unlike Torin-2, Bafilomycin A1 prevented the CC-induced increase in the mean intensity and mean area of the PINK1 SunTag clusters (Fig. 24g-i). Furthermore, the SunTag clusters did not localize to the endolysosomal compartment when the neurons were treated with both CC and Bafilomycin A1 (Fig. 24j-l). This indicates that the upregulation and localization of PINK1 translation is dependent on the degradative capacity of the endolysosomal compartment but not on mTORC1 signaling.
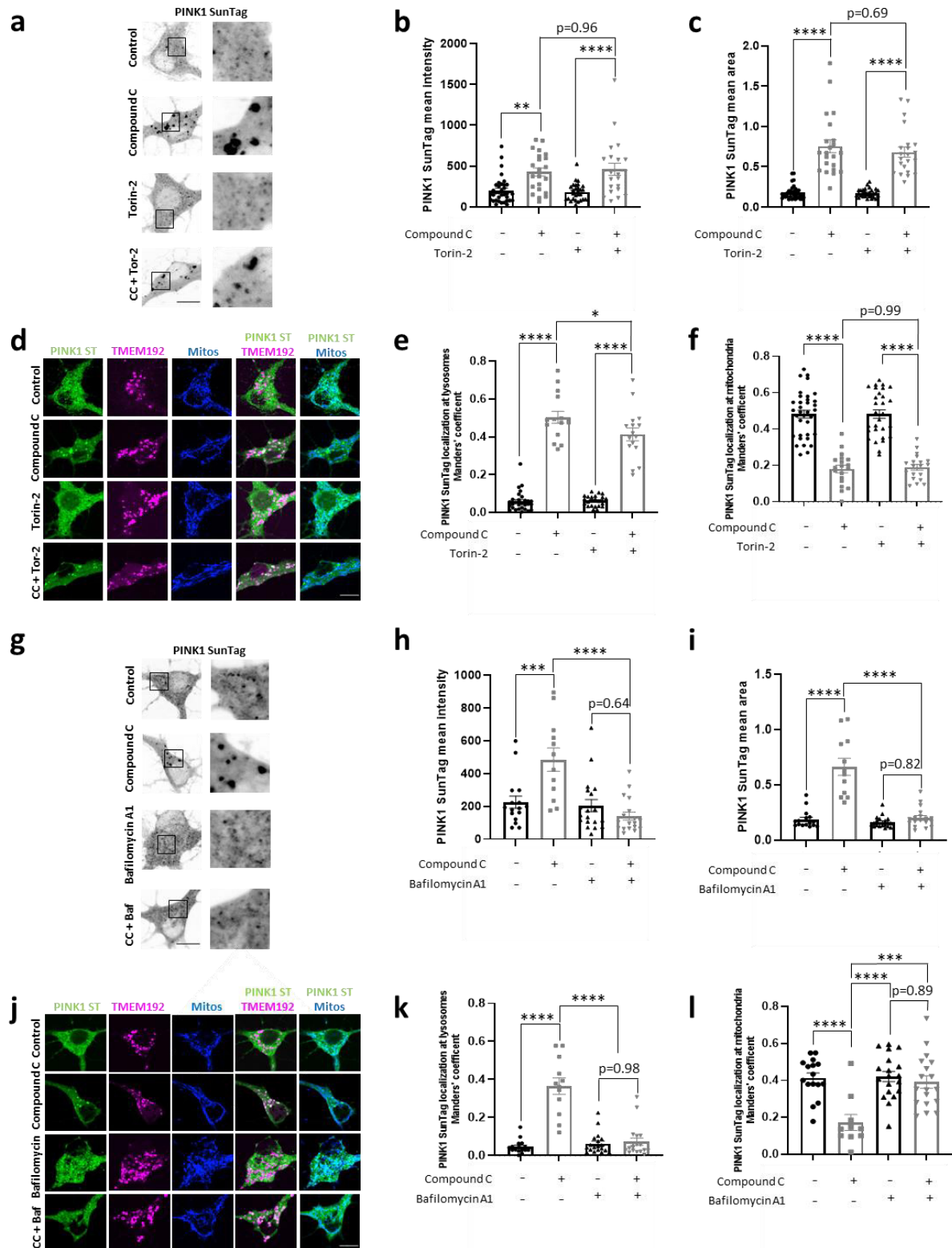
Figure 24: Increased PINK1 translation is not dependent on mTORC1 signaling but on endolysosomal activity. **(a)** Representative images of PINK1 SunTag clusters following control or CC (20 µM, 2 h) treatment in the presence or absence of Torin-2 (10 nM, 2 h) in the soma of primary hippocampal neurons. **(b)** Quantification of the mean intensity of the PINK1 SunTag clusters as in **a**. One-way ANOVA with Tukey's post hoc test; n = 22 - 35; p < 0.01 (**), p < 0.0001 (****). **(c)** Quantification of the mean area of the PINK1 SunTag clusters as in **a**. One-way ANOVA with Tukey's post hoc test; n = 22 - 35; p < 0.0001 (****). **(d)** Representative images of PINK1 SunTag clusters as well as mitochondria and endolysosomes visualized by overexpression of mitochondrially-targeted

_____

BFP and RFP-tagged TMEM192, respectively, in the soma of primary hippocampal neurons following control or CC (20 µM, 2 h) treatment in the presence or absence of Torin-2 (10 nM, 2 h). **(e)** Manders' coefficient-based quantification of the colocalization between the PINK1 SunTag and the endolysosomal channel as in **d**. One-way ANOVA with Tukey's post hoc test; n = 15 - 29; p < 0.05 (*), p < 0.0001 (****). **(f)** Manders' coefficient-based quantification of the colocalization between the PINK1 SunTag and the mitochondrial channel as in **d**. One-way ANOVA with Tukey's post hoc test; n = 19 - 35; p < 0.0001 (****). **(g)** Representative images of PINK1 SunTag clusters following control or CC (20 µM, 2 h) treatment in the presence or absence of Bafilomycin A1 (100 nM, 2 h) in the soma of primary hippocampal neurons. **(h)** Quantification of the mean intensity of the PINK1 SunTag clusters as in **g**. One-way ANOVA with Tukey's post hoc test; n = 12 - 19; p < 0.001 (***), p < 0.0001 (****). **(i)** Quantification of the mean area of the PINK1 SunTag clusters as in **g**. One-way ANOVA with Tukey's post hoc test; n = 12 - 19; p < 0.0001 (****). **(j)** Representative images of PINK1 SunTag clusters as well as mitochondria and endolysosomes visualized by overexpression of mitochondrially-targeted BFP and RFP-tagged TMEM192, respectively, in the soma of primary hippocampal neurons following control or CC (20 µM, 2 h) treatment in the presence or absence of Bafilomycin A1 (100 nM, 2 h). **(k)** Manders' coefficient-based quantification of the colocalization between the PINK1 SunTag and the endolysosomal channel as in **j**. One-way ANOVA with Tukey's post hoc test; n = 12 - 19; p < 0.0001 (****). **(l)** Manders' coefficient-based quantification of the colocalization between the PINK1 SunTag and the mitochondrial channel as in **j**. One-way ANOVA with Tukey's post hoc test; n = 10 - 19; p < 0.001 (***), p < 0.0001 (****).

All data are presented as mean ± SEM. Data points correspond to single cells obtained from ≥3 biological replicates (**b,c,e,f,h,i,k,l**). Scale bars, 10 µm.

3.16   DNAJB6 might guide PINK1 to mitochondria via the ER-SURF pathway after translation

In order to have a closer look at the involvement of the different organelles in PINK1 translation upon AMPK inhibition, I performed correlative light-electron microscopy (CLEM) imaging in collaboration with Martina Fetting from the electron microscopy hub at the German Center for Neurodegenerative Diseases (DZNE), Munich, Germany. I could confirm the localization of the PINK1 SunTag signal next to endolysosomes visualized by expression of RFP-tagged TMEM192. At the same time, lysosomal engulfment of the signal as would be expected during bulk autophagy could be ruled out. Apart from endolysosomes, mitochondria visualized by mitochondrially-targeted BFP were also present in close proximity to the SunTag signal (Fig. 25a).

Interestingly, when having a closer look at the CLEM image, instead of cytosolic polysome structures I could also detect an ER tubule that seems to resemble rough ER. In yeast, a mechanism called ER-SURF has recently been described (Hansen et al., 2018). The ER-anchored chaperone Djp1 has been shown to guide mitochondrial proteins from the cytosol towards the mitochondrial surface. I therefore investigated the localization of its mammalian homolog DnaJ heat shock protein family (Hsp40) member B6 (DNAJB6) in neurons upon CC treatment. Interestingly, I observed colocalization between the PINK1 SunTag signal and DNAJB6 only upon CC treatment (Fig. 25b) indicating that the chaperone DNAJB6 may be indeed involved in guiding PINK1 to the mitochondria.
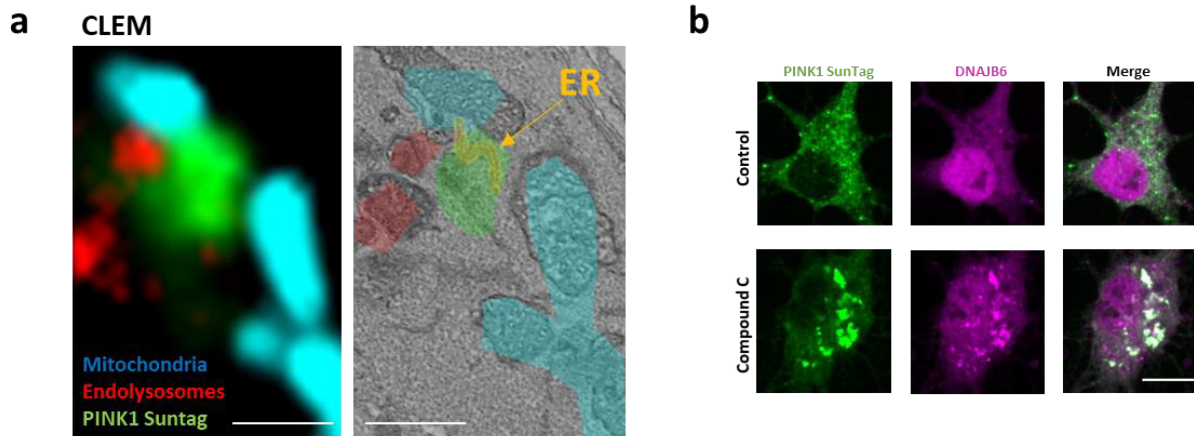
Figure 25: DNAJB6 might guide PINK1 to mitochondria via the ER-SURF pathway after translation. **(a)** Correlative light-electron microscopy image of PINK1 SunTag clusters as well as mitochondria and endolysosomes visualized by overexpression of mitochondrially-targeted BFP and RFP-tagged TMEM192, respectively, in the soma of primary hippocampal neurons following CC (20 µM, 2 h) treatment. Note the arrow marks an ER tubule that resembles rough ER. **(b)** Representative images of PINK1 SunTag clusters and DNAJB6 immunostaining in the soma of primary hippocampal neurons following control and CC (20 µM, 2 h) treatment.

Scale bars, 1 µm **(a)** and 10 µm **(b)**.

3.17   Insulin supports PINK1 activation and mitophagy

PINK1 acts as a sensor for mitochondrial quality control and tags defective mitochondria with phosphorylated ubiquitin (p-ubiquitin) in a combined action with the E3-ubiquitin ligase Parkin, which eventually results in recruitment of the autophagy receptor optineurin and lysosomal delivery of damaged mitochondria (Lazarou et al., 2015). As I observed increased translation of PINK1 upon AMPK inhibition mediated by CC or insulin treatment, I tested whether the function of PINK1 as a ubiquitin kinase during mitophagy was affected by insulin. To this end, I used a phospho-specific antibody against ubiquitin (S65) and took advantage of the decreased mitochondrial density in dendrites compared to the soma to visualize p-ubiquitin localization to mitochondria. In the presence of insulin, I detected increased p-ubiquitin generation at mitochondria upon mitophagy induction using the complex III inhibitor Antimycin A (AA). This was, indeed, significantly impaired in neurons grown in insulin-free medium (Fig. 26a,b), which is in line with reduced PINK1 protein levels under this condition (Fig. 19,f,g). As phosphorylated ubiquitin serves as Parkin receptor (Okatsu et al., 2015), I next examined whether Parkin recruitment to mitochondria upon induction of mitophagy was also affected in the absence of insulin. Using live cell microscopy, I observed impaired mitochondrial Parkin recruitment in the absence of insulin (Fig. 26c,d), providing additional support for the positive regulation of mitophagy via insulin signaling. To further investigate the impact of insulin signaling on the engulfment of damaged mitochondria into autophagosomes, I also assessed mitochondrial

recruitment of optineurin, a key autophagy receptor in the PINK1/Parkin-dependent mitophagy pathway. In line with decreased PINK1 protein levels (Fig. 19f,g) as well as reduced p-ubiquitin (Fig. 26a,b) and Parkin localization to mitochondria (Fig. 26c,d), AA-induced optineurin recruitment was also significantly impaired in the absence of insulin (Fig. 26e,f). As the final step of mitophagy, colocalization of mitochondria with LAMP1-positive lysosomes following AA treatment was only observed when the neurons were cultured in the presence of insulin overnight (Fig. 26g,h).

Figure 26: Insulin supports PINK1 activation and mitophagy.

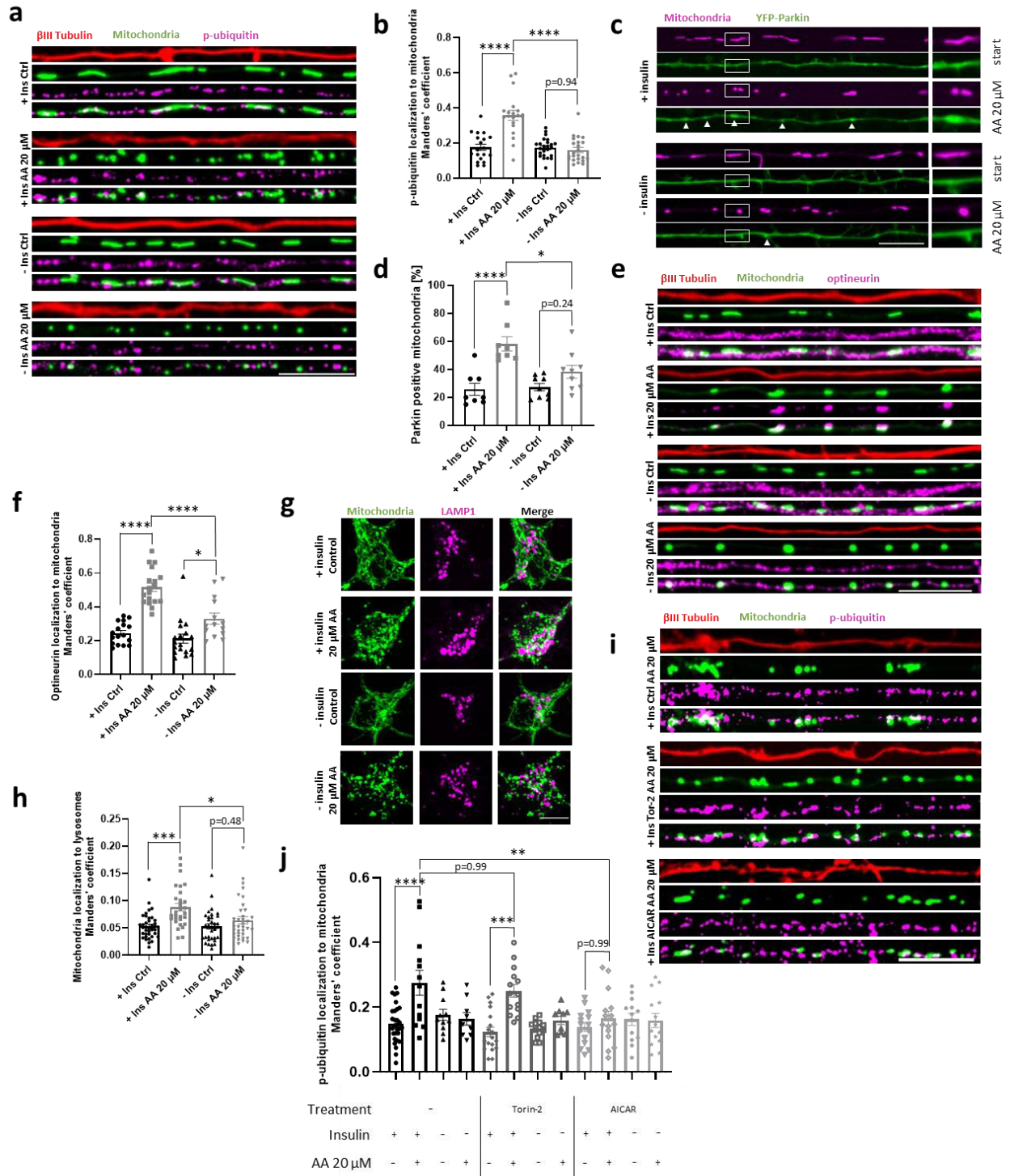**(a)** Representative dendrite images of primary hippocampal neurons grown with or without insulin overnight before treatment with or without 20 µM AA overexpressing mito-meGFP and immunostained for βIII tubulin and phospho-ubiquitin (S65). **(b)** Manders' coefficient-based quantification of the colocalization between the phospho-ubiquitin (S65) and the mitochondrial channel as in a. One-way ANOVA with Tukey's post hoc test; n = 19 - 24: p < 0.0001 (****). **(c)** Representative dendrite images of primary hippocampal neurons overexpressing YFP-Parkin and mitochondrially targeted mRaspberry grown with or without insulin overnight before treatment with 20 µM AA. The white arrowheads highlight Parkin-positive mitochondria observed through live cell imaging before (start) and 30 min after AA treatment. **(d)** Quantification of Parkin-positive mitochondria before and after AA addition as in c. One-way ANOVA with Tukey's post hoc test; n = 8 - 9; p < 0.05 (*), p < 0.0001 (****). **(e)** Representative dendrite images of primary hippocampal neurons grown with or without insulin overnight before treatment with or without 20 µM AA overexpressing mito-meGFP and immunostained for βIII tubulin and optineurin. **(f)** Manders' coefficient-based quantification of the colocalization between the optineurin and the mitochondrial channel as in e. One-way ANOVA with Tukey's post hoc test; n = 14 - 18; p < 0.05 (*), p < 0.0001 (****). **(g)** Representative soma images of primary hippocampal neurons grown with or without insulin overnight before treatment with or without 20 µM AA overexpressing mito-meGFP and LAMP1-mCherry. **(h)** Manders' coefficient-based quantification of the colocalization between the mitochondrial and the lysosomal channel as in g. One-way ANOVA with Tukey's post hoc test; n = 30 - 38; p < 0.05 (*), p < 0.001 (***). **(i)** Representative dendrite images of primary hippocampal neurons grown in the presence of insulin overnight before treatment with Torin-2 (10 nM, 30 min) or AICAR (1 mM, 2 h) as well as 20 µM AA. The neurons overexpress mito-meGFP and are immunostained for βIII tubulin and phospho-ubiquitin (S65). **(j)** Manders' coefficient-based quantification of the colocalization between the phospho-ubiquitin (S65) and the mitochondrial channel following different treatments as indicated. One-way ANOVA with Tukey's post hoc test; n = 9 - 29; p < 0.01 (**), p < 0.001 (***), p < 0.0001 (****).

All data are presented as mean ± SEM. Data points correspond to single cells obtained from ≥3 biological replicates (**b,d,f,h,j**). Scale bars, 10 µm (adapted from Hees & Harbauer, 2023 and from the unpublished data in the revised manuscript Hees et al., 2023 (under review)).

Importantly, the insulin-induced effect on PINK1 availability and function was not dependent on general translational regulation by mTOR signaling as the mTOR inhibitor Torin-2 did not prevent the mitochondrial p-ubiquitination (Fig. 26i,j). AMPK activation using AICAR, however, inhibited generation of p-ubiquitin at mitochondria also in the presence of insulin (Fig. 26i,j). Thus, PINK1 activation and its function as ubiquitin kinase is mediated by AMPK downstream of insulin signaling.

3.18 Insulin effect on PINK1 activation and mitophagy is mediated through SYNJ2BP dephosphorylation

Given the insulin-mediated effect on PINK1 activity and mitophagy I next investigated whether this effect is regulated by SYNJ2BP phosphorylation and consequently *Pink1* mRNA localization. Therefore, I examined whether overexpression of the phospho-ablative SYNJ2BP S21A mutant would be able to boost PINK1 activity upon insulin withdrawal as measured by p-ubiquitin localization at mitochondria. Indeed, if instead of SYNJ2BP WT the phospho-ablative SYNJ2BP S21A mutant was overexpressed, p-ubiquitin localized to mitochondria also in the absence of insulin upon AA treatment indicating PINK1 activity (Fig. 27a,b). Accordingly, overexpression of the phospho-mimetic SYNJ2BP S21E mutant in neurons cultured in the presence of insulin inhibited PINK1's function as a ubiquitin kinase (Fig. 27c,d).

_____

In SYNJ2BP S21E overexpressing neurons, *Pink1* mRNA is associated with mitochondria even in the presence of insulin (Fig. 17d-f). Hence, insulin-induced dissociation of *Pink1* mRNA from mitochondria via SYNJ2BP dephosphorylation positively regulates PINK1 availability and its function in the PINK1/Parkin-dependent mitophagy pathway.
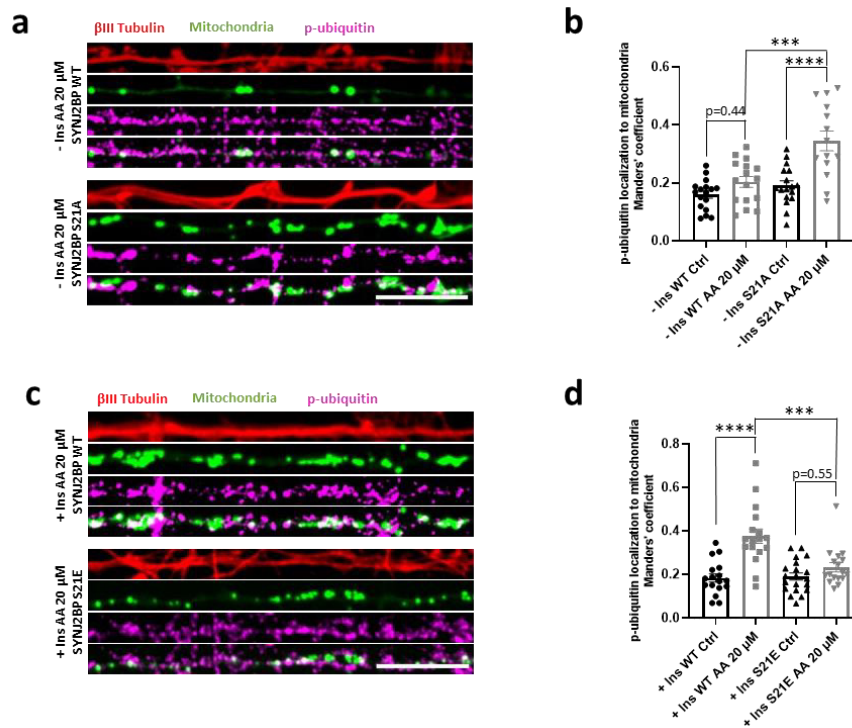
Figure 27: Insulin effect on PINK1 activation and mitophagy is mediated through SYNJ2BP dephosphorylation. **(a)** Representative dendrite images of primary hippocampal neurons grown without insulin overnight before treatment with 20 µM AA. The neurons overexpress mito-meGFP as well as SYNJ2BP WT or S21A and are immunostained for βIII tubulin and phospho-ubiquitin (S65). **(b)** Manders' coefficient-based quantification of the colocalization between the phospho-ubiquitin (S65) and the mitochondrial channel under different conditions as indicated. One-way ANOVA with Tukey's post hoc test; n = 14 - 17; p < 0.001 (***), p < 0.0001 (****). **(c)** Representative dendrite images of primary hippocampal neurons grown in the presence of insulin overnight before treatment with 20 µM AA. The neurons overexpress mito-meGFP as well as SYNJ2BP WT or S21E and are immunostained for βIII tubulin and phospho-ubiquitin (S65). **(d)** Manders' coefficient-based quantification of the colocalization between the phospho-ubiquitin (S65) and the mitochondrial channel under different conditions as indicated. One-way ANOVA with Tukey's post hoc test; n = 17 - 20; p < 0.001 (***), p < 0.0001 (****).

All data are presented as mean ± SEM. Data points correspond to single cells obtained from ≥3 biological replicates (**b,d**). Scale bars, 10 µm (adapted from Hees & Harbauer, 2023).

3.19   ApoE4 inhibits insulin-regulated *Pink1* mRNA localization and PINK1 activation

Brain insulin resistance as well as mitochondrial dysfunction are closely associated with the pathology of AD (Arnold et al., 2018). However, so far, no direct link has been shown between the two phenomena. The presence of the ε4 allele of the apolipoprotein E (ApoE4) has been identified as the strongest genetic risk factor for late onset AD (Bu, 2009; C.-C. Liu et al., 2013). Interestingly, a recent

study showed that addition of ApoE4 to neuronal cultures causes insulin resistance *in vitro* by trapping the IR in endosomes (N. Zhao et al., 2017). I therefore investigated whether ApoE4 treatment prevents the insulin-mediated effects on *Pink1* mRNA localization as well as PINK1 function. To address this question, I first confirmed that ApoE4 inhibits the insulin-mediated reduction in AMPK activity. By measuring the donor lifetime of the AMPK FRET-based activity sensor I indeed observed that the insulin-induced decrease in AMPK activity was prevented upon ApoE4 addition overnight (Fig. 28a). Importantly, this was not the case when its homolog ApoE3 was added to the cultured neurons (Fig. 28a).

Figure 28: ApoE4 inhibits insulin-regulated *Pink1* mRNA localization and PINK1 activation.
(a) Analysis of AMPK activity by performing fluorescence lifetime imaging of the FRET-based AMPK activity sensor donor in primary hippocampal neurons following control or insulin (500 nM, 1 h) treatment in the presence or absence of ApoE3 (50 nM, overnight) or ApoE4 (50 nM, overnight). One-way ANOVA with Tukey's post hoc test; n = 31 - 47; $p < 0.05$ (*), $p < 0.01$ (**), $p < 0.001$ (***). **(b)** Representative images of *Pink1* mRNA as visualized using the MS2/PP7-split Venus approach and mRaspberry-labeled mitochondria in the soma an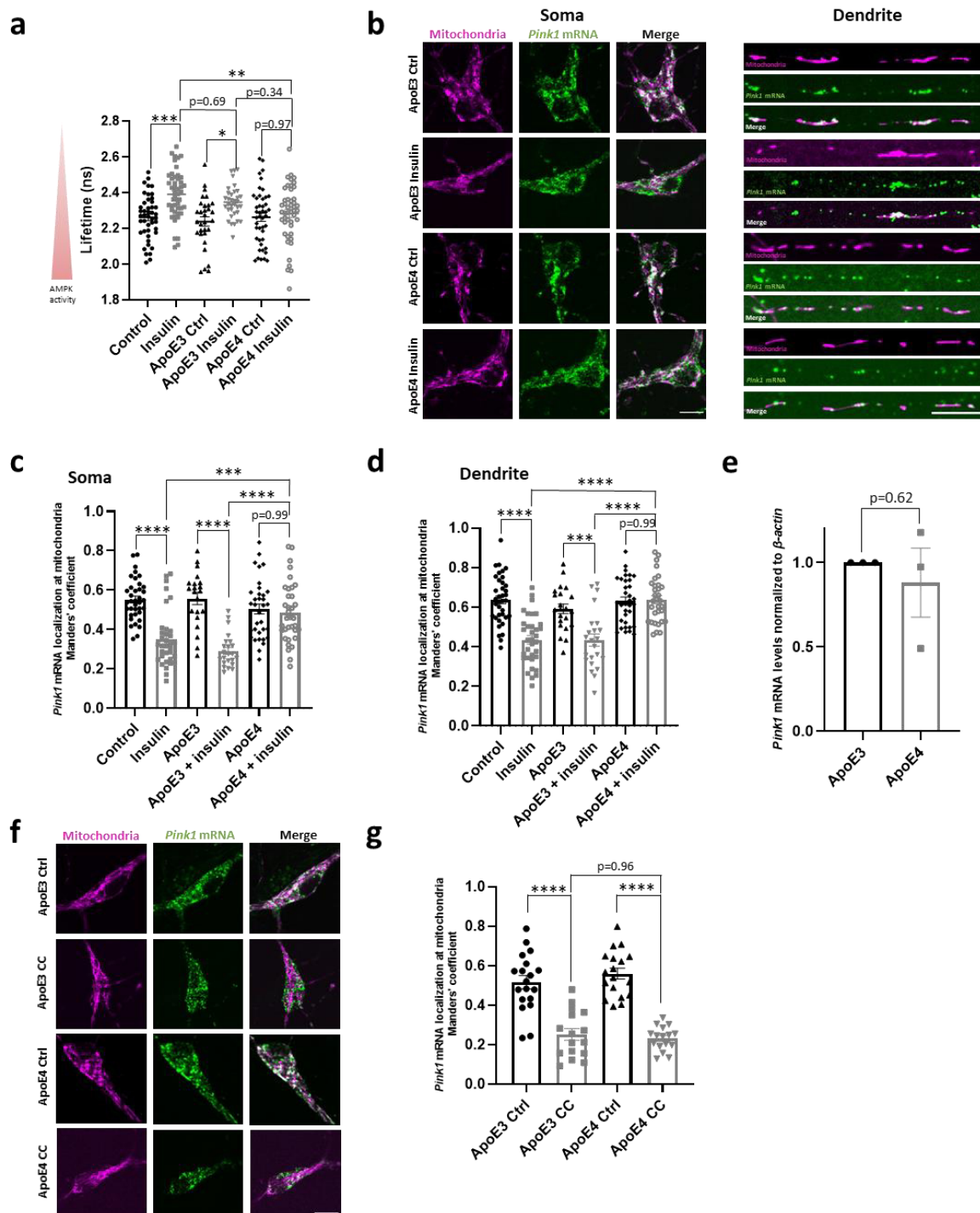d dendrites of primary hippocampal neurons following control or insulin (500 nM, 1 h) treatment in the presence of ApoE3 (50 nM, overnight) or ApoE4 (50 nM, overnight). **(c)** Manders' coefficient-based quantification of the colocalization between the *Pink1* mRNA and the mitochondrial channel in the soma as in **b**. One-way ANOVA with Tukey's post hoc test; n = 21 - 30; $p < 0.001$ (***), $p < 0.0001$ (****). **(d)** Manders' coefficient-based quantification of the colocalization between the *Pink1* mRNA and the mitochondrial channel in dendrites as in **b**. One-way ANOVA with Tukey's post hoc test; n = 22 - 37; $p < 0.001$ (***), $p < 0.0001$ (****). **(e)** *Pink1* transcript levels normalized to β-*actin* transcript levels as assessed by RT-qPCR from primary cortical neurons treated cultured in the presence of ApoE3 (50 nM, overnight) or ApoE4 (50 nM, overnight). Two-tailed Welch's t-test; n = 3. **(f)** Representative images of *Pink1* mRNA as visualized using the MS2/PP7-split Venus approach and mRaspberry-labeled mitochondria in primary hippocampal neurons following control or CC (20 μM, 2 h) treatment in the presence of ApoE3 (50 nM, overnight) or ApoE4 (50 nM, overnight). **(g)** Manders' coefficient-based quantification of the colocalization between the *Pink1* mRNA and the mitochondrial channel as in **f**. One-way ANOVA with Tukey's post hoc test; n = 16 - 19; $p < 0.0001$ (****).

All data are presented as mean ± SEM. Data points correspond to single cells obtained from ≥3 biological replicates (**a,c,d,e,g**). Scale bars, 10 μm (adapted from Hees & Harbauer, 2023 and from the unpublished data in the revised manuscript Hees et al., 2023 (under review)).

In line with that observation, ApoE4 but not ApoE3 prevented the insulin effect on *Pink1* mRNA localization visualized using the MS2/PP7 split-Venus approach. In the presence of ApoE4, *Pink1* mRNA remained tethered to the mitochondria both in the soma and in dendrites despite addition of insulin (Fig. 28b-d). Importantly, the effect on colocalization was not caused by altered *Pink1* mRNA levels upon ApoE3 or ApoE4 treatment (Fig. 28e). Furthermore, ApoE4 did not prevent the CC-mediated dissociation of *Pink1* mRNA from mitochondria suggesting that the ApoE4-induced effect on *Pink1* mRNA localization occurs upstream of AMPK (Fig. 28f,g).

As I observed that *Pink1* mRNA association to mitochondria is dependent on AMPK-mediated SYNJ2BP phosphorylation (Fig. 16a,b), I next tested whether overexpression of the phospho-ablative SYNJ2BP S21A mutant would rescue the ApoE4-induced phenotype. Indeed, mitochondrial *Pink1* mRNA localization was significantly reduced in insulin- and ApoE4-treated neurons, when instead of SYNJ2BP WT the phospho-ablative SYNJ2BP S21A mutant was overexpressed (Fig. 29a,b). Given the observation of reduced PINK1 availability and activation in the absence of insulin (Fig. 19f,g and Fig. 25a,b), I tested whether ApoE4 would also inhibit the insulin-induced effect on PINK1 activity as measured by mitochondrial p-ubiquitin generation. Unlike its homolog ApoE3, ApoE4 abolished mitochondrial p-ubiquitination upon induction of mitochondrial damage using AA in the presence of insulin (Fig. 29c,d). Taken together, insulin resistance *in vitro* induced by ApoE4 application dysregulates *Pink1* mRNA localization and consequently PINK1's function in the removal of damaged mitochondria via mitophagy.
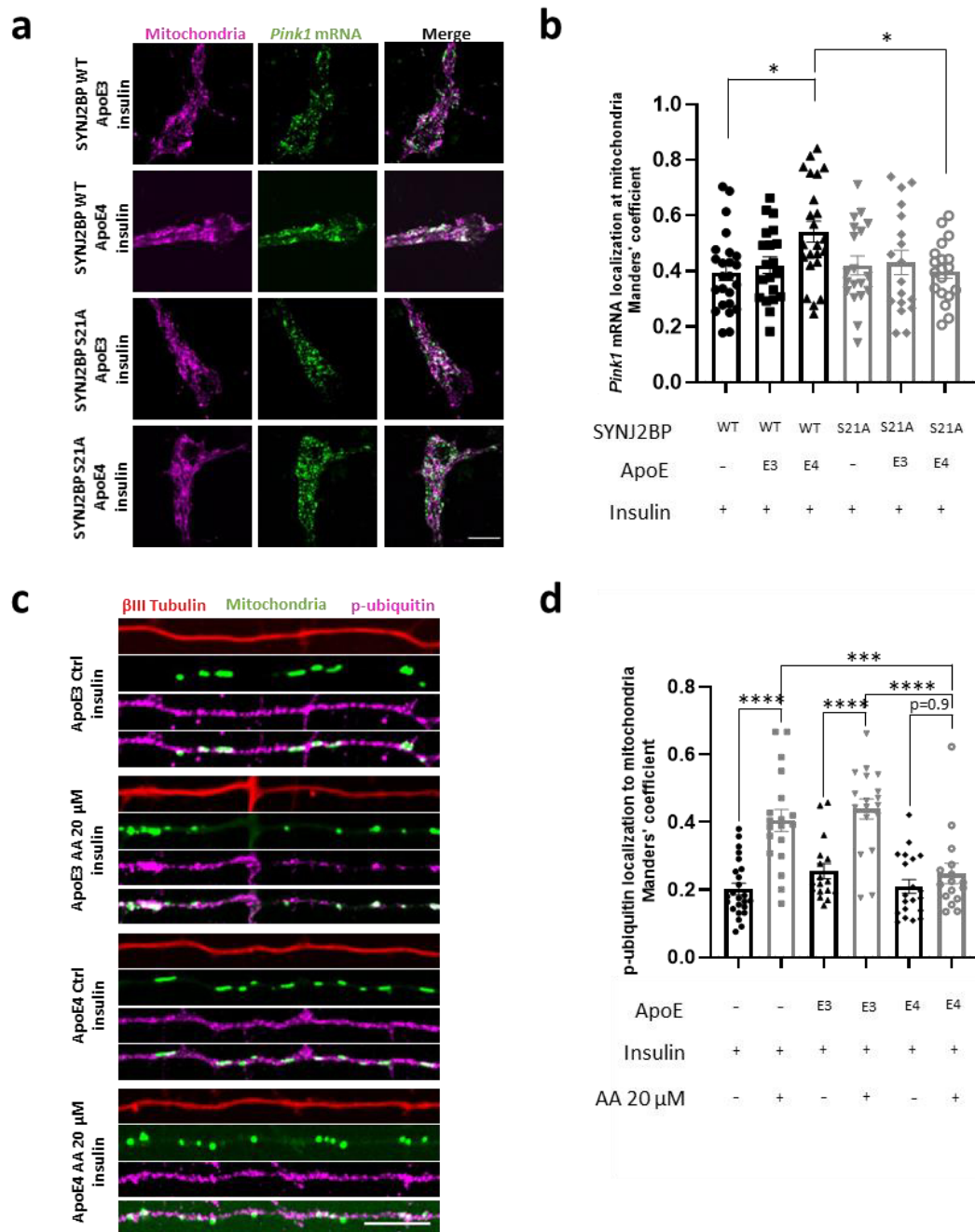
Figure 29: ApoE4 inhibits insulin-regulated PINK1 activation.
(a) Representative images of *Pink1* mRNA as visualized using the MS2/PP7-split Venus approach and mRaspberry-labeled mitochondria in primary hippocampal neurons grown in the presence of insulin and treated with ApoE3 (50 nM, overnight) or ApoE4 (50 nM, overnight). The neurons overexpress SYNJ2BP WT or S21A. **(b)** Manders' coefficient-based quantification of the colocalization between the *Pink1* mRNA and the mitochondrial channel under different conditions as indicated. One-way ANOVA with Tukey's post hoc test; n = 18 - 24; p < 0.05 (*).
(c) Representative dendrite images of primary hippocampal neurons grown in the presence of insulin as well as ApoE3 (50 nM, overnight) or ApoE4 (50 nM, overnight) before treatment with or without 20 µM AA. The neurons overexpress mito-meGFP and are immunostained for βIII tubulin and phospho-ubiquitin (S65). **(d)** Manders' coefficient-based quantification of the colocalization between the phospho-ubiquitin (S65) and the mitochondrial channel following different treatments as indicated. One-way ANOVA with Tukey's post hoc test; n = 17 - 24; p < 0.001 (***), p < 0.0001 (****).

All data are presented as mean ± SEM. Data points correspond to single cells obtained from ≥3 biological replicates (**b,d**). Scale bars, 10 µm (adapted from Hees & Harbauer, 2023).

4 DISCUSSION

In my project, I discovered a metabolically regulated switch that controls *Pink1* mRNA localization, translation as well as PINK1 function in response to insulin and AMPK signaling. I have shown that AMPK phosphorylates the mitochondrial anchor protein SYNJ2BP at S21, which leads to a strengthened interaction with the RNA-binding protein SYNJ2a, thereby increasing the association of *Pink1* mRNA with mitochondria. In this way, efficient transport of *Pink1* mRNA into distal parts of the neuron is ensured, which allows for on-demand local translation of the short-lived PINK1 protein (Harbauer et al., 2022). However, during AMPK-mediated mitochondrial binding of *Pink1* mRNA, its translation as well as PINK1/Parkin-dependent mitophagy is reduced. This might serve to increase the mitochondrial content during times of ATP shortage as signaled by AMPK activity (Fig. 30a). Insulin-mediated AMPK inhibition untethers *Pink1* mRNA from mitochondria resulting in translocation of *Pink1* mRNA to endolysosomes. At the endolysosomal compartment, amino acids derived from lysosomal protein degradation fuel local translation of the PINK1 protein, potentially at ER-associated ribosomes. Transfer of the PINK1 precursor to mitochondria with the help of chaperones like DNAJB6 facilitates PINK1 protein import and also PINK1/Parkin-dependent mitophagy during times of energy abundance (Fig. 30b). Disturbance of proper metabolic regulation, such as insulin resistance in AD, directly impacts the ability of neurons to upregulate PINK1 translation as needed, which most likely contributes to the mitochondrial dysfunction observed in AD.
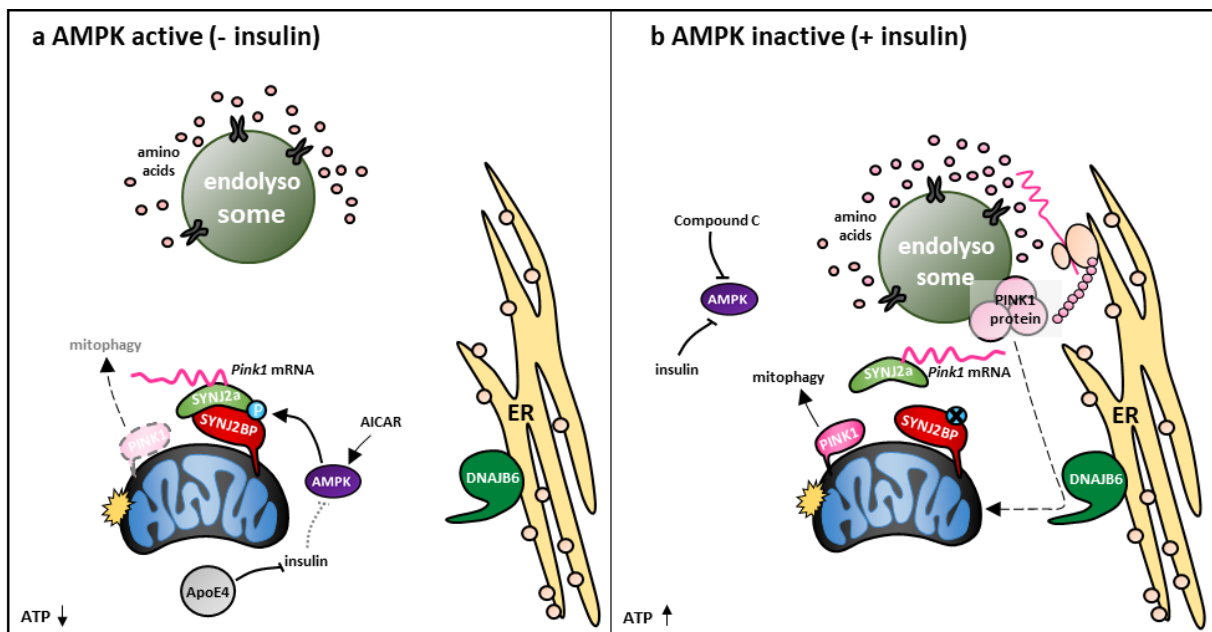
Figure 30: Insulin signaling regulates *Pink1* mRNA localization and translation via modulation of AMPK activity. **(a)** During periods of energy shortage, characterized by low ATP levels, increased AMPK activity and decreased insulin levels, *Pink1* mRNA is tethered to mitochondria via SYNJ2BP and SYNJ2a. The interaction between SYNJ2BP and SYNJ2a is enhanced by AMPK-mediated phosphorylation of SYNJ2BP at S21. Mitochondrial *Pink1*

_____

mRNA association results in reduced translation of PINK1 and a subsequent decrease in mitophagy levels. ApoE4 mimics this condition by impeding the insulin-mediated effects. **(b)** During periods of energy abundance, characterized by high ATP levels, decreased AMPK activity and increased insulin levels, less *Pink1* mRNA is tethered to mitochondria due to a reduced interaction between SYNJ2BP and SYNJ2a. This results in increased PINK1 translation at the endolysosomal compartment in close proximity to the ER and mitochondria. DNAJB6 might be involved in guiding the PINK1 protein back to its mitochondrial destination. In this state of energy abundance, mitophagy is favored samples (adapted from Hees & Harbauer, 2023).

4.1 AMPK does not universally promote autophagy

While AMPK is widely recognized for its role in promoting autophagy, including mitophagy, through the phosphorylation and activation of ULK1 (Egan et al., 2011; J. Kim et al., 2011), the model proposed in this thesis suggests that AMPK negatively regulates PINK1/Parkin-dependent mitophagy in neurons (Fig. 26). Notably, a very recent study conducted in non-neuronal cells has challenged the traditional view by demonstrating that starvation-induced AMPK-mediated phosphorylation of ULK1 inhibits ULK1 activity, thereby impeding the initiation of autophagy (Park et al., 2023). This discovery aligns with the findings of this thesis and emphasizes that the current understanding of the relationship between autophagy initiation and AMPK is still too simplified and requires further investigation. Autophagy itself is an energy-consuming process and hence, during energy shortage, the cell might first prioritize other critical processes. Although AMPK initially inhibits autophagy, it does preserve the cellular ability to perform autophagy by protecting the ULK1-associated autophagy machinery from caspase-mediated degradation (Park et al., 2023). As neurons are very energy-demanding cells, this mechanism of initial inhibition of autophagy as well as mitophagy mediated by AMPK might be particularly pronounced in neurons.

Both starvation-induced activation of AMPK and inhibition of mTOR signaling are generally known to increase bulk autophagy (Bagherniya et al., 2018). Interestingly, in cultured neurons, however, neither starvation nor inhibition of mTOR signaling result in enhanced autophagy (Maday & Holzbaur, 2016). Consistent with these findings, I also observed differences between neurons and non-neuronal cells. The increased PINK1 translation following AMPK inhibition (Fig. 18b-d,i-k; Fig. 19f,g,j,k) and potentially also its impact on mitophagy appear to be specific to neurons. The primary function of neuronal autophagy, including mitophagy, might be the maintenance of cellular homeostasis by degrading aging organelles and proteins rather than the mobilization of biosynthetic building blocks such as amino acids as observed in other cell types (Maday & Holzbaur, 2016). The homeostatic function of autophagy is particularly important in neurons as these cells are postmitotic and need to last an entire lifetime. Consequently, they heavily rely on quality-control pathways as they cannot divide to dilute out toxic proteins or organelles.

Finally, there is relatively limited research focused on the role of AMPK in PINK1/Parkin-dependent mitophagy. However, in a recent study, a link between the AMPK substrate ULK1 and the PINK1/Parkin-dependent mitophagy pathway has been identified (C.-M. Hung et al., 2021). Parkin has been shown to be phosphorylated at S108 by AMPK-dependent ULK1 within five minutes upon induction of mitochondrial damage (C.-M. Hung et al., 2021). This represents a very early step in the mitophagy pathway as activation of PINK1 only occurs 30 to 60 minutes later (C.-M. Hung et al., 2021). The phosphorylation of Parkin at S108 by ULK1 has also been detected in human embryonic stem cell line-derived neurons (C.-M. Hung et al., 2021). Importantly, the findings of this thesis add another layer to this complex relationship by demonstrating the necessity of AMPK inhibition for proper PINK1 function and consequently mitophagy in neurons (Fig. 26). Further research is needed to fully understand the intricate interplay between AMPK and PINK1/Parkin-mediated mitophagy in neurons.

4.2 Neurons require cell type-specific mitophagy mechanisms

Morphologically, neurons have a very complex structure, which makes maintaining a healthy mitochondrial network very challenging (Misgeld & Schwarz, 2017) and thus might require neuron-specific mechanisms. Apart from the challenging mitostasis, neurons heavily rely on mitochondrial function due to their high energy demand. Therefore, PINK1/Parkin-dependent mitophagy might only be activated if sufficient energy supply is ensured or if the mitochondrion is severely damaged and thus harmful to the cell. This hypothesis is supported by the findings presented in this thesis. Fittingly, PINK1/Parkin-dependent mitophagy is not detectable under basal conditions in neurons (Goldsmith et al., 2022; Le Guerroué et al., 2017; McWilliams et al., 2018; Ordureau et al., 2021) but can be induced by stressors such as exhaustive exercise or the progression of aging (Cornelissen et al., 2018; Y.-T. Liu et al., 2021).

Upon induction of mitochondrial damage, I observed PINK1/Parkin-dependent mitophagy only in the presence of insulin (Fig. 26), which indicates sufficient ATP levels along with decreased activity of AMPK. A recent study showed that low concentrations of AA are not sufficient to recruit Parkin to mitochondria in cultured hippocampal neurons (M.-Y. Lin et al., 2017). Interestingly, these neurons were imaged in a medium that did not contain any growth factors including insulin. Additionally, variations in the effectiveness of PINK1/Parkin-dependent mitophagy have also been reported in human iPSC-derived neurons. While some studies were able to observe mitochondrial Parkin recruitment upon induction of mitochondrial damage (Oh et al., 2017; Seibler et al., 2011), others claim that PINK1/Parkin-mediated mitophagy does not occur in human neurons (Rakovic et al., 2013). As I only observed PINK1/Parkin-dependent mitophagy when insulin was present in the medium, it is possible that different media composition might explain the different experimental outcomes.

_____

My findings are in line with previous studies that link PINK1/Parkin-mediated mitophagy to insulin signaling and AKT activity in neurons (McCoy et al., 2014; Soutar et al., 2018). While AKT inhibition reduces mitochondrial PINK1 accumulation, Parkin recruitment, ubiquitin phosphorylation as well as overall mitophagy levels, insulin-mediated AKT stimulation increases the mitophagy pathway (Soutar et al., 2018). AKT is activated by increased PIP_3 levels. Interestingly, PIP_3 levels have also been shown to be upregulated by PINK1 itself (Furlong et al., 2019). This could suggest a positive feedback mechanism, in which PINK1 can promote untethering of its own mRNA by ensuring local AKT activity and thus AMPK inhibition.

AMPK is known to affect several aspects of mitochondrial homeostasis in neurons. It not only induces mitochondrial fission but also suppresses retrograde transport of axonal mitochondria and promotes their anchoring at synapses (S. Li et al., 2020; Toyama et al., 2016; Watters et al., 2020). All of these pathways ensure the presence of mitochondria in axons and synapses undergoing energy shortage. Our finding that AMPK activity reduces PINK1 synthesis as well as PINK1/Parkin-dependent mitophagy fits into the picture as it also increases the mitochondrial content and hence counteracts the energy shortage. Furthermore, it might serve a second purpose: Reducing the mitophagy process also saves energy as it is an energy-consuming process itself. Interestingly, PINK1 has also been shown to recruit mRNAs encoding for mitochondrial OXPHOS proteins to mitochondria and to upregulate their translation (Gehrke et al., 2015) apart from its role in mitophagy. Protein synthesis is a very energy-demanding process. Therefore, restraining PINK1 biogenesis to periods of energy abundance as signaled by increased insulin levels might also restrict translation of other mitochondrial proteins thereby reducing energy-consuming local translation during ATP shortage.

It is very likely that severely damaged mitochondria are still delivered to degradative lysosomes even in the absence of insulin. As PINK1/Parkin-dependent mitophagy is less active under these conditions, it is possible that other mitophagy pathways are upregulated during these energy-limiting conditions in the absence of insulin. One potential compensatory pathway is the FUNDC1-mediated mitophagy. FUNDC1 is a protein in the outer mitochondrial membrane and an identified mitophagy receptor (L. Liu et al., 2012). ULK1, activated by AMPK-mediated phosphorylation (Egan et al., 2011; J. Kim et al., 2011), translocates to mitochondria and phosphorylates and thereby activates FUNDC1 (Tian et al., 2015; W. Wu et al., 2014). As AMPK signaling is increased during energy-limiting conditions, activation of ULK1 and FUNDC1 might provide an alternative mitophagy pathway, which allows for removal of damaged mitochondria when PINK1/Parkin-dependent mitophagy is reduced. It remains to be determined whether AMPK/ULK1-mediated phosphorylation of FUNDC1 contributes to mitophagy in neurons.

4.3 The SunTag system reports increased PINK1 translation upon AMPK inhibition

Inhibition of AMPK leads to a significant increase in the mean intensity as well as the mean area of PINK1 SunTag clusters suggesting that translation of PINK1 is upregulated (Fig. 18b-d). The SunTag system visualizes translation of single mRNAs by fluorescently labeling the nascent polypeptide using an scFv-GFP (Khuperkar et al., 2020). The observed increase in PINK1 SunTag cluster formation upon AMPK inhibition could represent the accumulation of multiple mRNAs undergoing translation simultaneously, the presence of multiple ribosomes associated with a single mRNA molecule, or a combination of both phenomena. In addition to analyzing the mean intensity and area of the SunTag clusters, another informative parameter is typically the number of clusters per cell. However, due to the unusually large size and the resolution limits present during confocal light microscopy, it is possible that multiple individual dots contribute to each large SunTag cluster. Hence, this particular measurement cannot be utilized in the context of this experiment. Besides an upregulated synthesis of PINK1, the possibility of impaired degradation of PINK1 also needs to be considered. Based on the very short half-life of PINK1 and the assumption that scFv-GFP can no longer bind to the construct upon mitochondrial PINK1 import, only freshly synthesized PINK1 precursors are visualized. This is also corroborated by the puromycin sensitivity of the SunTag signal (Fig. 18e-g). However, PINK1 protein that is not properly degraded and hence accumulates in the cell would also very likely be recognized by the scFv-GFP resulting in SunTag signal. Therefore, the data needs to be confirmed by alternative methods. One complementary experiment using neuronal cultures from the RiboTag mice showed a trend towards increased ribosomal *Pink1* mRNA association upon AMPK inhibition (Fig. 19b,c), which supports the hypothesis of upregulated PINK1 synthesis. PINK1 protein levels on Western blot also mirrored the effect seen with the SunTag system (Fig. 19d-g). Additionally, polysome profiling using sucrose gradient centrifugation could be performed in the future to specifically determine *Pink1* mRNA association with monosomes versus polysomes. An increased association with the translationally active polysomes upon AMPK inhibition would further confirm that PINK1 translation is enhanced. Lastly, the possibility of impaired degradation of PINK1 should be ruled out by a cycloheximide chase assay.

4.4 PINK1 translation occurs at organellar MCSs

According to the model presented in this thesis, *Pink1* mRNA is associated and co-transported with mitochondria, increasingly translated in proximity to the ER and endolysosomes to finally exert its function back at mitochondria. The back and forth of the mRNA as well as the protein between mitochondria and endolysosomes seems to be very inefficient at first sight. However, the mRNA molecules as well as the protein do not have to travel a long way because there are MCSs between

organelles such as mitochondria, ER and endolysosomes, which are critically involved in maintaining cellular functions (Elbaz & Schuldiner, 2011; Murley & Nunnari, 2016; Phillips & Voeltz, 2016; H. Wu et al., 2018). Interestingly, translation of proteins seems to preferentially occur at organellar contact sites in neurons (reviewed in Hees & Harbauer, 2022). Rab7-positive endolysosomes have been shown to serve as translation platform for nuclear-encoded mitochondrial transcripts in axons (Cioni et al., 2019). The endolysosomes stop in close proximity to mitochondria thereby forming mitochondria-endolysosome MCSs. In line with that, I observed increased PINK1 translation as visualized by the SunTag system at the endolysosomal compartment upon AMPK inhibition (Fig. 22a,b). This compartment serves as an ideal platform for protein translation as its environment is rich in amino acids and other building blocks that are transported back into the cytosol following degradation inside the organelle. Supporting its importance as a metabolic signaling hub, both AMPK and mTORC1 are localized to the endolysosomes (Carroll & Dunlop, 2017; Lamming & Bar-Peled, 2019). While PINK1 translation was not dependent on mTORC1 signaling (Fig. 24a-f), inhibition of the degradative capacity of the endolysosomes using Bafilomycin A1 prevented the effect on PINK1 synthesis mediated by AMPK inhibition (Fig. 24g-l). Translation of PINK1 was not only no longer localized to the endolysosomal compartment but also significantly reduced confirming the importance on this organelle in protein synthesis.

Intriguingly, I also observed the ER in close proximity to the PINK1 translation hotspot as well as next to the mitochondria and endolysosomes (Fig. 25a). To date, only one MCS involving all three organelles (mitochondria, ER, and endolysosomes) has been characterized in mammalian cells including the ER transmembrane proteins PDZD8 and Protrudin as well as the late endosomal protein Rab7 as important tethers (Elbaz-Alon et al., 2020). As indicated by the name, PDZD8 contains a PDZ domain similar to the mitochondrial anchor protein SYNJ2BP. It is interesting to speculate that the RNA-binding protein SYNJ2a, which contains the complementary PDZ motif, might be able to interact with PDZD8 thereby bringing *Pink1* mRNA along. However, both presence and function of this three-way MCS remains to be elucidated in neurons. Another open question is how ribosomes localize to those translation hotspots in neurons. Interestingly, apart from interacting with SYNJ2a, SYNJ2BP also has a known interaction partner at the rough ER: RRBP1 (V. Hung et al., 2017). As the rough ER is associated with ribosomes, this tether pair has been shown to play an important role in protein translation (V. Hung et al., 2017). It is intriguing to speculate that the interaction between SYNJ2BP and RRBP1 increases upon AMPK inhibition, oppositely regulated compared to SYNJ2BP and SYNJ2a interaction, which could potentially facilitate translation of *Pink1* mRNA.

After all, PINK1 is a mitochondrial protein, which raises the question how PINK1 finds its way back to mitochondria after being translated at another organelle. In a recent study, the so-called ER-SURF pathway has been identified in yeast (Hansen et al., 2018). Mitochondrial membrane protein

_____

precursors are bound by ER-associated chaperones such as Djp1, which facilitate their transfer to the mitochondria (Hansen et al., 2018). Interestingly, I found the mammalian homolog of Djp1, DNAJB6, to colocalize with the PINK1 SunTag clusters in my experiments (Fig. 25b). This suggests that PINK1 protein translated at endolysosomes in close proximity to the ER gets translocated back to the mitochondria with the help of the chaperone DNAJB6. In line with that DNAJB6 has been found to restore mitophagy in the neuron-like cell line SK-N-SH overexpressing the PD-associated Parkin C289G mutant (Rose et al., 2011). DNAJB6 prevents aggregation of Parkin C289G and promotes its localization to damaged mitochondria (Rose et al., 2011). It is intriguing to speculate that DNAJB6 plays a similar role in mitochondrial PINK1 localization in neurons. It remains to be determined whether knockdown of DNAJB6 affects PINK1/Parkin-dependent mitophagy or even prevents the formation of PINK1 SunTag clusters.

In another recent study in yeast, so-called MitoStores have been identified (Krämer et al., 2023). MitoStores are cytosolic deposits that transiently store nuclear-encoded mitochondrial proteins containing N-terminal mitochondrial targeting signals. The MitoStore formation, which is controlled by the chaperones Hsp42 and Hsp104 in yeast, counteracts potentially aberrantly accumulating mitochondrial precursor proteins when protein synthesis exceeds the capacity of the mitochondrial import system (Krämer et al., 2023). It is possible that the observed PINK1 SunTag clusters upon AMPK inhibition represent chaperone-controlled MitoStores. This could mean that during energy abundance PINK1 is increasingly synthesized and then transiently stored until needed. However, it remains to be investigated if this is the nature of PINK1 SunTag clusters.

Finally, proximity-specific ribosome profiling could be conducted in the future. In this approach, a selective biotin ligase (BirA) biotinylates a specific acceptor tag sequence (Avi-Tag), which is placed on the ribosomal protein Rpl10a (Williams et al., 2014). Purification of the biotinylated ribosomes by performing a streptavidin pull down would also allow to investigate ribosomal *Pink1* mRNA association upon AMPK inhibition. Moreover, BirA could also be targeted to specific organelles such as mitochondria, endolysosomes and the ER to investigate the localization of PINK1 translation. This approach could be used to confirm my finding that PINK1 may be synthesized by ER-associated ribosomes upon AMPK inhibition.

4.5 *Pink1* mRNA tethering and translation are inversely regulated

My findings indicate that there is metabolically regulated switching between mitochondrial association of *Pink1* mRNA and translation of *Pink1* mRNA at endolysosomes. This metabolic control is mediated by AMPK downstream of insulin signaling. The insulin signaling off/AMPK on state is required for *Pink1* mRNA association with mitochondria allowing for co-transport into distal parts of the neuron. In

_____

contrast, the insulin signaling on/AMPK off state favors translation of PINK1 at endolysosomes as well as mitophagy. AMPK is generally known to upregulate mitochondrial biogenesis via activation of the transcription factor PGC-1α (Jäger et al., 2007). According to my model, AMPK reduces biogenesis of PINK1 and potentially other nuclear-encoded mitochondrial proteins that are regulated in the same way such as Atp5f1β. This AMPK-mediated downregulation, however, occurs at the translational level, while *Pink1* transcript levels do not change. In line with that, insulin signaling, which reduces AMPK activity, has been shown to induce translation of nuclear-encoded mitochondrial transcripts via activation of mTORC1, which in turn stimulates the eIF4E (Morita et al., 2013). Hence, there is a differential regulation of mitochondrial biogenesis at the transcriptional versus the translational level (Hees & Harbauer, 2022). While insulin- and mTORC1-mediated AMPK inhibition downregulates PGC-1α-dependent transcription, it may increase translation of mitochondrial proteins. In line with that, other studies also hypothesized that AMPK might inhibit mitochondrial biogenesis (Cardanho-Ramos & Morais, 2021) as it counteracts mTORC1-induced protein synthesis in neurons (Ishizuka et al., 2013). While my findings support the hypothesis, the mechanism is not dependent on mTORC1 as inhibition of mTOR signaling does not prevent the effect on PINK1 translation (Fig. 24a-f). Instead, it is dependent on reversible phosphorylation of SYNJ2BP. AMPK-mediated SYNJ2BP phosphorylation increases *Pink1* mRNA binding to mitochondria. Dephosphorylation, in contrast, untethers *Pink1* mRNA from mitochondria and allows for efficient translation at the endolysosomal compartment. Interestingly, multiple sequences within the coding region of the mRNA seem to be required for efficient binding to the RNA-binding protein SYNJ2a (Harbauer et al., 2022). This is not only in line with other studies reporting that the coding region rather than the UTRs are required for binding (Cohen et al., 2022; Popovic et al., 2020) but also supports the model that *Pink1* mRNA binding and translation by ribosomes cannot occur simultaneously. While translation is required for the first round of tethering (Harbauer et al., 2022), the *Pink1* transcript needs to dissociate from mitochondria to enable efficient reading of the sequence by ribosomes.

Furthermore, unraveling the identity of the phosphatase dephosphorylating SYNJ2BP at S21 and thereby enabling dissociation of *Pink1* mRNA from mitochondria would immensely contribute to a better understanding of the underlying regulatory mechanisms. Constructing an interactome centered around SYNJ2BP and the implementation of proximity labeling strategies might offer valuable insights, given that the phosphatase should exhibit at least transient interactions with SYNJ2BP. Moreover, the phosphatase's scope should extend beyond mere mitochondrial localization; it should also be enriched at endolysosomes and the ER. This is crucial as these organelles emerge as plausible sites for *Pink1* mRNA dissociation from mitochondria and subsequent translation. Importantly, my observations have revealed diminished AMPK activity at endolysosomes in contrast to mitochondria (Fig. 22e), thereby providing a conducive environment for the phosphatase's action. Taken together, the identification of

_____

the phosphatase, positioned to promote PINK1/Parkin-dependent mitophagy in contrast to its counterpart kinase AMPK, has the potential to unveil a new layer of regulatory complexities within this intricate mechanism.

4.6 Ribosomes might be stalled during AMPK-mediated mitochondrial *Pink1* mRNA tethering

In neurons, ribosomes are mainly detected in the somato-dendritic compartment, while their presence in the axonal compartment is still controversial. Hence, local translation in axons is also a matter of debate. However, it has recently been shown that axonal ribosomes are only rarely seen grouped into polysomes. Instead, 80S monosomes mainly contribute to axonal local translation (Biever et al., 2020), which explains the scarce ribosomal distribution in axons.

While I could show that ribosomes are localized to the somatic PINK1 SunTag clusters by performing a PLA experiment (Fig. 20a-d), the origin of these ribosomes still needs to be determined. They might either accompany mitochondria and their mRNA cargo during transport or their recruitment could depend on specific signaling cues. During energy shortage, characterized by AMPK activation and consequently mitochondrial *Pink1* mRNA association, I observed reduced translation of PINK1 (Fig. 18b-d). Hence, if ribosomes are associated with the traveling mRNA, translation might be limited to monosomes or even stalled under these circumstances. The binding of SYNJ2a within the coding region of *Pink1* mRNA (Harbauer et al., 2022) might block the ribosome from translating the transcript. Employing ribosomal footprinting would allow to identify the sequences with increased ribosomal occupancy, thereby serving as a method to test whether ribosomes are mainly localized upstream of the SYNJ2a binding region during periods of energy insufficiency. Furthermore, polysome profiling could help to assess whether *Pink1* mRNA association shifts from monosomes to polysomes upon translational activation, which is induced by AMPK inhibition.

There are two spatially separate populations of cytosolic ribosomes: free ribosomes and membrane-bound ribosomes attached to the cytosolic side of the ER. My findings show that upon AMPK inhibition PINK1 translation occurs in close proximity to the ER suggesting that the PINK1 protein is synthesized on ER-associated ribosomes and not free cytosolic ribosomes as previously assumed. As discussed in chapter 4.4, PINK1 may therefore be the first mammalian protein that follows the ER-SURF pathway (Hansen et al., 2018). Considering the limited availability of free cytoplasmic ribosomes in axons, translating on the ER membrane could potentially increase the chances of PINK1 translation upon formation of contact sites between mitochondria and the ER. However, it still remains to be shown whether stretches of rough ER are present in axons.

_____

4.7 Insulin resistance causes mitochondrial dysfunction in the context of AD *in vitro*

Brain insulin resistance as well as mitochondrial dysfunction are a frequent characteristic of both metabolic and cognitive dysfunctions including type 2 diabetes and AD (Kullmann et al., 2016; Laws et al., 2017; Perez Ortiz & Swerdlow, 2019; Rovira-Llopis et al., 2017; Talbot et al., 2012). However, to date, the intricate relationship between insulin resistance and mitochondrial dysfunction and how this contributes to the pathogenesis of various diseases are not completely understood. On one hand, impaired mitochondrial function compromises cellular energy production, which can contribute to insulin resistance by disrupting insulin signaling pathways. On the other hand, insulin resistance can directly affect mitochondrial function by impairing mitochondrial biogenesis and function (Gonzalez-Franquesa & Patti, 2017). My findings shed light on the question by providing evidence for the cause and the consequence in the interplay of insulin resistance and mitochondrial dysfunction in the context of AD. According to my findings, mitochondrial dysfunction can be directly caused by insulin resistance, which was induced by addition of the key genetic AD-risk factor ApoE4 *in vitro*. ApoE4 traps the IR in early endosomes thereby impairing proper insulin signaling (N. Zhao et al., 2017) and disturbing AMPK-regulated *Pink1* mRNA localization. As a result, *Pink1* mRNA remains tethered to mitochondria even in the presence of insulin (Fig. 28b-d), which impairs the removal of damaged mitochondria via mitophagy (Fig. 29c,d) potentially leading to the accumulation of dysfunctional mitochondria. In line with that, other studies have already shown that ApoE4 impairs PINK1/Parkin-dependent mitophagy (reviewed in H. Chen et al., 2022). Human ApoE4 carriers have reduced total PINK1 levels as well as reduced p-ubiquitin levels in the brain (Sohn et al., 2021). Furthermore, ApoE4 transgenic mice show lower cleaved PINK1 levels in hippocampal neurons, while full-length PINK1 levels are increased (Simonovitch et al., 2019). Using my experimental setup, it remains to be determined whether addition of ApoE4 also prevents insulin-mediated translation of PINK1. Nevertheless, my findings indicate that impaired mitophagy resulting in accumulation of defective mitochondria might be a direct consequence of insulin resistance *in vitro*. Interestingly, mitophagy has also been suggested as a potential therapeutic strategy for insulin resistance (P. Ning et al., 2022) thereby again turning the causal relation of the two phenomena and demonstrating the complex relationship between mitochondrial dysfunction and insulin resistance.

Considering that type 2 diabetes is also characterized by both insulin resistance and mitochondrial dysfunction, the outcomes of my research could potentially hold relevance for understanding and addressing the neurological parts of this metabolic disorder. While it is widely recognized that mitochondrial dynamics, mitochondrial biogenesis, and mitochondrial function are compromised in type 2 diabetes, there is relatively limited research focused on the specific aspects of neuronal PINK1/Parkin-dependent mitophagy (Galizzi & Di Carlo, 2022; Luo et al., 2022; Rovira-Llopis et al., 2017). A recent study, however, showed that PINK1 levels are reduced in the midbrain of diabetic mice

_____

(Su et al., 2020). In line with that, high glucose as observed in diabetes also decreases PINK1 protein expression in neuron-like PC12 cells thereby inhibiting PINK1/Parkin-mediated mitophagy (Su et al., 2020). Based on these findings, it is plausible to consider the applicability of my model not only in AD but also in metabolic disorders associated with insulin resistance such as type 2 diabetes.

While, on one hand, application of insulin has been shown to be beneficial in both diabetes and neurodegeneration (Benedict et al., 2007; Brünner et al., 2015; Claxton et al., 2015; Craft, 2012; Novak et al., 2014; Reger et al., 2008; H. Zhang et al., 2015), a reduction in insulin signaling, on the other hand, extends the lifespan in multiple organisms, a phenomenon known as longevity (Clancy et al., 2001; S.-S. Kim & Lee, 2019; Ogg et al., 1997). In line with this, AMPK, which is inhibited by insulin signaling, has also been shown to promote longevity (Apfeld et al., 2004; Mair et al., 2011; Martin-Montalvo et al., 2013; Stenesen et al., 2013). However, the involvement of AMPK activity in the treatment of neurodegenerative diseases is still a subject of controversy (Muraleedharan & Dasgupta, 2022). The seemingly contradictory findings on the role of insulin-related signaling in neurodegeneration and longevity implies that both insufficient and excessive levels of insulin (Kolb et al., 2020) as well as both inhibition and overactivation of AMPK are detrimental to the physiological balance. This again shows the complex biology of insulin signaling and is in line with my model that both metabolic states (insulin signaling on/off) are required for proper mitochondrial quality control and hence neuronal survival.

4.8 Conclusion and perspectives

The findings of my project provide new insights into the role of insulin and AMPK signaling in PINK1-dependent mitophagy in neurons. Throughout the study, I thoroughly investigated the five aims and research questions stated in chapter 1.10. I found that AMPK signaling regulates mitochondrial *Pink1* mRNA localization downstream of insulin signaling in neurons (1). Mechanistically, AMPK phosphorylates the mitochondrial anchor protein SYNJ2BP at S21, thereby increasing its interaction with the RNA-binding protein SYNJ2a (2). AMPK-mediated mitochondrial binding of *Pink1* mRNA reduces its translation, while insulin-induced untethering of *Pink1* mRNA from mitochondria leads to increased translation at the endolysosomal compartment in close proximity to the ER and mitochondria (3). As a result, insulin promotes mitochondrial quality control via the PINK1/Parkin-dependent mitophagy pathway (4). Finally, ApoE4-induced insulin resistance prevents the effects on *Pink1* mRNA localization, translation and PINK1 function, which is relevant in the context of AD (5) (Fig. 30).

Apart from providing valuable insights into the significance of insulin and AMPK signaling in PINK1-dependent mitochondrial quality control, this thesis has also given rise to several emerging questions that require further investigation and have the potential to bring significant advancements in the field.

At the molecular and mechanistic level, the project has uncovered the inverse regulation of AMPK-mediated binding of *Pink1* mRNA on one hand and the increased PINK1 translation at endolysosomes/ER contact sites upon AMPK inhibition on the other hand. However, the exact mechanism of transfer of the transcript and the protein between the different organelles remains to be elucidated (chapter 4.4). Another aspect that remains unanswered is the mechanism through which ribosomes are directed towards the translation hotspot in neurons. It is unclear whether ribosomes are always associated with *Pink1* mRNA and blocked from translating by SYNJ2a or whether they are only recruited during episodes of active translation. Furthermore, my experiments were carried out within the somatodendritic compartment. Although the occurrence of mitochondrial transport of *Pink1* mRNA in axons has been previously established (Harbauer et al., 2022), the AMPK-mediated regulation of both transcript and protein specifically in axons remains to be shown.

At the translational and therapeutic level, the project has revealed an interesting connection between mitochondrial dysfunction, insulin resistance, and neurodegeneration. The topic of AMPK activity in neurodegenerative diseases is still controversial. Some studies claim that AMPK activation is neuroprotective while other studies suggest the opposite (Muraleedharan & Dasgupta, 2022). Similarly, insulin has been observed to have both positive and negative effects (Kolb et al., 2020). This shows the complexity of insulin and AMPK signaling and suggests that a fine balance between both metabolic states is required for neuronal health. How this can be translated into pharmacological or dietary interventions will be an interesting but also challenging task, which requires more basic research into the metabolic regulation of neuronal health.

Overall, the project has not only provided crucial insights into the fundamental processes of mitophagy regulation via AMPK and insulin signaling but has also sparked numerous avenues for further research, both at the molecular and mechanistic level, and at the translational and therapeutic level. Exploring these questions will advance our knowledge and potentially lead to innovative treatments for various diseases including AD, PD and type 2 diabetes.

5 REFERENCES

Agrawal, R., Reno, C. M., Sharma, S., Christensen, C., Huang, Y., & Fisher, S. J. (2021). Insulin action in the brain regulates both central and peripheral functions. *American Journal of Physiology-Endocrinology and Metabolism*, *321*(1), E156–E163. https://doi.org/10.1152/ajpendo.00642.2020

Andreassi, C., Zimmermann, C., Mitter, R., Fusco, S., De Vita, S., Devita, S., Saiardi, A., & Riccio, A. (2010). An NGF-responsive element targets myo-inositol monophosphatase-1 mRNA to sympathetic neuron axons. *Nature Neuroscience*, *13*(3), 291–301. https://doi.org/10.1038/nn.2486

Apfeld, J., O'Connor, G., McDonagh, T., DiStefano, P. S., & Curtis, R. (2004). The AMP-activated protein kinase AAK-2 links energy levels and insulin-like signals to lifespan in C. elegans. *Genes & Development*, *18*(24), 3004–3009. https://doi.org/10.1101/gad.1255404

Archibald, J. M. (2015). Endosymbiosis and Eukaryotic Cell Evolution. *Current Biology*, *25*(19), R911–R921. https://doi.org/10.1016/j.cub.2015.07.055

Armstrong, R. A. (2019). Risk factors for Alzheimer's disease. *Folia Neuropathologica*, *57*(2), 87–105. https://doi.org/10.5114/fn.2019.85929

Arnold, S. E., Arvanitakis, Z., Macauley-Rambach, S. L., Koenig, A. M., Wang, H.-Y., Ahima, R. S., Craft, S., Gandy, S., Buettner, C., Stoeckel, L. E., Holtzman, D. M., & Nathan, D. M. (2018). Brain insulin resistance in type 2 diabetes and Alzheimer disease: Concepts and conundrums. *Nature Reviews. Neurology*, *14*(3), 168–181. https://doi.org/10.1038/nrneurol.2017.185

Aschrafi, A., Kar, A. N., Gale, J. R., Elkahloun, A. G., Vargas, J. N. S., Sales, N., Wilson, G., Tompkins, M., Gioio, A. E., & Kaplan, B. B. (2016). A heterogeneous population of nuclear-encoded mitochondrial mRNAs is present in the axons of primary sympathetic neurons. *Mitochondrion*, *30*, 18–23. https://doi.org/10.1016/j.mito.2016.06.002

Ashrafi, G., Schlehe, J. S., LaVoie, M. J., & Schwarz, T. L. (2014). Mitophagy of damaged mitochondria occurs locally in distal neuronal axons and requires PINK1 and Parkin. *Journal of Cell Biology*, *206*(5), 655–670. https://doi.org/10.1083/jcb.201401070

Attwell, D., & Laughlin, S. B. (2001). An energy budget for signaling in the grey matter of the brain. *Journal of Cerebral Blood Flow and Metabolism: Official Journal of the International Society of Cerebral Blood Flow and Metabolism*, *21*(10), 1133–1145. https://doi.org/10.1097/00004647-200110000-00001

Bagherniya, M., Butler, A. E., Barreto, G. E., & Sahebkar, A. (2018). The effect of fasting or calorie restriction on autophagy induction: A review of the literature. *Ageing Research Reviews*, *47*, 183–197. https://doi.org/10.1016/j.arr.2018.08.004

Bai, X., Ma, D., Liu, A., Shen, X., Wang, Q. J., Liu, Y., & Jiang, Y. (2007). Rheb activates mTOR by antagonizing its endogenous inhibitor, FKBP38. *Science (New York, N.Y.)*, *318*(5852), 977–980. https://doi.org/10.1126/science.1147379

Baldwin, D., Prince, M., Marshall, S., Davies, P., & Olefsky, J. M. (1980). Regulation of insulin receptors: Evidence for involvement of an endocytotic internalization pathway. *Proceedings of the National Academy of Sciences of the United States of America*, *77*(10), 5975–5978. https://doi.org/10.1073/pnas.77.10.5975

Bar-Peled, L., Chantranupong, L., Cherniack, A. D., Chen, W. W., Ottina, K. A., Grabiner, B. C., Spear, E. D., Carter, S. L., Meyerson, M., & Sabatini, D. M. (2013). A Tumor suppressor complex with GAP activity for the Rag GTPases that signal amino acid sufficiency to mTORC1. *Science (New York, N.Y.)*, *340*(6136), 1100–1106. https://doi.org/10.1126/science.1232044

Bar-Peled, L., Schweitzer, L. D., Zoncu, R., & Sabatini, D. M. (2012). Ragulator is a GEF for the rag GTPases that signal amino acid levels to mTORC1. *Cell*, *150*(6), 1196–1208. https://doi.org/10.1016/j.cell.2012.07.032

Belloy, M. E., Napolioni, V., Han, S. S., Le Guen, Y., Greicius, M. D., & for the Alzheimer's Disease Neuroimaging Initiative. (2020). Association of *Klotho* -VS Heterozygosity With Risk of Alzheimer Disease in Individuals Who Carry *APOE4*. *JAMA Neurology*, *77*(7), 849. https://doi.org/10.1001/jamaneurol.2020.0414

Benedict, C., Hallschmid, M., Schmitz, K., Schultes, B., Ratter, F., Fehm, H. L., Born, J., & Kern, W. (2007). Intranasal Insulin Improves Memory in Humans: Superiority of Insulin Aspart. *Neuropsychopharmacology*, *32*(1), 239–243. https://doi.org/10.1038/sj.npp.1301193

Bereiter-Hahn, J., & Vöth, M. (1994). Dynamics of mitochondria in living cells: Shape changes, dislocations, fusion, and fission of mitochondria: DYNAMICS OF MITOCHONDRIA. *Microscopy Research and Technique*, *27*(3), 198–219. https://doi.org/10.1002/jemt.1070270303

Berggreen, C., Gormand, A., Omar, B., Degerman, E., & Göransson, O. (2009). Protein kinase B activity is required for the effects of insulin on lipid metabolism in adipocytes. *American Journal of Physiology. Endocrinology and Metabolism*, *296*(4), E635-646. https://doi.org/10.1152/ajpendo.90596.2008

Biever, A., Glock, C., Tushev, G., Ciirdaeva, E., Dalmay, T., Langer, J. D., & Schuman, E. M. (2020). Monosomes actively translate synaptic mRNAs in neuronal processes. *Science*, *367*(6477), eaay4991. https://doi.org/10.1126/science.aay4991

Bolam, J. P., & Pissadaki, E. K. (2012). Living on the edge with too many mouths to feed: Why dopamine neurons die. *Movement Disorders: Official Journal of the Movement Disorder Society*, *27*(12), 1478–1483. https://doi.org/10.1002/mds.25135

Bolte, S., & Cordelières, F. P. (2006). A guided tour into subcellular colocalization analysis in light microscopy. *Journal of Microscopy*, *224*(Pt 3), 213–232. https://doi.org/10.1111/j.1365-2818.2006.01706.x

Boschert, U., Merlo-Pich, E., Higgins, G., Roses, A. D., & Catsicas, S. (1999). Apolipoprotein E Expression by Neurons Surviving Excitotoxic Stress. *Neurobiology of Disease*, *6*(6), 508–514. https://doi.org/10.1006/nbdi.1999.0251

Briese, M., Saal, L., Appenzeller, S., Moradi, M., Baluapuri, A., & Sendtner, M. (2016). Whole transcriptome profiling reveals the RNA content of motor axons. *Nucleic Acids Research*, *44*(4), e33. https://doi.org/10.1093/nar/gkv1027

Bros, H., Hauser, A., Paul, F., Niesner, R., & Infante-Duarte, C. (2015). Assessing Mitochondrial Movement Within Neurons: Manual Versus Automated Tracking Methods. *Traffic, 16*(8), 906–917. https://doi.org/10.1111/tra.12291

Brunet, A., Bonni, A., Zigmond, M. J., Lin, M. Z., Juo, P., Hu, L. S., Anderson, M. J., Arden, K. C., Blenis, J., & Greenberg, M. E. (1999). Akt promotes cell survival by phosphorylating and inhibiting a Forkhead transcription factor. *Cell*, *96*(6), 857–868. https://doi.org/10.1016/s0092-8674(00)80595-4

Brünner, Y. F., Kofoet, A., Benedict, C., & Freiherr, J. (2015). Central Insulin Administration Improves Odor-Cued Reactivation of Spatial Memory in Young Men. *The Journal of Clinical Endocrinology & Metabolism*, *100*(1), 212–219. https://doi.org/10.1210/jc.2014-3018

Bu, G. (2009). Apolipoprotein E and its receptors in Alzheimer's disease: Pathways, pathogenesis and therapy. *Nature Reviews. Neuroscience*, *10*(5), 333–344. https://doi.org/10.1038/nrn2620

Cardanho-Ramos, C., & Morais, V. A. (2021). Mitochondrial Biogenesis in Neurons: How and Where. *International Journal of Molecular Sciences*, *22*(23), 13059. https://doi.org/10.3390/ijms222313059

Carroll, B., & Dunlop, E. A. (2017). The lysosome: A crucial hub for AMPK and mTORC1 signalling. *The Biochemical Journal*, *474*(9), 1453–1466. https://doi.org/10.1042/BCJ20160780

Chatterjee, S., & Mudher, A. (2018). Alzheimer's Disease and Type 2 Diabetes: A Critical Assessment of the Shared Pathological Traits. *Frontiers in Neuroscience*, *12*, 383. https://doi.org/10.3389/fnins.2018.00383

Chen, H., Chen, F., Jiang, Y., Zhang, L., Hu, G., Sun, F., Zhang, M., Ji, Y., Chen, Y., Che, G., Zhou, X., & Zhang, Y. (2022). A Review of ApoE4 Interference Targeting Mitophagy Molecular Pathways for Alzheimer's Disease. *Frontiers in Aging Neuroscience*, *14*, 881239. https://doi.org/10.3389/fnagi.2022.881239

Chen, H., Chomyn, A., & Chan, D. C. (2005). Disruption of fusion results in mitochondrial heterogeneity and dysfunction. *The Journal of Biological Chemistry*, *280*(28), 26185–26192. https://doi.org/10.1074/jbc.M503062200

Chen, M., Chen, Z., Wang, Y., Tan, Z., Zhu, C., Li, Y., Han, Z., Chen, L., Gao, R., Liu, L., & Chen, Q. (2016). Mitophagy receptor FUNDC1 regulates mitochondrial dynamics and mitophagy. *Autophagy*, *12*(4), 689–702. https://doi.org/10.1080/15548627.2016.1151580

Cheng, Z., Guo, S., Copps, K., Dong, X., Kollipara, R., Rodgers, J. T., Depinho, R. A., Puigserver, P., & White, M. F. (2009). Foxo1 integrates insulin signaling with mitochondrial function in the liver. *Nature Medicine*, *15*(11), 1307–1311. https://doi.org/10.1038/nm.2049

Cheung, P. C., Salt, I. P., Davies, S. P., Hardie, D. G., & Carling, D. (2000). Characterization of AMP-activated protein kinase gamma-subunit isoforms and their role in AMP binding. *The Biochemical Journal*, *346 Pt 3*(Pt 3), 659–669.

Chua, L.-M., Lim, M.-L., Chong, P.-R., Hu, Z. P., Cheung, N. S., & Wong, B.-S. (2012). Impaired Neuronal Insulin Signaling Precedes Aβ42 Accumulation in Female AβPPsw/PS1ΔE9 Mice. *Journal of Alzheimer's Disease*, *29*(4), 783–791. https://doi.org/10.3233/JAD-2012-111880

Cioni, J.-M., Lin, J. Q., Holtermann, A. V., Koppers, M., Jakobs, M. A. H., Azizi, A., Turner-Bridger, B., Shigeoka, T., Franze, K., Harris, W. A., & Holt, C. E. (2019). Late Endosomes Act as mRNA Translation Platforms and Sustain Mitochondria in Axons. *Cell*, *176*(1–2), 56-72.e15. https://doi.org/10.1016/j.cell.2018.11.030

Cipolat, S., Martins de Brito, O., Dal Zilio, B., & Scorrano, L. (2004). OPA1 requires mitofusin 1 to promote mitochondrial fusion. *Proceedings of the National Academy of Sciences of the United States of America*, *101*(45), 15927–15932. https://doi.org/10.1073/pnas.0407043101

Cisneros, J., Belton, T. B., Shum, G. C., Molakal, C. G., & Wong, Y. C. (2022). Mitochondria-lysosome contact site dynamics and misregulation in neurodegenerative diseases. *Trends in Neurosciences*, *45*(4), 312–322. https://doi.org/10.1016/j.tins.2022.01.005

Clancy, D. J., Gems, D., Harshman, L. G., Oldham, S., Stocker, H., Hafen, E., Leevers, S. J., & Partridge, L. (2001). Extension of life-span by loss of CHICO, a Drosophila insulin receptor substrate protein. *Science (New York, N.Y.)*, *292*(5514), 104–106. https://doi.org/10.1126/science.1057991

Claxton, A., Baker, L. D., Hanson, A., Trittschuh, E. H., Cholerton, B., Morgan, A., Callaghan, M., Arbuckle, M., Behl, C., & Craft, S. (2015). Long-acting intranasal insulin detemir improves cognition for adults with mild cognitive impairment or early-stage Alzheimer's disease dementia. *Journal of Alzheimer's Disease: JAD*, *44*(3), 897–906. https://doi.org/10.3233/JAD-141791

Cohen, B., Altman, T., Golani-Armon, A., Savulescu, A. F., Ibraheem, A., Mhlanga, M. M., Perlson, E., & Arava, Y. S. (2022). Co-transport of the nuclear-encoded *Cox7c* mRNA with mitochondria along axons occurs through a coding-region-dependent mechanism. *Journal of Cell Science*, *135*(16), jcs259436. https://doi.org/10.1242/jcs.259436

Corder, E. H., Saunders, A. M., Strittmatter, W. J., Schmechel, D. E., Gaskell, P. C., Small, G. W., Roses, A. D., Haines, J. L., & Pericak-Vance, M. A. (1993). Gene dose of apolipoprotein E type 4 allele and the risk of Alzheimer's disease in late onset families. *Science (New York, N.Y.)*, *261*(5123), 921–923. https://doi.org/10.1126/science.8346443

Cornelissen, T., Vilain, S., Vints, K., Gounko, N., Verstreken, P., & Vandenberghe, W. (2018). Deficiency of parkin and PINK1 impairs age-dependent mitophagy in Drosophila. *ELife*, *7*, e35878. https://doi.org/10.7554/eLife.35878

Corton, J. M., Gillespie, J. G., Hawley, S. A., & Hardie, D. G. (1995). 5-aminoimidazole-4-carboxamide ribonucleoside. A specific method for activating AMP-activated protein kinase in intact cells? *European Journal of Biochemistry*, *229*(2), 558–565. https://doi.org/10.1111/j.1432-1033.1995.tb20498.x

Cox, J., & Mann, M. (2008). MaxQuant enables high peptide identification rates, individualized p.p.b.-range mass accuracies and proteome-wide protein quantification. *Nature Biotechnology*, *26*(12), 1367–1372. https://doi.org/10.1038/nbt.1511

Craft, S. (2012). Intranasal Insulin Therapy for Alzheimer Disease and Amnestic Mild Cognitive Impairment: A Pilot Clinical Trial. *Archives of Neurology*, *69*(1), 29. https://doi.org/10.1001/archneurol.2011.233

Dagon, Y., Hur, E., Zheng, B., Wellenstein, K., Cantley, L. C., & Kahn, B. B. (2012). P70S6 kinase phosphorylates AMPK on serine 491 to mediate leptin's effect on food intake. *Cell Metabolism*, *16*(1), 104–112. https://doi.org/10.1016/j.cmet.2012.05.010

Dalla Costa, I., Buchanan, C. N., Zdradzinski, M. D., Sahoo, P. K., Smith, T. P., Thames, E., Kar, A. N., & Twiss, J. L. (2021). The functional organization of axonal mRNA transport and translation. *Nature Reviews Neuroscience*, *22*(2), 77–91. https://doi.org/10.1038/s41583-020-00407-7

Das, S., Singer, R. H., & Yoon, Y. J. (2019). The travels of mRNAs in neurons: Do they know where they are going? *Current Opinion in Neurobiology*, *57*, 110–116. https://doi.org/10.1016/j.conb.2019.01.016

Dasgupta, B., & Seibel, W. (2018). Compound C/Dorsomorphin: Its Use and Misuse as an AMPK Inhibitor. *Methods in Molecular Biology (Clifton, N.J.)*, *1732*, 195–202. https://doi.org/10.1007/978-1-4939-7598-3_12

Davies, S. P., Helps, N. R., Cohen, P. T., & Hardie, D. G. (1995). 5'-AMP inhibits dephosphorylation, as well as promoting phosphorylation, of the AMP-activated protein kinase. Studies using

bacterially expressed human protein phosphatase-2C alpha and native bovine protein phosphatase-2AC. *FEBS Letters*, *377*(3), 421–425. https://doi.org/10.1016/0014-5793(95)01368-7

de la Monte, S. M., & Wands, J. R. (2008). Alzheimer's Disease is Type 3 Diabetes—Evidence Reviewed. *Journal of Diabetes Science and Technology*, *2*(6), 1101–1113. https://doi.org/10.1177/193229680800200619

Deas, E., Plun-Favreau, H., Gandhi, S., Desmond, H., Kjaer, S., Loh, S. H. Y., Renton, A. E. M., Harvey, R. J., Whitworth, A. J., Martins, L. M., Abramov, A. Y., & Wood, N. W. (2011). PINK1 cleavage at position A103 by the mitochondrial protease PARL. *Human Molecular Genetics*, *20*(5), 867–879. https://doi.org/10.1093/hmg/ddq526

Detmer, S. A., & Chan, D. C. (2007). Functions and dysfunctions of mitochondrial dynamics. *Nature Reviews. Molecular Cell Biology*, *8*(11), 870–879. https://doi.org/10.1038/nrm2275

Diaz, F., & Moraes, C. T. (2008). Mitochondrial biogenesis and turnover. *Cell Calcium*, *44*(1), 24–35. https://doi.org/10.1016/j.ceca.2007.12.004

Dibble, C. C., Elis, W., Menon, S., Qin, W., Klekota, J., Asara, J. M., Finan, P. M., Kwiatkowski, D. J., Murphy, L. O., & Manning, B. D. (2012). TBC1D7 Is a Third Subunit of the TSC1-TSC2 Complex Upstream of mTORC1. *Molecular Cell*, *47*(4), 535–546. https://doi.org/10.1016/j.molcel.2012.06.009

Didier, S., Sauvé, F., Domise, M., Buée, L., Marinangeli, C., & Vingtdeux, V. (2018). AMP-activated Protein Kinase Controls Immediate Early Genes Expression Following Synaptic Activation Through the PKA/CREB Pathway. *International Journal of Molecular Sciences*, *19*(12), 3716. https://doi.org/10.3390/ijms19123716

Digman, M. A., Caiolfa, V. R., Zamai, M., & Gratton, E. (2008). The phasor approach to fluorescence lifetime imaging analysis. *Biophysical Journal*, *94*(2), L14-16. https://doi.org/10.1529/biophysj.107.120154

Ducommun, S., Deak, M., Sumpton, D., Ford, R. J., Núñez Galindo, A., Kussmann, M., Viollet, B., Steinberg, G. R., Foretz, M., Dayon, L., Morrice, N. A., & Sakamoto, K. (2015). Motif affinity and mass spectrometry proteomic approach for the discovery of cellular AMPK targets: Identification of mitochondrial fission factor as a new AMPK substrate. *Cellular Signalling*, *27*(5), 978–988. https://doi.org/10.1016/j.cellsig.2015.02.008

Efeyan, A., Zoncu, R., Chang, S., Gumper, I., Snitkin, H., Wolfson, R. L., Kirak, O., Sabatini, D. D., & Sabatini, D. M. (2013). Regulation of mTORC1 by the Rag GTPases is necessary for neonatal autophagy and survival. *Nature*, *493*(7434), 679–683. https://doi.org/10.1038/nature11745

Egan, D. F., Shackelford, D. B., Mihaylova, M. M., Gelino, S., Kohnz, R. A., Mair, W., Vasquez, D. S., Joshi, A., Gwinn, D. M., Taylor, R., Asara, J. M., Fitzpatrick, J., Dillin, A., Viollet, B., Kundu, M.,

Hansen, M., & Shaw, R. J. (2011). Phosphorylation of ULK1 (hATG1) by AMP-activated protein kinase connects energy sensing to mitophagy. *Science (New York, N.Y.)*, *331*(6016), 456–461. https://doi.org/10.1126/science.1196371

Eisenberg-Bord, M., Shai, N., Schuldiner, M., & Bohnert, M. (2016). A Tether Is a Tether Is a Tether: Tethering at Membrane Contact Sites. *Developmental Cell*, *39*(4), 395–409. https://doi.org/10.1016/j.devcel.2016.10.022

Elbaz, Y., & Schuldiner, M. (2011). Staying in touch: The molecular era of organelle contact sites. *Trends in Biochemical Sciences*, *36*(11), 616–623. https://doi.org/10.1016/j.tibs.2011.08.004

Elbaz-Alon, Y., Guo, Y., Segev, N., Harel, M., Quinnell, D. E., Geiger, T., Avinoam, O., Li, D., & Nunnari, J. (2020). PDZD8 interacts with Protrudin and Rab7 at ER-late endosome membrane contact sites associated with mitochondria. *Nature Communications*, *11*(1), 3645. https://doi.org/10.1038/s41467-020-17451-7

Erecińska, M., & Silver, I. A. (1994). Ions and energy in mammalian brain. *Progress in Neurobiology*, *43*(1), 37–71. https://doi.org/10.1016/0301-0082(94)90015-9

Eura, Y., Ishihara, N., Yokota, S., & Mihara, K. (2003). Two mitofusin proteins, mammalian homologues of FZO, with distinct functions are both required for mitochondrial fusion. *Journal of Biochemistry*, *134*(3), 333–344. https://doi.org/10.1093/jb/mvg150

Forgac, M. (2007). Vacuolar ATPases: Rotary proton pumps in physiology and pathophysiology. *Nature Reviews. Molecular Cell Biology*, *8*(11), 917–929. https://doi.org/10.1038/nrm2272

Fransson, S., Ruusala, A., & Aspenström, P. (2006). The atypical Rho GTPases Miro-1 and Miro-2 have essential roles in mitochondrial trafficking. *Biochemical and Biophysical Research Communications*, *344*(2), 500–510. https://doi.org/10.1016/j.bbrc.2006.03.163

Fröhlich, C., Grabiger, S., Schwefel, D., Faelber, K., Rosenbaum, E., Mears, J., Rocks, O., & Daumke, O. (2013). Structural insights into oligomerization and mitochondrial remodelling of dynamin 1-like protein. *The EMBO Journal*, *32*(9), 1280–1292. https://doi.org/10.1038/emboj.2013.74

Furlong, R. M., Lindsay, A., Anderson, K. E., Hawkins, P. T., Sullivan, A. M., & O'Neill, C. (2019). The Parkinson's disease gene PINK1 activates Akt via PINK1 kinase-dependent regulation of the phospholipid PI(3,4,5)P3. *Journal of Cell Science*, *132*(20), jcs233221. https://doi.org/10.1242/jcs.233221

Galizzi, G., & Di Carlo, M. (2022). Insulin and Its Key Role for Mitochondrial Function/Dysfunction and Quality Control: A Shared Link between Dysmetabolism and Neurodegeneration. *Biology*, *11*(6), 943. https://doi.org/10.3390/biology11060943

Gandre-Babbe, S., & van der Bliek, A. M. (2008). The novel tail-anchored membrane protein Mff controls mitochondrial and peroxisomal fission in mammalian cells. *Molecular Biology of the Cell*, *19*(6), 2402–2412. https://doi.org/10.1091/mbc.e07-12-1287

_____

Ganley, I. G., Lam, D. H., Wang, J., Ding, X., Chen, S., & Jiang, X. (2009). ULK1.ATG13.FIP200 complex mediates mTOR signaling and is essential for autophagy. *The Journal of Biological Chemistry*, *284*(18), 12297–12305. https://doi.org/10.1074/jbc.M900573200

Gehrke, S., Wu, Z., Klinkenberg, M., Sun, Y., Auburger, G., Guo, S., & Lu, B. (2015). PINK1 and Parkin Control Localized Translation of Respiratory Chain Component mRNAs on Mitochondria Outer Membrane. *Cell Metabolism*, *21*(1), 95–108. https://doi.org/10.1016/j.cmet.2014.12.007

Ghasemi, R., Haeri, A., Dargahi, L., Mohamed, Z., & Ahmadiani, A. (2013). Insulin in the Brain: Sources, Localization and Functions. *Molecular Neurobiology*, *47*(1), 145–171. https://doi.org/10.1007/s12035-012-8339-9

Glater, E. E., Megeath, L. J., Stowers, R. S., & Schwarz, T. L. (2006). Axonal transport of mitochondria requires milton to recruit kinesin heavy chain and is light chain independent. *The Journal of Cell Biology*, *173*(4), 545–557. https://doi.org/10.1083/jcb.200601067

Goldberg, A. L. (2003). Protein degradation and protection against misfolded or damaged proteins. *Nature*, *426*(6968), 895–899. https://doi.org/10.1038/nature02263

Goldsmith, J., Ordureau, A., Harper, J. W., & Holzbaur, E. L. F. (2022). Brain-derived autophagosome profiling reveals the engulfment of nucleoid-enriched mitochondrial fragments by basal autophagy in neurons. *Neuron*, *110*(6), 967-976.e8. https://doi.org/10.1016/j.neuron.2021.12.029

Gomes, C., Merianda, T. T., Lee, S. J., Yoo, S., & Twiss, J. L. (2014). Molecular determinants of the axonal mRNA transcriptome. *Developmental Neurobiology*, *74*(3), 218–232. https://doi.org/10.1002/dneu.22123

Gonzalez-Franquesa, A., & Patti, M.-E. (2017). Insulin Resistance and Mitochondrial Dysfunction. *Advances in Experimental Medicine and Biology*, *982*, 465–520. https://doi.org/10.1007/978-3-319-55330-6_25

Gowans, G. J., Hawley, S. A., Ross, F. A., & Hardie, D. G. (2013). AMP is a true physiological regulator of AMP-activated protein kinase by both allosteric activation and enhancing net phosphorylation. *Cell Metabolism*, *18*(4), 556–566. https://doi.org/10.1016/j.cmet.2013.08.019

Graber, T. E., Hébert-Seropian, S., Khoutorsky, A., David, A., Yewdell, J. W., Lacaille, J.-C., & Sossin, W. S. (2013). Reactivation of stalled polyribosomes in synaptic plasticity. *Proceedings of the National Academy of Sciences of the United States of America*, *110*(40), 16205–16210. https://doi.org/10.1073/pnas.1307747110

Gray, S. M., & Barrett, E. J. (2018). Insulin transport into the brain. *American Journal of Physiology. Cell Physiology*, *315*(2), C125–C136. https://doi.org/10.1152/ajpcell.00240.2017

_____

Greene, A. W., Grenier, K., Aguileta, M. A., Muise, S., Farazifard, R., Haque, M. E., McBride, H. M., Park, D. S., & Fon, E. A. (2012). Mitochondrial processing peptidase regulates PINK1 processing, import and Parkin recruitment. *EMBO Reports*, *13*(4), 378–385. https://doi.org/10.1038/embor.2012.14

Griparic, L., van der Wel, N. N., Orozco, I. J., Peters, P. J., & van der Bliek, A. M. (2004). Loss of the intermembrane space protein Mgm1/OPA1 induces swelling and localized constrictions along the lengths of mitochondria. *The Journal of Biological Chemistry*, *279*(18), 18792–18798. https://doi.org/10.1074/jbc.M400920200

Guan, R., Zou, W., Dai, X., Yu, X., Liu, H., Chen, Q., & Teng, W. (2018). Mitophagy, a potential therapeutic target for stroke. *Journal of Biomedical Science*, *25*(1), 87. https://doi.org/10.1186/s12929-018-0487-4

Gumy, L. F., Yeo, G. S. H., Tung, Y.-C. L., Zivraj, K. H., Willis, D., Coppola, G., Lam, B. Y. H., Twiss, J. L., Holt, C. E., & Fawcett, J. W. (2011). Transcriptome analysis of embryonic and adult sensory axons reveals changes in mRNA repertoire localization. *RNA (New York, N.Y.)*, *17*(1), 85–98. https://doi.org/10.1261/rna.2386111

Gwinn, D. M., Shackelford, D. B., Egan, D. F., Mihaylova, M. M., Mery, A., Vasquez, D. S., Turk, B. E., & Shaw, R. J. (2008). AMPK phosphorylation of raptor mediates a metabolic checkpoint. *Molecular Cell*, *30*(2), 214–226. https://doi.org/10.1016/j.molcel.2008.03.003

Hall, C. N., Klein-Flügge, M. C., Howarth, C., & Attwell, D. (2012). Oxidative phosphorylation, not glycolysis, powers presynaptic and postsynaptic mechanisms underlying brain information processing. *The Journal of Neuroscience: The Official Journal of the Society for Neuroscience*, *32*(26), 8940–8951. https://doi.org/10.1523/JNEUROSCI.0026-12.2012

Han, W., & Li, C. (2010). Linking type 2 diabetes and Alzheimer's disease. *Proceedings of the National Academy of Sciences*, *107*(15), 6557–6558. https://doi.org/10.1073/pnas.1002555107

Hansen, K. G., Aviram, N., Laborenz, J., Bibi, C., Meyer, M., Spang, A., Schuldiner, M., & Herrmann, J. M. (2018). An ER surface retrieval pathway safeguards the import of mitochondrial membrane proteins in yeast. *Science (New York, N.Y.)*, *361*(6407), 1118–1122. https://doi.org/10.1126/science.aar8174

Harbauer, A. B., Hees, J. T., Wanderoy, S., Segura, I., Gibbs, W., Cheng, Y., Ordonez, M., Cai, Z., Cartoni, R., Ashrafi, G., Wang, C., Perocchi, F., He, Z., & Schwarz, T. L. (2022). Neuronal mitochondria transport Pink1 mRNA via synaptojanin 2 to support local mitophagy. *Neuron*, S0896-6273(22)00105-2. https://doi.org/10.1016/j.neuron.2022.01.035

Hardie, D. G. (2007). AMP-activated/SNF1 protein kinases: Conserved guardians of cellular energy. *Nature Reviews. Molecular Cell Biology*, *8*(10), 774–785. https://doi.org/10.1038/nrm2249

_____

Hardie, D. G., Carling, D., & Gamblin, S. J. (2011). AMP-activated protein kinase: Also regulated by ADP? *Trends in Biochemical Sciences*, *36*(9), 470–477. https://doi.org/10.1016/j.tibs.2011.06.004

Harris, J. J., Jolivet, R., & Attwell, D. (2012). Synaptic energy use and supply. *Neuron*, *75*(5), 762–777. https://doi.org/10.1016/j.neuron.2012.08.019

Havrankova, J., Brownstein, M., & Roth, J. (1981). Insulin and insulin receptors in rodent brain. *Diabetologia*, *20 Suppl*, 268–273.

Havrankova, J., Schmechel, D., Roth, J., & Brownstein, M. (1978). Identification of insulin in rat brain. *Proceedings of the National Academy of Sciences of the United States of America*, *75*(11), 5737–5741. https://doi.org/10.1073/pnas.75.11.5737

Hawley, S. A., Boudeau, J., Reid, J. L., Mustard, K. J., Udd, L., Mäkelä, T. P., Alessi, D. R., & Hardie, D. G. (2003). Complexes between the LKB1 tumor suppressor, STRAD alpha/beta and MO25 alpha/beta are upstream kinases in the AMP-activated protein kinase cascade. *Journal of Biology*, *2*(4), 28. https://doi.org/10.1186/1475-4924-2-28

Hawley, S. A., Davison, M., Woods, A., Davies, S. P., Beri, R. K., Carling, D., & Hardie, D. G. (1996). Characterization of the AMP-activated Protein Kinase Kinase from Rat Liver and Identification of Threonine 172 as the Major Site at Which It Phosphorylates AMP-activated Protein Kinase. *Journal of Biological Chemistry*, *271*(44), 27879–27887. https://doi.org/10.1074/jbc.271.44.27879

Hawley, S. A., Pan, D. A., Mustard, K. J., Ross, L., Bain, J., Edelman, A. M., Frenguelli, B. G., & Hardie, D. G. (2005). Calmodulin-dependent protein kinase kinase-beta is an alternative upstream kinase for AMP-activated protein kinase. *Cell Metabolism*, *2*(1), 9–19. https://doi.org/10.1016/j.cmet.2005.05.009

Hees, J. T., & Harbauer, A. B. (2022). Metabolic Regulation of Mitochondrial Protein Biogenesis from a Neuronal Perspective. *Biomolecules*, *12*(11), 1595. https://doi.org/10.3390/biom12111595

Hees, J. T., & Harbauer, A. B. (2023). *Insulin signaling regulates* Pink1 *mRNA localization via modulation of AMPK activity to support PINK1 function in neurons*. BioRxiv. https://doi.org/10.1101/2023.02.06.527276

Heo, J.-M., Ordureau, A., Paulo, J. A., Rinehart, J., & Harper, J. W. (2015). The PINK1-PARKIN Mitochondrial Ubiquitylation Pathway Drives a Program of OPTN/NDP52 Recruitment and TBK1 Activation to Promote Mitophagy. *Molecular Cell*, *60*(1), 7–20. https://doi.org/10.1016/j.molcel.2015.08.016

Herzig, S., & Shaw, R. J. (2018). AMPK: Guardian of metabolism and mitochondrial homeostasis. *Nature Reviews. Molecular Cell Biology*, *19*(2), 121–135. https://doi.org/10.1038/nrm.2017.95

Hill, J. M., Lesniak, M. A., Pert, C. B., & Roth, J. (1986). Autoradiographic localization of insulin receptors in rat brain: Prominence in olfactory and limbic areas. *Neuroscience*, *17*(4), 1127–1138. https://doi.org/10.1016/0306-4522(86)90082-5

Hinde, E., Digman, M. A., Welch, C., Hahn, K. M., & Gratton, E. (2012). Biosensor Förster resonance energy transfer detection by the phasor approach to fluorescence lifetime imaging microscopy. *Microscopy Research and Technique*, *75*(3), 271–281. https://doi.org/10.1002/jemt.21054

Hirabayashi, Y., Kwon, S.-K., Paek, H., Pernice, W. M., Paul, M. A., Lee, J., Erfani, P., Raczkowski, A., Petrey, D. S., Pon, L. A., & Polleux, F. (2017). ER-mitochondria tethering by PDZD8 regulates Ca^{2+} dynamics in mammalian neurons. *Science*, *358*(6363), 623–630. https://doi.org/10.1126/science.aan6009

Hirokawa, N., & Takemura, R. (2005). Molecular motors and mechanisms of directional transport in neurons. *Nature Reviews. Neuroscience*, *6*(3), 201–214. https://doi.org/10.1038/nrn1624

Hollenbeck, P. J., & Saxton, W. M. (2005). The axonal transport of mitochondria. *Journal of Cell Science*, *118*(Pt 23), 5411–5419. https://doi.org/10.1242/jcs.02745

Hopkins, D. F., & Williams, G. (1997). Insulin receptors are widely distributed in human brain and bind human and porcine insulin with equal affinity. *Diabetic Medicine: A Journal of the British Diabetic Association*, *14*(12), 1044–1050. https://doi.org/10.1002/(SICI)1096-9136(199712)14:12<1044::AID-DIA508>3.0.CO;2-F

Horman, S., Vertommen, D., Heath, R., Neumann, D., Mouton, V., Woods, A., Schlattner, U., Wallimann, T., Carling, D., Hue, L., & Rider, M. H. (2006). Insulin antagonizes ischemia-induced Thr172 phosphorylation of AMP-activated protein kinase alpha-subunits in heart via hierarchical phosphorylation of Ser485/491. *The Journal of Biological Chemistry*, *281*(9), 5335–5340. https://doi.org/10.1074/jbc.M506850200

Hsu, F., & Mao, Y. (2015). The structure of phosphoinositide phosphatases: Insights into substrate specificity and catalysis. *Biochimica Et Biophysica Acta*, *1851*(6), 698–710. https://doi.org/10.1016/j.bbalip.2014.09.015

Huang, T.-J., Price, S. A., Chilton, L., Calcutt, N. A., Tomlinson, D. R., Verkhratsky, A., & Fernyhough, P. (2003). Insulin prevents depolarization of the mitochondrial inner membrane in sensory neurons of type 1 diabetic rats in the presence of sustained hyperglycemia. *Diabetes*, *52*(8), 2129–2136. https://doi.org/10.2337/diabetes.52.8.2129

Hudson, E. R., Pan, D. A., James, J., Lucocq, J. M., Hawley, S. A., Green, K. A., Baba, O., Terashima, T., & Hardie, D. G. (2003). A novel domain in AMP-activated protein kinase causes glycogen storage bodies similar to those seen in hereditary cardiac arrhythmias. *Current Biology: CB*, *13*(10), 861–866. https://doi.org/10.1016/s0960-9822(03)00249-5

Hung, C.-M., Lombardo, P. S., Malik, N., Brun, S. N., Hellberg, K., Van Nostrand, J. L., Garcia, D., Baumgart, J., Diffenderfer, K., Asara, J. M., & Shaw, R. J. (2021). AMPK/ULK1-mediated phosphorylation of Parkin ACT domain mediates an early step in mitophagy. *Science Advances*, *7*(15), eabg4544. https://doi.org/10.1126/sciadv.abg4544

Hung, V., Lam, S. S., Udeshi, N. D., Svinkina, T., Guzman, G., Mootha, V. K., Carr, S. A., & Ting, A. Y. (2017). Proteomic mapping of cytosol-facing outer mitochondrial and ER membranes in living human cells by proximity biotinylation. *ELife*, *6*, e24463. https://doi.org/10.7554/eLife.24463

Hurley, R. L., Anderson, K. A., Franzone, J. M., Kemp, B. E., Means, A. R., & Witters, L. A. (2005). The Ca2+/calmodulin-dependent protein kinase kinases are AMP-activated protein kinase kinases. *The Journal of Biological Chemistry*, *280*(32), 29060–29066. https://doi.org/10.1074/jbc.M503824200

Ingerman, E., Perkins, E. M., Marino, M., Mears, J. A., McCaffery, J. M., Hinshaw, J. E., & Nunnari, J. (2005). Dnm1 forms spirals that are structurally tailored to fit mitochondria. *The Journal of Cell Biology*, *170*(7), 1021–1027. https://doi.org/10.1083/jcb.200506078

Inoki, K., Li, Y., Xu, T., & Guan, K.-L. (2003). Rheb GTPase is a direct target of TSC2 GAP activity and regulates mTOR signaling. *Genes & Development*, *17*(15), 1829–1834. https://doi.org/10.1101/gad.1110003

Inoki, K., Li, Y., Zhu, T., Wu, J., & Guan, K.-L. (2002). TSC2 is phosphorylated and inhibited by Akt and suppresses mTOR signalling. *Nature Cell Biology*, *4*(9), 648–657. https://doi.org/10.1038/ncb839

Inoki, K., Zhu, T., & Guan, K.-L. (2003). TSC2 Mediates Cellular Energy Response to Control Cell Growth and Survival. *Cell*, *115*(5), 577–590. https://doi.org/10.1016/S0092-8674(03)00929-2

Iraburu, M. J., Garner, T., & Montiel-Duarte, C. (2021). Revising Endosomal Trafficking under Insulin Receptor Activation. *International Journal of Molecular Sciences*, *22*(13), 6978. https://doi.org/10.3390/ijms22136978

Ishihara, N., Nomura, M., Jofuku, A., Kato, H., Suzuki, S. O., Masuda, K., Otera, H., Nakanishi, Y., Nonaka, I., Goto, Y.-I., Taguchi, N., Morinaga, H., Maeda, M., Takayanagi, R., Yokota, S., & Mihara, K. (2009). Mitochondrial fission factor Drp1 is essential for embryonic development and synapse formation in mice. *Nature Cell Biology*, *11*(8), 958–966. https://doi.org/10.1038/ncb1907

Ishizuka, Y., Kakiya, N., Witters, L. A., Oshiro, N., Shirao, T., Nawa, H., & Takei, N. (2013). AMP-activated protein kinase counteracts brain-derived neurotrophic factor-induced mammalian target of rapamycin complex 1 signaling in neurons. *Journal of Neurochemistry*, *127*(1), 66–77. https://doi.org/10.1111/jnc.12362

Jäger, S., Handschin, C., St-Pierre, J., & Spiegelman, B. M. (2007). AMP-activated protein kinase (AMPK) action in skeletal muscle via direct phosphorylation of PGC-1alpha. *Proceedings of the National Academy of Sciences of the United States of America*, *104*(29), 12017–12022. https://doi.org/10.1073/pnas.0705070104

Jin, S. M., Lazarou, M., Wang, C., Kane, L. A., Narendra, D., & Youle, R. J. (2010). Mitochondrial membrane potential regulates PINK1 import and proteolytic destabilization by PARL. *The Journal of Cell Biology*, *191*(5), 933–942. https://doi.org/10.1083/jcb.201008084

Jin, S. M., & Youle, R. J. (2013). The accumulation of misfolded proteins in the mitochondrial matrix is sensed by PINK1 to induce PARK2/Parkin-mediated mitophagy of polarized mitochondria. *Autophagy*, *9*(11), 1750–1757. https://doi.org/10.4161/auto.26122

Jornayvaz, F. R., & Shulman, G. I. (2010). Regulation of mitochondrial biogenesis. *Essays in Biochemistry*, *47*, 69–84. https://doi.org/10.1042/bse0470069

Kamer, K. J., & Mootha, V. K. (2015). The molecular era of the mitochondrial calcium uniporter. *Nature Reviews Molecular Cell Biology*, *16*(9), 545–553. https://doi.org/10.1038/nrm4039

Kanai, Y., Dohmae, N., & Hirokawa, N. (2004). Kinesin transports RNA: Isolation and characterization of an RNA-transporting granule. *Neuron*, *43*(4), 513–525. https://doi.org/10.1016/j.neuron.2004.07.022

Kang, J.-S., Tian, J.-H., Pan, P.-Y., Zald, P., Li, C., Deng, C., & Sheng, Z.-H. (2008). Docking of axonal mitochondria by syntaphilin controls their mobility and affects short-term facilitation. *Cell*, *132*(1), 137–148. https://doi.org/10.1016/j.cell.2007.11.024

Khuperkar, D., Hoek, T. A., Sonneveld, S., Verhagen, B. M. P., Boersma, S., & Tanenbaum, M. E. (2020). Quantification of mRNA translation in live cells using single-molecule imaging. *Nature Protocols*, *15*(4), 1371–1398. https://doi.org/10.1038/s41596-019-0284-x

Kim, E., Goraksha-Hicks, P., Li, L., Neufeld, T. P., & Guan, K.-L. (2008). Regulation of TORC1 by Rag GTPases in nutrient response. *Nature Cell Biology*, *10*(8), 935–945. https://doi.org/10.1038/ncb1753

Kim, J., Kundu, M., Viollet, B., & Guan, K.-L. (2011). AMPK and mTOR regulate autophagy through direct phosphorylation of Ulk1. *Nature Cell Biology*, *13*(2), 132–141. https://doi.org/10.1038/ncb2152

Kim, K. H., & Lee, M.-S. (2014). Autophagy—A key player in cellular and body metabolism. *Nature Reviews. Endocrinology*, *10*(6), 322–337. https://doi.org/10.1038/nrendo.2014.35

Kim, S.-S., & Lee, C.-K. (2019). Growth signaling and longevity in mouse models. *BMB Reports*, *52*(1), 70–85. https://doi.org/10.5483/BMBRep.2019.52.1.299

Kinoshita, E., Kinoshita-Kikuta, E., Takiyama, K., & Koike, T. (2006). Phosphate-binding tag, a new tool to visualize phosphorylated proteins. *Molecular & Cellular Proteomics: MCP*, *5*(4), 749–757. https://doi.org/10.1074/mcp.T500024-MCP200

Kislinger, G., Gnägi, H., Kerschensteiner, M., Simons, M., Misgeld, T., & Schifferer, M. (2020). ATUM-FIB microscopy for targeting and multiscale imaging of rare events in mouse cortex. *STAR Protocols*, *1*(3), 100232. https://doi.org/10.1016/j.xpro.2020.100232

Kislinger, G., Niemann, C., Rodriguez, L., Jiang, H., Fard, M. K., Snaidero, N., Schumacher, A.-M., Kerschensteiner, M., Misgeld, T., & Schifferer, M. (2023). Neurons on tape: Automated Tape Collecting Ultramicrotomy-mediated volume EM for targeting neuropathology. In *Methods in Cell Biology* (p. S0091679X23000225). Elsevier. https://doi.org/10.1016/bs.mcb.2023.01.012

Kitada, T., Asakawa, S., Hattori, N., Matsumine, H., Yamamura, Y., Minoshima, S., Yokochi, M., Mizuno, Y., & Shimizu, N. (1998). Mutations in the parkin gene cause autosomal recessive juvenile parkinsonism. *Nature*, *392*(6676), 605–608. https://doi.org/10.1038/33416

Koch, S., Donarski, N., Goetze, K., Kreckel, M., Stuerenburg, H. J., Buhmann, C., & Beisiegel, U. (2001). Characterization of four lipoprotein classes in human cerebrospinal fluid. *Journal of Lipid Research*, *42*(7), 1143–1151.

Kolb, H., Kempf, K., Röhling, M., & Martin, S. (2020). Insulin: Too much of a good thing is bad. *BMC Medicine*, *18*(1), 224. https://doi.org/10.1186/s12916-020-01688-6

Konagaya, Y., Terai, K., Hirao, Y., Takakura, K., Imajo, M., Kamioka, Y., Sasaoka, N., Kakizuka, A., Sumiyama, K., Asano, T., & Matsuda, M. (2017). A Highly Sensitive FRET Biosensor for AMPK Exhibits Heterogeneous AMPK Responses among Cells and Organs. *Cell Reports*, *21*(9), 2628–2638. https://doi.org/10.1016/j.celrep.2017.10.113

Kops, G. J., de Ruiter, N. D., De Vries-Smits, A. M., Powell, D. R., Bos, J. L., & Burgering, B. M. (1999). Direct control of the Forkhead transcription factor AFX by protein kinase B. *Nature*, *398*(6728), 630–634. https://doi.org/10.1038/19328

Kovacic, S., Soltys, C.-L. M., Barr, A. J., Shiojima, I., Walsh, K., & Dyck, J. R. B. (2003). Akt activity negatively regulates phosphorylation of AMP-activated protein kinase in the heart. *The Journal of Biological Chemistry*, *278*(41), 39422–39427. https://doi.org/10.1074/jbc.M305371200

Krämer, L., Dalheimer, N., Räschle, M., Storchová, Z., Pielage, J., Boos, F., & Herrmann, J. M. (2023). MitoStores: Chaperone-controlled protein granules store mitochondrial precursors in the cytosol. *The EMBO Journal*, *42*(7), e112309. https://doi.org/10.15252/embj.2022112309

Kullmann, S., Heni, M., Hallschmid, M., Fritsche, A., Preissl, H., & Häring, H.-U. (2016). Brain Insulin Resistance at the Crossroads of Metabolic and Cognitive Disorders in Humans. *Physiological Reviews*, *96*(4), 1169–1209. https://doi.org/10.1152/physrev.00032.2015

_____

Lalier, L., Mignard, V., Joalland, M.-P., Lanoé, D., Cartron, P.-F., Manon, S., & Vallette, F. M. (2021). TOM20-mediated transfer of Bcl2 from ER to MAM and mitochondria upon induction of apoptosis. *Cell Death & Disease*, *12*(2), 182. https://doi.org/10.1038/s41419-021-03471-8

Lamming, D. W., & Bar-Peled, L. (2019). Lysosome: The metabolic signaling hub. *Traffic (Copenhagen, Denmark)*, *20*(1), 27–38. https://doi.org/10.1111/tra.12617

Laws, S. M., Gaskin, S., Woodfield, A., Srikanth, V., Bruce, D., Fraser, P. E., Porter, T., Newsholme, P., Wijesekara, N., Burnham, S., Doré, V., Li, Q.-X., Maruff, P., Masters, C. L., Rainey-Smith, S., Rowe, C. C., Salvado, O., Villemagne, V. L., Martins, R. N., & Verdile, G. (2017). Insulin resistance is associated with reductions in specific cognitive domains and increases in CSF tau in cognitively normal adults. *Scientific Reports*, *7*(1), 9766. https://doi.org/10.1038/s41598-017-09577-4

Lazarou, M., Sliter, D. A., Kane, L. A., Sarraf, S. A., Wang, C., Burman, J. L., Sideris, D. P., Fogel, A. I., & Youle, R. J. (2015). The ubiquitin kinase PINK1 recruits autophagy receptors to induce mitophagy. *Nature*, *524*(7565), 309–314. https://doi.org/10.1038/nature14893

Le Guerroué, F., Eck, F., Jung, J., Starzetz, T., Mittelbronn, M., Kaulich, M., & Behrends, C. (2017). Autophagosomal Content Profiling Reveals an LC3C-Dependent Piecemeal Mitophagy Pathway. *Molecular Cell*, *68*(4), 786-796.e6. https://doi.org/10.1016/j.molcel.2017.10.029

Li, S., Xiong, G.-J., Huang, N., & Sheng, Z.-H. (2020). The cross-talk of energy sensing and mitochondrial anchoring sustains synaptic efficacy by maintaining presynaptic metabolism. *Nature Metabolism*, *2*(10), 1077–1095. https://doi.org/10.1038/s42255-020-00289-0

Li, Y., Zheng, W., Lu, Y., Zheng, Y., Pan, L., Wu, X., Yuan, Y., Shen, Z., Ma, S., Zhang, X., Wu, J., Chen, Z., & Zhang, X. (2021). BNIP3L/NIX-mediated mitophagy: Molecular mechanisms and implications for human disease. *Cell Death & Disease*, *13*(1), 14. https://doi.org/10.1038/s41419-021-04469-y

Li, Z., Okamoto, K.-I., Hayashi, Y., & Sheng, M. (2004). The importance of dendritic mitochondria in the morphogenesis and plasticity of spines and synapses. *Cell*, *119*(6), 873–887. https://doi.org/10.1016/j.cell.2004.11.003

Liao, Y.-C., Fernandopulle, M. S., Wang, G., Choi, H., Hao, L., Drerup, C. M., Patel, R., Qamar, S., Nixon-Abell, J., Shen, Y., Meadows, W., Vendruscolo, M., Knowles, T. P. J., Nelson, M., Czekalska, M. A., Musteikyte, G., Gachechiladze, M. A., Stephens, C. A., Pasolli, H. A., … Ward, M. E. (2019). RNA Granules Hitchhike on Lysosomes for Long-Distance Transport, Using Annexin A11 as a Molecular Tether. *Cell*, *179*(1), 147-164.e20. https://doi.org/10.1016/j.cell.2019.08.050

Ligon, L. A., & Steward, O. (2000). Movement of mitochondria in the axons and dendrites of cultured hippocampal neurons. *The Journal of Comparative Neurology*, *427*(3), 340–350. https://doi.org/10.1002/1096-9861(20001120)427:3<340::aid-cne2>3.0.co;2-y

Lin, M.-Y., Cheng, X.-T., Tammineni, P., Xie, Y., Zhou, B., Cai, Q., & Sheng, Z.-H. (2017). Releasing Syntaphilin Removes Stressed Mitochondria from Axons Independent of Mitophagy under Pathophysiological Conditions. *Neuron*, *94*(3), 595-610.e6. https://doi.org/10.1016/j.neuron.2017.04.004

Lin, W., & Kang, U. J. (2008). Characterization of PINK1 processing, stability, and subcellular localization. *Journal of Neurochemistry*, *106*(1), 464–474. https://doi.org/10.1111/j.1471-4159.2008.05398.x

Ling, N. X. Y., Kaczmarek, A., Hoque, A., Davie, E., Ngoei, K. R. W., Morrison, K. R., Smiles, W. J., Forte, G. M., Wang, T., Lie, S., Dite, T. A., Langendorf, C. G., Scott, J. W., Oakhill, J. S., & Petersen, J. (2020). MTORC1 directly inhibits AMPK to promote cell proliferation under nutrient stress. *Nature Metabolism*, *2*(1), 41–49. https://doi.org/10.1038/s42255-019-0157-1

Liu, C.-C., Liu, C.-C., Kanekiyo, T., Xu, H., & Bu, G. (2013). Apolipoprotein E and Alzheimer disease: Risk, mechanisms and therapy. *Nature Reviews. Neurology*, *9*(2), 106–118. https://doi.org/10.1038/nrneurol.2012.263

Liu, G. Y., & Sabatini, D. M. (2020). MTOR at the nexus of nutrition, growth, ageing and disease. *Nature Reviews Molecular Cell Biology*, *21*(4), 183–203. https://doi.org/10.1038/s41580-019-0199-y

Liu, L., Feng, D., Chen, G., Chen, M., Zheng, Q., Song, P., Ma, Q., Zhu, C., Wang, R., Qi, W., Huang, L., Xue, P., Li, B., Wang, X., Jin, H., Wang, J., Yang, F., Liu, P., Zhu, Y., … Chen, Q. (2012). Mitochondrial outer-membrane protein FUNDC1 mediates hypoxia-induced mitophagy in mammalian cells. *Nature Cell Biology*, *14*(2), 177–185. https://doi.org/10.1038/ncb2422

Liu, Q., Wang, J., Kang, S. A., Thoreen, C. C., Hur, W., Ahmed, T., Sabatini, D. M., & Gray, N. S. (2011). Discovery of 9-(6-aminopyridin-3-yl)-1-(3-(trifluoromethyl)phenyl)benzo[h][1,6]naphthyridin-2(1H)-one (Torin2) as a potent, selective, and orally available mammalian target of rapamycin (mTOR) inhibitor for treatment of cancer. *Journal of Medicinal Chemistry*, *54*(5), 1473–1480. https://doi.org/10.1021/jm101520v

Liu, Q., Xu, C., Kirubakaran, S., Zhang, X., Hur, W., Liu, Y., Kwiatkowski, N. P., Wang, J., Westover, K. D., Gao, P., Ercan, D., Niepel, M., Thoreen, C. C., Kang, S. A., Patricelli, M. P., Wang, Y., Tupper, T., Altabef, A., Kawamura, H., … Gray, N. S. (2013). Characterization of Torin2, an ATP-competitive inhibitor of mTOR, ATM, and ATR. *Cancer Research*, *73*(8), 2574–2586. https://doi.org/10.1158/0008-5472.CAN-12-1702

_____

Liu, Y.-T., Sliter, D. A., Shammas, M. K., Huang, X., Wang, C., Calvelli, H., Maric, D. S., & Narendra, D. P. (2021). Mt-Keima detects PINK1-PRKN mitophagy in vivo with greater sensitivity than mito-QC. *Autophagy*, *17*(11), 3753–3762. https://doi.org/10.1080/15548627.2021.1896924

López-Doménech, G., Covill-Cooke, C., Ivankovic, D., Halff, E. F., Sheehan, D. F., Norkett, R., Birsa, N., & Kittler, J. T. (2018). Miro proteins coordinate microtubule- and actin-dependent mitochondrial transport and distribution. *The EMBO Journal*, *37*(3), 321–336. https://doi.org/10.15252/embj.201696380

Losón, O. C., Song, Z., Chen, H., & Chan, D. C. (2013). Fis1, Mff, MiD49, and MiD51 mediate Drp1 recruitment in mitochondrial fission. *Molecular Biology of the Cell*, *24*(5), 659–667. https://doi.org/10.1091/mbc.E12-10-0721

Luo, J.-S., Ning, J.-Q., Chen, Z.-Y., Li, W.-J., Zhou, R.-L., Yan, R.-Y., Chen, M.-J., & Ding, L.-L. (2022). The Role of Mitochondrial Quality Control in Cognitive Dysfunction in Diabetes. *Neurochemical Research*, *47*(8), 2158–2172. https://doi.org/10.1007/s11064-022-03631-y

Maday, S., & Holzbaur, E. L. F. (2016). Compartment-Specific Regulation of Autophagy in Primary Neurons. *The Journal of Neuroscience: The Official Journal of the Society for Neuroscience*, *36*(22), 5933–5945. https://doi.org/10.1523/JNEUROSCI.4401-15.2016

Mair, W., Morantte, I., Rodrigues, A. P. C., Manning, G., Montminy, M., Shaw, R. J., & Dillin, A. (2011). Lifespan extension induced by AMPK and calcineurin is mediated by CRTC-1 and CREB. *Nature*, *470*(7334), 404–408. https://doi.org/10.1038/nature09706

Manning, B. D., Tee, A. R., Logsdon, M. N., Blenis, J., & Cantley, L. C. (2002). Identification of the tuberous sclerosis complex-2 tumor suppressor gene product tuberin as a target of the phosphoinositide 3-kinase/akt pathway. *Molecular Cell*, *10*(1), 151–162. https://doi.org/10.1016/s1097-2765(02)00568-3

Markovinovic, A., Greig, J., Martín-Guerrero, S. M., Salam, S., & Paillusson, S. (2022). Endoplasmic reticulum–mitochondria signaling in neurons and neurodegenerative diseases. *Journal of Cell Science*, *135*(3), jcs248534. https://doi.org/10.1242/jcs.248534

Martin-Montalvo, A., Mercken, E. M., Mitchell, S. J., Palacios, H. H., Mote, P. L., Scheibye-Knudsen, M., Gomes, A. P., Ward, T. M., Minor, R. K., Blouin, M.-J., Schwab, M., Pollak, M., Zhang, Y., Yu, Y., Becker, K. G., Bohr, V. A., Ingram, D. K., Sinclair, D. A., Wolf, N. S., … de Cabo, R. (2013). Metformin improves healthspan and lifespan in mice. *Nature Communications*, *4*, 2192. https://doi.org/10.1038/ncomms3192

Maruszczak, K. K., Jung, M., Rasool, S., Trempe, J.-F., & Rapaport, D. (2022). The role of the individual TOM subunits in the association of PINK1 with depolarized mitochondria. *Journal of Molecular Medicine*, *100*(5), 747–762. https://doi.org/10.1007/s00109-022-02191-6

_____

Matsuda, N., Sato, S., Shiba, K., Okatsu, K., Saisho, K., Gautier, C. A., Sou, Y.-S., Saiki, S., Kawajiri, S., Sato, F., Kimura, M., Komatsu, M., Hattori, N., & Tanaka, K. (2010). PINK1 stabilized by mitochondrial depolarization recruits Parkin to damaged mitochondria and activates latent Parkin for mitophagy. *The Journal of Cell Biology*, *189*(2), 211–221. https://doi.org/10.1083/jcb.200910140

Matsuda, W., Furuta, T., Nakamura, K. C., Hioki, H., Fujiyama, F., Arai, R., & Kaneko, T. (2009). Single Nigrostriatal Dopaminergic Neurons Form Widely Spread and Highly Dense Axonal Arborizations in the Neostriatum. *Journal of Neuroscience*, *29*(2), 444–453. https://doi.org/10.1523/JNEUROSCI.4029-08.2009

McBride, H. M., Neuspiel, M., & Wasiak, S. (2006). Mitochondria: More Than Just a Powerhouse. *Current Biology*, *16*(14), R551–R560. https://doi.org/10.1016/j.cub.2006.06.054

McClintock, M. A., Dix, C. I., Johnson, C. M., McLaughlin, S. H., Maizels, R. J., Hoang, H. T., & Bullock, S. L. (2018). RNA-directed activation of cytoplasmic dynein-1 in reconstituted transport RNPs. *ELife*, *7*, e36312. https://doi.org/10.7554/eLife.36312

McCoy, M. K., Kaganovich, A., Rudenko, I. N., Ding, J., & Cookson, M. R. (2014). Hexokinase activity is required for recruitment of parkin to depolarized mitochondria. *Human Molecular Genetics*, *23*(1), 145–156. https://doi.org/10.1093/hmg/ddt407

McWilliams, T. G., Prescott, A. R., Montava-Garriga, L., Ball, G., Singh, F., Barini, E., Muqit, M. M. K., Brooks, S. P., & Ganley, I. G. (2018). Basal Mitophagy Occurs Independently of PINK1 in Mouse Tissues of High Metabolic Demand. *Cell Metabolism*, *27*(2), 439-449.e5. https://doi.org/10.1016/j.cmet.2017.12.008

Meissner, C., Lorenz, H., Weihofen, A., Selkoe, D. J., & Lemberg, M. K. (2011). The mitochondrial intramembrane protease PARL cleaves human Pink1 to regulate Pink1 trafficking. *Journal of Neurochemistry*, *117*(5), 856–867. https://doi.org/10.1111/j.1471-4159.2011.07253.x

Mertins, P., Yang, F., Liu, T., Mani, D. R., Petyuk, V. A., Gillette, M. A., Clauser, K. R., Qiao, J. W., Gritsenko, M. A., Moore, R. J., Levine, D. A., Townsend, R., Erdmann-Gilmore, P., Snider, J. E., Davies, S. R., Ruggles, K. V., Fenyo, D., Kitchens, R. T., Li, S., … Carr, S. A. (2014). Ischemia in tumors induces early and sustained phosphorylation changes in stress kinase pathways but does not affect global protein levels. *Molecular & Cellular Proteomics: MCP*, *13*(7), 1690–1704. https://doi.org/10.1074/mcp.M113.036392

Mielke, J. G., & Wang, Y.-T. (2011). Insulin, synaptic function, and opportunities for neuroprotection. *Progress in Molecular Biology and Translational Science*, *98*, 133–186. https://doi.org/10.1016/B978-0-12-385506-0.00004-1

Mindell, J. A. (2012). Lysosomal acidification mechanisms. *Annual Review of Physiology*, *74*, 69–86. https://doi.org/10.1146/annurev-physiol-012110-142317

_____

Minokoshi, Y., Alquier, T., Furukawa, N., Kim, Y.-B., Lee, A., Xue, B., Mu, J., Foufelle, F., Ferré, P., Birnbaum, M. J., Stuck, B. J., & Kahn, B. B. (2004). AMP-kinase regulates food intake by responding to hormonal and nutrient signals in the hypothalamus. *Nature*, *428*(6982), 569–574. https://doi.org/10.1038/nature02440

Misgeld, T., & Schwarz, T. L. (2017). Mitostasis in Neurons: Maintaining Mitochondria in an Extended Cellular Architecture. *Neuron*, *96*(3), 651–666. https://doi.org/10.1016/j.neuron.2017.09.055

Miyamoto, T., Rho, E., Sample, V., Akano, H., Magari, M., Ueno, T., Gorshkov, K., Chen, M., Tokumitsu, H., Zhang, J., & Inoue, T. (2015). Compartmentalized AMPK signaling illuminated by genetically encoded molecular sensors and actuators. *Cell Reports*, *11*(4), 657–670. https://doi.org/10.1016/j.celrep.2015.03.057

Mizushima, N., & Komatsu, M. (2011). Autophagy: Renovation of cells and tissues. *Cell*, *147*(4), 728–741. https://doi.org/10.1016/j.cell.2011.10.026

Mootha, V. K., Lindgren, C. M., Eriksson, K.-F., Subramanian, A., Sihag, S., Lehar, J., Puigserver, P., Carlsson, E., Ridderstråle, M., Laurila, E., Houstis, N., Daly, M. J., Patterson, N., Mesirov, J. P., Golub, T. R., Tamayo, P., Spiegelman, B., Lander, E. S., Hirschhorn, J. N., … Groop, L. C. (2003). PGC-1alpha-responsive genes involved in oxidative phosphorylation are coordinately downregulated in human diabetes. *Nature Genetics*, *34*(3), 267–273. https://doi.org/10.1038/ng1180

Morita, M., Gravel, S.-P., Chénard, V., Sikström, K., Zheng, L., Alain, T., Gandin, V., Avizonis, D., Arguello, M., Zakaria, C., McLaughlan, S., Nouet, Y., Pause, A., Pollak, M., Gottlieb, E., Larsson, O., St-Pierre, J., Topisirovic, I., & Sonenberg, N. (2013). MTORC1 Controls Mitochondrial Activity and Biogenesis through 4E-BP-Dependent Translational Regulation. *Cell Metabolism*, *18*(5), 698–711. https://doi.org/10.1016/j.cmet.2013.10.001

Morris, R. L., & Hollenbeck, P. J. (1993). The regulation of bidirectional mitochondrial transport is coordinated with axonal outgrowth. *Journal of Cell Science*, *104 (Pt 3)*, 917–927. https://doi.org/10.1242/jcs.104.3.917

Mullari, M., Lyon, D., Jensen, L. J., & Nielsen, M. L. (2017). Specifying RNA-Binding Regions in Proteins by Peptide Cross-Linking and Affinity Purification. *Journal of Proteome Research*, *16*(8), 2762–2772. https://doi.org/10.1021/acs.jproteome.7b00042

Muraleedharan, R., & Dasgupta, B. (2022). AMPK in the brain: Its roles in glucose and neural metabolism. *The FEBS Journal*, *289*(8), 2247–2262. https://doi.org/10.1111/febs.16151

Murley, A., & Nunnari, J. (2016). The Emerging Network of Mitochondria-Organelle Contacts. *Molecular Cell*, *61*(5), 648–653. https://doi.org/10.1016/j.molcel.2016.01.031

Nakae, J., Park, B. C., & Accili, D. (1999). Insulin stimulates phosphorylation of the forkhead transcription factor FKHR on serine 253 through a Wortmannin-sensitive pathway. *The*

_____

Journal of Biological Chemistry, *274*(23), 15982–15985.

https://doi.org/10.1074/jbc.274.23.15982

Narendra, D., Jin, S. M., Tanaka, A., Suen, D.-F., Gautier, C. A., Shen, J., Cookson, M. R., & Youle, R. J. (2010). PINK1 is selectively stabilized on impaired mitochondria to activate Parkin. *PLoS Biology*, *8*(1), e1000298. https://doi.org/10.1371/journal.pbio.1000298

Narendra, D., Tanaka, A., Suen, D.-F., & Youle, R. J. (2008). Parkin is recruited selectively to impaired mitochondria and promotes their autophagy. *The Journal of Cell Biology*, *183*(5), 795–803. https://doi.org/10.1083/jcb.200809125

Nemoto, Y., & De Camilli, P. (1999). Recruitment of an alternatively spliced form of synaptojanin 2 to mitochondria by the interaction with the PDZ domain of a mitochondrial outer membrane protein. *The EMBO Journal*, *18*(11), 2991–3006. https://doi.org/10.1093/emboj/18.11.2991

Nguyen, T. T., Ta, Q. T. H., Nguyen, T. K. O., Nguyen, T. T. D., & Giau, V. V. (2020). Type 3 Diabetes and Its Role Implications in Alzheimer's Disease. *International Journal of Molecular Sciences*, *21*(9), 3165. https://doi.org/10.3390/ijms21093165

Nikoletopoulou, V., Markaki, M., Palikaras, K., & Tavernarakis, N. (2013). Crosstalk between apoptosis, necrosis and autophagy. *Biochimica et Biophysica Acta (BBA) - Molecular Cell Research*, *1833*(12), 3448–3459. https://doi.org/10.1016/j.bbamcr.2013.06.001

Ning, J., Xi, G., & Clemmons, D. R. (2011). Suppression of AMPK activation via S485 phosphorylation by IGF-I during hyperglycemia is mediated by AKT activation in vascular smooth muscle cells. *Endocrinology*, *152*(8), 3143–3154. https://doi.org/10.1210/en.2011-0155

Ning, P., Jiang, X., Yang, J., Zhang, J., Yang, F., & Cao, H. (2022). Mitophagy: A potential therapeutic target for insulin resistance. *Frontiers in Physiology*, *13*, 957968. https://doi.org/10.3389/fphys.2022.957968

Novak, V., Milberg, W., Hao, Y., Munshi, M., Novak, P., Galica, A., Manor, B., Roberson, P., Craft, S., & Abduljalil, A. (2014). Enhancement of Vasoreactivity and Cognition by Intranasal Insulin in Type 2 Diabetes. *Diabetes Care*, *37*(3), 751–759. https://doi.org/10.2337/dc13-1672

Nunnari, J., & Suomalainen, A. (2012). Mitochondria: In Sickness and in Health. *Cell*, *148*(6), 1145–1159. https://doi.org/10.1016/j.cell.2012.02.035

Oeding, S. J., Majstrowicz, K., Hu, X.-P., Schwarz, V., Freitag, A., Honnert, U., Nikolaus, P., & Bähler, M. (2018). Identification of Miro1 and Miro2 as mitochondrial receptors for myosin XIX. *Journal of Cell Science*, *131*(17), jcs219469. https://doi.org/10.1242/jcs.219469

Ogg, S., Paradis, S., Gottlieb, S., Patterson, G. I., Lee, L., Tissenbaum, H. A., & Ruvkun, G. (1997). The Fork head transcription factor DAF-16 transduces insulin-like metabolic and longevity signals in C. elegans. *Nature*, *389*(6654), 994–999. https://doi.org/10.1038/40194

Oh, C.-K., Sultan, A., Platzer, J., Dolatabadi, N., Soldner, F., McClatchy, D. B., Diedrich, J. K., Yates, J. R., Ambasudhan, R., Nakamura, T., Jaenisch, R., & Lipton, S. A. (2017). S-Nitrosylation of PINK1 Attenuates PINK1/Parkin-Dependent Mitophagy in hiPSC-Based Parkinson's Disease Models. *Cell Reports*, *21*(8), 2171–2182. https://doi.org/10.1016/j.celrep.2017.10.068

Okatsu, K., Koyano, F., Kimura, M., Kosako, H., Saeki, Y., Tanaka, K., & Matsuda, N. (2015). Phosphorylated ubiquitin chain is the genuine Parkin receptor. *The Journal of Cell Biology*, *209*(1), 111–128. https://doi.org/10.1083/jcb.201410050

Okatsu, K., Oka, T., Iguchi, M., Imamura, K., Kosako, H., Tani, N., Kimura, M., Go, E., Koyano, F., Funayama, M., Shiba-Fukushima, K., Sato, S., Shimizu, H., Fukunaga, Y., Taniguchi, H., Komatsu, M., Hattori, N., Mihara, K., Tanaka, K., & Matsuda, N. (2012). PINK1 autophosphorylation upon membrane potential dissipation is essential for Parkin recruitment to damaged mitochondria. *Nature Communications*, *3*, 1016. https://doi.org/10.1038/ncomms2016

Ordureau, A., Kraus, F., Zhang, J., An, H., Park, S., Ahfeldt, T., Paulo, J. A., & Harper, J. W. (2021). Temporal proteomics during neurogenesis reveals large-scale proteome and organelle remodeling via selective autophagy. *Molecular Cell*, *81*(24), 5082-5098.e11. https://doi.org/10.1016/j.molcel.2021.10.001

Palmer, C. S., Osellame, L. D., Laine, D., Koutsopoulos, O. S., Frazier, A. E., & Ryan, M. T. (2011). MiD49 and MiD51, new components of the mitochondrial fission machinery. *EMBO Reports*, *12*(6), 565–573. https://doi.org/10.1038/embor.2011.54

Panchaud, N., Péli-Gulli, M.-P., & De Virgilio, C. (2013). Amino acid deprivation inhibits TORC1 through a GTPase-activating protein complex for the Rag family GTPase Gtr1. *Science Signaling*, *6*(277), ra42. https://doi.org/10.1126/scisignal.2004112

Papa, S., Martino, P. L., Capitanio, G., Gaballo, A., De Rasmo, D., Signorile, A., & Petruzzella, V. (2012). The oxidative phosphorylation system in mammalian mitochondria. *Advances in Experimental Medicine and Biology*, *942*, 3–37. https://doi.org/10.1007/978-94-007-2869-1_1

Park, J.-M., Lee, D.-H., & Kim, D.-H. (2023). Redefining the role of AMPK in autophagy and the energy stress response. *Nature Communications*, *14*(1), 2994. https://doi.org/10.1038/s41467-023-38401-z

Patti, M. E., Butte, A. J., Crunkhorn, S., Cusi, K., Berria, R., Kashyap, S., Miyazaki, Y., Kohane, I., Costello, M., Saccone, R., Landaker, E. J., Goldfine, A. B., Mun, E., DeFronzo, R., Finlayson, J., Kahn, C. R., & Mandarino, L. J. (2003). Coordinated reduction of genes of oxidative metabolism in humans with insulin resistance and diabetes: Potential role of PGC1 and NRF1.

Proceedings of the National Academy of Sciences of the United States of America, *100*(14), 8466–8471. https://doi.org/10.1073/pnas.1032913100

Perez Ortiz, J. M., & Swerdlow, R. H. (2019). Mitochondrial dysfunction in Alzheimer's disease: Role in pathogenesis and novel therapeutic opportunities. *British Journal of Pharmacology*, *176*(18), 3489–3507. https://doi.org/10.1111/bph.14585

Periasamy, A., Mazumder, N., Sun, Y., Christopher, K. G., & Day, R. N. (2015). FRET Microscopy: Basics, Issues and Advantages of FLIM-FRET Imaging. In W. Becker (Ed.), *Advanced Time-Correlated Single Photon Counting Applications* (Vol. 111, pp. 249–276). Springer International Publishing. https://doi.org/10.1007/978-3-319-14929-5_7

Petit, A., Kawarai, T., Paitel, E., Sanjo, N., Maj, M., Scheid, M., Chen, F., Gu, Y., Hasegawa, H., Salehi-Rad, S., Wang, L., Rogaeva, E., Fraser, P., Robinson, B., St George-Hyslop, P., & Tandon, A. (2005). Wild-type PINK1 Prevents Basal and Induced Neuronal Apoptosis, a Protective Effect Abrogated by Parkinson Disease-related Mutations. *Journal of Biological Chemistry*, *280*(40), 34025–34032. https://doi.org/10.1074/jbc.M505143200

Phillips, M. J., & Voeltz, G. K. (2016). Structure and function of ER membrane contact sites with other organelles. *Nature Reviews. Molecular Cell Biology*, *17*(2), 69–82. https://doi.org/10.1038/nrm.2015.8

Popovic, D., Nijenhuis, W., Kapitein, L. C., & Pelkmans, L. (2020). *Co-translational targeting of transcripts to endosomes*. BioRxiv. https://doi.org/10.1101/2020.07.17.208652

Qin, W., Myers, S. A., Carey, D. K., Carr, S. A., & Ting, A. Y. (2021). Spatiotemporally-resolved mapping of RNA binding proteins via functional proximity labeling reveals a mitochondrial mRNA anchor promoting stress recovery. *Nature Communications*, *12*(1), 4980. https://doi.org/10.1038/s41467-021-25259-2

Quintero, O. A., DiVito, M. M., Adikes, R. C., Kortan, M. B., Case, L. B., Lier, A. J., Panaretos, N. S., Slater, S. Q., Rengarajan, M., Feliu, M., & Cheney, R. E. (2009). Human Myo19 is a novel myosin that associates with mitochondria. *Current Biology: CB*, *19*(23), 2008–2013. https://doi.org/10.1016/j.cub.2009.10.026

Rakovic, A., Shurkewitsch, K., Seibler, P., Grünewald, A., Zanon, A., Hagenah, J., Krainc, D., & Klein, C. (2013). Phosphatase and tensin homolog (PTEN)-induced putative kinase 1 (PINK1)-dependent ubiquitination of endogenous Parkin attenuates mitophagy: Study in human primary fibroblasts and induced pluripotent stem cell-derived neurons. *The Journal of Biological Chemistry*, *288*(4), 2223–2237. https://doi.org/10.1074/jbc.M112.391680

Rambold, A. S., & Pearce, E. L. (2018). Mitochondrial Dynamics at the Interface of Immune Cell Metabolism and Function. *Trends in Immunology*, *39*(1), 6–18. https://doi.org/10.1016/j.it.2017.08.006

_____

Reger, M. A., Watson, G. S., Green, P. S., Wilkinson, C. W., Baker, L. D., Cholerton, B., Fishel, M. A., Plymate, S. R., Breitner, J. C. S., DeGroodt, W., Mehta, P., & Craft, S. (2008). Intranasal insulin improves cognition and modulates beta-amyloid in early AD. *Neurology*, *70*(6), 440–448. https://doi.org/10.1212/01.WNL.0000265401.62434.36

Ribeiro, M., Rosenstock, T. R., Oliveira, A. M., Oliveira, C. R., & Rego, A. C. (2014). Insulin and IGF-1 improve mitochondrial function in a PI-3K/Akt-dependent manner and reduce mitochondrial generation of reactive oxygen species in Huntington's disease knock-in striatal cells. *Free Radical Biology & Medicine*, *74*, 129–144. https://doi.org/10.1016/j.freeradbiomed.2014.06.023

Rose, J. M., Novoselov, S. S., Robinson, P. A., & Cheetham, M. E. (2011). Molecular chaperone-mediated rescue of mitophagy by a Parkin RING1 domain mutant. *Human Molecular Genetics*, *20*(1), 16–27. https://doi.org/10.1093/hmg/ddq428

Ross, F. A., Jensen, T. E., & Hardie, D. G. (2016). Differential regulation by AMP and ADP of AMPK complexes containing different γ subunit isoforms. *The Biochemical Journal*, *473*(2), 189–199. https://doi.org/10.1042/BJ20150910

Ross, F. A., MacKintosh, C., & Hardie, D. G. (2016). AMP-activated protein kinase: A cellular energy sensor that comes in 12 flavours. *The FEBS Journal*, *283*(16), 2987–3001. https://doi.org/10.1111/febs.13698

Rovira-Llopis, S., Bañuls, C., Diaz-Morales, N., Hernandez-Mijares, A., Rocha, M., & Victor, V. M. (2017). Mitochondrial dynamics in type 2 diabetes: Pathophysiological implications. *Redox Biology*, *11*, 637–645. https://doi.org/10.1016/j.redox.2017.01.013

Ruegsegger, G. N., Creo, A. L., Cortes, T. M., Dasari, S., & Nair, K. S. (2018). Altered mitochondrial function in insulin-deficient and insulin-resistant states. *Journal of Clinical Investigation*, *128*(9), 3671–3681. https://doi.org/10.1172/JCI120843

Ruegsegger, G. N., Manjunatha, S., Summer, P., Gopala, S., Zabeilski, P., Dasari, S., Vanderboom, P. M., Lanza, I. R., Klaus, K. A., & Nair, K. S. (2019). Insulin deficiency and intranasal insulin alter brain mitochondrial function: A potential factor for dementia in diabetes. *FASEB Journal: Official Publication of the Federation of American Societies for Experimental Biology*, *33*(3), 4458–4472. https://doi.org/10.1096/fj.201802043R

Ruijtenberg, S., Hoek, T. A., Yan, X., & Tanenbaum, M. E. (2018). Imaging Translation Dynamics of Single mRNA Molecules in Live Cells. *Methods in Molecular Biology (Clifton, N.J.)*, *1649*, 385–404. https://doi.org/10.1007/978-1-4939-7213-5_26

Sancak, Y., Bar-Peled, L., Zoncu, R., Markhard, A. L., Nada, S., & Sabatini, D. M. (2010). Ragulator-Rag complex targets mTORC1 to the lysosomal surface and is necessary for its activation by amino acids. *Cell*, *141*(2), 290–303. https://doi.org/10.1016/j.cell.2010.02.024

Sancak, Y., Peterson, T. R., Shaul, Y. D., Lindquist, R. A., Thoreen, C. C., Bar-Peled, L., & Sabatini, D. M. (2008). The Rag GTPases bind raptor and mediate amino acid signaling to mTORC1. *Science (New York, N.Y.)*, *320*(5882), 1496–1501. https://doi.org/10.1126/science.1157535

Sandoval, H., Thiagarajan, P., Dasgupta, S. K., Schumacher, A., Prchal, J. T., Chen, M., & Wang, J. (2008). Essential role for Nix in autophagic maturation of erythroid cells. *Nature*, *454*(7201), 232–235. https://doi.org/10.1038/nature07006

Sanz, E., Yang, L., Su, T., Morris, D. R., McKnight, G. S., & Amieux, P. S. (2009). Cell-type-specific isolation of ribosome-associated mRNA from complex tissues. *Proceedings of the National Academy of Sciences of the United States of America*, *106*(33), 13939–13944. https://doi.org/10.1073/pnas.0907143106

Sarraf, S. A., Raman, M., Guarani-Pereira, V., Sowa, M. E., Huttlin, E. L., Gygi, S. P., & Harper, J. W. (2013). Landscape of the PARKIN-dependent ubiquitylome in response to mitochondrial depolarization. *Nature*, *496*(7445), 372–376. https://doi.org/10.1038/nature12043

Saucedo, L. J., Gao, X., Chiarelli, D. A., Li, L., Pan, D., & Edgar, B. A. (2003). Rheb promotes cell growth as a component of the insulin/TOR signalling network. *Nature Cell Biology*, *5*(6), 566–571. https://doi.org/10.1038/ncb996

Schell, M., Wardelmann, K., & Kleinridders, A. (2021). Untangling the effect of insulin action on brain mitochondria and metabolism. *Journal of Neuroendocrinology*, *33*(4). https://doi.org/10.1111/jne.12932

Schindelin, J., Arganda-Carreras, I., Frise, E., Kaynig, V., Longair, M., Pietzsch, T., Preibisch, S., Rueden, C., Saalfeld, S., Schmid, B., Tinevez, J.-Y., White, D. J., Hartenstein, V., Eliceiri, K., Tomancak, P., & Cardona, A. (2012). Fiji: An open-source platform for biological-image analysis. *Nature Methods*, *9*(7), 676–682. https://doi.org/10.1038/nmeth.2019

Schubert, M., Gautam, D., Surjo, D., Ueki, K., Baudler, S., Schubert, D., Kondo, T., Alber, J., Galldiks, N., Küstermann, E., Arndt, S., Jacobs, A. H., Krone, W., Kahn, C. R., & Brüning, J. C. (2004). Role for neuronal insulin resistance in neurodegenerative diseases. *Proceedings of the National Academy of Sciences*, *101*(9), 3100–3105. https://doi.org/10.1073/pnas.0308724101

Schuhmacher, J. S., tom Dieck, S., Christoforidis, S., Landerer, C., Davila Gallesio, J., Hersemann, L., Seifert, S., Schäfer, R., Giner, A., Toth-Petroczy, A., Kalaidzidis, Y., Bohnsack, K. E., Bohnsack, M. T., Schuman, E. M., & Zerial, M. (2023). The Rab5 effector FERRY links early endosomes with mRNA localization. *Molecular Cell*, *83*(11), 1839-1855.e13. https://doi.org/10.1016/j.molcel.2023.05.012

_____

Schulingkamp, R. J., Pagano, T. C., Hung, D., & Raffa, R. B. (2000). Insulin receptors and insulin action in the brain: Review and clinical implications. *Neuroscience and Biobehavioral Reviews*, *24*(8), 855–872. https://doi.org/10.1016/s0149-7634(00)00040-3

Seibler, P., Graziotto, J., Jeong, H., Simunovic, F., Klein, C., & Krainc, D. (2011). Mitochondrial Parkin recruitment is impaired in neurons derived from mutant PINK1 induced pluripotent stem cells. *The Journal of Neuroscience: The Official Journal of the Society for Neuroscience*, *31*(16), 5970–5976. https://doi.org/10.1523/JNEUROSCI.4441-10.2011

Serrano-Pozo, A., Das, S., & Hyman, B. T. (2021). APOE and Alzheimer's disease: Advances in genetics, pathophysiology, and therapeutic approaches. *The Lancet Neurology*, *20*(1), 68–80. https://doi.org/10.1016/S1474-4422(20)30412-9

Shackelford, D. B., & Shaw, R. J. (2009). The LKB1-AMPK pathway: Metabolism and growth control in tumour suppression. *Nature Reviews. Cancer*, *9*(8), 563–575. https://doi.org/10.1038/nrc2676

Shaw, R. J., Kosmatka, M., Bardeesy, N., Hurley, R. L., Witters, L. A., DePinho, R. A., & Cantley, L. C. (2004). The tumor suppressor LKB1 kinase directly activates AMP-activated kinase and regulates apoptosis in response to energy stress. *Proceedings of the National Academy of Sciences of the United States of America*, *101*(10), 3329–3335. https://doi.org/10.1073/pnas.0308061100

Shigeoka, T., Jung, H., Jung, J., Turner-Bridger, B., Ohk, J., Lin, J. Q., Amieux, P. S., & Holt, C. E. (2016). Dynamic Axonal Translation in Developing and Mature Visual Circuits. *Cell*, *166*(1), 181–192. https://doi.org/10.1016/j.cell.2016.05.029

Simonovitch, S., Schmukler, E., Masliah, E., Pinkas-Kramarski, R., & Michaelson, D. M. (2019). The Effects of APOE4 on Mitochondrial Dynamics and Proteins in vivo. *Journal of Alzheimer's Disease: JAD*, *70*(3), 861–875. https://doi.org/10.3233/JAD-190074

Smirnova, E., Griparic, L., Shurland, D. L., & van der Bliek, A. M. (2001). Dynamin-related protein Drp1 is required for mitochondrial division in mammalian cells. *Molecular Biology of the Cell*, *12*(8), 2245–2256. https://doi.org/10.1091/mbc.12.8.2245

Sohn, H.-Y., Kim, S.-I., Park, J.-Y., Park, S.-H., Koh, Y. H., Kim, J., & Jo, C. (2021). ApoE4 attenuates autophagy via FoxO3a repression in the brain. *Scientific Reports*, *11*(1), 17604. https://doi.org/10.1038/s41598-021-97117-6

Soltys, C.-L. M., Kovacic, S., & Dyck, J. R. B. (2006). Activation of cardiac AMP-activated protein kinase by LKB1 expression or chemical hypoxia is blunted by increased Akt activity. *American Journal of Physiology. Heart and Circulatory Physiology*, *290*(6), H2472-2479. https://doi.org/10.1152/ajpheart.01206.2005

Soutar, M. P. M., Kempthorne, L., Miyakawa, S., Annuario, E., Melandri, D., Harley, J., O'Sullivan, G. A., Wray, S., Hancock, D. C., Cookson, M. R., Downward, J., Carlton, M., & Plun-Favreau, H. (2018). AKT signalling selectively regulates PINK1 mitophagy in SHSY5Y cells and human iPSC-derived neurons. *Scientific Reports*, *8*(1), 8855. https://doi.org/10.1038/s41598-018-26949-6

Spillane, M., Ketschek, A., Merianda, T. T., Twiss, J. L., & Gallo, G. (2013). Mitochondria Coordinate Sites of Axon Branching through Localized Intra-axonal Protein Synthesis. *Cell Reports*, *5*(6), 1564–1575. https://doi.org/10.1016/j.celrep.2013.11.022

Stapleton, D., Mitchelhill, K. I., Gao, G., Widmer, J., Michell, B. J., Teh, T., House, C. M., Fernandez, C. S., Cox, T., Witters, L. A., & Kemp, B. E. (1996). Mammalian AMP-activated protein kinase subfamily. *The Journal of Biological Chemistry*, *271*(2), 611–614. https://doi.org/10.1074/jbc.271.2.611

Steinberg, G. R., & Hardie, D. G. (2022). New insights into activation and function of the AMPK. *Nature Reviews. Molecular Cell Biology*. https://doi.org/10.1038/s41580-022-00547-x

Stenesen, D., Suh, J. M., Seo, J., Yu, K., Lee, K.-S., Kim, J.-S., Min, K.-J., & Graff, J. M. (2013). Adenosine nucleotide biosynthesis and AMPK regulate adult life span and mediate the longevity benefit of caloric restriction in flies. *Cell Metabolism*, *17*(1), 101–112. https://doi.org/10.1016/j.cmet.2012.12.006

Stolz, A., Ernst, A., & Dikic, I. (2014). Cargo recognition and trafficking in selective autophagy. *Nature Cell Biology*, *16*(6), 495–501. https://doi.org/10.1038/ncb2979

Stowers, R. S., Megeath, L. J., Górska-Andrzejak, J., Meinertzhagen, I. A., & Schwarz, T. L. (2002). Axonal transport of mitochondria to synapses depends on milton, a novel Drosophila protein. *Neuron*, *36*(6), 1063–1077. https://doi.org/10.1016/s0896-6273(02)01094-2

Strittmatter, W. J., Saunders, A. M., Schmechel, D., Pericak-Vance, M., Enghild, J., Salvesen, G. S., & Roses, A. D. (1993). Apolipoprotein E: High-avidity binding to beta-amyloid and increased frequency of type 4 allele in late-onset familial Alzheimer disease. *Proceedings of the National Academy of Sciences of the United States of America*, *90*(5), 1977–1981. https://doi.org/10.1073/pnas.90.5.1977

Strittmatter, W. J., Weisgraber, K. H., Huang, D. Y., Dong, L. M., Salvesen, G. S., Pericak-Vance, M., Schmechel, D., Saunders, A. M., Goldgaber, D., & Roses, A. D. (1993). Binding of human apolipoprotein E to synthetic amyloid beta peptide: Isoform-specific effects and implications for late-onset Alzheimer disease. *Proceedings of the National Academy of Sciences of the United States of America*, *90*(17), 8098–8102. https://doi.org/10.1073/pnas.90.17.8098

Su, C.-J., Shen, Z., Cui, R.-X., Huang, Y., Xu, D.-L., Zhao, F.-L., Pan, J., Shi, A.-M., Liu, T., & Yu, Y.-L. (2020). Thioredoxin-Interacting Protein (TXNIP) Regulates Parkin/PINK1-mediated Mitophagy in Dopaminergic Neurons Under High-glucose Conditions: Implications for Molecular Links

Between Parkinson's Disease and Diabetes. *Neuroscience Bulletin*, *36*(4), 346–358. https://doi.org/10.1007/s12264-019-00459-5

Suter, M., Riek, U., Tuerk, R., Schlattner, U., Wallimann, T., & Neumann, D. (2006). Dissecting the role of 5'-AMP for allosteric stimulation, activation, and deactivation of AMP-activated protein kinase. *The Journal of Biological Chemistry*, *281*(43), 32207–32216. https://doi.org/10.1074/jbc.M606357200

Talbot, K., Wang, H.-Y., Kazi, H., Han, L.-Y., Bakshi, K. P., Stucky, A., Fuino, R. L., Kawaguchi, K. R., Samoyedny, A. J., Wilson, R. S., Arvanitakis, Z., Schneider, J. A., Wolf, B. A., Bennett, D. A., Trojanowski, J. Q., & Arnold, S. E. (2012). Demonstrated brain insulin resistance in Alzheimer's disease patients is associated with IGF-1 resistance, IRS-1 dysregulation, and cognitive decline. *The Journal of Clinical Investigation*, *122*(4), 1316–1338. https://doi.org/10.1172/JCI59903

Tanenbaum, M. E., Gilbert, L. A., Qi, L. S., Weissman, J. S., & Vale, R. D. (2014). A Protein-Tagging System for Signal Amplification in Gene Expression and Fluorescence Imaging. *Cell*, *159*(3), 635–646. https://doi.org/10.1016/j.cell.2014.09.039

Taniguchi, C. M., Emanuelli, B., & Kahn, C. R. (2006). Critical nodes in signalling pathways: Insights into insulin action. *Nature Reviews. Molecular Cell Biology*, *7*(2), 85–96. https://doi.org/10.1038/nrm1837

Tauber, D., Tauber, G., & Parker, R. (2020). Mechanisms and Regulation of RNA Condensation in RNP Granule Formation. *Trends in Biochemical Sciences*, *45*(9), 764–778. https://doi.org/10.1016/j.tibs.2020.05.002

Tee, A. R., Manning, B. D., Roux, P. P., Cantley, L. C., & Blenis, J. (2003). Tuberous sclerosis complex gene products, Tuberin and Hamartin, control mTOR signaling by acting as a GTPase-activating protein complex toward Rheb. *Current Biology: CB*, *13*(15), 1259–1268. https://doi.org/10.1016/s0960-9822(03)00506-2

Thies, W. & Bleiler, L. (2011). Alzheimer's Association Report: 2011 Alzheimer's Disease Facts and Figures. *Alzheimer's & Dementia*, *7*, 208–244. https://doi.org/10.1016/j.jalz.2011.02.004

Thornton, C., Snowden, M. A., & Carling, D. (1998). Identification of a novel AMP-activated protein kinase beta subunit isoform that is highly expressed in skeletal muscle. *The Journal of Biological Chemistry*, *273*(20), 12443–12450. https://doi.org/10.1074/jbc.273.20.12443

Tian, W., Li, W., Chen, Y., Yan, Z., Huang, X., Zhuang, H., Zhong, W., Chen, Y., Wu, W., Lin, C., Chen, H., Hou, X., Zhang, L., Sui, S., Zhao, B., Hu, Z., Li, L., & Feng, D. (2015). Phosphorylation of ULK1 by AMPK regulates translocation of ULK1 to mitochondria and mitophagy. *FEBS Letters*, *589*(15), 1847–1854. https://doi.org/10.1016/j.febslet.2015.05.020

Tilokani, L., Russell, F. M., Hamilton, S., Virga, D. M., Segawa, M., Paupe, V., Gruszczyk, A. V., Protasoni, M., Tabara, L.-C., Johnson, M., Anand, H., Murphy, M. P., Hardie, D. G., Polleux, F., & Prudent, J. (2022). AMPK-dependent phosphorylation of MTFR1L regulates mitochondrial morphology. *Science Advances*, *8*(45), eabo7956. https://doi.org/10.1126/sciadv.abo7956

Toyama, E. Q., Herzig, S., Courchet, J., Lewis, T. L., Losón, O. C., Hellberg, K., Young, N. P., Chen, H., Polleux, F., Chan, D. C., & Shaw, R. J. (2016). Metabolism. AMP-activated protein kinase mediates mitochondrial fission in response to energy stress. *Science (New York, N.Y.)*, *351*(6270), 275–281. https://doi.org/10.1126/science.aab4138

Trischitta, V., Wong, K. Y., Brunetti, A., Scalisi, R., Vigneri, R., & Goldfine, I. D. (1989). Endocytosis, recycling, and degradation of the insulin receptor. Studies with monoclonal antireceptor antibodies that do not activate receptor kinase. *The Journal of Biological Chemistry*, *264*(9), 5041–5046.

Valente, E. M., Abou-Sleiman, P. M., Caputo, V., Muqit, M. M. K., Harvey, K., Gispert, S., Ali, Z., Del Turco, D., Bentivoglio, A. R., Healy, D. G., Albanese, A., Nussbaum, R., González-Maldonado, R., Deller, T., Salvi, S., Cortelli, P., Gilks, W. P., Latchman, D. S., Harvey, R. J., … Wood, N. W. (2004). Hereditary early-onset Parkinson's disease caused by mutations in PINK1. *Science (New York, N.Y.)*, *304*(5674), 1158–1160. https://doi.org/10.1126/science.1096284

Valentine, R. J., Coughlan, K. A., Ruderman, N. B., & Saha, A. K. (2014). Insulin inhibits AMPK activity and phosphorylates AMPK Ser485/491 through Akt in hepatocytes, myotubes and incubated rat skeletal muscle. *Archives of Biochemistry and Biophysics*, *562*, 62–69. https://doi.org/10.1016/j.abb.2014.08.013

van Spronsen, M., Mikhaylova, M., Lipka, J., Schlager, M. A., van den Heuvel, D. J., Kuijpers, M., Wulf, P. S., Keijzer, N., Demmers, J., Kapitein, L. C., Jaarsma, D., Gerritsen, H. C., Akhmanova, A., & Hoogenraad, C. C. (2013). TRAK/Milton motor-adaptor proteins steer mitochondrial trafficking to axons and dendrites. *Neuron*, *77*(3), 485–502. https://doi.org/10.1016/j.neuron.2012.11.027

Vance, J. E., & Hayashi, H. (2010). Formation and function of apolipoprotein E-containing lipoproteins in the nervous system. *Biochimica Et Biophysica Acta*, *1801*(8), 806–818. https://doi.org/10.1016/j.bbalip.2010.02.007

Vincow, E. S., Merrihew, G., Thomas, R. E., Shulman, N. J., Beyer, R. P., MacCoss, M. J., & Pallanck, L. J. (2013). The PINK1-Parkin pathway promotes both mitophagy and selective respiratory chain turnover in vivo. *Proceedings of the National Academy of Sciences of the United States of America*, *110*(16), 6400–6405. https://doi.org/10.1073/pnas.1221132110

Vitali, C., Wellington, C. L., & Calabresi, L. (2014). HDL and cholesterol handling in the brain. *Cardiovascular Research*, *103*(3), 405–413. https://doi.org/10.1093/cvr/cvu148

_____

Vives-Bauza, C., Zhou, C., Huang, Y., Cui, M., de Vries, R. L. A., Kim, J., May, J., Tocilescu, M. A., Liu, W., Ko, H. S., Magrané, J., Moore, D. J., Dawson, V. L., Grailhe, R., Dawson, T. M., Li, C., Tieu, K., & Przedborski, S. (2010). PINK1-dependent recruitment of Parkin to mitochondria in mitophagy. *Proceedings of the National Academy of Sciences of the United States of America*, *107*(1), 378–383. https://doi.org/10.1073/pnas.0911187107

Vrijsen, S., Vrancx, C., Del Vecchio, M., Swinnen, J. V., Agostinis, P., Winderickx, J., Vangheluwe, P., & Annaert, W. (2022). Inter-organellar Communication in Parkinson's and Alzheimer's Disease: Looking Beyond Endoplasmic Reticulum-Mitochondria Contact Sites. *Frontiers in Neuroscience*, *16*, 900338. https://doi.org/10.3389/fnins.2022.900338

Warner, J. R., & Knopf, P. M. (2002). The discovery of polyribosomes. *Trends in Biochemical Sciences*, *27*(7), 376–380. https://doi.org/10.1016/s0968-0004(02)02126-6

Warner, J. R., Knopf, P. M., & Rich, A. (1963). A multiple ribosomal structure in protein synthesis. *Proceedings of the National Academy of Sciences of the United States of America*, *49*(1), 122–129. https://doi.org/10.1073/pnas.49.1.122

Warner, J. R., & Rich, A. (1964). THE NUMBER OF SOLUBLE RNA MOLECULES ON RETICULOCYTE POLYRIBOSOMES. *Proceedings of the National Academy of Sciences of the United States of America*, *51*(6), 1134–1141. https://doi.org/10.1073/pnas.51.6.1134

Watters, O., Connolly, N. M. C., König, H.-G., Düssmann, H., & Prehn, J. H. M. (2020). AMPK Preferentially Depresses Retrograde Transport of Axonal Mitochondria during Localized Nutrient Deprivation. *The Journal of Neuroscience: The Official Journal of the Society for Neuroscience*, *40*(25), 4798–4812. https://doi.org/10.1523/JNEUROSCI.2067-19.2020

Weisgraber, K. H. (1990). Apolipoprotein E distribution among human plasma lipoproteins: Role of the cysteine-arginine interchange at residue 112. *Journal of Lipid Research*, *31*(8), 1503–1511.

Williams, C. C., Jan, C. H., & Weissman, J. S. (2014). Targeting and plasticity of mitochondrial proteins revealed by proximity-specific ribosome profiling. *Science (New York, N.Y.)*, *346*(6210), 748–751. https://doi.org/10.1126/science.1257522

Wilson, E. L., & Metzakopian, E. (2021). ER-mitochondria contact sites in neurodegeneration: Genetic screening approaches to investigate novel disease mechanisms. *Cell Death & Differentiation*, *28*(6), 1804–1821. https://doi.org/10.1038/s41418-020-00705-8

Wong, Y. C., & Holzbaur, E. L. F. (2014). Optineurin is an autophagy receptor for damaged mitochondria in parkin-mediated mitophagy that is disrupted by an ALS-linked mutation. *Proceedings of the National Academy of Sciences of the United States of America*, *111*(42), E4439-4448. https://doi.org/10.1073/pnas.1405752111

Woods, A., Dickerson, K., Heath, R., Hong, S.-P., Momcilovic, M., Johnstone, S. R., Carlson, M., & Carling, D. (2005). Ca2+/calmodulin-dependent protein kinase kinase-beta acts upstream of AMP-activated protein kinase in mammalian cells. *Cell Metabolism*, *2*(1), 21–33. https://doi.org/10.1016/j.cmet.2005.06.005

Woods, A., Johnstone, S. R., Dickerson, K., Leiper, F. C., Fryer, L. G. D., Neumann, D., Schlattner, U., Wallimann, T., Carlson, M., & Carling, D. (2003). LKB1 is the upstream kinase in the AMP-activated protein kinase cascade. *Current Biology: CB*, *13*(22), 2004–2008. https://doi.org/10.1016/j.cub.2003.10.031

Wu, B., Chen, J., & Singer, R. H. (2014). Background free imaging of single mRNAs in live cells using split fluorescent proteins. *Scientific Reports*, *4*, 3615. https://doi.org/10.1038/srep03615

Wu, H., Carvalho, P., & Voeltz, G. K. (2018). Here, there, and everywhere: The importance of ER membrane contact sites. *Science (New York, N.Y.)*, *361*(6401), eaan5835. https://doi.org/10.1126/science.aan5835

Wu, W., Tian, W., Hu, Z., Chen, G., Huang, L., Li, W., Zhang, X., Xue, P., Zhou, C., Liu, L., Zhu, Y., Zhang, X., Li, L., Zhang, L., Sui, S., Zhao, B., & Feng, D. (2014). ULK1 translocates to mitochondria and phosphorylates FUNDC1 to regulate mitophagy. *EMBO Reports*, *15*(5), 566–575. https://doi.org/10.1002/embr.201438501

Xiao, B., Heath, R., Saiu, P., Leiper, F. C., Leone, P., Jing, C., Walker, P. A., Haire, L., Eccleston, J. F., Davis, C. T., Martin, S. R., Carling, D., & Gamblin, S. J. (2007). Structural basis for AMP binding to mammalian AMP-activated protein kinase. *Nature*, *449*(7161), 496–500. https://doi.org/10.1038/nature06161

Xu, Q., Bernardo, A., Walker, D., Kanegawa, T., Mahley, R. W., & Huang, Y. (2006). Profile and Regulation of Apolipoprotein E (ApoE) Expression in the CNS in Mice with Targeting of Green Fluorescent Protein Gene to the ApoE Locus. *The Journal of Neuroscience*, *26*(19), 4985–4994. https://doi.org/10.1523/JNEUROSCI.5476-05.2006

Yamaguchi, O., Murakawa, T., Nishida, K., & Otsu, K. (2016). Receptor-mediated mitophagy. *Journal of Molecular and Cellular Cardiology*, *95*, 50–56. https://doi.org/10.1016/j.yjmcc.2016.03.010

Yamano, K., & Youle, R. J. (2013). PINK1 is degraded through the N-end rule pathway. *Autophagy*, *9*(11), 1758–1769. https://doi.org/10.4161/auto.24633

Yan, D., Cai, Y., Luo, J., Liu, J., Li, X., Ying, F., Xie, X., Xu, A., Ma, X., & Xia, Z. (2020). FOXO1 contributes to diabetic cardiomyopathy via inducing imbalanced oxidative metabolism in type 1 diabetes. *Journal of Cellular and Molecular Medicine*, *24*(14), 7850–7861. https://doi.org/10.1111/jcmm.15418

Yang, H., Yu, Z., Chen, X., Li, J., Li, N., Cheng, J., Gao, N., Yuan, H.-X., Ye, D., Guan, K.-L., & Xu, Y. (2021). Structural insights into TSC complex assembly and GAP activity on Rheb. *Nature Communications*, *12*(1), 339. https://doi.org/10.1038/s41467-020-20522-4

Yoon, B. C., Jung, H., Dwivedy, A., O'Hare, C. M., Zivraj, K. H., & Holt, C. E. (2012). Local translation of extranuclear lamin B promotes axon maintenance. *Cell*, *148*(4), 752–764. https://doi.org/10.1016/j.cell.2011.11.064

Yousefi, R., Fornasiero, E. F., Cyganek, L., Montoya, J., Jakobs, S., Rizzoli, S. O., Rehling, P., & Pacheu-Grau, D. (2021). Monitoring mitochondrial translation in living cells. *EMBO Reports*, *22*(4), e51635. https://doi.org/10.15252/embr.202051635

Zakharova, I. O., Sokolova, T. V., Bayunova, L. V., Zorina, I. I., Rychkova, M. P., Shpakov, A. O., & Avrova, N. F. (2019). The Protective Effect of Insulin on Rat Cortical Neurons in Oxidative Stress and Its Dependence on the Modulation of Akt, GSK-3beta, ERK1/2, and AMPK Activities. *International Journal of Molecular Sciences*, *20*(15), E3702. https://doi.org/10.3390/ijms20153702

Zhang, C.-S., Jiang, B., Li, M., Zhu, M., Peng, Y., Zhang, Y.-L., Wu, Y.-Q., Li, T. Y., Liang, Y., Lu, Z., Lian, G., Liu, Q., Guo, H., Yin, Z., Ye, Z., Han, J., Wu, J.-W., Yin, H., Lin, S.-Y., & Lin, S.-C. (2014). The lysosomal v-ATPase-Ragulator complex is a common activator for AMPK and mTORC1, acting as a switch between catabolism and anabolism. *Cell Metabolism*, *20*(3), 526–540. https://doi.org/10.1016/j.cmet.2014.06.014

Zhang, H., Hao, Y., Manor, B., Novak, P., Milberg, W., Zhang, J., Fang, J., & Novak, V. (2015). Intranasal Insulin Enhanced Resting-State Functional Connectivity of Hippocampal Regions in Type 2 Diabetes. *Diabetes*, *64*(3), 1025–1034. https://doi.org/10.2337/db14-1000

Zhang, Y., Pak, C., Han, Y., Ahlenius, H., Zhang, Z., Chanda, S., Marro, S., Patzke, C., Acuna, C., Covy, J., Xu, W., Yang, N., Danko, T., Chen, L., Wernig, M., & Südhof, T. C. (2013). Rapid single-step induction of functional neurons from human pluripotent stem cells. *Neuron*, *78*(5), 785–798. https://doi.org/10.1016/j.neuron.2013.05.029

Zhang, Y.-L., Guo, H., Zhang, C.-S., Lin, S.-Y., Yin, Z., Peng, Y., Luo, H., Shi, Y., Lian, G., Zhang, C., Li, M., Ye, Z., Ye, J., Han, J., Li, P., Wu, J.-W., & Lin, S.-C. (2013). AMP as a low-energy charge signal autonomously initiates assembly of AXIN-AMPK-LKB1 complex for AMPK activation. *Cell Metabolism*, *18*(4), 546–555. https://doi.org/10.1016/j.cmet.2013.09.005

Zhao, H., Shen, A., Xiang, Y. K., & Corey, D. P. (2016). Three Recombinant Engineered Antibodies against Recombinant Tags with High Affinity and Specificity. *PLOS ONE*, *11*(3), e0150125. https://doi.org/10.1371/journal.pone.0150125

Zhao, N., Liu, C.-C., Van Ingelgom, A. J., Martens, Y. A., Linares, C., Knight, J. A., Painter, M. M., Sullivan, P. M., & Bu, G. (2017). Apolipoprotein E4 Impairs Neuronal Insulin Signaling by

Trapping Insulin Receptor in the Endosomes. *Neuron*, *96*(1), 115-129.e5. https://doi.org/10.1016/j.neuron.2017.09.003

Zhou, G., Myers, R., Li, Y., Chen, Y., Shen, X., Fenyk-Melody, J., Wu, M., Ventre, J., Doebber, T., Fujii, N., Musi, N., Hirshman, M. F., Goodyear, L. J., & Moller, D. E. (2001). Role of AMP-activated protein kinase in mechanism of metformin action. *The Journal of Clinical Investigation*, *108*(8), 1167–1174. https://doi.org/10.1172/JCI13505

Zivraj, K. H., Tung, Y. C. L., Piper, M., Gumy, L., Fawcett, J. W., Yeo, G. S. H., & Holt, C. E. (2010). Subcellular Profiling Reveals Distinct and Developmentally Regulated Repertoire of Growth Cone mRNAs. *Journal of Neuroscience*, *30*(46), 15464–15478. https://doi.org/10.1523/JNEUROSCI.1800-10.2010

Zoncu, R., Bar-Peled, L., Efeyan, A., Wang, S., Sancak, Y., & Sabatini, D. M. (2011). MTORC1 senses lysosomal amino acids through an inside-out mechanism that requires the vacuolar H(+)-ATPase. *Science (New York, N.Y.)*, *334*(6056), 678–683. https://doi.org/10.1126/science.1207056

6 ACKNOWLEDGMENTS

First of all, I would like to thank my supervisor Prof. Dr. Angelika Harbauer for choosing me and giving me the opportunity to do my PhD in her lab. Angie, thank you for your trust, your honest feedback, your encouragement, and your constant belief in me. Furthermore, I would also like to express my appreciation to Prof. Dr. Danny Nedialkova and Prof. Dr. Thomas Misgeld for their support as members of my thesis advisory committee. Your insights and suggestions have been important for refining the direction of my research. Additionally, I want to thank Martina, Barbara, Sabine, Leo, Robert, Claudio, Eva, Martin and Markus from the core facilities for their assistance and involvements, which have greatly contributed to the success of my research.

A very special thank you goes to all my colleagues who have been with me throughout these years. Jana, your care, understanding and help meant a lot to me. I will always remember our talks. My fellow PhD students have been much more than just colleagues; they have become an irreplaceable part of this journey. Simone, I am very glad that you have been with me since the beginning, sharing this journey together along with all its ups and downs. Hari, no matter the subject, I can talk to you about anything, and you are always there to listen and make time. Alina, we have experienced so much together, and you have shown me the importance of balance beyond work. Isabel, seeing you and your smile always makes my day better. Marlena, your calming presence and our conversations helped me reduce stress in so many situations. Luciano, your approachable nature, daily hugs, and the smell of your perfume wherever you have been always bring a smile to my face. Furthermore, I am very grateful for our postdocs, Inma and Ben. Inma, your vast knowledge and help have been really important to my progress. My students Caro and Andrea, your enthusiasm and commitment have helped me a lot in my project.

Lastly, my deepest thank you goes to my sister Femke and Jan. Both of you have always been my go-to for recharging my batteries. You have consistently listened to all of my stories, ups and downs and dissected everything with me. Perhaps one day, we will still produce that daily soap we often joke about. I am also incredibly grateful for my parents, Claudia and Andreas, as well as Jan's family. You have always been there for me and supported me, no matter what. I am equally thankful for all of my friends, particularly Janik, Lea, Thea, Elena, Gina, and Laura. Your patient listening and support have helped me through many challenges. I would not have reached this point without each and every one of you.